



Durham E-Theses

Vibrational modes of massive Skyrmons within the rational map ansatz

Lin, Wen-Tsan

How to cite:

Lin, Wen-Tsan (2007) *Vibrational modes of massive Skyrmons within the rational map ansatz*, Durham theses, Durham University. Available at Durham E-Theses Online: <http://etheses.dur.ac.uk/2486/>

Use policy

The full-text may be used and/or reproduced, and given to third parties in any format or medium, without prior permission or charge, for personal research or study, educational, or not-for-profit purposes provided that:

- a full bibliographic reference is made to the original source
- a [link](#) is made to the metadata record in Durham E-Theses
- the full-text is not changed in any way

The full-text must not be sold in any format or medium without the formal permission of the copyright holders.

Please consult the [full Durham E-Theses policy](#) for further details.

Vibrational Modes of Massive Skyrmions within the Rational Map Ansatz

by

WEN-TSAN LIN

The copyright of this thesis rests with the author or the university to which it was submitted. No quotation from it, or information derived from it may be published without the prior written consent of the author or university, and any information derived from it should be acknowledged.

A Thesis presented for the degree of
Doctor of Philosophy



Centre for Particle Theory
Department of Mathematical Sciences
University of Durham
England

September 2007

0 1 SEP 2008



Dedicated to

my parents

Vibrational Modes of Massive Skyrmions within the Rational Map Ansatz

by

WEN-TSAN LIN

Submitted for the degree of Doctor of Philosophy
September 2007

Abstract

In this thesis, we study the vibrational modes of some Skyrmion solutions within the rational map approximation. When the Skyrme field is perturbed around a static solution, the radial and angular vibrations of the field are decoupled; this gives us two sets of eigenvalue equations that provide us the vibrational modes of the solutions when solved. Using the symmetry properties of the solutions of the equation of motion of the model, the conjugate relations among these solutions can be identified. With a physical constraint on the dispersion relation between the mass and the vibration frequency, we obtain an upper bound for the critical pion mass. Finally, we compare between our results with some numerical results obtained by Houghton et al.

Declaration

The work in this thesis is based on research carried out at CPT, the Department of Mathematical Sciences, University of Durham, England. No part of this thesis has been submitted elsewhere for any other degree or qualification and it all my own work unless referenced to the contrary in the text.

Copyright © 2007 by WEN-TSAN LIN.

“The copyright of this thesis rests with the author. No quotations from it should be published without the author’s prior written consent and information derived from it should be acknowledged”.

Acknowledgements

Thank my parents and family for the full support. Thanks to my supervisor, Dr. B.M.A.G. Piette, for his guidance and patience.

Contents

Abstract	iii
Declaration	iv
Acknowledgements	v
1 Introduction	1
2 Skyrme Model	9
2.1 The Model	9
2.2 Rational Map and Rational Map Ansatz	13
2.3 Energy Density	20
2.4 Symmetry of The Skyrme Model, Skyrmion and Rational Map	24
2.5 Asymptotic Behavior of Rational Map Profile	30
3 Vibration	34
3.1 Vibration of profile function	34
3.2 Vibrations of Rational Map	38
4 Eigen Mode of Profile Function	46
4.1 Eigenvalues	46
4.2 Asymptotic Fields	51
4.3 Critical Mass	56
5 Eigen Mode of Rational Map (I)	60
5.1 Determination of \mathcal{X}_2 , \mathcal{Y}_2 , and \mathcal{I}_2	60
5.2 Eigenvalues and Eigenvectors	70

5.3	Broken Zero Mode	79
5.4	Conjugacy Relation	84
5.4.1	Möbius Transformation	85
5.4.2	Conjugacy relation, $B = 1$	95
5.4.3	Conjugacy relation, $B = 2$	98
5.4.4	Finding the Iso-rotational Zero Mode, $B = 2$	101
5.4.5	Conjugacy Relation Between $R_7(\xi)$ and $R_8(\xi)$, $B = 2$	103
5.5	Plots of Rational Maps and Energy Density	108
5.5.1	$B = 1$	108
5.5.2	$B = 2$	113
6	Eigen Mode of Rational Map (II)	126
6.1	$R_{18}(\xi)$, $B = 4$	126
6.2	$R_{16}(\xi)$ & $R_{17}(\xi)$, $B = 4$	135
6.3	$R_{15}(\xi)$, $R_{14}(\xi)$ & $R_{13}(\xi)$, $B = 4$	142
6.4	$R_{12}(\xi)$, $R_{11}(\xi)$ & $R_{10}(\xi)$, $B = 4$	148
6.5	$R_9(\xi)$, $R_8(\xi)$ & $R_7(\xi)$, $B = 4$	153
6.6	Zero Modes, $B = 4$	158
6.6.1	Identification of Iso-rotational Modes, $B = 4$	169
6.6.2	Plots of the Zero Modes, $B = 4$	174
7	Conclusion	183
7.1	Comparisons	183
7.1.1	Analysis for $B = 2$ case	184
7.1.2	Analysis for $B = 4$ case	189
7.2	Conclusion	194
	Bibliography	198
	Appendix	205
A	Symmetry Groups	205
A.1	Introduction to Symmetry Groups	205

A.2	Fundamental Symmetry Transformations	206
A.2.1	Finite rotation.	206
A.2.2	Reflection.	206
A.3	Groups of Pure Rotations	208
A.3.1	Uniaxial Group: C_n	208
A.3.2	Dihedral Group: D_n	209
A.3.3	Regular Polyhedron (Platonic Solids)	209
A.4	Groups with Pure Rotations and Rotation Reflections	213
A.4.1	Adjunction of Reflection to C_n	213
A.4.2	Adjunction of Reflection to D_n	214
A.4.3	Adjunction of Reflection to T, O	215
A.5	Character Tables for Some Important Point Groups	216

List of Figures

2.1	Ansatz for Profile function for $B=2$, $m = 0.2$, $p = 1$	23
2.2	Ansatz for Profile function for $B=4$, $m = 0.2$, $p = 1$	24
2.3	Pictures of the energy density isosurface for (a) $B = 1$, (b) $B = 2$, and (c) $B = 4$	27
4.1	Vibrational frequencies ω vs pion mass m for $B=1$, $B=2$, and $B=4$. . .	50
4.2	Critical Mass M_c for different baryon number p and potential param- eter p	57
5.1	The eigenvalues versus mass for different potential parameters p . (Left) $B = 1$, (Right) $B = 2$	78
5.2	The eigenvalues versus mass for different potential parameters p for $B = 4$. (Left) $p = 1$, (Right) $p = 2$	78
5.3	The eigenvalues versus mass for $B = 4$. (Left) $p = 3$, (Right) $p = 4$. . .	79
5.4	$\pi/2$ rotation of Riemann sphere about x -axis.	89
5.5	(Left) Green dots: The sample points of the domain(or physical) space. Red circles: The corresponding sample points of the deformed domain space of R_4 of $B = 1$. (Right) A slice of the stereographic projection of the complex plane.	109
5.6	Perturbed rational map R_5 of $B = 1$	109
5.7	Perturbed rational map R_6 of $B = 1$	109
5.8	R_6 , $B=1$	110
5.9	$B = 1$: (Left) $R_6(\xi)$, $\varepsilon = 2$; (Right) $R_6(\xi)$, $\varepsilon = -0.670$	112
5.10	$B = 1$, $R_6(\xi)$, side view: (Left) $\varepsilon = 2$; (Right) $\varepsilon = -0.67$	112
5.11	R_1 , $B=2$	115

5.12 Northern(left) and southern(right) hemisphere of Riemann sphere of $R_1, B=2$	115
5.13 $R_3, B=2$	116
5.14 Northern(left) and southern(right) hemisphere of Riemann sphere of $R_3, B=2$	116
5.15 $R_5, B=2$	117
5.16 Northern(left) and southern(right) hemisphere of Riemann sphere of $R_5, B=2$	117
5.17 $R_6, B=2$	118
5.18 Northern(left) and southern(right) hemisphere of Riemann sphere of $R_6, B=2$	118
5.19 $B = 2, R_6(\xi)$: (Left) $\varepsilon > 0$; (Right) $\varepsilon < 0$	119
5.20 $B = 2, R_6(\xi)$, half side view: (Left) $\varepsilon > 0$; (Right) $\varepsilon < 0$	119
5.21 $R_8, B=2$	120
5.22 Northern(left) and southern(right) hemisphere of Riemann sphere of $R_8, B=2$	120
5.23 $B = 2, R_8(\xi)$: (Left) $\varepsilon > 0$; (Right) $\varepsilon < 0$	121
5.24 $B = 2, R_8(\xi)$, half side view: (Left) $\varepsilon > 0$; (Right) $\varepsilon < 0$	121
5.25 $R_{10}, B=2$	122
5.26 Northern(left) and southern(right) hemisphere of Riemann sphere of $R_{10}, B=2$	122
5.27 $B = 2, R_{10}(\xi)$: (Left) $\varepsilon > 0$; (Right) $\varepsilon < 0$	123
5.28 $B = 2, R_{10}(\xi)$, half side view: (Left) $\varepsilon > 0$; (Right) $\varepsilon < 0$	123
6.1 $R_{18}, B=4$	127
6.2 $R_{18}, B=4$	127
6.3 Northern(left) and southern(right) hemisphere of Riemann sphere of $R_{18}, B=4$	128
6.4 $B = 4, R_{18}(\xi)$: (Left) $\varepsilon > 0$; (Right) $\varepsilon < 0$	128
6.5 The neighborhood of $\xi = 1$	130
6.6 Parameter $\varepsilon = 0$, (left)upper half plane and (right)lower half plane of the target space of the rational map $R_{18}(\xi), B=4$	130

6.7	Parameter $\varepsilon = 0.01$, (left)upper half plane and (right)lower half plane of the target space of the rational map $R_{18}(\xi)$, $B=4$	131
6.8	Parameter $\varepsilon = 0.05$, (left)upper half plane and (right)lower half plane of the target space of the rational map $R_{18}(\xi)$, $B=4$	131
6.9	Parameter $\varepsilon = 0.1$, (left)upper half plane and (right)lower half plane of the target space of the rational map $R_{18}(\xi)$, $B=4$	132
6.10	Neighborhood of $\xi = 1$ under the perturbed rational map R_{18} , $B=4$, with parameter $\varepsilon = 0$ (left) and parameter $\varepsilon = 0.01$ (right)	133
6.11	Neighborhood of $\xi = 1$ under the perturbed rational map R_{18} , $B=4$, with parameter $\varepsilon = 0.05$ (left) and parameter $\varepsilon = 0.1$ (right)	133
6.12	Northern(left) and southern(right) hemisphere of Riemann sphere of $R_{16}(\xi)$, $B=4$	140
6.13	$R_{16}(\xi)$, $B=4$	140
6.14	$B = 4$, $R_{16}(\xi)$: (Left) $\varepsilon > 0$; (Right) $\varepsilon < 0$	141
6.15	Northern(left) and southern(right) hemisphere of Riemann sphere of $R_{13}(\xi)$, $B=4$	146
6.16	$R_{13}(\xi)$, $B=4$	146
6.17	$B = 4$, $R_{13}(\xi)$: (Left) $\varepsilon > 0$; (Right) $\varepsilon < 0$	147
6.18	Northern(left) and southern(right) hemisphere of Riemann sphere of $R_{10}(\xi)$, $B=4$	151
6.19	$R_{10}(\xi)$, $B=4$	151
6.20	$B = 4$, $R_{10}(\xi)$: (Left) $\varepsilon > 0$; (Right) $\varepsilon < 0$	152
6.21	Northern(left) and southern(right) hemisphere of Riemann sphere of $R_7(\xi)$, $B=4$	156
6.22	$R_7(\xi)$, $B=4$	156
6.23	$B = 4$, $R_7(\xi)$: (Left) $\varepsilon > 0$; (Right) $\varepsilon < 0$	157
6.24	Northern(left) and southern(right) hemisphere of Riemann sphere of $R_{rot,x}(\xi)$, $B=4$	174
6.25	$R_{rot,x}(\xi)$, $B=4$	174
6.26	Northern(left) and southern(right) hemisphere of Riemann sphere of $R_{rot,y}(\xi)$, $B=4$	175

6.27	$R_{rot,y}(\xi), B=4$	175
6.28	Northern(left) and southern(right) hemisphere of Riemann sphere of $R_{rot,z}(\xi), B=4$	176
6.29	$R_{rot,z}(\xi), B=4$	176
6.30	Northern(left) and southern(right) hemisphere of Riemann sphere of $R_{iso,x}(\xi), B=4$	177
6.31	$R_{iso,x}(\xi), B=4$	177
6.32	Northern(left) and southern(right) hemisphere of Riemann sphere of $R_{iso,y}(\xi), B=4$	178
6.33	$R_{iso,y}(\xi), B=4$	178
6.34	Northern(left) and southern(right) hemisphere of Riemann sphere of $R_{iso,z}(\xi), B=4$	179
6.35	$R_{iso,z}(\xi), B=4$	179
A.1	Five regular polyhedra (or platonic solids).	211
A.2	Tetrahedron and the rotation axes.	211
A.3	Octahedron and the rotation axes.	212
A.4	T_h, T_d and O_h	215

List of Tables

2.1	Symmetry of Skyrmion for different baryon number B	27
2.2	The values for Baryon number B for integers s	33
4.1	Vibrational frequencies ω for $B=1$	47
4.2	Vibrational frequencies ω for $B=2$	48
4.3	Vibrational frequencies ω for $B=4$	49
4.4	Critical Mass for different B and potential parameter p	57
5.1	Fixed Points of Perturbed Rational Map in Baryon Number $B = 1$. .	93
5.2	Fixed Points of Perturbed Rational Map in Baryon Number $B = 2$. .	94
5.3	Conjugacy Classes of Perturbed Rational Maps of Baryon Number $B = 1$	98
5.4	Conjugacy Classes of Perturbed Rational Maps in Baryon Number $B = 2$	107
5.5	Description of the energy density of the perturbed rational maps, $B = 1$.	113
5.6	Description of the energy density of the perturbed rational maps, $B = 2$.	124
6.1	Descriptions of the zero modes and the broken zero modes of the perturbed rational maps, $B = 4$	180
6.2	Description of the energy density for the vibrational modes of the per- turbed rational maps, $B = 4$	181
7.1	Character table for $D_{\infty h}$	185
7.2	Comparison of vibrational frequency between the numerical results and the rational map ansatz, $B = 2$	192

7.3	Comparison of vibrational frequency between the numerical result and the rational map ansatz, $B = 4$	193
A.1	Notations for the elements of point groups	208
A.2	Combinatorial properties of the polyhedron.	210

Chapter 1

Introduction

Quantum Chromodynamics (QCD) is believed to be the fundamental theory of the strong interactions. By the energy scale, it can be basically divided into three regimes or phases:

1. High energy domain - distance of order of 0.1 fm or smaller. This domain is called **asymptotic freedom phase**, where the effective coupling constant g is small enough that one is allowed to use the perturbation theory in this region.
2. Intermediate energy domain - distance between 0.1 fm and 1 fm. This is a phase of quark-gluon plasma; the dynamical problems here are very difficult to solve.
3. Low energy domain - distance of order of 1 fm and larger. In this domain, QCD is a nonperturbative theory, and the quarks and gluons are confined within the hadrons without being seen. Since the only degree of freedom in this regime is the hadrons, this region is known as **the confinement phase**.

In the high energy domain of QCD, the asymptotic freedom can be well described in terms of the quark model; however, in the low energy domain (or long-wavelength approximation), QCD still lacks a quantitative understanding. Most of the low-energy models can only approximate QCD qualitatively.

The conventional model to QCD is the quark model. Besides the color, QCD involves different flavors, u , d , s , c , t , and b , among which the three light quarks



u , d , and s can be used to explain most of the low-energy phenomena in QCD. If the masses of three light quarks can be ignored, as they are small compared to the QCD cutoff Λ , the QCD Lagrangian is then invariant under $SU(2)_L \otimes SU(2)_R$ chiral symmetry, which can be spontaneously broken via the Nambu-Goldstone mechanism [39] [64] to obtain 3 massless pions.

Apart from the quark model, there is an alternative choice to understanding the QCD in the low-energy domain: the chiral field models, which are effective chiral descriptions of QCD. Among them, the nonlinear σ -model is one with interesting structure, whose generalization is the Skyrme model. Although in general the quantum range for chiral field models is confined to the low-energy domain due to the short and long-distance singularities that result in the nonrenormalizable character, the relative success of the chiral phenomenology encouraged people that it is worthwhile to study their quantum behavior.

Among these chiral fields models, the Skyrme model has some interesting features. The motivation of developing the Skyrme model, which was the “Mesonic Fluid” model at the time, is to study nucleons as being immersed into the “Mesonic Fluid”. Quote T. H. R. Skyrme’s words, “... it would be fun to see if I could get everything out of self-interacting boson field theory” [87].

The discovery of the violation of the parity symmetry in the weak interactions [53] motivated people to look for the enlargement of the isotopic internal symmetry group $SU(2)$ to include the parity-violating transformation into a new internal symmetry group of the strong interactions. One of the possibilities to construct this realization was studied by Pais [70] [71] but confronted one difficulty that it is impossible to have a linear representation of a symmetry group with more than six parameters in the 3-dimensional isotopic space.

There are two different directions to search for the possible solutions: one is to extend the isotopic space by introducing more components in the isotopic space; the other is to look for a nonlinear realization for this symmetry group. Skyrme chose the latter option and adopted the chiral symmetry to his “Mesonic Fluid” model, *i.e.* to realize the chiral symmetry nonlinearly: he added an auxiliary field ϕ_0 to the isotriplet of pion fields $\vec{\phi}$ and in order to prevent unphysical consequence he imposed

on the fields $\phi_\mu = (\phi_0, \vec{\phi})$ with $\mu=0, 1, 2, 3$, a constraint: $\phi_0^2 + \phi_i\phi^i = 1$, $i = 1, 2, 3$.

However, the Skyrme model did not attract much attention until 't Hooft [68] suggested to generalize the color number from 3 to N_c to simplify QCD in the large N_c limit, and indeed that for $N_c \rightarrow \infty$, QCD can be treated as an effective theory of meson fields using $1/N_c$ as an implicit expansion parameter. Later, Witten [93] argued that in the limit $N_c \rightarrow \infty$, the baryons masses are of the order N_c . With some development of the nonlinear field theory, for which it is possible to have some non-trivial field configurations (solitons), Witten's results suggest that one may think of the baryons as soliton solutions of the effective meson field theory without involving the quarks. Further attention was brought up by the work of G. S. Adkins et al. [2], who showed that the static properties of the baryons derived from the solitons of the Skyrme model is within about 30% of the experimental data. This comeback is from the belief there exists some models which is the long-wavelength limit of QCD, *e.g.* in [26] [4]. Furthermore, the basic Skyrme model can be modified to apply to several different directions, which are the inclusion of higher-order terms in the model [57] [58], the model with higher unitary groups [92], the model in the curved space [56], and the addition of the vector mesons [59] [61] [46]. A more fundamental modification that can be made to the theory is to incorporate the Wess-Zumino term.

The Skyrme model now is identified as the nonlinear field theory of pions described in terms of the $SU(2)$ -valued Skyrme field. It has several interesting features:

1. The space of the Skyrme field configurations consists of all the based maps $U : \mathbb{R}^3 \rightarrow \mathbb{S}^3$ with the finite energy boundary condition $U(|\vec{x}| \rightarrow \infty) \rightarrow 1$, which compactifies \mathbb{R}^3 to \mathbb{S}^3 . The configuration space then is divided into different connected components, each of which is labelled by the degree which is an element of the homotopy group $\pi_3(\mathbb{S}^3) \simeq \mathbb{Z}$ [41].
2. It has topological solitons that can be interpreted as baryons, whose baryon number B is identified as the winding number of the Skyrme field. Static minimal energy configurations for a given B are called Skyrmions.
3. With the help of the Finkelstein-Rubenstein constraints [35], it is possible

for the Skyrmion of the odd baryon number to be quantized as a fermion even though the Skyrme field is $SU(2)$ -valued scalar field modelling the strong interactions.

Although the Skyrme model has several attractive characteristics, it is hard to deal with because of its nonlinearity and therefore one must solve it numerically. But one needs an analytic method to study, at least approximately, the Skyrme model and this is where the rational map ansatz [42] comes in. Rational maps are holomorphic maps from $\mathbb{R}^2 \rightarrow \mathbb{S}^2$ whereas the Skyrme fields are the maps from $\mathbb{R}^3 \rightarrow \mathbb{S}^3$. However the rational map ansatz is a good approximation approach for studying the Skyrmion with massless pions since Skyrme configuration with zero pion mass have a fullerene-like appearance. The Skyrmion in terms of the rational map ansatz is of the form, $U = \exp(-if(r) \hat{n}_R \cdot \vec{\sigma})$, where $f(r)$ is a radial profile function, \hat{n}_R is a directional unit vector associated with the rational map, and $\vec{\sigma}$ is the triplet of the Pauli matrices.

When inserting the ansatz-generated Skyrme field configuration into the Hamiltonian, the minimization of this energy functional will lead to a simple expression consisting of two parts: one is for the radial profile function to be calculated, and the other is for the angular part to be obtained. Since the Skyrme model is a nonlinear model of pions whose topological solitons are identified with the nucleons, it is necessary to consider the mass of pions to have a realistic model. When the pion mass is taken into consideration, *i.e.* the pion mass term is added into the Lagrangian, only the radial profile function is affected; the angular behavior remains the same as taking zero pion mass. The effect of the pion mass on the radial profile function is to have a more rapid fall-off. It is necessary to emphasize that the Skyrmions with massless pions have a shell-like structure [12] [13] but those with massive pions can have very different structures [15]. The rational map ansatz is a good approximation to the massless Skyrmions and to massive Skyrmions with a low baryon number.

The symmetry group of the Skyrme model Lagrangian is the direct product of the Poincaré group and $SU(2)_L \otimes SU(2)_R$ chiral symmetry group. However, the symmetry group of the model is different from that of the solutions of the equation of motion of the model. After considering the finite energy constraint

and the requirement that the invariant Skyrme field must be in the non-trivial homotopy class, meaning that the change of the field under the spatial rotation must be counteracted by its associated iso-rotation, the symmetry group that admits the non-trivial invariant fields is $G = \text{diag}[SO(3)_S \otimes SO(3)_I]$. In other words, group G is the symmetry group of the Skyrmions. The other nice feature of the rational map ansatz is that the symmetry of the known minimal energy Skyrme field configuration can be clearly realized by the corresponding symmetric rational map.

The mass term in the Skyrme model did not have too much attention since it was thought that, for the low baryon number, the effect of including the pion mass is to change the asymptotic behavior of the Skyrmion from algebraically to exponentially localized. From Battye et al. [12] [13], for massless pions, all the known Skyrmions have same feature in their structure, namely the shell-like structure. There are some good approximate approaches for studying Skyrmions with massless pions. One of them is the instanton method [6], which utilizes instantons solutions [27] of $SU(2)$ Yang-Mills theory in Euclidean space \mathbb{R}^4 , and the approximation of Skyrmion with massless pions via this method can be realized by computing the holonomy of the instantons. Through some examples [7] [54] [85] [88], the instanton method seems to be capable of approximating all the minimal energy Skyrmions by computing the holonomy of a proper instanton. However, Battye et al. [15] has shown that the inclusion of the massive pions to the Skyrme model can cause effects beyond the expectation. For massive pions, some of the Skyrmion configurations are not the bound states any more. The Skyrmions with massless pions which are generated via the instanton method have the correct asymptotic behavior, namely the algebraic decay. But the instanton method can not be applied to approximate the Skyrmions with the massive pions since it requires the exponential decay to have the energy finite, instead of the algebraic decay. The instanton method can be generalized to produce the exponential decay for the massive pions case, which is shown in [8].

Another good approach for the study of Skyrmions with massless pions is the rational map ansatz, which will be taken in this thesis for the massive pions case. In this thesis, we are interested in studying the vibrational modes of Skyrmions using the rational map ansatz for a family of mass terms. The Skyrmions are candidates

to describe real nuclei; however, the classical Skyrme solutions, obtained from the numerical work, for the standard mass parameter, have a shell-like configuration, unlike real nuclei. A further numerical study from Battye et al. [15], which is not captured by the rational map ansatz, shows that there are some important qualitative changes when the pion mass is taken to larger values than the standard one. Battye et al. pointed out that the features of the multi-Skyrmions which are obtained from the Lagrangian with these larger values of the pion mass appear to be similar to real nuclei. But the form of the mass term in the Skyrme model is not unique; there is actually a family of mass terms [49], some of which seems to have non-shell-like solutions for smaller values of the mass parameters.

To perturb the Skyrme field, we will perturb the radial profile function and every parameter of the rational map of a given degree, around the minimum energy configurations. Inserting the perturbed field into the Lagrangian, collecting the terms of different order of perturbation, and applying the variational principle, we will have the Euler-Lagrange equation of the perturbed Skyrme field. Since there are no cross terms for the perturbed profile function and the perturbed rational map, we have two independent sets of the Euler-Lagrange equation of motion. Solving these two equations of motion, we can get the vibrational modes of the Skyrme using the rational map ansatz. Afterwards, comparisons of our results to the numerical results from Barnes et al. [10] [11] and the analytical analysis of the group theory from Houghton et al. [42] will be done.

All the work done in this thesis is to try to help the understanding more of the quantization of the Skyrme model, which is necessary for the comparison of the predictions of the model with the experimental results from the nuclear physics. Since the Skyrme model is non-renormalizable, only semi-classical quantization can be done. Before the quantization, the degrees of freedom of the configuration space are reduced from infinite to finite, consisting of the classical field configurations only in connection with the low energy dynamics. That how many degrees of freedom do people have to include is the problem. It is obvious that the more degrees of freedom are included, the more accurate properties of the system can be described but then more difficult to be analyzed. Besides, the aspect of the problem of the

quantization are considered in [3]. Also, the problem of the stability about the quantization of radial oscillations is discussed in [80] [82]. In addition, some other quantization methods which are performed on the Skyrme model include cutoff quantization [9], the general covariant Hamiltonian approach for the quantization [32] [30] [31], Kerman-Klein quantization approach [25] and the quantization method in the framework of collective-coordinate for $SU(2)$ case [36].

The translational and rotational zero modes of the $B = 1$ Skyrmion with zero and nonzero pion mass, respectively, were quantized in [2] [1]. The quantization of the Skyrmions of the baryon number $B = 2$ is performed in [21] [48] [90], and in [55] the massive modes are considered to improve the approximation. The Skyrmion of the $B = 3$ was quantized in [24] and in [91] is for the $B = 4$ Skyrmion quantization. More recently, a zero mode quantization of $SU(2)$ Skyrmions for baryon number $B = 4$ to $B = 9$ and $B = 17$ is done in [43] using the rational map ansatz. Some of the quantization of the Skyrmions using the rational map ansatz are described in [50] [51]. Although there are still some problems for quantizing the Skyrmions, we hope that the work done in this thesis can do some help.

Here is the brief review of every chapter in this thesis. Chapter 1 is the introduction to the relation between Skyrme model and QCD, and the motivation of this thesis. In chapter 2, some of the technical details of the Skyrme model are introduced to give the background knowledge. We also talk about the symmetry of the Skyrme model and that of the solutions of the Skyrme equation, which is the Euler-Lagrange equation obtained from least action principle. The motivation and the benefit of using rational map ansatz are also explained. Then the Lagrangian and Hamiltonian are rewritten in terms of the rational map ansatz. Chapter 3 is to give the idea and the derivation of the vibration of the Skyrme field using the rational map ansatz to have two separate equations of motion of the perturbed radial profile function and the perturbed rational maps. In chapter 4, we solve the equation of motion of the perturbed radial profile function to obtain its eigenvalues. Furthermore, the critical mass of the pion is determined under the rational map ansatz. In chapter 5, the equation of motion of the perturbed rational map for baryon number $B = 1$ and $B = 2$ is solved to give their eigenvalues and eigen-modes. These eigen-modes are

then sorted into different conjugacy classes by taking use of the symmetry of the solutions of the Skyrmons. Afterwards, the plots of the perturbed rational maps and the energy density associated to these eigen-modes are shown. In chapter 6, we repeat the procedure in chapter 5 to find out the eigenvalues, eigen-modes, and plots of perturbed rational maps and energy density of them, for the $B = 4$ case. In chapter 7, the comparisons between our results, which are obtained by using the rational map ansatz, with the numerical results from Barnes et al. [10] [11] and with the analytical results from Houghton et al. [42], are done.

Chapter 2

Skyrme Model

2.1 The Model

The Skyrme Model [86], which is a classical field theory modelling the strong interaction between atomic nuclei, is modified to take the mass of pion into account by the following Lagrangian

$$L_p = \int_{R^3} \left\{ \frac{F_\pi^2}{16} \text{Tr}(\partial_\mu U \partial^\mu U^\dagger) + \frac{1}{32e^2} \text{Tr}([\partial_\mu U U^\dagger, \partial_\nu U U^\dagger]^2) + \frac{F_\pi^2 m_\pi^2}{8p^2} \text{Tr}(U^p - \mathbf{1}) \right\} d^3x, \quad (2.1)$$

where $U = U(\vec{x}, t)$ is an $SU(2)$ chiral field and $p \in \mathbb{Z}^+$; $\mathbf{1}$ is the 2×2 unit matrix; $\partial_\mu \equiv \frac{\partial}{\partial x^\mu} = (\frac{\partial}{\partial t}, \vec{\nabla})$ and $\partial^\mu \equiv \frac{\partial}{\partial x_\mu} = (\frac{\partial}{\partial t}, -\vec{\nabla})$; F_π and e are free parameters of the model, whose values are fixed by comparison with experimental data.

It is convenient to describe the model in dimensionless units by performing the scaling and redefining mass m

$$\begin{aligned} x &\rightarrow \left(\frac{2}{F_\pi e}\right) x, \\ m &\equiv \left(\frac{2}{F_\pi e}\right) m_\pi, \end{aligned}$$

then the Lagrangian L_p is replaced by L in the following way

$$\begin{aligned}
L &= \frac{e}{3\pi^2 F_\pi} L_p \\
&= \frac{1}{12\pi^2} \int \left\{ \frac{1}{2} \text{Tr}(\partial_\mu U \partial^\mu U^\dagger) + \frac{1}{16} \text{Tr}([\partial_\mu U]U^\dagger, (\partial_\nu U)U^\dagger)^2 \right. \\
&\quad \left. + \frac{m^2}{p^2} \text{Tr}(U^p - \mathbf{1}) \right\} d^3x \\
&= \frac{1}{12\pi^2} \int \left\{ -\frac{1}{2} \text{Tr}(R_\mu R^\mu) + \frac{1}{16} \text{Tr}([R_\mu, R_\nu][R^\mu, R^\nu]) + \frac{m^2}{p^2} \text{Tr}(U^p - \mathbf{1}) \right\} d^3x,
\end{aligned} \tag{2.2}$$

where we have introduced the $su(2)$ -valued current $R_\mu = (\partial_\mu U)U^\dagger$.

The Skyrme energy functional derived from Lagrangian (2.2) is

$$H = \frac{1}{12\pi^2} \int \left\{ -\frac{1}{2} \text{Tr}(R_i R^i) - \frac{1}{16} \text{Tr}([R_i, R_j][R^i, R^j]) - \frac{m^2}{p^2} \text{Tr}(U^p - \mathbf{1}) \right\} d^3x. \tag{2.3}$$

The $SU(2)$ chiral field can be parameterized as

$$U = \phi_0 \mathbf{1} + i \sigma_i \phi_i, \tag{2.4}$$

by the quaternion representation of mesonic scalar fields $\phi_\alpha = (\phi_0, \phi_i) = (\phi_0, \vec{\phi})$ with $\alpha = 0, 1, 2, 3$; $i = 1, 2, 3$, and Pauli matrices $\vec{\sigma} = (\sigma_1, \sigma_2, \sigma_3)$. The chiral field U has the boundary condition

$$U(\vec{x}, t) \rightarrow \mathbf{1}_{2 \times 2}, \text{ as } |\vec{x}| \rightarrow \infty, \tag{2.5}$$

and the constraint

$$U U^\dagger = \phi_0^2 + \phi_i^2 = \phi_\alpha^2 = 1, \quad \alpha = 0, 1, 2, 3; \quad i = 1, 2, 3. \tag{2.6}$$

Since we have the quaternion representation of $U(\vec{x}, t)$, we would like to write the Lagrangian, (2.2), in terms of the mesonic fields, ϕ_α . Meanwhile, the quaternion representation of $U(\vec{x}, t)$ involve the Pauli matrices, and therefore here we list some useful formulae and identities of Pauli matrices for the latter computation. One has to note that the repeated index summation rule is applied.

□ Properties of Pauli Matrices

$$\sigma_i \sigma_j = i \varepsilon_{ijk} \sigma_k + \delta_{ij} ,$$

$$\text{Tr}(\sigma_i) = 0 ,$$

$$(\vec{\sigma} \cdot \vec{A})(\vec{\sigma} \cdot \vec{B}) = (\vec{A} \cdot \vec{B}) + i(\vec{A} \times \vec{B}) \cdot \vec{\sigma} .$$

□ Identities

$$(\sigma_i \phi_i)^{2n} = (\phi_i)^{2n} ,$$

$$(\sigma_i \phi_i)^{2n+1} = (\phi_i)^{2n} (\sigma_j \phi_j) .$$

These identities are easily proven using the above properties of the Pauli matrices. In the above formulae, i , j and k can be 1, 2 or 3 respectively. ε_{ijk} is the Levi-Civita symbol with the definition $\varepsilon_{ijk} = 1$ if (ijk) is an even permutation of (123), $\varepsilon_{ijk} = -1$ if (ijk) is an odd permutation of (123), and $\varepsilon_{ijk} = 0$ otherwise. δ_{ij} is the Kronecker delta with $\delta_{ij}=1$ if $i = j$; $\delta_{ij} = 0$ if $i \neq j$. \vec{A} and \vec{B} are arbitrary vectors.

Let us briefly demonstrate the process of the calculation of the first term $\frac{1}{2} \text{Tr}(\partial_\mu U \partial^\mu U^\dagger)$ in (2.2):

$$U = \phi_0 \mathbf{1} + i \sigma_i \phi_i ,$$

$$\partial_\mu U = (\partial_\mu \phi_0) \mathbf{1} + i (\partial_\mu \phi_i) \sigma_i ,$$

$$\frac{1}{2} \text{Tr}(\partial_\mu U \partial^\mu U^\dagger) = (\partial_\mu \phi_0 \partial^\mu \phi_0) + (\partial_\mu \phi_i \partial^\mu \phi_i) .$$

In the last step, we use the properties $\text{Tr}(\sigma_i) = 0$ and $\text{Tr}(\mathbf{1}) = 2$.

Using the similar idea and after some work, we have three terms in (2.2) as

$$\frac{1}{2} \text{Tr}(\partial_\mu U \partial^\mu U^\dagger) = (\partial_\mu \phi_\alpha)^2 , \quad (2.7)$$

$$\frac{1}{16} \text{Tr}([(\partial_\mu U) U^\dagger, (\partial_\nu U) U^\dagger]^2) = \frac{1}{2} [(\partial_\mu \phi_\alpha \partial_\nu \phi_\alpha)^2 - (\partial_\mu \phi_\alpha)^4] , \quad (2.8)$$

$$\frac{m^2}{p^2} \text{Tr}(U^p - \mathbf{1}) = m^2 V_p(\phi_0) , \quad (2.9)$$

where, by convenience, we define

$$\begin{aligned} V_p(\phi_0) &\equiv \frac{1}{p^2} \text{Tr}(U^p - \mathbf{1}) \\ &= \frac{2}{p^2} \left\{ \left[\sum_{k=0}^{\lfloor \frac{p}{2} \rfloor} (-1)^k \binom{p}{2k} \phi_0^{p-2k} (1 - \phi_0^2)^k \right] - 1 \right\}, \end{aligned} \quad (2.10)$$

with $\binom{p}{2k} = \frac{p(p-1)\cdots(p-2k+1)}{(2k)!}$ and $\lfloor \frac{p}{2} \rfloor = n \in \mathbb{Z}^+$ if $p = 2n + 1$. Since the parameter $p = 0$ results in a singular potential, we will not use this parameter in this thesis.

From (2.10), we list the first 4 terms of V_p series

$$\begin{aligned} V_1(\phi_0) &= 2(\phi_0 - 1), \\ V_2(\phi_0) &= (\phi_0^2 - 1), \\ V_3(\phi_0) &= \frac{2}{9}(4\phi_0^3 - 3\phi_0 - 1), \\ V_4(\phi_0) &= (\phi_0^4 - \phi_0^2). \end{aligned}$$

Hence, combining the three terms (2.7), (2.8) and (2.9) obtained above, we have the following expression of (2.2) in terms of ϕ_α

$$L = \int_{R^3} \left\{ (\partial_\mu \phi_\alpha)^2 + \frac{1}{2} \left[(\partial_\mu \phi_\alpha \partial_\nu \phi_\alpha)^2 - (\partial_\mu \phi_\alpha)^4 \right] + m^2 V_p(\phi_0) \right\} d^3x. \quad (2.11)$$

The equation of motion for the Lagrangian (2.11) is derived as

$$\begin{aligned} &\partial_\mu \partial^\mu \phi_\alpha - (\partial_\mu \partial^\mu \phi_\eta) \phi_\eta \phi_\alpha + (\partial_\mu \partial^\mu \phi_\beta) (\partial_\nu \phi_\alpha \partial^\nu \phi_\beta) - (\partial_\mu \partial^\mu \phi_\alpha) (\partial_\nu \phi_\beta \partial^\nu \phi_\beta) \\ &+ (\partial_\mu \partial^\mu \phi_\eta) (\partial_\nu \phi_\beta \partial^\nu \phi_\beta) \phi_\eta \phi_\alpha - (\partial_\mu \partial^\nu \phi_\beta) (\partial^\mu \phi_\beta \partial_\nu \phi_\alpha) + (\partial_\mu \partial^\nu \phi_\alpha) (\partial^\mu \phi_\beta \partial_\nu \phi_\beta) \\ &- (\partial_\mu \partial^\nu \phi_\eta) (\partial^\mu \phi_\beta \partial_\nu \phi_\beta) \phi_\eta \phi_\alpha + \frac{m^2}{2} \frac{\partial V_p(\phi_0)}{\partial \phi_0} \phi_0 \phi_\alpha - \frac{m^2}{2} \frac{\partial V_p(\phi_0)}{\partial \phi_0} \delta_{\alpha 0} = 0, \end{aligned} \quad (2.12)$$

where

$$\begin{aligned} \frac{\partial V_p(\phi_0)}{\partial \phi_0} &= \frac{2}{p^2} \left\{ \sum_{k=0}^{\lfloor \frac{p}{2} \rfloor} (-1)^k \binom{p}{2k} \right. \\ &\quad \left. \left[(p - 2k) \phi_0^{p-2k-1} (1 - \phi_0^2)^k - 2k \phi_0^{p-2k+1} (1 - \phi_0^2)^{k-1} \right] \right\}. \end{aligned}$$

The first four terms for the $\frac{\partial V_p(\phi_0)}{\partial \phi_0}$ are as follows

$$\begin{aligned}\frac{\partial V_1(\phi_0)}{\partial \phi_0} &= 2, \\ \frac{\partial V_2(\phi_0)}{\partial \phi_0} &= 2\phi_0, \\ \frac{\partial V_3(\phi_0)}{\partial \phi_0} &= \frac{2}{3}(4\phi_0^2 - 1), \\ \frac{\partial V_4(\phi_0)}{\partial \phi_0} &= 4\phi_0^3 - 2\phi_0.\end{aligned}$$

Beside using the quaternion representation of the mesonic field ϕ_α to express chiral field U , there is another way to do it by utilizing a hermitian projector. We use the following ansatz to present an $SU(2)$ chiral field U :

$$U = e^{if(2\mathbf{P}-1)}, \quad (2.13)$$

where f is a real function, $\mathbf{1}$ is the 2×2 unit matrix, and \mathbf{P} is a 2×2 hermitian projector, which, by definition, satisfies the property $\mathbf{P} = \mathbf{P}^\dagger = \mathbf{P}^2$. As

$$\mathbf{P}^n = \mathbf{P}, \quad \forall n \in \mathbb{Z}^+,$$

$e^{2if\mathbf{P}}$ can be expanded in Taylor series as

$$\begin{aligned}e^{2if\mathbf{P}} &= \sum_{n=0}^{\infty} \frac{(2if)^n}{n!} \mathbf{P}^n = 1 + \sum_{n=1}^{\infty} \frac{(2if)^n}{n!} \mathbf{P}^n \\ &= (\mathbf{1} - \mathbf{P}) + \mathbf{P} e^{2if}.\end{aligned}$$

Therefore, we are able to rewrite U as

$$U = e^{2if\mathbf{P}} e^{-if} = (\mathbf{1} - \mathbf{P}) e^{-if} + \mathbf{P} e^{if}. \quad (2.14)$$

2.2 Rational Map and Rational Map Ansatz

The Skyrmions, *i.e.* static Skyrme field configurations minimizing the Hamiltonian for a given baryon number B , can only be obtained numerically by varying the

Hamiltonian (2.3). Studying the properties of the Skyrme model with these numerical solutions is hard. However, there is an ansatz called the rational map ansatz [42] that can be used as a good approximation to the shell-like Skyrmions.

A rational map of degree \mathcal{N} is a holomorphic function from $\mathbb{S}^2 \mapsto \mathbb{S}^2$. Regarding the domain space \mathbb{S}^2 as a Riemann space with coordinate ξ , the rational map is defined as

$$R(\xi) = \frac{P(\xi)}{Q(\xi)},$$

where $P(\xi)$ and $Q(\xi)$ are the polynomials with the properties:

1. The maximal polynomial degree of $P(\xi)$ or $Q(\xi)$ must be \mathcal{N} .
2. $P(\xi)$ and $Q(\xi)$ do not have the common factors.

The Skyrmions are maps from $\mathbb{R}^3 \rightarrow \mathbb{S}^3$, whereas the rational maps are the maps from $\mathbb{S}^2 \rightarrow \mathbb{S}^2$. The main idea of adapting the rational map to the Skyrmions is to identify the domain \mathbb{R}^3 as the product of the angular part, (θ, ϕ) , which is recognized as \mathbb{S}^2 and radial part, and to identify the target \mathbb{S}^2 , which is mapped from the domain \mathbb{S}^2 by the rational map, with spheres of latitude on \mathbb{S}^3 .

To present the rational map ansatz, recall that we can identify the angular coordinates (θ, ϕ) on the unit sphere \mathbb{S}^2 with the complex coordinate ξ via stereographic projection by $\xi = (\tan \frac{\theta}{2}) e^{i\phi}$. Hence a point ξ on the complex plane corresponds to a unit vector \hat{n}_ξ on the unit sphere \mathbb{S}^2

$$\hat{n}_\xi = \frac{1}{1 + |\xi|^2} \left(2\Re(\xi), 2\Im(\xi), 1 - |\xi|^2 \right).$$

Under the rational map, the point ξ on the complex plane is mapped to another point $R(\xi)$ on the complex plane which can be associated with the unit vector on \mathbb{S}^2

$$\hat{n}_{R(\xi)} = \frac{1}{1 + |R(\xi)|^2} \left(2\Re(R(\xi)), 2\Im(R(\xi)), 1 - |R(\xi)|^2 \right).$$

Denoting the coordinate of a point in \mathbb{R}^3 by (r, ξ) , the rational map ansatz assumes that the Skyrmion has the following form

$$U = e^{2if(r)\hat{n}_{R(\xi)} \cdot \vec{\sigma}}, \quad (2.15)$$

where $\vec{\sigma} = (\sigma_1, \sigma_2, \sigma_3)$ represents the triplet of Pauli matrices, $R(\xi)$ is the rational map and $f(r)$ is a radial profile function, which satisfies the boundary conditions: $f(r = 0) = \pi$ and $f(r = \infty) = 0$. The constraint on the profile function as r approaches infinity comes from the requirement $U = 1$ as $r \rightarrow \infty$.

The rational map ansatz has several attractive features:

1. It gives the Hamiltonian a simple expression. By minimizing the Hamiltonian with respect to the rational map and the profile function, it leads to the energies that are close to those of some known Skyrmion configurations, which are shell-like structures in the massless case.
2. It provides not only a good approximation to the Skyrmion configuration but also particularly to the symmetries of the configurations.
3. The topology of the function space of the rational maps is also a good approximation to that of the configuration space of the Skyrme model. [50]

Here we rewrite the Lagrangian (2.2) and Hamiltonian (2.3) in terms of the rational map ansatz; however, we found that it would be easier for the calculation to take advantage of the properties of the hermitian projector \mathbf{P} than to deal with (2.15) directly. By this ansatz, the function $f(r)$ in (2.13) depends only on the radial coordinate r and the projector \mathbf{P} depends only on the angular coordinates, *i.e.* $\mathbf{P}(\theta, \phi)$. Through the stereographic projection and changing the variables from (θ, ϕ) to $(\xi, \bar{\xi})$, the projector $\mathbf{P}(\xi, \bar{\xi})$ takes the following form

$$\mathbf{P} = \frac{v \otimes v^\dagger}{|v|^2} = \frac{1}{1 + |R|^2} \begin{pmatrix} 1 & R^* \\ R & |R|^2 \end{pmatrix}, \quad (2.16)$$

where

$$v = \begin{pmatrix} 1 \\ R \end{pmatrix}; \quad R = R(\xi) = \frac{v_1(\xi)}{v_2(\xi)},$$

$$|v|^2 = v^\dagger v = 1 + |R|^2.$$

Before doing the integration over the angular coordinates to have the one-dimensional energy functional for $f(r)$, we present some useful properties of \mathbf{P} for

the future calculations.

$$\left. \begin{aligned} \mathbf{P}(\partial\mathbf{P}) &= 0, & (\partial\mathbf{P})\mathbf{P} &= \partial\mathbf{P} \\ (\bar{\partial}\mathbf{P})\mathbf{P} &= 0, & \mathbf{P}(\bar{\partial}\mathbf{P}) &= \bar{\partial}\mathbf{P} \\ (\partial\mathbf{P})(\partial\mathbf{P}) &= 0, & (\bar{\partial}\mathbf{P})(\bar{\partial}\mathbf{P}) &= 0 \\ Tr(\partial\mathbf{P}) &= 0, & Tr(\bar{\partial}\mathbf{P}) &= 0 \\ Tr(\dot{\mathbf{P}}) &= 0, & Tr(\mathbf{P}\dot{\mathbf{P}}) &= 0 \end{aligned} \right\}, \quad (2.17)$$

where $\partial \equiv \frac{\partial}{\partial\xi}$, $\bar{\partial} \equiv \frac{\partial}{\partial\bar{\xi}}$, and $\dot{\mathbf{P}} \equiv \frac{\partial\mathbf{P}}{\partial t}$. Here we show how to derive some of the above formulae.

□ **Proof of $\mathbf{P}(\partial\mathbf{P}) = 0$**

$$\begin{aligned} \mathbf{P}(\partial\mathbf{P}) &= \frac{vv^\dagger}{|v|^2} \partial\left(\frac{vv^\dagger}{|v|^2}\right) \\ &= \frac{vv^\dagger}{|v|^2} \left[\frac{v_\xi v^\dagger}{|v|^2} - \frac{vv^\dagger}{|v|^4} (v^\dagger v + v^\dagger v_\xi) \right] \\ &= \frac{vv^\dagger}{|v|^2} \frac{v_\xi v^\dagger}{|v|^2} - \frac{vv^\dagger}{|v|^2} \frac{vv^\dagger}{|v|^4} (v^\dagger v_\xi) \\ &= \frac{vv^\dagger}{|v|^4} (v^\dagger v_\xi) - \frac{vv^\dagger}{|v|^4} (v^\dagger v_\xi) \\ &= 0, \end{aligned}$$

where $v_\xi \equiv \frac{\partial v}{\partial\xi}$.

□ **Proof of $(\partial\mathbf{P})\mathbf{P} = (\partial\mathbf{P})$**

$$\begin{aligned} (\partial\mathbf{P})\mathbf{P} &= \left[\partial\left(\frac{vv^\dagger}{|v|^2}\right) \right] \frac{vv^\dagger}{|v|^2} \\ &= \left[\frac{v_\xi v^\dagger}{|v|^2} - \frac{vv^\dagger}{|v|^4} (v^\dagger v_\xi) \right] \frac{vv^\dagger}{|v|^2} \\ &= \frac{v_\xi v^\dagger}{|v|^2} - \frac{vv^\dagger}{|v|^4} (v^\dagger v_\xi) \\ &= (\partial\mathbf{P}). \end{aligned}$$

□ **Proof of $(\partial\mathbf{P})(\partial\mathbf{P}) = 0$**

$$\begin{aligned}
(\partial\mathbf{P})(\partial\mathbf{P}) &= \left[\partial \left(\frac{vv^\dagger}{|v|^2} \right) \right] \left[\partial \left(\frac{vv^\dagger}{|v|^2} \right) \right] \\
&= \left[\frac{v_\xi v^\dagger}{|v|^2} - \frac{vv^\dagger}{|v|^4} (v^\dagger v_\xi) \right] \left[\frac{v_\xi v^\dagger}{|v|^2} - \frac{vv^\dagger}{|v|^4} (v^\dagger v_\xi) \right] \\
&= \frac{v_\xi v^\dagger}{|v|^2} \frac{v_\xi v^\dagger}{|v|^2} - \frac{vv^\dagger}{|v|^4} (v^\dagger v_\xi) \frac{v_\xi v^\dagger}{|v|^2} - \frac{v_\xi v^\dagger}{|v|^2} \frac{vv^\dagger}{|v|^4} (v^\dagger v_\xi) + \frac{vv^\dagger}{|v|^4} (v^\dagger v_\xi) \frac{vv^\dagger}{|v|^4} (v^\dagger v_\xi) \\
&= \frac{v_\xi v^\dagger}{|v|^4} (v^\dagger v_\xi) - \frac{vv^\dagger}{|v|^6} (v^\dagger v_\xi)^2 - \frac{v_\xi v^\dagger}{|v|^4} (v^\dagger v_\xi) + \frac{vv^\dagger}{|v|^6} (v^\dagger v_\xi)^2 \\
&= 0.
\end{aligned}$$

□ **Proof of $Tr(\partial\mathbf{P}) = 0$**

$$\begin{aligned}
v &= \begin{pmatrix} 1 \\ R \end{pmatrix}; \quad v^\dagger = \begin{pmatrix} 1 & R^* \end{pmatrix} \\
vv^\dagger &= \begin{pmatrix} 1 & R^* \\ R & |R|^2 \end{pmatrix}; \quad Tr(vv^\dagger) = 1 + |R|^2 = |v|^2 \\
v_\xi v^\dagger &= \begin{pmatrix} 0 & 0 \\ \partial R & R^*(\partial R) \end{pmatrix}; \quad Tr(v_\xi v^\dagger) = R^*(\partial R) \\
v^\dagger v_\xi &= R^*(\partial R) \\
(\partial\mathbf{P}) &= \frac{v_\xi v^\dagger}{|v|^2} - \frac{vv^\dagger}{|v|^4} (v^\dagger v_\xi) \\
Tr(\partial\mathbf{P}) &= Tr \left(\frac{v_\xi v^\dagger}{|v|^2} \right) - Tr \left(\frac{vv^\dagger}{|v|^4} (v^\dagger v_\xi) \right) \\
&= \frac{1}{|v|^2} [R^*(\partial R)] - \frac{1}{|v|^4} (1 + |R|^2) [R^*(\partial R)] \\
&= 0.
\end{aligned}$$

Consider the most general situation that the Skyrme field U is time-dependent. It is assumed that both the projector \mathbf{P} (or rational map R) and the profile function f have time dependence. The three terms in (2.2) are obtained respectively as

$$\begin{aligned}
& Tr\left(\frac{1}{2}\partial_\mu U\partial^\mu U^\dagger\right) \\
&= \left\{2(\sin^2 f)Tr[(\dot{\mathbf{P}})^2] + 2\dot{f}(\sin 2f)Tr(\mathbf{P}\dot{\mathbf{P}}) + \dot{f}^2\right\} \\
&\quad - \left\{\frac{2(\sin^2 f)(1+|\xi|^2)^2}{r^2}Tr[(\partial\mathbf{P})(\bar{\partial}\mathbf{P})] + f'^2\right\} \\
&= \left\{\frac{4(\sin^2 f)|\dot{R}|^2}{(1+|R|^2)^2} + \dot{f}^2\right\} - \left\{\frac{2\sin^2 f}{r^2(1+|R|^2)^2}(1+|\xi|^2)^2\left|\frac{dR}{d\xi}\right|^2 + f'^2\right\}, \quad (2.18)
\end{aligned}$$

$$\begin{aligned}
& \frac{1}{16}Tr\left([\partial_\mu U U^\dagger, \partial_\nu U U^\dagger]^2\right) \\
&= \left\{\frac{2f'^2(1-\cos 2f)|\dot{R}|^2}{(1+|R|^2)^2} + \frac{(1-\cos 2f)^2(1+|\xi|^2)^2}{r^2(1+|R|^2)^4}\left|\frac{dR}{d\xi}\right|^2|\dot{R}|^2\right. \\
&\quad \left. + \frac{\dot{f}^2(1-\cos 2f)(1+|\xi|^2)^2}{r^2(1+|R|^2)^2}\left|\frac{dR}{d\xi}\right|^2\right\} - \left\{\frac{2f'^2(\sin^2 f)(1+|\xi|^2)^2}{r^2(1+|R|^2)^2}\left|\frac{dR}{d\xi}\right|^2\right. \\
&\quad \left. + \frac{(\sin^4 f)(1+|\xi|^2)^4}{r^4(1+|R|^2)^4}\left|\frac{dR}{d\xi}\right|^4\right\}, \quad (2.19)
\end{aligned}$$

$$Tr(U^p - \mathbf{1}) = 2[\cos(pf) - 1], \quad (2.20)$$

where $f' \equiv \frac{\partial f}{\partial r}$, $\dot{f} \equiv \frac{\partial f}{\partial t}$, and $\dot{R} \equiv \frac{\partial R}{\partial t}$.

Putting the above three terms back into (2.2) will allow us to have the Lagrangian in terms of the rational maps R and the profile function f . We then can simplify the Lagrangian to be the functional of the profile function $f(r)$ only, by integrating the rational maps R with respect to the complex variables $(\xi, \bar{\xi})$. Before doing the integration, we have to rewrite the volume element d^3x in terms of ξ and $\bar{\xi}$. Since, while making use of the rational maps ansatz, we have already changed from Cartesian coordinates to the polar coordinates and the stereographic projection has been done to transform the angular coordinates (θ, ϕ) to the set of complex variables $(\xi, \bar{\xi})$, it is necessary to do the corresponding change to the volume element d^3x ,

$$d^3x = |J| dr d\xi d\bar{\xi} = \frac{2ir^2}{(1+|\xi|^2)^2} dr d\xi d\bar{\xi},$$

where $|J|$ is the Jacobian of this coordinate transformation, defined as

$$|J| = \left|\frac{\partial(x, y, z)}{\partial(r, \xi, \bar{\xi})}\right| = \left|\frac{\partial(x, y, z)}{\partial(r, \theta, \phi)} \frac{\partial(r, \theta, \phi)}{\partial(r, \xi, \bar{\xi})}\right|.$$

By combining (2.18), (2.19) and (2.20), putting them back to (2.2), and doing the integration with respect to variables $(\xi, \bar{\xi})$, the Lagrangian then becomes

$$L = \frac{1}{3\pi} \int \left\{ \left[4r^2 \mathcal{X}(1 + f'^2) \sin^2 f + 4\mathcal{Y} \sin^4 f + 2f'^2 B \sin^2 f + r^2 f'^2 \right] - \left\{ r^2 f'^2 + 2B(1 + f'^2) \sin^2 f + \mathcal{I} \frac{\sin^4 f}{r^2} + \frac{2m^2 r^2}{p^2} [1 - \cos(pf)] \right\} \right\} dr, \quad (2.21)$$

where

$$B \equiv \frac{1}{4\pi} \int \left(\frac{1 + |\xi|^2}{1 + |R|^2} \left| \frac{dR}{d\xi} \right| \right)^2 \frac{2i d\xi d\bar{\xi}}{(1 + |\xi|^2)^2}, \quad (2.22)$$

$$\mathcal{I} \equiv \frac{1}{4\pi} \int \left(\frac{1 + |\xi|^2}{1 + |R|^2} \left| \frac{dR}{d\xi} \right| \right)^4 \frac{2i d\xi d\bar{\xi}}{(1 + |\xi|^2)^2}, \quad (2.23)$$

$$\mathcal{X} \equiv \frac{1}{4\pi} \int \frac{|\dot{R}|^2}{(1 + |R|^2)^2} \frac{2i d\xi d\bar{\xi}}{(1 + |\xi|^2)^2}, \quad (2.24)$$

$$\mathcal{Y} \equiv \frac{1}{4\pi} \int \frac{(1 + |\xi|^2)^2}{(1 + |R|^2)^4} \left| \frac{dR}{d\xi} \right|^2 |\dot{R}|^2 \frac{2i d\xi d\bar{\xi}}{(1 + |\xi|^2)^2}. \quad (2.25)$$

Then the Skyrme energy functional derived from the Lagrangian (2.21) is

$$H = \frac{1}{3\pi} \int \left\{ r^2 f'^2 + 2(1 + f'^2)(2r^2 \mathcal{X} + B) \sin^2 f + \frac{\sin^4 f}{r^2} (4r^2 \mathcal{Y} + \mathcal{I}) + f'^2 (r^2 + 2B \sin^2 f) + \frac{2m^2 r^2}{p^2} [1 - \cos(pf)] \right\} dr. \quad (2.26)$$

For convenience, we rewrite the Lagrangian (2.21) as follows

$$L = \frac{1}{3\pi} \int \left\{ \left[(4r^2 \mathcal{X} - 2B) \sin^2 f \right] + \left[(4r^2 \mathcal{X} - 2B) \sin^2 f - r^2 \right] f'^2 + (2B \sin^2 f + r^2) f'^2 + \left(4\mathcal{Y} - \frac{\mathcal{I}}{r^2} \right) \sin^4 f - \frac{2m^2 r^2}{p^2} [1 - \cos(pf)] \right\} dr. \quad (2.27)$$

Here, we first derive the Lagrangian and its energy functional for the static Skyrme field from (2.21) and (2.26). When considering the time-independent Skyrme field U , *i.e.* the static rational maps and profile function $f(r)$, when $\dot{f}(r) = 0$ and $\mathcal{X} = \mathcal{Y} = 0$, the Lagrangian (2.21) is reduced to the following form

$$L = \frac{-1}{3\pi} \int \left\{ r^2 f'^2 + 2B(1 + f'^2) \sin^2 f + \mathcal{I} \frac{\sin^4 f}{r^2} + \frac{2m^2 r^2}{p^2} [1 - \cos(pf)] \right\} dr, \quad (2.28)$$

and the corresponding energy functional derived from Lagrangian (2.28) is

$$H = \frac{1}{3\pi} \int \left\{ r^2 f'^2 + 2B(1 + f'^2) \sin^2 f + \mathcal{I} \frac{\sin^4 f}{r^2} + \frac{2m^2 r^2}{p^2} [1 - \cos(pf)] \right\} dr . \quad (2.29)$$

By applying the variational principle to the Lagrangian (2.28), the equation of motion for the profile function $f(r)$ is given as

$$(r^2 + 2B \sin^2 f) f'' + 2r f' + B(f'^2 - 1) \sin 2f - \frac{2\mathcal{I}}{r^2} (\sin^3 f) (\cos f) - \frac{m^2 r^2}{p} \sin(pf) = 0 . \quad (2.30)$$

There is an important thing that we should notice: since we do not know how to solve analytically the equation of motion for the Skyrme field derived from Lagrangian (2.2), we then take an ansatz for a Skyrme field $U(x, t)$ in terms of a rational map as a starting point. By using this ansatz, the Skyrme energy functional (2.3) takes a simpler expression, (2.26) or (2.29) for static Skyrme field, that can be minimized with respect to the rational map R and the profile function f . Hence the $f_0(r)$, found by solving (2.30), with the optimized rational map, minimizing \mathcal{I} in (2.23), is a low energy configuration approximating the exact solution and assuming that \mathcal{I} in (2.30) is the value which minimizes (2.23) and then solving (2.30), we can find the configuration $f_0(r)$ which minimizes the energy functional (2.26).

2.3 Energy Density

The energy functional for static Skyrmion, (2.29), is

$$\begin{aligned} H &= \frac{1}{3\pi} \int \left\{ r^2 f'^2 + 2B(1 + f'^2) \sin^2 f + \mathcal{I} \frac{\sin^4 f}{r^2} + \frac{2m^2 r^2}{p^2} [1 - \cos(pf)] \right\} dr \\ &= H_1 + H_2 + H_3 + H_4 , \end{aligned}$$

where

$$\begin{aligned}
 H_1 &= \frac{1}{3\pi} \int r^2 f'^2 dr , \\
 H_2 &= \frac{1}{3\pi} \int 2B(1 + f'^2) \sin^2 f dr , \\
 H_3 &= \frac{1}{3\pi} \int \mathcal{I} \frac{\sin^4 f}{r^2} dr , \\
 H_4 &= \frac{1}{3\pi} \int \frac{2m^2 r^2}{p^2} [1 - \cos(pf)] dr .
 \end{aligned}$$

We now try to plot the energy density of Skyrmion with rational map ansatz, which contributes to B and \mathcal{I} in (2.29). Meanwhile, we need to change the integration variables to Cartesian coordinate to make the plotting work easier.

$$\begin{aligned}
 H_1 &= \frac{1}{3\pi} \int r^2 f'^2 dr \\
 &= \frac{1}{3\pi \cdot 4\pi} \int r^2 f'^2 \left(\int \sin \theta d\theta d\phi \right) dr \\
 &= \frac{1}{12\pi^2} \int f'^2 d^3x ,
 \end{aligned}$$

$$\begin{aligned}
 H_2 &= \frac{1}{3\pi} \int 2B(1 + f'^2) \sin^2 f dr \\
 &= \frac{2}{3\pi} \int (1 + f'^2) \sin^2 f \left(\frac{1}{4\pi} \int \left(\frac{1 + |\xi|^2}{1 + |R|^2} \left| \frac{dR}{d\xi} \right| \right)^2 \frac{2i d\xi d\bar{\xi}}{(1 + |\xi|^2)^2} \right) dr \\
 &= \frac{1}{6\pi^2} \int (1 + f'^2) \frac{\sin^2 f}{r^2} \left(\frac{1 + |\xi|^2}{1 + |R|^2} \left| \frac{dR}{d\xi} \right| \right)^2 d^3x ,
 \end{aligned}$$

$$\begin{aligned}
H_3 &= \frac{1}{3\pi} \int \mathcal{I} \frac{\sin^4 f}{r^2} dr \\
&= \frac{1}{3\pi} \int \frac{\sin^4 f}{r^2} \left(\frac{1}{4\pi} \int \left(\frac{1 + |\xi|^2}{1 + |R|^2} \left| \frac{dR}{d\xi} \right| \right)^4 \frac{2i d\xi d\bar{\xi}}{(1 + |\xi|^2)^2} \right) dr \\
&= \frac{1}{12\pi^2} \int \frac{\sin^4 f}{r^2} \left(\frac{1 + |\xi|^2}{1 + |R|^2} \left| \frac{dR}{d\xi} \right| \right)^4 d^3x,
\end{aligned}$$

$$\begin{aligned}
H_4 &= \frac{1}{3\pi} \int \frac{2m^2 r^2}{p^2} [1 - \cos(pf)] dr \\
&= \frac{2m^2}{p^2 \cdot 3\pi \cdot 4\pi} \int r^2 [1 - \cos(pf)] \left(\int \sin \theta d\theta d\phi \right) d^3x \\
&= \frac{m^2}{6p^2 \pi^2} \int [1 - \cos(pf)] d^3x.
\end{aligned}$$

So the energy functional is rewritten in terms of Cartesian coordinates as

$$\begin{aligned}
H &= \frac{1}{6\pi^2} \int \frac{1}{2} f'^2 + (1 + f'^2) \frac{\sin^2 f}{r^2} \left(\frac{1 + |\xi|^2}{1 + |R|^2} \left| \frac{dR}{d\xi} \right| \right)^2 \\
&\quad + \frac{\sin^4 f}{r^2} \left(\frac{1 + |\xi|^2}{1 + |R|^2} \left| \frac{dR}{d\xi} \right| \right)^4 + \frac{m^2}{p^2} [1 - \cos(pf)] d^3x.
\end{aligned}$$

Before the work is carried out, one more thing needs to be done, which is about determining the profile function.

To produce energy density plots more easily, we have decided to use some approximations of the profile functions instead of the ones obtained numerically. The plots obtained like this are good enough to show what the vibrational modes correspond to. To compute the actual vibrational modes and the frequencies, we will use the numerical profile for maximum accuracy.

An approximate profile function ansatz [66] for $B = 1$ is given by

$$f(r) = 2 \cos^{-1}(1 - e^{-\frac{r}{a}}), \quad \text{with } a = 0.94510062. \quad (2.31)$$

Hence the ansatz for $B = 2$ can be modified from the one for $B = 1$ to be

$$f(r) = 4 \tan^{-1}(e^{-\frac{r^2}{2}}), \quad (2.32)$$

and ansatz for $B = 4$ case will be

$$f(r) = 4 \tan^{-1}(e^{-\frac{2r^2}{7}}). \quad (2.33)$$

The reason why we choose the profile function ansatz to be the function of \tan^{-1} rather than the previous one \cos^{-1} is that for $B > 1$ cases, the derivative value of profile function should be zero of $r = 0$. The constants, $1/2$ and $2/7$, in the exponentials in (2.32) and (2.33) are for the profile functions of the pion mass $m = 0.2$ and the potential parameter $p = 1$ in $B = 2$ and $B = 4$ case respectively. These constants are determined by matching approximately the curves, which are generated by the ansatz, with the numerical data and they are moderate for our need although it is not a very good approximation. Actually any reasonable choice of these constants will do since only qualitative features of the angular dependence of the Skyrme field is highlighted in later plots of the energy density. Except for plotting the energy density, this profile function ansatz is not used in any quantitative work.

Base on the argument above, we can generalize this profile function ansatz, taking the baryon number $B > 1$, the pion mass paramter m , and the potential parameter p as the parameters to determine the constant, to the following form:

$$f(r) = 4 \tan^{-1} \left(e^{\frac{-r^2}{\alpha(B,m,p)}} \right),$$

where $\alpha(2, 0.2, 1) = 2$, and $\alpha(4, 0.2, 1) = 7/2$.

In the following two figures are the approximate profile functions for $B = 2$ and $B = 4$ respectively, where the solid line is the profile function ansatz and the dash line is the profile function obtained numerically from solving equation (2.30):

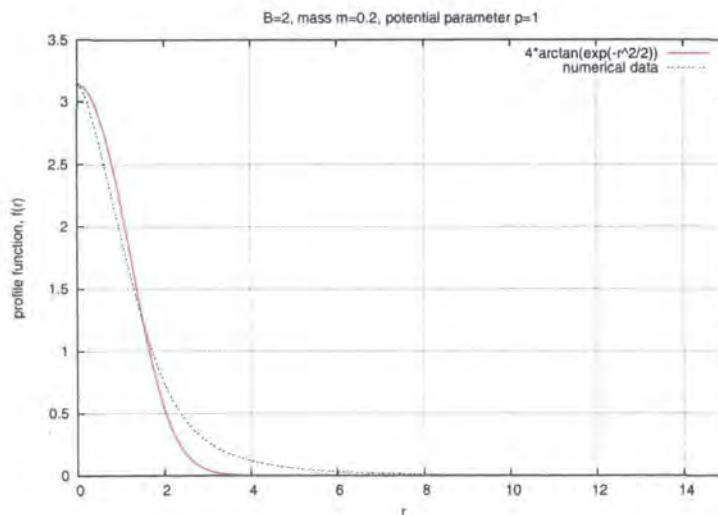


Figure 2.1: Ansatz for Profile function for $B=2$, $m = 0.2$, $p = 1$.

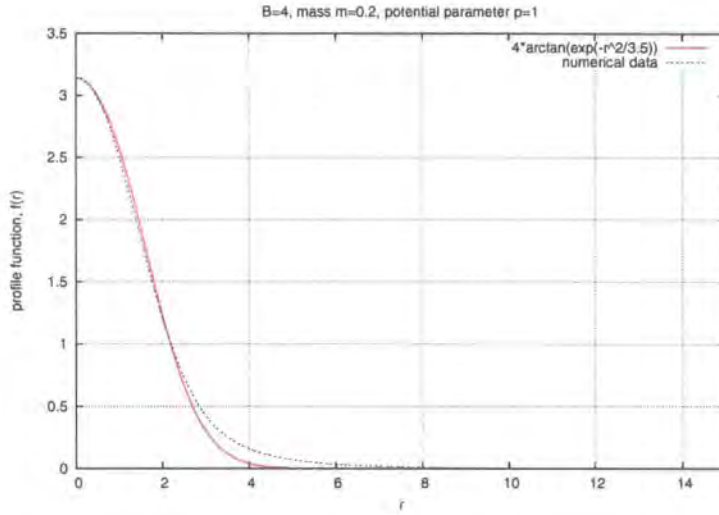


Figure 2.2: Ansatz for Profile function for $B=4$, $m = 0.2$, $p = 1$.

With the help of an analytic profile function ansatz and the rational map ansatz, we can have the energy density for $B = 1$, $B = 2$, and $B = 4$ which will be listed separately in the following chapters.

2.4 Symmetry of The Skyrme Model, Skyrmion and Rational Map

Since the Skyrme model is the theory of the pion, the Lagrangian should be Lorentz invariant and is supposed to have the symmetry of QCD, *i.e.* the chiral symmetry. The symmetry group of the Skyrme model is the direct product of the Poincaré group (geometrical symmetry) and the chiral group (internal symmetry):

$$\text{Poincaré Group} \otimes \underbrace{(SU(2)_L \otimes SU(2)_R)}_{\text{Chiral Group}} \otimes P, \quad (2.34)$$

where P is the parity operator, which has the property: $PU(\vec{x}) = U(-\vec{x})$. But we will not consider the effect caused by the parity operator P hereafter. Nevertheless, this symmetry group is too big to be useful for searching for the invariant (or symmetric) fields, which are believed to extremize the Hamiltonian and will be defined clearly later, and so it is necessary to impose some restrictions to find its maximal compact subgroup.

The Hamiltonian (2.3) is invariant under the chiral transformation of the Skyrme field $U(x)$:

$$U'(x) = VU(x)W^{-1}; \quad V \in SU(2)_L, \quad W \in SU(2)_R.$$

However, the chiral symmetry is not shared by the vacuum state of the Skyrme model,

$$U(\infty, t) = U_{vacuum}(\vec{x}, t) = \mathbf{1}_{2 \times 2}, \quad \text{unless } V = W.$$

Therefore the internal symmetry of the Skyrme model then is

$$\text{diag}(SU(2)_L \otimes SU(2)_R) \simeq SU(2)_I \simeq SO(3)_I.$$

It is stated that the chiral symmetry is spontaneously broken by the boundary condition, imposed by the finite energy requirement, to the isospin $SO(3)$ symmetry given by the conjugation

$$U(\vec{x}) \mapsto VU(\vec{x})V^\dagger, \quad V \in SU(2).$$

For the restrictions on the Poincaré group and for later use, we need to define the invariant fields of a group G of the transformations.

Definition A field $\phi(\vec{x})$ is said to be invariant¹ under the transformation from a group G , if it satisfies [66]

$$\phi(\vec{x}) = \phi_g(\vec{x}) = T_g \phi(g^{-1} \cdot \vec{x}), \quad g \in G,$$

where T_g is a linear operator in a representation space of G which is associated to a group element g . There is one observation from which it is possible to have a restriction on the Poincaré group:

Proposition Because the Hamiltonian has the quadratic term of the time derivatives of fields, the invariant fields of the Hamiltonian are in the class of static fields. [66]

¹To be precise, it is equivariant.

Since only considering the static fields, the Poincaré group can be replaced with the Euclidean group. Therefore the symmetry group for the time-independent field configurations, such as static Skyrmions, is reduced from (2.34) to

$$SO(3)_I \otimes \text{Euclidean Group of } \mathbb{R}^3 \otimes P . \quad (2.35)$$

However, there is one further requirement for the aforementioned maximal compact subgroup that it is necessary for the invariant fields to belong to a nontrivial homotopy class, then **“the change of the field under a spatial rotation must be compensated by an isospace transformation”** [76]. This means when the maximal compact symmetry subgroup, which will be called the symmetry group for short, acts on a static Skyrmion $U_B(\vec{x})$, it will generate a new set of static solutions²

$$U(\vec{x}) = VU_B(R_V(\vec{x} - \vec{X}))V^\dagger ,$$

where V is a $SU(2)$ matrix belonging to $SO(3)_I$, R_V is the $SO(3)$ space rotation associated with V , and \vec{X} is a vector. This tells us that when any Skyrmion configuration is translated, rotated or iso-rotated, its energy will not be changed, and these configurations are called zero modes.

It should be noted that the symmetry of the Lagrangian of the model, or in short, the symmetry of the model, might be different from that of the solution of the model. The symmetry of the model, when applied to a field configuration whether it is a solution of the model or not, will leave the Lagrangian (or the Hamiltonian) invariant. However, the symmetry of the solution of the model will leave the solution itself invariant and then, of course, its energy will remain the same.

We list the symmetry of the Skyrmion for different baryon number B in the table [42] [69] below

²The parity transformation is not taken into consideration here.

B	Symmetry	Remarks
1	$O(3)$	Spherical Symmetry
2	$D_{\infty h}$	Axial Symmetry
3	T_d	Tetrahedral Symmetry
4	O_h	Octahedral Symmetry
5	D_{2d}	Extended Cyclic Symmetry
6	D_{4d}	Extended Cyclic Symmetry
7	Y_h	Icosahedral Symmetry
8	D_{6d}	Extended Cyclic Symmetry
9	T_d	Tetrahedral Symmetry

Table 2.1: Symmetry of Skyrmion for different baryon number B .

Now we would like to display the Skyrmions by showing the pictures of the surfaces of the constant energy density (or called the energy density isosurface), although it is conventional to plot the baryon density isosurfaces, for baryon number $B = 1, 2,$ and $4,$ of which their vibrational modes will be investigated in the later chapter, as follows

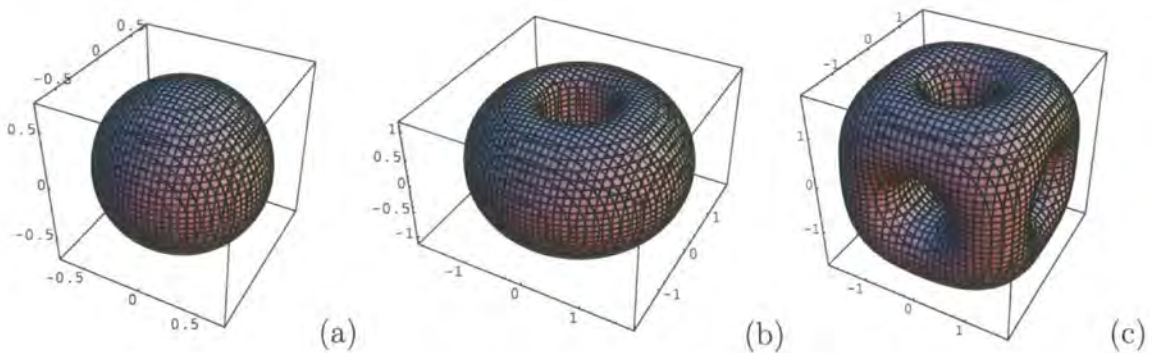


Figure 2.3: Pictures of the energy density isosurface for (a) $B = 1,$ (b) $B = 2,$ and (c) $B = 4.$

The shapes of the energy density isosurface for $B = 1, 2,$ and 4 are a sphere, torus, and cube with a hole in each face respectively, which obviously has the aforementioned symmetry $O(3), D_{\infty h},$ and O_h listed in the Table 2.1.

□ **Symmetry of the rational map**

As stated in the former section that the Skyrmion can be approximated by the rational map ansatz, we present the rational map with the same symmetry of the Skyrmion of $B = 1, B = 2,$ and $B = 4$ in the rest of this section.

A rational map is said to be symmetric or invariant under some transformations if there exists a set of transformation pairs $(g, D_g),$ where $g \in G \subset SO(3)$ is acting on the domain space \mathbb{S}^2 and, associated with g, D_g is the Möbius transformation³ acting on the target space $\mathbb{S}^2,$ such that

$$R(g(\xi)) = D_g R(\xi) .$$

It also would be helpful to use the following commutative diagram to illustrate the symmetry mentioned above

$$\begin{array}{ccc}
 \xi & \xrightarrow{R} & R(\xi) \\
 \downarrow g & & \downarrow D_g \\
 \xi' = g(\xi) & \xrightarrow{R} & R(g(\xi)) = D_g R(\xi)
 \end{array}$$

The symmetric rational maps [42] of degree $\mathcal{N} = 1, 2,$ and 4 are listed below

³Some properties of Möbius transformation will be given in more details in the later chapter.

\mathcal{N}	Symmetric Rational Map $R(\xi)$
1	ξ
2	ξ^2
4	$\frac{\xi^4 + 2\sqrt{3}i\xi^2 + 1}{\xi^4 - 2\sqrt{3}i\xi^2 + 1}$

Let us verify the symmetric rational maps given previously to see whether they have the same symmetry as required for the associated Skyrmion configuration.

$\mathcal{N} = 1$

Besides for any $g \in SU(2)$, $R(g(\xi)) = g(R(\xi))$, the rational map $R(\xi)$ also has the symmetry

$$R\left(\frac{-1}{\bar{\xi}}\right) = -\frac{1}{\bar{\xi}} = -\frac{1}{R(\xi)}.$$

Therefore the rational map of degree 1, $R(\xi) = \xi$, indeed has the same symmetry as the standard hedgehog Skyrmion solution.

$\mathcal{N} = 2$

The \mathbb{Z}_2 symmetry $\xi \mapsto 1/\bar{\xi}$ and the rotation about z -axis for any angle θ , $\xi \mapsto e^{i\theta}\xi$, can be realized by the requirements

$$\mathbb{Z}_2 : \xi \mapsto \frac{1}{\bar{\xi}} \Rightarrow R\left(\frac{1}{\bar{\xi}}\right) = \frac{1}{\bar{\xi}^2} = \frac{1}{R(\xi)},$$

$$C_\infty : \xi \mapsto e^{i\theta}\xi \Rightarrow R(e^{i\theta}\xi) = e^{2i\theta}R(\xi).$$

So the Skyrme field taking this rational map $R(\xi) = \xi^2$ will have the same symmetry as the $B = 2$ Skyrmion.

$\mathcal{N} = 4$

There are four conjugacy classes in the octahedral group O , which is the symmetry group of the $B = 4$ Skyrmion. They are C_4 , C_4^2 , C_2 and C_3 respectively, where C_2 is different from C_4^2 . We demonstrate these symmetry operations for the rational map of degree $\mathcal{N} = 4$ as follows

$$C_4: \xi \mapsto i\xi \quad \Rightarrow \quad R(i\xi) = \frac{\xi^4 - 2\sqrt{3}i\xi^2 + 1}{\xi^4 + 2\sqrt{3}i\xi^2 + 1} = \frac{1}{R(\xi)},$$

$$C_4^2: \xi \mapsto -\xi \quad \Rightarrow \quad R(-\xi) = \frac{\xi^4 + 2\sqrt{3}i\xi^2 + 1}{\xi^4 - 2\sqrt{3}i\xi^2 + 1} = R(\xi),$$

$$C_2: \xi \mapsto \frac{i}{\xi} \quad \Rightarrow \quad R\left(\frac{i}{\xi}\right) = \frac{1}{R(\xi)},$$

$$C_3: \xi \mapsto \frac{i\xi + 1}{-i\xi + 1} \quad \Rightarrow \quad R\left(\frac{i\xi + 1}{-i\xi + 1}\right) = \exp(2\pi i/3)R(\xi).$$

Using this rational map in the Skyrme field ansatz, the symmetry that the derivative Skyrmion has will be the same as that of the Skyrmion of $B = 4$.

2.5 Asymptotic Behavior of Rational Map Profile

In this section, we try to find the asymptotic behavior of the profile function $f(r)$ near the origin. It is an important task to search for this asymptotic function, because we can not solve the equation of motion for the profile function $f(r)$ analytically. The only way to do it is numerical. Therefore we need to determine its asymptotic behavior, when r approaches the origin. So we briefly introduce the method of getting the asymptotic function as follows.

Dividing (2.30) by r^2 , we have

$$\left(1 + \frac{2B \sin^2 f}{r^2}\right) f'' + \frac{2}{r} f' + \frac{B}{r^2} (f'^2 - 1) \sin(2f) - \frac{2\mathcal{I}}{r^4} (\sin^3 f) (\cos f) - \frac{m^2}{p} \sin(pf) = 0.$$

We take the asymptotic function of $f(r)$ near $r = 0$ as $f(r) = \pi + ar^s$, in which $a \neq 0$ and $s > 0$. The constant π in the expression is due to the boundary condition,

$f(0) = \pi$. Then plugging the asymptotic function of $f(r)$ into the equation above, we have

$$\left[(s(s-1) + 2s - 2B) r^{s-2} + a^3 \left[2Bs(s-1) + 2Bs^2 - 2\mathcal{I} \right] r^{3s-4} - a(-1)^p m^2 r^s = 0. \quad (2.36)$$

For the equation to be satisfied, the coefficient of the lowest order term of r must be set to zero, since, when $r \rightarrow 0$, the asymptotic function of $f(r)$ is taken as $f(r) = \pi + ar^s$ as we are only interested in the lowest order. Therefore, any terms other than the one of the lowest order will be neglected. Our next step is to decide which terms is of the lowest order and once it is done we set its coefficient to zero to determine the value of s .

There are three terms, r^s , r^{s-2} , and r^{3s-4} , in (2.36). By inspection, we can easily find that the order of r^s is always higher than that of r^{s-2} . After some comparisons, we have the following relations:

$$0 < s < 1 \quad , \quad O(r^s) > O(r^{s-2}) > O(r^{3s-4}) ; \quad (2.37)$$

$$s = 1 \quad , \quad O(r^s) > O(r^{3s-4}) = O(r^{s-2}) ; \quad (2.38)$$

$$1 < s < 2 \quad , \quad O(r^s) > O(r^{3s-4}) > O(r^{s-2}) ; \quad (2.39)$$

$$s = 2 \quad , \quad O(r^s) = O(r^{3s-4}) > O(r^{s-2}) ; \quad (2.40)$$

$$s > 2 \quad , \quad O(r^{3s-4}) > O(r^s) > O(r^{s-2}) . \quad (2.41)$$

While examining the relations above, we find (2.38) can not be satisfied for baryon number $B \geq 2$ because the values of s determined from setting the coefficients of r^{s-2} and r^{3s-4} to zero, are not the expected value $s = 1$. Based on the similar reason neither can (2.40) be for $B \geq 2$. We also realize that it is possible to combine (2.39) and (2.41), since what we are concerned is the lowest order term. Then r^{s-2} is the term of the lowest order when $s > 1$ but $s \neq 2$. From (2.37), a further inspection

shows that r^{3s-4} is the lowest order term when $0 < s < 1$; however, it is not self-consistent. This means that, while setting the coefficient of r^{3s-4} to be zero to find the value of s , the resultant s does not satisfy the relation $0 < s < 1$. In the end, we have determined the lowest order term for $B = 1$ is r^{s-2} as $s \geq 1 \cap s \neq 2$, and for $B \geq 2$ it also is r^{s-2} as $s > 1 \cap s \neq 2$.

This method of analysis can be applied to any value of baryon number B . Here take $B = 1, 2$, and 4 cases, in which we are interested, as an example, and we get

$$\begin{aligned} B = 1, \quad s(s-1) + 2s - 2 = 0 &\Rightarrow s = 1, \\ B = 2, \quad s(s-1) + 2s - 4 = 0 &\Rightarrow s = \frac{-1 + \sqrt{17}}{2} \cong 1.5616, \\ B = 4, \quad s(s-1) + 2s - 8 = 0 &\Rightarrow s = \frac{-1 + \sqrt{33}}{2} \cong 2.3723. \end{aligned}$$

The value of s in the asymptotic function, $f(r) = \pi + ar^s$, for $B = 1, 2$, and 4 are shown above. The reason of neglecting the negative value of s is that the profile function $f(r)$ does not have an singularity at the origin.

Obviously, in the case of $B = 2$ and 4 the values of s , 1.5617 and 2.3723 , are not integers. However, what does this non-integer s mean?

If the derivative $f'(x)$ exists at all points x of a region \mathbb{R} , then $f(x)$ is said to be analytic in \mathbb{R} and is referred to as an analytic function in \mathbb{R} or a function analytic in \mathbb{R} . A function $f(x)$ is said to be analytic at a point x_0 if there exists a neighborhood $|x - x_0| < \delta$ at all points of which $f'(x)$ exists.

So when s is not an integer, as we take the Taylor expansion at the origin, the value of the n -th derivative $f^{(n)}(r)$, where $n = [s] + 1$, will not exist. Here $[s]$ is the floor function of s , whose definition is: $[s] = \max\{m \in \mathbb{Z} \mid m \leq s\}$. This is because after taking the n -th derivative of the asymptotic function $f(r)$, the power of r will be negative. When we insert the value of $r = 0$, the value of this derivative will be infinite and of course does not exist. Therefore this asymptotic function of $f(r)$ is not an analytic function.

This is not a good news to us, since the field function we expect should be analytic. From the practical point of view, we do not find any singularity in our everyday life, *i.e.* we don't see any point around us with infinite value. However, this result comes from the rational map ansatz. That means it is only an approximate

solution rather than an exact solution to the field equation. Due to this reason, the fact that this profile function is non-analytic is acceptable.

Since it seems that for most of the baryon number B the value of s are non-integers, here we raise a question: for what specific values of B can we have an integer value for s ? Furthermore, is there any connection between these integers s and B ? This question can be easily answered by rewriting $s(s - 1) + 2s - 2B = 0$ and inserting the integer as the value of s into it to obtain the value of B , which will be an integer, because the connection between s and B can be expressed as follows

$$B(s) = \frac{1}{2}s(s + 1), \quad \forall s \in \mathbb{Z}.$$

Here, we list the first ten values of s and B in the table below

s	1	2	3	4	5	6	7	8	9	10
B	1	3	6	10	15	21	28	36	45	55

Table 2.2: The values for Baryon number B for integers s .

Chapter 3

Vibration

The functional H , (2.26), is the energy for the time-dependent Skyrme field $U(x, t)$. Our purpose is to study the time-dependent behavior of the Skyrme field U , which is in terms of the profile function $f(r, t)$ and the rational map $R(\xi, \bar{\xi}, t)$, around the minimum energy configuration of the functional H , (2.26). The field configuration of the minimum energy can be obtained by solving the static version of (2.26). When it is done, we perform a perturbation around this static solution by allowing the field configuration to have the time-dependent fluctuations in both $f(r)$ and $R(\xi, \bar{\xi})$. Inserting the perturbed Skyrme field in terms of the perturbed rational map ansatz into the Skyrme Lagrangian and assuming the behavior of the perturbed field configuration away from minimal energy configuration would be the simple harmonic vibration, we then expand the Skyrme Lagrangian up to the second order of perturbation since we will show later that the first order of perturbation is zero. The application of the Euler-Lagrange equation to the Skyrme Lagrangian will lead us to have the equation of motion for the perturbed profile function and perturbed rational map. In the following sections, we will demonstrate the procedures mentioned above.

3.1 Vibration of profile function

In order to investigate the behavior of time-dependent fluctuation around the extremum solution $f_0(r)$, the perturbation which will be performed in the Lagrangian

(2.21) is taken in the following form

$$f(r, t) \rightarrow f_0(r) + g(r, t) . \quad (3.1)$$

The conditions which we have to impose on the function $g(r, t)$ are

$$g(r = 0) = g(r \rightarrow \infty) = 0 .$$

Inserting the perturbed profile function (3.1) into Lagrangian (2.27), we briefly demonstrate the process of calculation.

Expanding $\sin[f(r, t)]$ in terms of $f_0(r)$ and $g(r, t)$, the first term in (2.27) can be written as

$$\begin{aligned} & (4r^2\mathcal{X} - 2B) \sin^2 f \\ = & \left[(4r^2\mathcal{X} - 2B) \sin^2 f_0 \right] + g \left[(4r^2\mathcal{X} - 2B) \sin(2f_0) \right] + g^2 \left[(4r^2\mathcal{X} - 2B) \cos(2f_0) \right] . \end{aligned}$$

Besides the expansion of $\sin[f(r, t)]$, the second term in (2.27) also needs to be considered to expand the spatial derivative of $f(r, t)$. Therefore it is

$$\begin{aligned} & \left[(4r^2\mathcal{X} - 2B) \sin^2 f - r^2 \right] f'^2 \\ = & \left\{ \left[(4r^2\mathcal{X} - 2B) \sin^2 f_0 - r^2 \right] + g(4r^2\mathcal{X} - 2B) \sin(2f_0) \right. \\ & \left. + g^2(4r^2\mathcal{X} - 2B) \cos(2f_0) \right\} f_0'^2 \\ & + \left\{ \left[(4r^2\mathcal{X} - 2B) \sin^2 f_0 - r^2 \right] + g(4r^2\mathcal{X} - 2B) \sin(2f_0) \right. \\ & \left. + g^2(4r^2\mathcal{X} - 2B) \cos(2f_0) \right\} g'^2 \\ & + \left\{ \left[(4r^2\mathcal{X} - 2B) \sin^2 f_0 - r^2 \right] + g(4r^2\mathcal{X} - 2B) \sin(2f_0) \right. \\ & \left. + g^2(4r^2\mathcal{X} - 2B) \cos(2f_0) \right\} 2f_0'g' . \end{aligned}$$

For the third term in (2.27), we have to equate both the time derivative of $f(r, t)$

and $\sin f(r, t)$:

$$\begin{aligned}
& (2B \sin^2 f + r^2) \dot{f}^2 \\
&= \left\{ [2B \sin^2 f_0 + r^2] + g [2B \sin 2f_0] + g^2 [2B \cos 2f_0] \right\} \dot{f}_0^2 \\
&+ \left\{ [2B \sin^2 f_0 + r^2] + g [2B \sin 2f_0] + g^2 [2B \cos 2f_0] \right\} \dot{g}^2 \\
&+ \left\{ [2B \sin^2 f_0 + r^2] + g [2B \sin 2f_0] + g^2 [2B \cos 2f_0] \right\} 2\dot{f}_0 \dot{g} .
\end{aligned}$$

It is simple to deal with the fourth term in (2.27), since we only need to expand $\sin^4 f(r, t)$

$$\begin{aligned}
& (4\mathcal{Y} - \frac{\mathcal{I}}{r^2}) \sin^4 f \\
&= \left[(4\mathcal{Y} - \frac{\mathcal{I}}{r^2}) \sin^4 f_0 \right] + g \left[4(4\mathcal{Y} - \frac{\mathcal{I}}{r^2}) \sin^3 f_0 \cos f_0 \right] \\
&+ g^2 \left[(4\mathcal{Y} - \frac{\mathcal{I}}{r^2}) (6 \sin^2 f_0 \cos^2 f_0 - 2 \sin^4 f_0) \right] .
\end{aligned}$$

The final term in (2.27) is then

$$\begin{aligned}
& \frac{2m^2 r^2}{p^2} [1 - \cos(pf)] \\
&= \left\{ \frac{2m^2 r^2}{p^2} [1 - \cos(pf_0)] \right\} + g \left[\frac{2m^2 r^2}{p} \sin(pf_0) \right] + g^2 \left[m^2 r^2 \cos(pf_0) \right] .
\end{aligned}$$

Putting each term computed above into (2.27), after a bit of calculation, and collecting all the terms of the same order of perturbation, we then can write the Lagrangian as

$$L = L_0 + L_1 + L_2 = \int_{R^3} \mathcal{L} d^3x ,$$

where L_0 , L_1 and L_2 are defined below and the integer lower index indicates the order of the perturbation.

$$\begin{aligned}
L_0 = \frac{1}{3\pi} \int \left\{ \left[(4r^2 \mathcal{X} - 2B) \sin^2 f_0 \right] + \left[(4r^2 \mathcal{X} - 2B) \sin^2 f_0 - r^2 \right] f_0'^2 \right. \\
\left. + (4\mathcal{Y} - \frac{\mathcal{I}}{r^2}) \sin^4 f_0 - \frac{2m^2 r^2}{p^2} [1 - \cos(pf_0)] \right\} dr , \quad (3.2)
\end{aligned}$$

where $f_0' \equiv \frac{df_0}{dr}$.

$$\begin{aligned}
L_1 &= \frac{1}{3\pi} \int \left\{ \frac{\partial \mathcal{L}}{\partial f} \Big|_{f=f_0} \cdot g + \frac{\partial \mathcal{L}}{\partial f'} \Big|_{f=f_0} \cdot g' + \frac{\partial \mathcal{L}}{\partial \dot{f}} \Big|_{f=f_0} \cdot \dot{g} \right\} dr \\
&= \frac{1}{3\pi} \int \left\{ g \left[(4r^2 \mathcal{X} - 2B) \sin 2f_0 \right] + g \left[(4r^2 \mathcal{X} - 2B) \sin 2f_0 \right] f_0'^2 \right. \\
&\quad \left. + 2g' \left[(4r^2 \mathcal{X} - 2B) \sin^2 f_0 - r^2 \right] f_0' + 4g \left(4\mathcal{Y} - \frac{\mathcal{I}}{r^2} \right) (\sin^3 f_0) (\cos f_0) \right. \\
&\quad \left. - g \frac{2m^2 r^2}{p} \sin(pf_0) \right\} dr, \tag{3.3}
\end{aligned}$$

with $g' \equiv \frac{\partial g}{\partial r}$ and $\dot{g} \equiv \frac{\partial g}{\partial t}$.

When doing the integration in L_1 , we will find that it is zero, since

$$\begin{aligned}
&\frac{\partial \mathcal{L}}{\partial f} \Big|_{f=f_0} \cdot g + \frac{\partial \mathcal{L}}{\partial f'} \Big|_{f=f_0} \cdot g' + \frac{\partial \mathcal{L}}{\partial \dot{f}} \Big|_{f=f_0} \cdot \dot{g} \\
&= \frac{\partial \mathcal{L}}{\partial (\partial_\mu f)} \Big|_{f=f_0} \cdot (\partial_\mu g) + \frac{\partial \mathcal{L}}{\partial f} \Big|_{f=f_0} \cdot g \\
&= \partial_\mu \left(\frac{\partial \mathcal{L}}{\partial (\partial_\mu f)} \Big|_{f=f_0} \cdot g \right) - \left[\partial_\mu \left(\frac{\partial \mathcal{L}}{\partial (\partial_\mu f)} \Big|_{f=f_0} \right) - \frac{\partial \mathcal{L}}{\partial f} \Big|_{f=f_0} \right] \cdot g \\
&= \partial_\mu \left(\frac{\partial \mathcal{L}}{\partial (\partial_\mu f)} \Big|_{f=f_0} \cdot g \right),
\end{aligned}$$

$$\therefore \partial_\mu \left(\frac{\partial \mathcal{L}}{\partial (\partial_\mu f)} \Big|_{f=f_0} \right) - \frac{\partial \mathcal{L}}{\partial f} \Big|_{f=f_0} = 0, \quad \text{Euler-Lagrange equation.}$$

Then plugging the above result into the integration (3.3) and using Gauss' theorem with the boundary conditions imposed on $g(r, t)$, *i.e.* $g(r \rightarrow \infty) = 0$, we will see that the integration in L_1 vanishes as expected given that f_0 minimizes (2.28).

L_2 is given by

$$\begin{aligned}
L_2 &= \frac{1}{3\pi} \int \left\{ g^2 (4r^2 \mathcal{X} - 2B) \cos(2f_0) + g^2 (4r^2 \mathcal{X} - 2B) (\cos 2f_0) f_0'^2 \right. \\
&\quad \left. + g'^2 \left[(4r^2 \mathcal{X} - 2B) \sin^2 f_0 - r^2 \right] + 2gg' (4r^2 \mathcal{X} - 2B) (\sin 2f_0) f_0' \right. \\
&\quad \left. + g^2 (2B \cos 2f_0) f_0'^2 + \dot{g}^2 (2B \sin^2 f_0 + r^2) + 2g\dot{g} (2B \sin 2f_0) \dot{f}_0 \right. \\
&\quad \left. + g^2 \left(4\mathcal{Y} - \frac{\mathcal{I}}{r^2} \right) \left[6 (\sin^2 f_0) (\cos^2 f_0) - 2 \sin^4 f_0 \right] - g^2 m^2 r^2 \cos(pf_0) \right\} dr. \tag{3.4}
\end{aligned}$$

Applying the Euler-Lagrange equation on L_2 , we have the equation of motion for g :

$$K_0\ddot{g} = J_0g'' + N_0g' + M_0g, \quad (3.5)$$

where we define K_0 , J_0 , N_0 , and M_0 as follows

$$\left\{ \begin{array}{l} K_0 \equiv 2B \sin^2 f_0 + r^2 \\ J_0 \equiv r^2 - (4r^2\mathcal{X} - 2B) \sin^2 f_0 \\ N_0 \equiv 2r - 8r\mathcal{X} \sin^2 f_0 - f_0'(4r^2\mathcal{X} - 2B) \sin(2f_0) \\ M_0 \equiv (4r^2\mathcal{X} - 2B) \cos(2f_0) + f_0'^2(4r^2\mathcal{X} - 2B) \cos(2f_0) \\ \quad + \left(4\mathcal{Y} - \frac{\mathcal{I}}{r^2}\right) \left[6(\sin^2 f_0)(\cos^2 f_0) - 2\sin^4 f_0\right] - m^2r^2 \cos(pf_0) \\ \quad - 8r\mathcal{X}f_0' \sin(2f_0) - 2f_0'^2(4r^2\mathcal{X} - 2B) \cos(2f_0) - f_0''(4r^2\mathcal{X} - 2B) \sin(2f_0) \end{array} \right. \quad (3.6)$$

3.2 Vibrations of Rational Map

In the following, we want to find out how the value of \mathcal{I} varies as the perturbation of the rational map $R(\xi)$ is performed in both space and time. The definition of \mathcal{I} (2.23) is given as

$$\mathcal{I} = \frac{1}{4\pi} \int \left(\frac{1 + |\xi|^2}{1 + |R|^2} \right)^4 \left| \frac{dR}{d\xi} \right|^4 \frac{2i d\xi \bar{d}\xi}{(1 + |\xi|^2)^2}.$$

Now for the most general case, we require that the rational map be time-dependent with the following form:

$$R(\xi, t) = \frac{P(\xi, t)}{Q(\xi, t)}, \quad (3.7)$$

with

$$P(\xi, t) \equiv \sum_{i=0}^B (a_i + \delta a_i(t)) \xi^i = a_i \xi^i + (\delta a_i) \xi^i = P_0(\xi) + \delta P(\xi, t), \quad (3.8)$$

$$Q(\xi, t) \equiv \sum_{i=0}^B (b_i + \delta b_i(t)) \xi^i = b_i \xi^i + (\delta b_i) \xi^i = Q_0(\xi) + \delta Q(\xi, t). \quad (3.9)$$

In the above definitions, the a_i 's and b_i 's are the constant coefficients of ξ^i for the polynomials $P(\xi)$ and $Q(\xi)$ respectively. The δa_i and δb_i are very small time-dependent fluctuations of the rational map. The number B sitting on the top of the summation symbol is the baryon number of the Skyrmion configuration, *i.e.* the winding number of the rational map. The repeated indices summation rule is used here.

We can therefore have the expressions for the derivative with respect to the complex variable ξ and the time t as follows

$$\begin{aligned} \frac{\partial P(\xi, t)}{\partial \xi} &= P_\xi = P_{0,\xi} + (\delta P)_\xi ; & \frac{\partial P(\xi, t)}{\partial t} &= \dot{P} = (\delta \dot{P}) , \\ \frac{\partial Q(\xi, t)}{\partial \xi} &= Q_\xi = Q_{0,\xi} + (\delta Q)_\xi ; & \frac{\partial Q(\xi, t)}{\partial t} &= \dot{Q} = (\delta \dot{Q}) , \end{aligned}$$

as P_0 and Q_0 are time-independent.

With the definitions below,

$$\left\{ \begin{array}{l} \alpha_0 \equiv |P_0|^2 + |Q_0|^2 \\ \alpha_1 \equiv P_0(\delta \bar{P}) + \bar{P}_0(\delta P) + Q_0(\delta \bar{Q}) + \bar{Q}_0(\delta Q) \\ \alpha_2 \equiv (\delta P)(\delta \bar{P}) + (\delta Q)(\delta \bar{Q}) \\ \\ \beta_0 \equiv P_{0,\xi} Q_0 - P_0 Q_{0,\xi} \\ \beta_1 \equiv P_{0,\xi}(\delta Q) - P_0(\delta Q)_\xi - Q_{0,\xi}(\delta P) + Q_0(\delta P)_\xi \\ \beta_2 \equiv (\delta P)_\xi(\delta Q) - (\delta P)(\delta Q)_\xi \\ \\ \gamma_0 \equiv |\beta_0|^4 \\ \gamma_1 \equiv 2|\beta_0|^2(\beta_0 \bar{\beta}_1 + \bar{\beta}_0 \beta_1) \\ \gamma_2 \equiv 4|\beta_0|^2 |\beta_1|^2 + (\beta_0^2 \bar{\beta}_1^2 + \bar{\beta}_0^2 \beta_1^2) + 2|\beta_0|^2(\beta_0 \bar{\beta}_2 + \bar{\beta}_0 \beta_2) \end{array} \right. , \quad (3.10)$$

we can write our results in a simpler form.

Since the calculation is lengthy and tedious, we only show some crucial steps for

getting the results. The first term we consider in the integral of (2.23) is

$$\begin{aligned} \frac{1}{(1 + |R|^2)^4} &= \left(\frac{|Q|^2}{|P|^2 + |Q|^2} \right)^4 = \left(\frac{|Q|^2}{\alpha_0 + \alpha_1 + \alpha_2} \right)^4 \\ &= \frac{|Q|^8}{\alpha_0^4} \left[1 - \frac{4\alpha_1}{\alpha_0} + \left(\frac{10\alpha_1^2}{\alpha_0^2} - \frac{4\alpha_2}{\alpha_0} \right) \right], \end{aligned}$$

where α_0 , α_1 and α_2 and other coefficients appearing in the other calculations of the terms in (2.23), will be defined later on.

The next term which we need to deal with is

$$\left| \frac{dR}{d\xi} \right|^4 = \left| \frac{P_\xi Q - P Q_\xi}{Q^2} \right|^4 = \left(\frac{|\beta_0 + \beta_1 + \beta_2|}{|Q|^2} \right)^4 = \frac{\gamma_0 + \gamma_1 + \gamma_2}{|Q|^8}.$$

Therefore, after putting all the terms computed above back to (2.23), \mathcal{I} , on which the perturbation of rational map is performed, becomes

$$\begin{aligned} \mathcal{I} = \frac{1}{4\pi} \int \frac{(1 + |\xi|^2)^2}{\alpha_0^4} &\left[\gamma_0 + \left(\gamma_1 - 4\gamma_0 \frac{\alpha_1}{\alpha_0} \right) \right. \\ &\left. + \left(10\gamma_0 \frac{\alpha_1^2}{\alpha_0^2} - 4\gamma_0 \frac{\alpha_2}{\alpha_0} - 4\gamma_1 \frac{\alpha_1}{\alpha_0} + \gamma_2 \right) \right] 2i d\xi \bar{d}\xi, \quad (3.11) \end{aligned}$$

where the integer in the lower index of α and γ is the order of the perturbation, *i.e.* it means the first term in the above bracket is the perturbation of order one and so on.

A similar procedure can be applied to the calculation of finding the expression for \mathcal{X} and \mathcal{Y} under the perturbation of the rational map. We only give the outlines of the calculation here. Recalling from (2.24), the definition of \mathcal{X} , the part which is significantly different from the derivation of \mathcal{I} is the calculation for $|\dot{R}|^2$. The simplified computation for the term $|\dot{R}|^2$ is given by

$$\begin{aligned} |\dot{R}|^2 &= \left| \frac{\dot{P}Q - P\dot{Q}}{Q^2} \right|^2 \\ &= \frac{\left| [Q_0(\delta\dot{P}) - P_0(\delta\dot{Q})] + [(\delta\dot{P})(\delta Q) - (\delta P)(\delta\dot{Q})] \right|^2}{|Q|^4} \\ &\sim \frac{|Q_0(\delta\dot{P}) - P_0(\delta\dot{Q})|^2}{|Q|^4}. \end{aligned}$$

Since we only want to do the perturbation up to the second order, we neglect the higher order terms in the calculation of $|\dot{R}|^2$. Collecting and combing all the results

obtained in the previous computation, after a bit of work, we have

$$\mathcal{X} = \frac{1}{4\pi} \int \frac{|\lambda_1|^2}{\alpha_0^2} \frac{2i d\xi \bar{d}\xi}{(1 + |\xi|^2)^2}, \quad (3.12)$$

$$\mathcal{Y} = \frac{1}{4\pi} \int \frac{|\beta_0|^2 |\lambda_1|^2}{\alpha_0^4} 2i d\xi \bar{d}\xi, \quad (3.13)$$

where the $\lambda_1 = Q_0(\delta\dot{P}) - P_0(\delta\dot{Q})$

After the integration, the perturbed \mathcal{I} , \mathcal{X} and \mathcal{Y} in (3.11), (3.12) and (3.13) can be rewritten in terms of a more compact notation which we define as follows

$$\vec{V}(t) \equiv \begin{Bmatrix} \delta a_i \\ \delta b_i \end{Bmatrix} = \begin{Bmatrix} \delta a_B \\ \vdots \\ \delta a_0 \\ \delta b_B \\ \vdots \\ \delta b_0 \end{Bmatrix}; \quad \dot{\vec{V}}(t) \equiv \begin{Bmatrix} \delta \dot{a}_i \\ \delta \dot{b}_i \end{Bmatrix} = \begin{Bmatrix} \delta \dot{a}_B \\ \vdots \\ \delta \dot{a}_0 \\ \delta \dot{b}_B \\ \vdots \\ \delta \dot{b}_0 \end{Bmatrix}. \quad (3.14)$$

Therefore in the expression of \vec{V} , they becomes

$$\begin{cases} \mathcal{I} = \mathcal{I}_0 + \vec{\mathcal{I}}_1 \cdot \vec{V} + \vec{V}^T \mathcal{I}_2 \vec{V} = \mathcal{I}_0 + (\mathcal{I}_1)_i V_i + V_i (\mathcal{I}_2)_{ij} V_j \\ \mathcal{X} = \vec{V}^T \mathcal{X}_2 \vec{V} = \dot{V}_i (\mathcal{X}_2)_{ij} \dot{V}_j \\ \mathcal{Y} = \vec{V}^T \mathcal{Y}_2 \vec{V} = \dot{V}_i (\mathcal{Y}_2)_{ij} \dot{V}_j \end{cases}, \quad (3.15)$$

where $i, j = 0, 1, \dots, 2B$; $\vec{\mathcal{I}}_1$ is a vector which will be shown to vanish; \mathcal{I}_2 , \mathcal{X}_2 and \mathcal{Y}_2 are matrices which can be determined later; \vec{V}^T is the transpose of the vector \vec{V} . The expansions which we have done on \mathcal{I} , \mathcal{X} and \mathcal{Y} are up to the second order. The reason of our so doing on \mathcal{I} is that the initial value of \mathcal{I}_0 , around which the perturbation of the rational map is performed, is the minimum of \mathcal{I} . The answer to why it is a minimum is that the corresponding rational map is used as an ansatz to obtain the minimal energy of the field configuration of that baryon number. Since \mathcal{I}_0 is the minimum value, while doing the perturbation about \mathcal{I} , the first order variation with respect to the rational map appears to be zero, *i.e.* $\mathcal{I}_{1i} = 0$, we will show it in the following. Therefore we need to do this variation up to the second

order. For \mathcal{X} and \mathcal{Y} , because they involve the time derivative of the rational map, and their initial values of the rational map is time independent, \mathcal{X}_0 and \mathcal{Y}_0 are zero. A similar reason for the first order of variation to vanish is mentioned above, hence the perturbation for \mathcal{X} and \mathcal{Y} up to the second order is needed.

We then plug (3.15) and (3.1) into the Lagrangian (2.27). It is expanded up to second order of variation as

$$L = L_0 + L_1 + L_2 = \int (\mathcal{L}_0 + \mathcal{L}_1 + \mathcal{L}_2) dr ,$$

where

$$L_0 = \frac{1}{3\pi} \int \left\{ -2B \sin^2 f_0 - (2B \sin^2 f_0 + r^2) f_0'^2 - \frac{\mathcal{I}_0}{r^2} \sin^4 f_0 - \frac{2m^2 r^2}{p} [1 - \cos(pf_0)] \right\} dr , \quad (3.16)$$

$$L_1 = \frac{1}{3\pi} \int \left\{ -2gB \sin(2f_0) - 4g'B f_0' \sin^2 f_0 - 2gB f_0'^2 \sin(2f_0) - 2g'r^2 f_0' - \frac{4g\mathcal{I}_0}{r^2} (\sin^3 f_0)(\cos f_0) - \frac{2gm^2 r^2}{p} \sin(pf_0) - \frac{1}{r^2} \mathcal{I}_{1i} V_i \sin^4 f_0 \right\} dr , \quad (3.17)$$

$$L_2 = \frac{1}{3\pi} \int \left\{ 4r^2 \dot{V}_i \mathcal{X}_{2ij} \dot{V}_j \sin^2 f_0 + 2g^2 B \sin^2 f_0 - 2g^2 B \cos^2 f_0 + 4r^2 \dot{V}_i \mathcal{X}_{2ij} \dot{V}_j f_0'^2 \sin^2 f_0 - 2g'^2 B \sin^2 f_0 + 2g^2 B f_0'^2 \sin^2 f_0 - 4gg'B f_0' \sin(2f_0) - 2g^2 B f_0'^2 \cos^2 f_0 - r^2 g'^2 + 2\dot{g}^2 B \sin^2 f_0 + r^2 \dot{g}^2 + 4\dot{V}_i \mathcal{Y}_{2ij} \dot{V}_j \sin^4 f_0 + \frac{2g^2}{r^2} \mathcal{I}_0 \sin^4 f_0 - \frac{6g^2}{r^2} \mathcal{I}_0 (\sin^2 f_0)(\cos^2 f_0) - \frac{4g}{r^2} \mathcal{I}_{1i} V_i (\sin^3 f_0)(\cos f_0) - \frac{1}{r^2} V_i \mathcal{I}_{2ij} V_j \sin^4 f_0 - g^2 m^2 r^2 \cos(pf_0) \right\} dr . \quad (3.18)$$

General speaking, when expanding a Lagrangian $L[\phi(x^\mu), \partial_\mu \phi(x^\mu)]$ around a function $\phi_0(x^\mu)$ which minimize the Lagrangian, we have

$$\begin{aligned} L &= L^{(0)} + \left. \frac{\delta L}{\delta \phi} \right|_{\phi_0} \delta \phi + \left. \frac{\delta^2 L}{\delta \phi^2} \right|_{\phi_0} \delta \phi^2 + O(\delta \phi^3) \\ &\equiv L^{(0)} + L^{(1)} + L^{(2)} , \end{aligned}$$

where $L^{(0)} \equiv L[\phi_0(x^\mu), \partial_\mu \phi_0(x^\mu)]$.

If the Lagrangian can be written as a space volume integral over a density function \mathcal{L} , called the Lagrangian density:

$$L[\phi(x), \partial_\mu \phi(x^\mu)] = \int d^3x \mathcal{L}(\phi(x^\mu), \partial_\mu \phi(x^\mu)) ,$$

then we can express the variation of L as

$$\begin{aligned} \delta L &= \int d^3x \left(\frac{\partial \mathcal{L}}{\partial \phi(x^\mu)} \delta \phi(x^\mu) + \frac{\partial \mathcal{L}}{\partial (\partial_\mu \phi(x^\mu))} \delta \partial_\mu \phi(x^\mu) \right) ; \quad \delta (\partial_\mu \phi(x^\mu)) = \partial_\mu (\delta \phi(x^\mu)) \\ &= \int d^3x \left(\frac{\partial \mathcal{L}}{\partial \phi(x^\mu)} \delta \phi(x^\mu) + \partial_\mu \left(\frac{\partial \mathcal{L}}{\partial (\partial_\mu \phi(x^\mu))} \delta \phi(x^\mu) \right) - \left(\partial_\mu \frac{\partial \mathcal{L}}{\partial (\partial_\mu \phi(x^\mu))} \right) \delta \phi(x^\mu) \right) \\ &= \int d^3x \left(\left(\frac{\partial \mathcal{L}}{\partial \phi(x^\mu)} - \partial_\mu \frac{\partial \mathcal{L}}{\partial (\partial_\mu \phi(x^\mu))} \right) \delta \phi(x^\mu) + \partial_\mu \left(\frac{\partial \mathcal{L}}{\partial (\partial_\mu \phi(x^\mu))} \delta \phi(x^\mu) \right) \right) \\ &= \int d^3x \left(\frac{\partial \mathcal{L}}{\partial \phi(x^\mu)} - \partial_\mu \frac{\partial \mathcal{L}}{\partial (\partial_\mu \phi(x^\mu))} \right) \delta \phi(x^\mu) . \end{aligned}$$

In the last step, Gauss' theorem is applied with the boundary condition $\delta \phi(x^\mu) \rightarrow 0$ as $x^\mu \rightarrow \infty$. Therefore, we have

$$L^{(1)} = \frac{\delta L}{\delta \phi(x^\mu)} \Big|_{\phi_0(x^\mu)} \delta \phi(x^\mu) = \int d^3x \left(\frac{\partial \mathcal{L}}{\partial \phi(x^\mu)} - \partial_\mu \frac{\partial \mathcal{L}}{\partial (\partial_\mu \phi(x^\mu))} \right) \Big|_{\phi_0(x^\mu)} \delta \phi(x^\mu) = 0 ,$$

and this is because

$$\left(\frac{\partial \mathcal{L}}{\partial \phi(x^\mu)} - \partial_\mu \frac{\partial \mathcal{L}}{\partial (\partial_\mu \phi(x^\mu))} \right) \Big|_{\phi_0(x^\mu)} = 0$$

is the Euler-Lagrange equation for $\phi_0(x^\mu)$. And this result can be generalized to the Lagrangian of multi-functions, $L[\phi_i(x^\mu), \partial_\mu \phi_i(x^\mu)]$ for $i = 1 \dots n$:

$$\begin{aligned} L^{(1)} &= \frac{\delta L}{\delta \phi_i} \Big|_{\phi_0} \delta \phi_i \\ &= \sum_{i=1}^n \int d^3x \left(\frac{\partial \mathcal{L}}{\partial \phi_i} - \partial_\mu \frac{\partial \mathcal{L}}{\partial (\partial_\mu \phi_i)} \right) \Big|_{\phi_0} \delta \phi_i = 0 \end{aligned}$$

$$\therefore \left(\frac{\partial \mathcal{L}}{\partial \phi_i} - \partial_\mu \frac{\partial \mathcal{L}}{\partial (\partial_\mu \phi_i)} \right) \Big|_{\phi_0} = 0 \quad , \quad i = 1 \dots n .$$

As for L_1 in (3.17), according to the argument above, when the expansion of Lagrangian L around the profile function $f_0(r)$ and the rational map $R_0(\xi)$ which

minimize L to L_0 , is performed with $f(r) \rightarrow f_0(r) + g(r, t)$ and $R(\xi) \rightarrow R_0(\xi) + \delta R(\xi, t)$, $L_1 = 0$, and that results from

$$\left(\frac{\partial \mathcal{L}}{\partial f} - \partial_\mu \frac{\partial \mathcal{L}}{\partial (\partial_\mu f)} \right) \Big|_{f_0(r)} = 0 ,$$

$$\text{and } \left(\frac{\partial \mathcal{L}}{\partial V_i} - \partial_\mu \frac{\partial \mathcal{L}}{\partial (\partial_\mu V_i)} \right) \Big|_{R_0(\xi)} = 0 \quad \Rightarrow \quad \frac{1}{r^2} \mathcal{I}_{1i} \sin^4 f_0 = 0 .$$

Since $\sin^4 f_0$ is nonzero, we then have the conclusion

$$\mathcal{I}_{1i} = 0 .$$

The Lagrangian L now is

$$L = L_0 + L_2 .$$

Using the the Euler-Lagrange equation to \mathcal{L}_2 , we can have the equation of motion for $g(r, t)$ as follows

$$K_0 \ddot{g} = K_0 g'' + N_1 g' + M_1 g , \quad (3.19)$$

where

$$K_0 \equiv 2B \sin^2 f_0 + r^2 , \quad (3.6)$$

$$N_1 \equiv 2r + 2B f_0' \sin(2f_0) , \quad (3.20)$$

$$\begin{aligned} M_1 \equiv & -2B \cos(2f_0) + 2B f_0'^2 \cos(2f_0) + 2B f_0'' \sin(2f_0) \\ & - \frac{\mathcal{I}_0}{r^2} \left[6(\sin^2 f_0) (\cos^2 f_0) - 2 \sin^4 f_0 \right] - m^2 r^2 \cos(pf_0) . \end{aligned} \quad (3.21)$$

The \mathcal{I}_0 in (3.21) is the minimum value of \mathcal{I} around which the perturbation of the rational map is performed.

We can have not only the equation of motion for the small fluctuation field $g(r, t)$ of the profile function $f(r)$, but also that for the perturbed rational map. When we only allow the profile function f to have the time-dependent fluctuations $g(r, t)$ around its minimum energy configuration $f_0(r)$, we get the equation of motion for $g(r, t)$, (3.5). At first sight of (3.5), it seems that the motions of this time-dependent field $g(r, t)$ would couple to that of the rational map because of the coefficients

defined in (3.6). However, while we also take the time-dependent perturbations of the rational map into consideration, the situation is totally different. As we can see in (3.19) and (3.22) that the equation of motion for $g(r, t)$ does not involve any perturbed rational map, and the situation is the same to the case for the equation of motion of \vec{V} . This is because that in L_2 , (3.18), there is no cross term for perturbed profile function $g(r, t)$ and perturbed rational map V_i . Therefore, when applying the Euler-Lagrange equation to L_2 , we will find out that the equation of motion for $g(r, t)$ and V_i decouples from each other. We then separately have the equation of motion for $g(r, t)$ and that for V_i , which is the perturbation field of the rational map. This means that the motions of those two perturbation fields from profile function and rational map are decoupled. The equation of motion for V_i can be calculated using the Euler-Lagrange equation for L_2

$$A_{ij}\ddot{V}_j = -D_{ij}V_j, \quad (3.22)$$

where

$$\begin{aligned} A_{ij} &\equiv \int \left(r^2 \mathcal{X}_{2ij} \sin^2 f_0 + r^2 \mathcal{X}_{2ij} f_0'^2 \sin^2 f_0 + \mathcal{Y}_{2ij} \sin^4 f_0 \right) dr \\ &= \mathcal{X}_{2ij} \Gamma_1 + \mathcal{Y}_{2ij} \Gamma_2 \end{aligned} \quad (3.23)$$

$$\begin{aligned} D_{ij} &\equiv \int \left(\frac{1}{4r^2} \mathcal{I}_{2ij} \sin^4 f_0 \right) dr \\ &= \mathcal{I}_{2ij} \Gamma_3, \end{aligned} \quad (3.24)$$

with

$$\left\{ \begin{array}{l} \Gamma_1 \equiv \int (r^2 \sin^2 f_0 + r^2 f_0'^2 \sin^2 f_0) dr \\ \Gamma_2 \equiv \int (\sin^4 f_0) dr \\ \Gamma_3 \equiv \int \left(\frac{1}{4r^2} \sin^4 f_0 \right) dr \end{array} \right. \quad (3.25)$$

Since \mathcal{X}_{2ij} , \mathcal{Y}_{2ij} and \mathcal{I}_{2ij} are functions independent of r , we can treat them as constant and take them out of the integral.

Chapter 4

Eigen Mode of Profile Function

In this chapter, our intention is to study the eigenmode of the perturbed profile function. We will find its eigenvalues by solving the equation of motion for the perturbed profile function, (3.19), and then look for the asymptotic field to get the dispersion relation to determine the critical mass, which will tell whether the mode we are studying is a genuine vibrational mode or just a radiation mode.

4.1 Eigenvalues

In this section, we solve the equation of motion for the perturbed profile function, (3.5). Using the numerical method, we can determine the eigenvalues, ω^2 , for the perturbed profile functions for different masses of the pion fields, in the range from 0 to 5.0; different potential parameters p , from 0 to 4; and different baryon number, $B=1$, $B=2$, and $B=4$. We list this data in the following tables; however we use the vibrational frequency ω instead of the eigenvalues ω^2 .

$m \setminus p$	1	2	3	4
0.2	–	–	–	–
0.4	–	–	–	–
0.6	–	–	–	–
0.8	–	–	–	–
1.0	–	–	0.97890	0.91581
1.5	–	1.35574	1.18242	1.07668
2.0	1.85096	1.57960	1.33560	1.19920
2.5	2.12417	1.77053	1.46391	1.30233
3.0	2.36619	1.94006	1.57601	1.39285
3.5	2.58721	2.09397	1.67640	1.47429
4.0	2.79143	2.23582	1.76779	1.54837
4.5	2.98214	2.36798	1.85200	1.61675
5.0	3.16158	2.49213	1.93030	1.68023

Table 4.1: Vibrational frequencies ω for $B=1$.

The “–” symbol in Table 4.1, Table 4.2 and Table 4.3 is used to denote that no genuine vibrational mode, whose vibrational frequency is below the mass parameter, can be found. Although the eigenvalues are still available and the corresponding modes might be called pseudo-vibrational modes, we will not list them in the tables and put “–” symbol instead. In Table 4.1 and same for Table 4.2 and 4.3, the first column is the parameter for the rescaled pion mass, which is used as an input parameter for solving the eigenvalue equation. The second column is the vibrational frequency ω , derived from the eigenvalue ω^2 , for the potential parameter $p = 1$, and the third column for $p = 2$ and so on and so forth. We will analyze and discuss the data in Table 4.1, 4.2 and 4.3, in the section 4.3.

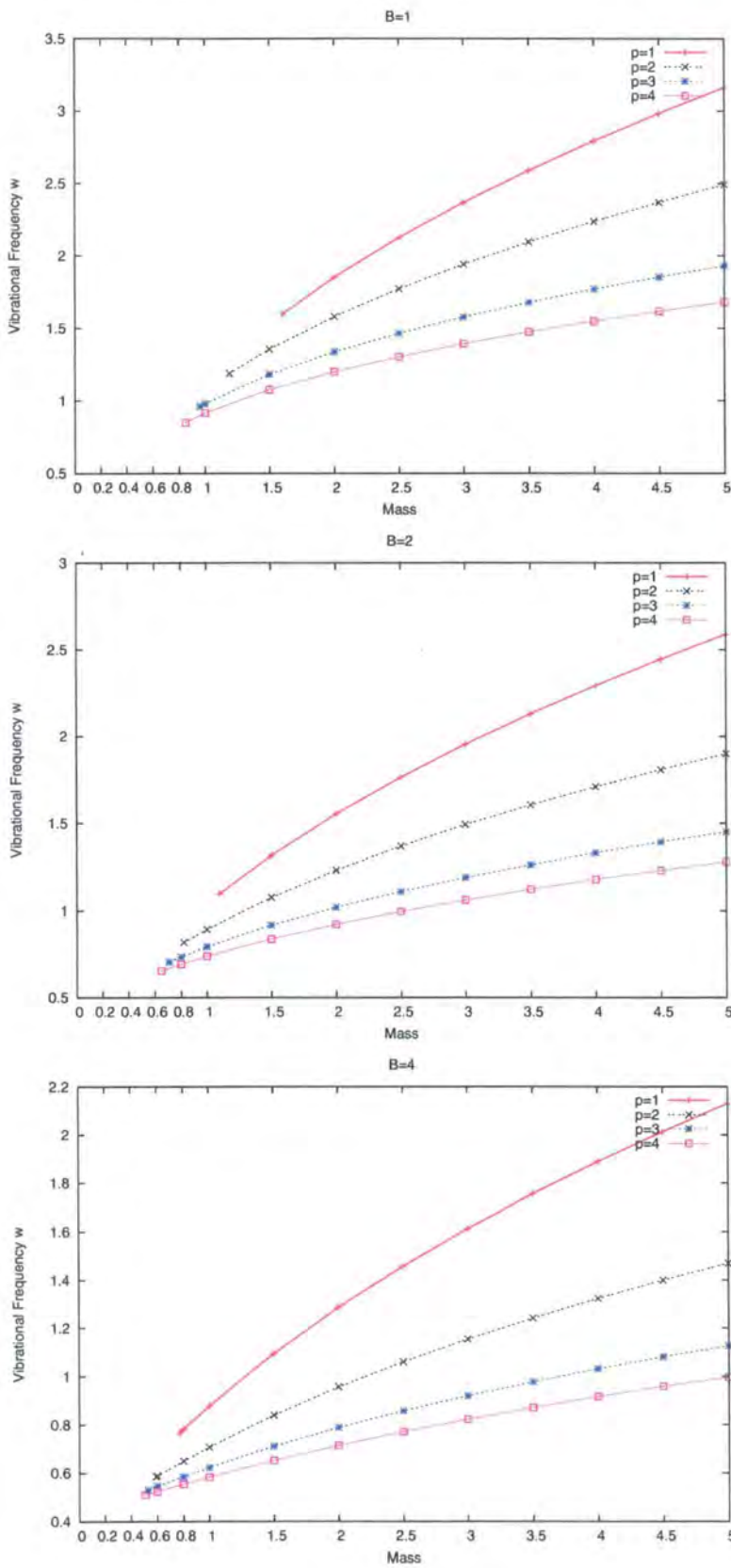
$m \setminus p$	1	2	3	4
0.2	—	—	—	—
0.4	—	—	—	—
0.6	—	—	—	—
0.8	—	—	0.73237	0.69121
1.0	—	0.89350	0.79137	0.73808
1.5	1.31555	1.07656	0.91527	0.83702
2.0	1.55270	1.23186	1.01843	0.92081
2.5	1.76302	1.36866	1.10848	0.99480
3.0	1.95350	1.49197	1.18892	1.06159
3.5	2.12854	1.60491	1.26198	1.12267
4.0	2.29117	1.70961	1.32918	1.17914
4.5	2.44359	1.80755	1.39159	1.23181
5.0	2.58737	1.89980	1.44982	1.28063

Table 4.2: Vibrational frequencies ω for $B=2$.

$m \setminus p$	1	2	3	4
0.2	—	—	—	—
0.4	—	—	—	—
0.6	—	0.58860	0.54534	0.52318
0.8	0.78191	0.64968	0.58380	0.55360
1.0	0.87679	0.70768	0.62215	0.58280
1.5	1.09438	0.84031	0.71014	0.65166
2.0	1.28544	0.95668	0.78723	0.71389
2.5	1.45607	1.06038	0.85630	0.77041
3.0	1.61134	1.15470	0.91886	0.82216
3.5	1.75416	1.24153	0.97638	0.87011
4.0	1.88719	1.32221	1.02916	0.91459
4.5	2.01188	1.39794	1.07851	0.95613
5.0	2.12966	1.46933	1.12478	0.99488

Table 4.3: Vibrational frequencies ω for $B=4$.

We put all the data of vibrational frequencies ω listed in Table 4.1, 4.2, and 4.3 into the following three plots respectively.

Figure 4.1: Vibrational frequencies ω vs pion mass m for $B=1$, $B=2$, and $B=4$.

4.2 Asymptotic Fields

Now, if we assume that the meson fields, ϕ_i , $i = 1, 2, 3$, fluctuate from the vacuum, *i.e.* $\phi_i = \epsilon \eta_i$, $\epsilon \ll 1$, then, because of the constraint for the meson fields $(\phi_\alpha)^2 = \phi_0^2 + \phi_i^2 = 1$, we have

$$\begin{aligned}\phi_0^2 &= 1 - \epsilon^2 \eta_i^2, \\ \phi_0 &\simeq \left(1 - \frac{1}{2} \epsilon^2 \eta_i^2\right) \approx 1.\end{aligned}$$

We next insert ϕ_i and ϕ_0 obtained above into (2.12)

$$\begin{aligned}&\partial_\mu \partial^\mu \phi_\alpha - (\partial_\mu \partial^\mu \phi_\eta) \phi_\eta \phi_\alpha + (\partial_\mu \partial^\mu \phi_\beta) (\partial_\nu \phi_\alpha \partial^\nu \phi_\beta) - (\partial_\mu \partial^\mu \phi_\alpha) (\partial_\nu \phi_\beta \partial^\nu \phi_\beta) \\ &+ (\partial_\mu \partial^\mu \phi_\eta) (\partial_\nu \phi_\beta \partial^\nu \phi_\beta) \phi_\eta \phi_\alpha - (\partial_\mu \partial^\nu \phi_\beta) (\partial^\mu \phi_\beta \partial_\nu \phi_\alpha) + (\partial_\mu \partial^\nu \phi_\alpha) (\partial^\mu \phi_\beta \partial_\nu \phi_\beta) \\ &- (\partial_\mu \partial^\nu \phi_\eta) (\partial^\mu \phi_\beta \partial_\nu \phi_\beta) \phi_\eta \phi_\alpha + \frac{m^2}{2} \frac{\partial V_p(\phi_0)}{\partial \phi_0} \phi_0 \phi_\alpha - \frac{m^2}{2} \frac{\partial V_p(\phi_0)}{\partial \phi_0} \delta_{\alpha 0} = 0, \quad (4.1)\end{aligned}$$

to get the equation of motion for the meson fields ϕ_α .

Here we give some details of the calculations for each of the terms in (4.1). To give clear results, we separate the computations into $\alpha = 0$ and $\alpha = i \neq 0$ to the first order in ϵ .

$$\partial_\mu \partial^\mu \phi_0 = \square \phi_0 = 0$$

$$\partial_\mu \partial^\mu \phi_i = \epsilon (\square \eta_i)$$

$$\begin{aligned}(\partial_\mu \partial^\mu \phi_\eta) \phi_\eta \phi_0 &= (\square \phi_0) \phi_0 \phi_0 + (\square \phi_i) \phi_i \phi_0 \\ &= 0 + \epsilon^2 (\square \eta_i) \eta_i \phi_0 \\ &\approx 0\end{aligned}$$

$$\begin{aligned}(\partial_\mu \partial^\mu \phi_\eta) \phi_\eta \phi_i &= (\square \phi_0) \phi_0 \phi_i + (\square \phi_j) \phi_j \phi_i \\ &= 0 + \epsilon^3 (\square \eta_j) \eta_j \eta_i \\ &\approx 0\end{aligned}$$

$$(\partial_\mu \partial^\mu \phi_\beta)(\partial_\nu \phi_0 \partial^\nu \phi_\beta) = 0$$

$$\begin{aligned} (\partial_\mu \partial^\mu \phi_\beta)(\partial_\nu \phi_i \partial^\nu \phi_\beta) &= (\square \phi_0)(\partial_\nu \phi_i \partial^\nu \phi_0) + (\square \phi_j)(\partial_\nu \phi_i \partial^\nu \phi_j) \\ &= 0 + \epsilon^3 (\square \eta_j)(\partial_\nu \eta_i \partial^\nu \eta_j) \\ &\approx 0 \end{aligned}$$

$$(\partial_\mu \partial^\mu \phi_0)(\partial_\nu \phi_\beta \partial^\nu \phi_\beta) = 0$$

$$\begin{aligned} (\partial_\mu \partial^\mu \phi_i)(\partial_\nu \phi_\beta \partial^\nu \phi_\beta) &= (\square \phi_i)(\partial_\nu \phi_0 \partial^\nu \phi_0) + (\square \phi_i)(\partial_\nu \phi_j \partial^\nu \phi_j) \\ &= 0 + \epsilon^3 (\square \eta_i)(\partial_\nu \eta_j \partial^\nu \eta_j) \\ &\approx 0 \end{aligned}$$

$$\begin{aligned} (\partial_\mu \partial^\mu \phi_\eta)(\partial_\nu \phi_\beta \partial^\nu \phi_\beta) \phi_\eta \phi_0 &= (\square \phi_\eta)(\partial_\nu \phi_0 \partial^\nu \phi_0) \phi_\eta \phi_0 + (\square \phi_\eta)(\partial_\nu \phi_i \partial^\nu \phi_i) \phi_\eta \phi_0 \\ &= 0 + \epsilon^2 (\square \phi_\eta)(\partial_\nu \eta_i \partial^\nu \eta_i) \phi_\eta \phi_0 \\ &\approx 0 \end{aligned}$$

$$\begin{aligned} (\partial_\mu \partial^\mu \phi_\eta)(\partial_\nu \phi_\beta \partial^\nu \phi_\beta) \phi_\eta \phi_i &= (\square \phi_\eta)(\partial_\nu \phi_0 \partial^\nu \phi_0) \phi_\eta \phi_i + (\square \phi_\eta)(\partial_\nu \phi_j \partial^\nu \phi_j) \phi_\eta \phi_i \\ &= 0 + \epsilon^3 (\square \phi_\eta)(\partial_\nu \eta_j \partial^\nu \eta_j) \phi_\eta \phi_i \\ &\approx 0 \end{aligned}$$

$$(\partial_\mu \partial^\nu \phi_\beta)(\partial^\mu \phi_\beta \partial_\nu \phi_0) = 0$$

$$\begin{aligned} (\partial_\mu \partial^\nu \phi_\beta)(\partial^\mu \phi_\beta \partial_\nu \phi_i) &= (\partial_\mu \partial^\nu \phi_0)(\partial^\mu \phi_0 \partial_\nu \phi_i) + (\partial_\mu \partial^\nu \phi_j)(\partial^\mu \phi_j \partial_\nu \phi_i) \\ &= 0 + \epsilon^3 (\partial_\mu \partial^\nu \eta_j)(\partial^\mu \eta_j \partial_\nu \eta_i) \\ &\approx 0 \end{aligned}$$

$$(\partial_\mu \partial^\nu \phi_0)(\partial^\mu \phi_\beta \partial_\nu \phi_\beta) = 0$$

$$\begin{aligned} (\partial_\mu \partial^\nu \phi_i)(\partial^\mu \phi_\beta \partial_\nu \phi_\beta) &= (\partial_\mu \partial^\nu \phi_i)(\partial^\mu \phi_0 \partial_\nu \phi_0) + (\partial_\mu \partial^\nu \phi_i)(\partial^\mu \phi_j \partial_\nu \phi_j) \\ &= 0 + \epsilon^3 (\partial_\mu \partial^\nu \eta_i)(\partial_\mu \eta_j \partial_\nu \eta_j) \\ &\approx 0 \end{aligned}$$

$$\begin{aligned} (\partial_\mu \partial^\nu \phi_\eta)(\partial^\mu \phi_\beta \partial_\nu \phi_\beta) \phi_\eta \phi_0 &= (\partial_\mu \partial^\nu \phi_\eta)(\partial^\mu \phi_0 \partial_\nu \phi_0) \phi_\eta \phi_0 + (\partial_\mu \partial^\nu \phi_\eta)(\partial^\mu \phi_i \partial_\nu \phi_i) \phi_\eta \phi_0 \\ &= 0 + \epsilon^2 (\partial_\mu \partial^\nu \phi_\eta)(\partial^\mu \eta_i \partial_\nu \eta_i) \phi_\eta \phi_0 \\ &\approx 0 \end{aligned}$$

$$\begin{aligned} (\partial_\mu \partial^\nu \phi_\eta)(\partial^\mu \phi_\beta \partial_\nu \phi_\beta) \phi_\eta \phi_i &= (\partial_\mu \partial^\nu \phi_\eta)(\partial^\mu \phi_0 \partial_\nu \phi_0) \phi_\eta \phi_i + (\partial_\mu \partial^\nu \phi_\eta)(\partial^\mu \phi_j \partial_\nu \phi_j) \phi_\eta \phi_i \\ &= 0 + \epsilon^3 (\partial_\mu \partial^\nu \phi_\eta)(\partial^\mu \eta_j \partial_\nu \eta_j) \phi_\eta \eta_i \\ &\approx 0 \end{aligned}$$

$$\begin{aligned} \frac{m^2}{2} \frac{\partial V_p(\phi_0)}{\partial \phi_0} \phi_0 \phi_0 &= \frac{m^2}{2} \frac{\partial V_p(\phi_0)}{\partial \phi_0} \\ \frac{m^2}{2} \frac{\partial V_p(\phi_0)}{\partial \phi_0} \phi_0 \phi_i &= \frac{\epsilon m^2}{2} \frac{\partial V_p(\phi_0)}{\partial \phi_0} \eta_i \end{aligned}$$

$$\begin{aligned} \frac{m^2}{2} \frac{\partial V_p(\phi_0)}{\partial \phi_0} \delta_{00} &= \frac{m^2}{2} \frac{\partial V_p(\phi_0)}{\partial \phi_0} \\ \frac{m^2}{2} \frac{\partial V_p(\phi_0)}{\partial \phi_0} \delta_{0i} &= 0 \end{aligned}$$

Combining all the terms for $\alpha = 0$, we find the equation of motion for ϕ_0 is trivial, $0 = 0$. But for $\alpha = i \neq 0$, hence $\phi_i = \epsilon \eta_i$, we have the following equation of motion

$$\square \eta_i + \frac{m^2}{2} \frac{\partial V_p(\phi_0)}{\partial \phi_0} \eta_i = 0 .$$

Taking the form of $\frac{\partial V_p}{\partial \phi_0}$ into account, the equation above leads to

$$\left(\square + m_p^2 \right) \eta_i = 0 , \tag{4.2}$$

with

$$m_p^2 \equiv \frac{m^2}{2} \left(\frac{\partial V_p(\phi_0)}{\partial \phi_0} \right) \Big|_{\phi_0 \rightarrow 1} .$$

(4.2) is the Klein-Gordon equation for a real scalar field $\phi(\vec{x}, t)$ in (3+1) dimensions:

$$(\square + m^2)\phi(\vec{x}, t) \equiv \left(\frac{\partial^2}{\partial t^2} - \nabla^2 + m^2 \right) \phi(\vec{x}, t) = 0 , \quad (4.3)$$

where we use the natural units and m is the mass of the field quanta.

Inserting the plane wave solution, $e^{i(kx-\omega t)}$, into Klein-Gordon equation, gives the dispersion relation:

$$\omega^2 = k^2 + m^2 . \quad (4.4)$$

As long as the vibrational frequency $\omega > m$, the wave number k is real, and the solution, $e^{i(kx-\omega t)}$, is a plane wave. Therefore, the energy of the plane wave solution with frequency ω is being carried away and we can call it radiation. It implies that the vibrational energy of the Skyrme will be carried away by the radiation of the meson field η_i . So any vibrational mode with $\omega > m$ is not a genuine vibrational mode of the Skyrme solutions.

However, with decreasing ω , we will come to meet the situation where m is greater than ω , *i.e.* $m > \omega$. Then the wave number k will become

$$k^2 = \omega^2 - m^2 = -\kappa^2 < 0 , \quad (4.5)$$

where $\kappa > 0$, and hence we have an imaginary wave number k . This means we have to replace k with $i\kappa$ in the plane wave solution, $e^{i(kx-\omega t)}$, and it leads to

$$e^{i(kx-\omega t)} \rightarrow e^{-\kappa x} e^{-i\omega t} . \quad (4.6)$$

This solution has a space-dependent exponential decay factor, $e^{-\kappa x}$. It indicates that at a fixed time the values of the field decay like an exponential function. The mass term in the equation of motion is important in determining if a solution radiates or vibrates.

When perturbing the Skyrme field $U(\vec{x}, t)$ from its minimum energy configuration, it is equivalent to exciting the vibrational modes of the Skyrme field or, in

other words, to making Skyrmion vibrate. The boundary condition for the Skyrme field is $U(\vec{x}, t) \rightarrow \mathbf{1}_{2 \times 2}$ as $|\vec{x}| \rightarrow \infty$. It implies that the meson fields are taken as $\phi_\alpha = (\phi_0, \phi_i) \sim (1, \epsilon \eta_i)$ while $|\vec{x}| \rightarrow \infty$. And we have the equation of motion for meson fields ϕ_α in the domain as (4.2). When the Skyrmion vibrates at the frequency ω , its far end, the field approaching to the infinity, will of course vibrate at the same frequency and behave by the equation of motion (4.2).

However, according to a recent research by Bizon et al. [18], the vibrational modes of the $B = 1$ Skyrmion without the pion mass term in the Lagrangian, are not as simple as expected. They numerically studied the relaxation to the stable equilibrium solution, namely the Skyrmion, and found that the relaxation process consists of two different stages, which are the oscillatory exponential decay, also called the quasinormal ringing, and the polynomial decay respectively.

The dispersion, *i.e.* the radiation carries away the excess of energy to infinity, is the main mechanism of decay as the state converging to the Skyrmion, since the system considered is not locally dissipative. In the first stage of evolution, dominates the quasinormal ringing, which, in linear scattering theory [52] [47], is a well-known effect, and its presence owed to the quasinormal mode with the damping factor. A quasinormal mode is a non-singular solution of the linearized equation of motion for the perturbations around the stable solution, taken the form:

$$\psi(r) \sim e^{ikr}, \quad k = \Omega - i\Gamma, \quad \Gamma > 0,$$

and fulfils the outgoing wave condition as $r \rightarrow \infty$. They showed that the behavior of the state from the Skyrmion is well-approximated by the quasinormal mode for intermediate times

In the second stage of the evolution, the main effect of the decay is no longer attributed to the quasinormal ringing but is taken over by the polynomial tail that is a decay in the form of the power-law. However, the decay rate of the tail, $\sim t^{-5}$, is different from the prediction by the linear scattering theory, $\sim t^{-8}$. But when taking the nonlinear perturbation into account, they showed that it is in a good agreement with the numerical result. Hence they revealed the nonlinear origin of the tail which, however, is not unusual but is a generic phenomenon in scattering theory for nonlinear wave equations.

To summarize, the asymptotic dynamics of approaching to the $B = 1$ Skyrmion is studied and they showd that two different kinds of decay are responsible for it: quasinormal ringring and polynomial tail. For intermediate times, the former, which is a linear effect, prevails; for later times, the latter, which is nonlinear, takes over.

4.3 Critical Mass

From the analysis of the linearized field equation, *i.e.* the Klein-Gordon equation, we find that if the vibrational frequency ω of the Skyrmion is higher than the mass of the pions, then the vibrational energy will be carried away by the pions. It indicates that it is not a genuine vibrational mode. But if the vibrational frequency ω is lower than the pion mass, then its vibrational energy will not be radiated away, and that means it is indeed a vibrational mode of the Skyrmion. From the argument above, it is important to find the critical mass that enables us to distinguish the radiation mode from the vibrational mode for the Skyrmion.

The critical pion mass is the value at which the pion mass m is equal to the vibrational frequency ω . A further observation on the data in Table 4.1, 4.2, and 4.3 can give us a clue of what value of the critical pion mass may be. In the following table and figure, the critical masses of baryon number $B = 1, 2$ and 4 for different potential parameter p , are shown.

$B \setminus p$	1	2	3	4
1	1.60	1.19	0.96	0.85
2	1.10	0.82	0.71	0.65
4	0.77	0.59	0.53	0.51
6	0.60	0.47	0.44	0.43
7	0.56	0.44	0.42	0.41
9	0.47	0.38	0.36	0.36
17	0.33	0.28	0.27	0.27

Table 4.4: Critical Mass for different B and potential parameter p .

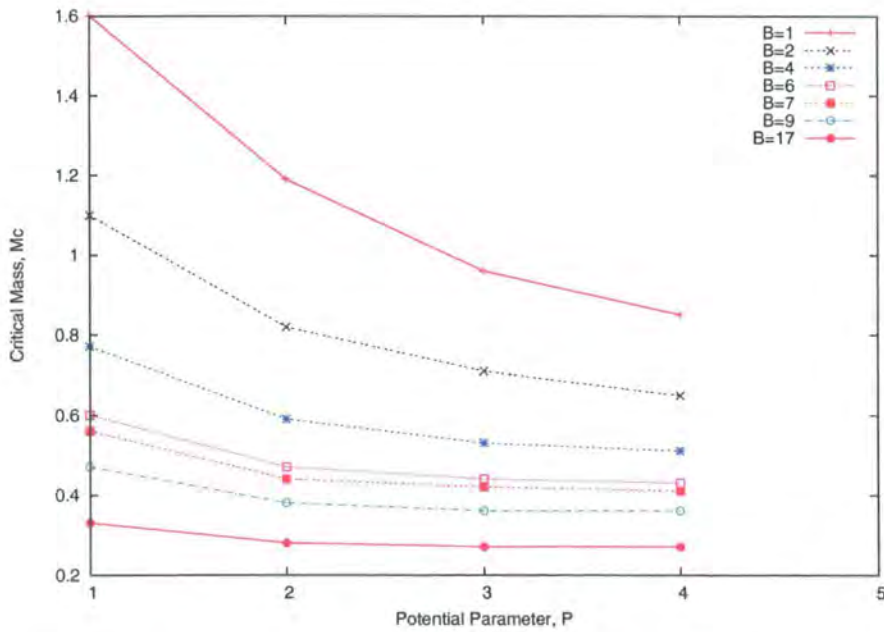


Figure 4.2: Critical Mass M_c for different baryon number p and potential parameter p .

We can obtain the vibrational frequency as a function of the rescaled pion mass m and potential parameters p . For a fixed value of the potential parameter p , as the mass varies, we have the associated frequency, and we do the comparison of the mass with the vibrational frequency to see whether the vibrational frequency is higher or lower than the mass. The critical mass is the value of m above which there exists a genuine vibrational mode, *i.e.* for which not all vibrational modes are radiative. By this, the critical mass is determined up to an accuracy of 10^{-2} . Then we change the value of the potential parameter p to find another critical mass.

From the Table 4.4 or Figure 4.2 above, we see that the critical mass decreases as the value of the potential parameter p increases for one fixed value of the baryon number. Similarly, with the same value of the potential parameter p , the critical mass also decreases as the baryon number B decreases.

The value of the critical mass obtained by us, seems to be relatively larger than the value from the standard Skyrme parameters [1], in which the pion mass is 138 MeV. Before a further discussion of our results, we give a basic idea of how the value of the pion mass can be fitted.

There are only three free parameters in the Lagrangian of the Skyrme model: m_π - the (tree-level) pion mass, F_π - the pion decay constant, and e - a dimensionless constant. The experimental values for the pion mass and pion decay constant are $m_\pi = 138$ MeV and $F_\pi = 186$ MeV respectively.

In the standard Skyrme parameters the pion mass is fixed to the experimental value, 138 MeV, and then F_π and e can be fixed by fitting the energies of the quantized spinning Skyrmion to the masses of the nucleons and the delta resonance, yielding $m_\pi = 138$ MeV, $F_\pi = 108$ MeV, and $e = 4.84$. However, this set of the standard Skyrme parameters are obtained by assuming that a Skyrmion does not deform while spinning, which is called the rigid body approximation(RBA). Some authors in early papers [73] [20] pointed out the limitation of the RBA and some [34] [78] have noted that the need to take into account the deformation of a spinning Skyrmion. Once the limitation is removed, Battye et al. [14] shows that the standard Skyrme parameters is merely an artifact of the RBA, using numerical computations of spinning Skyrmions in the full field theory with the only assumption

of an axial symmetry. For a range of Skyrme parameters, Battye et al. fitted the computed energies of spinning Skyrmions to the masses of the nucleons and delta resonance, and found that can be done only if the pion mass is taken to be larger than twice the experimental value, to be precise it is $m_\pi = 345$ MeV or in a rescaled pion mass of $m = 1.56$. That result is remarkably close to the value required in the study of the Roper resonance [22]. In the end, they concluded that a critical pion mass is in the range of $276 \text{ MeV} \leq m_\pi \leq 345 \text{ MeV}$.

Briefly speaking, Battye et al. relaxed the limitation of the RBA and allowed spinning Skyrmion to deform. The determination of their critical pion mass is under the constraint $\Omega^2 \leq m_\pi^2$, where Ω is the rotation frequency of a spinning Skyrmion, since the Skyrmion can only spin up to a certain frequency, beyond which the pion will be radiated. As a result, the critical pion mass obtained by this approach is larger than the experimental value. Our value for critical pion mass is determined under the similar constraint, namely $\omega^2 \leq m^2$, where the ω is the vibrational frequency.

We would also like to point out the following: for these values of the critical mass for the sets of the values of (B, p) , the values from $B = 1$, *i.e.* the values from $(1, p)$ with different p , are the most important since the hedgehog ansatz are exact solutions of the Skyrme equation for $B = 1$ that are derived from the Lagrangian with the mass terms $\frac{m^2}{p^2} \text{Tr}(U - \mathbf{1})$ for different p . It means that the upper bound for the pion mass that we can take for the Skyrme model is set by these values of the critical mass from $B = 1$ as any such vibrations, for $m > m_c$, would correspond to an excitation that does not exist as a stable particle. When $p = 1$, *i.e.* for the standard mass term, the critical value of the pion mass is $m = 1.6$.

Chapter 5

Eigen Mode of Rational Map (I)

5.1 Determination of \mathcal{X}_2 , \mathcal{Y}_2 , and \mathcal{I}_2

In order to solve (3.22), we rewrite it as

$$\frac{\partial^2}{\partial t^2} V_j = -A_{ij}^{-1} D_{ij} V_j. \quad (5.1)$$

Given the form of (5.1) we can assume that $V_j = e^{-i\omega t} v_j$, and (5.1) becomes the eigenvalue problem, $\omega^2 v_j = A_{ij}^{-1} D_{ij} v_j$. To solve this eigenvalue equation, one needs to determine A_{ij} , (3.23), and D_{ij} , (3.24). However, these two matrices can not be obtained without computing the matrices \mathcal{X}_2 , \mathcal{Y}_2 and \mathcal{I}_2 first. In this section, we will compute the matrices \mathcal{X}_2 , \mathcal{Y}_2 and \mathcal{I}_2 , and some of them will be presented.

According to the expression of the rational map in (3.7), the rational map of degree B can be written as

$$\begin{aligned} R(\xi, t) &= \frac{(a_0 + a_1 \xi + \cdots + a_B \xi^B) + [(\delta a_0) + (\delta a_1) \xi + \cdots + (\delta a_B) \xi^B]}{(b_0 + b_1 \xi + \cdots + b_B \xi^B) + [(\delta b_0) + (\delta b_1) \xi + \cdots + (\delta b_B) \xi^B]} \\ &= \frac{(a_0 + \delta a_0) + (a_1 + \delta a_1) \xi + (a_2 + \delta a_2) \xi^2 + \cdots + (a_B + \delta a_B) \xi^B}{(b_0 + \delta b_0) + (b_1 + \delta b_1) \xi + (b_2 + \delta b_2) \xi^2 + \cdots + (b_B + \delta b_B) \xi^B}. \end{aligned} \quad (5.2)$$

We are now considering the perturbation of rational map for $B = 1$ case. From Houghton et al., the rational map for $B = 1$ is

$$R(\xi) = \xi.$$

By (5.2), we have the perturbed rational map as

$$R(\xi, t) = \frac{[1 + (\delta a_1)]\xi + (\delta a_0)}{(\delta b_1)\xi + [1 + (\delta b_0)]}.$$

Without any loss of generality we can choose the coefficient of ξ to be 1 by dividing both the denominator and the numerator by $(1 + \delta a_1)$. Then, to leading order in δa_i and δb_i , we have

$$\begin{aligned} R(\xi, t) &= \frac{\xi + [1 - (\delta a_1)](\delta a_0)}{[1 - (\delta a_1)](\delta b_1)\xi + [1 - (\delta a_1)][1 + (\delta b_0)]} \\ &= \frac{\xi + (\delta a_0)}{(\delta b_1)\xi + [1 + (\tilde{\delta b}_0)]}. \end{aligned}$$

where $\tilde{\delta b}_0 = \delta b_0 - \delta a_1$. In the last step, we neglect the terms of order higher than one. Therefore, by the action of normalizing the coefficient of ξ to 1, we can eliminate one parameter in the above expression for the rational map. Following the procedure used to obtain (3.10), (3.12) and (3.13), we can determine the matrices \mathcal{X}_2 , \mathcal{Y}_2 and \mathcal{I}_2 in terms of the parameters δa_i 's and δb_i 's appearing implicitly in (3.15). Then it is relatively easy to obtain the matrices \mathcal{X}_2 , \mathcal{Y}_2 and \mathcal{I}_2 . It is important to note that these parameters, δa_i and δb_i , are complex parameters.

The rational map for $B = 2$ is

$$R(\xi) = \xi^2.$$

Therefore, the perturbed rational map is given by

$$R(\xi, t) = \frac{[1 + (\delta a_2)]\xi^2 + (\delta a_1)\xi + (\delta a_0)}{(\delta b_2)\xi^2 + (\delta b_1)\xi + [1 + (\delta b_0)]}.$$

As for $B = 2$, we can normalize the coefficient of the highest power of ξ in the numerator, *i.e.* ξ^2 , to one, which leads to the following expression

$$R(\xi, t) = \frac{\xi^2 + (\delta a_1)\xi + (\delta a_0)}{(\delta b_2)\xi^2 + (\delta b_1)\xi + [1 + (\tilde{\delta b}_0)]}.$$

By doing so we have (10×10) matrices for \mathcal{X}_2 , \mathcal{Y}_2 and \mathcal{I}_2 .

In the following, we will show how to derive the matrix expressions of \mathcal{X}_2 , \mathcal{Y}_2 and \mathcal{I}_2 in the general case, *i.e.* for any value of baryon number B . We will compute

the matrix \mathcal{I}_2 as an example; the procedure for computing the matrices \mathcal{X}_2 and \mathcal{Y}_2 is exactly the same. From (3.15), we know

$$\mathcal{I} = \mathcal{I}_0 + V_\alpha (\mathcal{I}_2)_{\alpha\beta} V_\beta .$$

Then we differentiate both sides of the above equality with respect to V_i first and then to V_j :

$$\begin{aligned} \frac{\partial^2 \mathcal{I}}{\partial V_j \partial V_i} &= \frac{\partial}{\partial V_j} \left[\left(\frac{\partial V_\alpha}{\partial V_i} \right) (\mathcal{I}_2)_{\alpha\beta} V_\beta + V_\alpha (\mathcal{I}_2)_{\alpha\beta} \left(\frac{\partial V_\beta}{\partial V_i} \right) \right] \\ &= \frac{\partial}{\partial V_j} \left[\delta_{\alpha i} (\mathcal{I}_2)_{\alpha\beta} V_\beta + V_\alpha (\mathcal{I}_2)_{\alpha\beta} \delta_{\beta i} \right] \\ &= \frac{\partial}{\partial V_j} \left[(\mathcal{I}_2)_{i\beta} V_\beta + V_\alpha (\mathcal{I}_2)_{\alpha i} \right] \\ &= (\mathcal{I}_2)_{i\beta} \delta_{\beta j} + \delta_{\alpha j} (\mathcal{I}_2)_{\alpha i} \\ &= (\mathcal{I}_2)_{ij} + (\mathcal{I}_2)_{ji} . \end{aligned}$$

The order in which one takes the differentiation of \mathcal{I} with respect to V_i and V_j does not affect the result, *i.e.*

$$\frac{\partial^2 \mathcal{I}}{\partial V_j \partial V_i} = \frac{\partial^2 \mathcal{I}}{\partial V_i \partial V_j} ,$$

therefore

$$(\mathcal{I}_2)_{ij} = (\mathcal{I}_2)_{ji} ,$$

which means that the matrix \mathcal{I}_2 is symmetric with respect to the exchange of the index i and j . This leads to the following explicit expression of the matrix of \mathcal{I}_2 :

$$(\mathcal{I}_2)_{ij} = \frac{1}{2} \left(\frac{\partial^2 \mathcal{I}}{\partial V_i \partial V_j} \right) ,$$

where \mathcal{I} is given in (3.11).

Here we list the matrices of \mathcal{X}_2 , \mathcal{Y}_2 and \mathcal{I}_2 for the different values of B 's.

$$\mathcal{Y}_2 = \begin{pmatrix} \lambda_2 & 0 & 0 & 0 & 0 & 0 & 0 & 0 & 0 & 0 \\ 0 & \lambda_2 & 0 & 0 & 0 & 0 & 0 & 0 & 0 & 0 \\ 0 & 0 & \frac{2}{3} & 0 & 0 & 0 & 0 & 0 & 0 & 0 \\ 0 & 0 & 0 & \frac{2}{3} & 0 & 0 & 0 & 0 & 0 & 0 \\ 0 & 0 & 0 & 0 & \frac{2}{3} & 0 & 0 & 0 & 0 & 0 \\ 0 & 0 & 0 & 0 & 0 & \frac{2}{3} & 0 & 0 & 0 & 0 \\ 0 & 0 & 0 & 0 & 0 & 0 & \lambda_2 & 0 & 0 & 0 \\ 0 & 0 & 0 & 0 & 0 & 0 & 0 & \lambda_2 & 0 & 0 \\ 0 & 0 & 0 & 0 & 0 & 0 & 0 & 0 & \frac{1}{3} & 0 \\ 0 & 0 & 0 & 0 & 0 & 0 & 0 & 0 & 0 & \frac{1}{3} \end{pmatrix},$$

$$\mathcal{I}_2 = \begin{pmatrix} \lambda_4 & 0 & 0 & 0 & 0 & 0 & \lambda_4 & 0 & 0 & 0 \\ 0 & \lambda_4 & 0 & 0 & 0 & 0 & 0 & -\lambda_4 & 0 & 0 \\ 0 & 0 & \lambda_5 & 0 & \lambda_5 & 0 & 0 & 0 & 0 & 0 \\ 0 & 0 & 0 & \lambda_5 & 0 & -\lambda_5 & 0 & 0 & 0 & 0 \\ 0 & 0 & \lambda_5 & 0 & \lambda_5 & 0 & 0 & 0 & 0 & 0 \\ 0 & 0 & 0 & -\lambda_5 & 0 & \lambda_5 & 0 & 0 & 0 & 0 \\ \lambda_4 & 0 & 0 & 0 & 0 & 0 & \lambda_4 & 0 & 0 & 0 \\ 0 & -\lambda_4 & 0 & 0 & 0 & 0 & 0 & \lambda_4 & 0 & 0 \\ 0 & 0 & 0 & 0 & 0 & 0 & 0 & 0 & \lambda_6 & 0 \\ 0 & 0 & 0 & 0 & 0 & 0 & 0 & 0 & 0 & 0 \end{pmatrix},$$

with $\lambda_1 = 0.1426990817$, $\lambda_2 = 0.3926990817$, $\lambda_3 = 0.1073009183$, $\lambda_4 = 2.118731497$, $\lambda_5 = 10.83112047$, and $\lambda_6 = 4\lambda_2 = 1.570796327$.

□ $B = 4$

$$\mathcal{X}_2 = \left(L_{18 \times 9} \mid R_{18 \times 9} \right) ;$$

$$L_{18 \times 9} = \begin{pmatrix} \lambda_7 & 0 & 0 & 0 & 0 & 0 & 0 & 0 & 0 \\ 0 & \lambda_7 & 0 & 0 & 0 & 0 & 0 & 0 & 0 \\ 0 & 0 & \lambda_{10} & 0 & 0 & 0 & 0 & \lambda_{11} & 0 \\ 0 & 0 & 0 & \lambda_{10} & 0 & 0 & -\lambda_{11} & 0 & -\lambda_{12} \\ 0 & 0 & 0 & 0 & \lambda_7 & 0 & 0 & 0 & 0 \\ 0 & 0 & 0 & 0 & 0 & \lambda_7 & 0 & 0 & 0 \\ 0 & 0 & 0 & -\lambda_{11} & 0 & 0 & \lambda_{14} & 0 & -\lambda_{15} \\ 0 & 0 & \lambda_{11} & 0 & 0 & 0 & 0 & \lambda_{14} & 0 \\ 0 & 0 & 0 & -\lambda_{12} & 0 & 0 & -\lambda_{15} & 0 & \lambda_{14} \\ 0 & 0 & \lambda_{12} & 0 & 0 & 0 & 0 & -\lambda_{15} & 0 \\ \lambda_8 & 0 & 0 & 0 & 0 & -\lambda_9 & 0 & 0 & 0 \\ 0 & \lambda_8 & 0 & 0 & \lambda_9 & 0 & 0 & 0 & 0 \\ 0 & 0 & \lambda_{13} & 0 & 0 & 0 & 0 & -\lambda_{12} & 0 \\ 0 & 0 & 0 & \lambda_{13} & 0 & 0 & \lambda_{12} & 0 & \lambda_{11} \\ 0 & -\lambda_9 & 0 & 0 & \lambda_8 & 0 & 0 & 0 & 0 \\ \lambda_9 & 0 & 0 & 0 & 0 & \lambda_8 & 0 & 0 & 0 \\ 0 & 0 & 0 & -\lambda_{12} & 0 & 0 & -\lambda_{16} & 0 & -\lambda_{17} \\ 0 & 0 & \lambda_{12} & 0 & 0 & 0 & 0 & -\lambda_{16} & 0 \end{pmatrix} ,$$

$$R_{18 \times 9} = \begin{pmatrix} 0 & \lambda_8 & 0 & 0 & 0 & 0 & \lambda_9 & 0 & 0 \\ 0 & 0 & \lambda_8 & 0 & 0 & -\lambda_9 & 0 & 0 & 0 \\ \lambda_{12} & 0 & 0 & \lambda_{13} & 0 & 0 & 0 & 0 & \lambda_{12} \\ 0 & 0 & 0 & 0 & \lambda_{13} & 0 & 0 & -\lambda_{12} & 0 \\ 0 & 0 & \lambda_9 & 0 & 0 & \lambda_8 & 0 & 0 & 0 \\ 0 & -\lambda_9 & 0 & 0 & 0 & 0 & \lambda_8 & 0 & 0 \\ 0 & 0 & 0 & 0 & \lambda_{12} & 0 & 0 & -\lambda_{16} & 0 \\ -\lambda_{15} & 0 & 0 & -\lambda_{12} & 0 & 0 & 0 & 0 & -\lambda_{16} \\ 0 & 0 & 0 & 0 & \lambda_{11} & 0 & 0 & -\lambda_{17} & 0 \\ \lambda_{14} & 0 & 0 & -\lambda_{11} & 0 & 0 & 0 & 0 & -\lambda_{17} \\ 0 & \lambda_7 & 0 & 0 & 0 & 0 & 0 & 0 & 0 \\ 0 & 0 & \lambda_7 & 0 & 0 & 0 & 0 & 0 & 0 \\ -\lambda_{11} & 0 & 0 & \lambda_{10} & 0 & 0 & 0 & 0 & -\lambda_{11} \\ 0 & 0 & 0 & 0 & \lambda_{10} & 0 & 0 & \lambda_{11} & 0 \\ 0 & 0 & 0 & 0 & 0 & \lambda_7 & 0 & 0 & 0 \\ 0 & 0 & 0 & 0 & 0 & 0 & \lambda_7 & 0 & 0 \\ 0 & 0 & 0 & 0 & \lambda_{11} & 0 & 0 & \lambda_{14} & 0 \\ -\lambda_{17} & 0 & 0 & -\lambda_{11} & 0 & 0 & 0 & 0 & \lambda_{14} \end{pmatrix},$$

$$\lambda_7 = 0.01592318262, \lambda_8 = 0.002753257980, \lambda_9 = 0.004768782708,$$

$$\lambda_{10} = 0.01041666666, \lambda_{11} = 0.003949376413, \lambda_{12} = 0.00704640975, \lambda_{13} = 0.004068246566,$$

$$\lambda_{14} = 0.06309636525, \lambda_{15} = 0.001191707776, \lambda_{16} = 0.02321777162, \lambda_{17} = 0.000596365255.$$

$$\mathcal{Y}_2 = \left(L_{18 \times 9} \mid R_{18 \times 9} \right) ;$$

$$L_{18 \times 9} = \begin{pmatrix} \lambda_{18} & 0 & 0 & 0 & 0 & 0 & 0 & 0 & 0 \\ 0 & \lambda_{18} & 0 & 0 & 0 & 0 & 0 & 0 & 0 \\ 0 & 0 & \lambda_{21} & 0 & 0 & 0 & 0 & \lambda_{22} & 0 \\ 0 & 0 & 0 & \lambda_{21} & 0 & 0 & -\lambda_{22} & 0 & -\lambda_{22} \\ 0 & 0 & 0 & 0 & \lambda_{18} & 0 & 0 & 0 & 0 \\ 0 & 0 & 0 & 0 & 0 & \lambda_{18} & 0 & 0 & 0 \\ 0 & 0 & 0 & -\lambda_{22} & 0 & 0 & \lambda_{24} & 0 & -\lambda_{25} \\ 0 & 0 & \lambda_{22} & 0 & 0 & 0 & 0 & \lambda_{24} & 0 \\ 0 & 0 & 0 & -\lambda_{22} & 0 & 0 & -\lambda_{25} & 0 & \lambda_{24} \\ 0 & 0 & \lambda_{22} & 0 & 0 & 0 & 0 & -\lambda_{25} & 0 \\ \lambda_{19} & 0 & 0 & 0 & 0 & -\lambda_{20} & 0 & 0 & 0 \\ 0 & \lambda_{19} & 0 & 0 & \lambda_{20} & 0 & 0 & 0 & 0 \\ 0 & 0 & \lambda_{23} & 0 & 0 & 0 & 0 & -\lambda_{22} & 0 \\ 0 & 0 & 0 & \lambda_{23} & 0 & 0 & \lambda_{22} & 0 & \lambda_{22} \\ 0 & -\lambda_{20} & 0 & 0 & \lambda_{19} & 0 & 0 & 0 & 0 \\ \lambda_{20} & 0 & 0 & 0 & 0 & \lambda_{19} & 0 & 0 & 0 \\ 0 & 0 & 0 & -\lambda_{22} & 0 & 0 & -\lambda_{26} & 0 & -\lambda_{27} \\ 0 & 0 & \lambda_{22} & 0 & 0 & 0 & 0 & -\lambda_{26} & 0 \end{pmatrix} ,$$

$$R_{18 \times 9} = \begin{pmatrix} 0 & \lambda_{19} & 0 & 0 & 0 & 0 & \lambda_{20} & 0 & 0 \\ 0 & 0 & \lambda_{19} & 0 & 0 & -\lambda_{20} & 0 & 0 & 0 \\ \lambda_{22} & 0 & 0 & \lambda_{23} & 0 & 0 & 0 & 0 & \lambda_{22} \\ 0 & 0 & 0 & 0 & \lambda_{23} & 0 & 0 & -\lambda_{22} & 0 \\ 0 & 0 & \lambda_{20} & 0 & 0 & \lambda_{19} & 0 & 0 & 0 \\ 0 & -\lambda_{20} & 0 & 0 & 0 & 0 & \lambda_{19} & 0 & 0 \\ 0 & 0 & 0 & 0 & \lambda_{22} & 0 & 0 & -\lambda_{26} & 0 \\ -\lambda_{25} & 0 & 0 & -\lambda_{22} & 0 & 0 & 0 & 0 & -\lambda_{26} \\ 0 & 0 & 0 & 0 & \lambda_{22} & 0 & 0 & -\lambda_{27} & 0 \\ \lambda_{24} & 0 & 0 & -\lambda_{22} & 0 & 0 & 0 & 0 & -\lambda_{27} \\ 0 & \lambda_{18} & 0 & 0 & 0 & 0 & 0 & 0 & 0 \\ 0 & 0 & \lambda_{18} & 0 & 0 & 0 & 0 & 0 & 0 \\ -\lambda_{22} & 0 & 0 & \lambda_{21} & 0 & 0 & 0 & 0 & -\lambda_{22} \\ 0 & 0 & 0 & 0 & \lambda_{21} & 0 & 0 & \lambda_{22} & 0 \\ 0 & 0 & 0 & 0 & 0 & \lambda_{18} & 0 & 0 & 0 \\ 0 & 0 & 0 & 0 & 0 & 0 & \lambda_{18} & 0 & 0 \\ 0 & 0 & 0 & 0 & \lambda_{22} & 0 & 0 & \lambda_{24} & 0 \\ -\lambda_{27} & 0 & 0 & -\lambda_{22} & 0 & 0 & 0 & 0 & \lambda_{24} \end{pmatrix},$$

$$\lambda_{18} = 0.06960881885, \lambda_{19} = 0.00791687494,$$

$$\lambda_{20} = 0.01371242963, \lambda_{21} = 0.04166666666, \lambda_{22} = 0.02405626122, \lambda_{23} = 0.01388888889,$$

$$\lambda_{24} = 0.26421763770, \lambda_{25} = 0.00999916692, \lambda_{26} = 0.07333416640, \lambda_{27} = 0.01421763772.$$

$$\mathcal{I}_2 = \left(L_{18 \times 9} \mid R_{18 \times 9} \right) ;$$

$$L_{18 \times 9} = \begin{pmatrix} \lambda_{28} & \lambda_{29} & 0 & 0 & -\lambda_{30} & 0 & 0 & 0 & 0 \\ \lambda_{29} & \lambda_{28} & 0 & 0 & 0 & \lambda_{30} & 0 & 0 & 0 \\ 0 & 0 & \lambda_{34} & 0 & 0 & 0 & 0 & \lambda_{35} & 0 \\ 0 & 0 & 0 & \lambda_{36} & 0 & 0 & \lambda_{37} & 0 & -\lambda_{38} \\ -\lambda_{30} & 0 & 0 & 0 & \lambda_{28} & \lambda_{29} & 0 & 0 & 0 \\ 0 & \lambda_{30} & 0 & 0 & \lambda_{29} & \lambda_{28} & 0 & 0 & 0 \\ 0 & 0 & 0 & \lambda_{37} & 0 & 0 & \lambda_{40} & 0 & \lambda_{41} \\ 0 & 0 & \lambda_{35} & 0 & 0 & 0 & 0 & \lambda_{43} & 0 \\ 0 & 0 & 0 & -\lambda_{38} & 0 & 0 & \lambda_{41} & 0 & \lambda_{40} \\ 0 & 0 & -\lambda_{35} & 0 & 0 & 0 & 0 & \lambda_{44} & 0 \\ \lambda_{31} & 0 & 0 & 0 & -\lambda_{32} & -\lambda_{33} & 0 & 0 & 0 \\ 0 & \lambda_{31} & 0 & 0 & \lambda_{33} & \lambda_{32} & 0 & 0 & 0 \\ 0 & 0 & \lambda_{34} & 0 & 0 & 0 & 0 & \lambda_{35} & 0 \\ 0 & 0 & 0 & \lambda_{39} & 0 & 0 & \lambda_{38} & 0 & -\lambda_{37} \\ -\lambda_{32} & -\lambda_{33} & 0 & 0 & \lambda_{31} & 0 & 0 & 0 & 0 \\ \lambda_{33} & \lambda_{32} & 0 & 0 & 0 & \lambda_{31} & 0 & 0 & 0 \\ 0 & 0 & 0 & -\lambda_{38} & 0 & 0 & -\lambda_{42} & 0 & \lambda_{45} \\ 0 & 0 & -\lambda_{35} & 0 & 0 & 0 & 0 & -\lambda_{43} & 0 \end{pmatrix} ,$$

$$R_{18 \times 9} = \begin{pmatrix} 0 & \lambda_{31} & 0 & 0 & 0 & -\lambda_{32} & \lambda_{33} & 0 & 0 \\ 0 & 0 & \lambda_{31} & 0 & 0 & -\lambda_{33} & \lambda_{32} & 0 & 0 \\ -\lambda_{35} & 0 & 0 & \lambda_{34} & 0 & 0 & 0 & 0 & -\lambda_{35} \\ 0 & 0 & 0 & 0 & \lambda_{39} & 0 & 0 & -\lambda_{38} & 0 \\ 0 & -\lambda_{32} & \lambda_{33} & 0 & 0 & \lambda_{31} & 0 & 0 & 0 \\ 0 & -\lambda_{33} & \lambda_{32} & 0 & 0 & 0 & \lambda_{31} & 0 & 0 \\ 0 & 0 & 0 & 0 & \lambda_{38} & 0 & 0 & -\lambda_{42} & 0 \\ \lambda_{44} & 0 & 0 & \lambda_{35} & 0 & 0 & 0 & 0 & -\lambda_{43} \\ 0 & 0 & 0 & 0 & -\lambda_{37} & 0 & 0 & \lambda_{45} & 0 \\ \lambda_{43} & 0 & 0 & -\lambda_{35} & 0 & 0 & 0 & 0 & -\lambda_{44} \\ 0 & \lambda_{28} & -\lambda_{29} & 0 & 0 & -\lambda_{30} & 0 & 0 & 0 \\ 0 & -\lambda_{29} & \lambda_{28} & 0 & 0 & 0 & \lambda_{30} & 0 & 0 \\ -\lambda_{35} & 0 & 0 & \lambda_{34} & 0 & 0 & 0 & 0 & -\lambda_{35} \\ 0 & 0 & 0 & 0 & \lambda_{36} & 0 & 0 & -\lambda_{37} & 0 \\ 0 & -\lambda_{30} & 0 & 0 & 0 & \lambda_{28} & -\lambda_{29} & 0 & 0 \\ 0 & 0 & \lambda_{30} & 0 & 0 & -\lambda_{29} & \lambda_{28} & 0 & 0 \\ 0 & 0 & 0 & 0 & -\lambda_{37} & 0 & 0 & \lambda_{40} & 0 \\ -\lambda_{44} & 0 & 0 & -\lambda_{35} & 0 & 0 & 0 & 0 & \lambda_{43} \end{pmatrix},$$

$$\lambda_{28} = 1.0073061060, \lambda_{29} = 0.2421657202,$$

$$\lambda_{30} = 0.1398144437, \lambda_{31} = 0.3961029148, \lambda_{32} = 0.0645286115, \lambda_{33} = 0.6860703735,$$

$$\lambda_{34} = 0.3979362461, \lambda_{35} = 0.6892457965, \lambda_{36} = 1.3228659620, \lambda_{37} = 0.9127794640,$$

$$\lambda_{38} = 2.2912710560, \lambda_{39} = 0.5269934690, \lambda_{40} = 6.5424678700, \lambda_{41} = 0.1324884752,$$

$$\lambda_{42} = 3.2944492900, \lambda_{43} = 2.6491631740, \lambda_{44} = 0.2615456982, \lambda_{45} = 1.3947278980,$$

5.2 Eigenvalues and Eigenvectors

In order to compute the A_{ij} and D_{ij} in (3.23) and (3.24) respectively, we need the matrices \mathcal{X}_2 , \mathcal{Y}_2 and \mathcal{I}_2 , and values of Γ_1 , Γ_2 and Γ_3 . With the matrices \mathcal{X}_2 , \mathcal{Y}_2

and \mathcal{I}_2 calculated and then listed above, we next have to find the values of Γ_1 , Γ_2 and Γ_3 . By the definition in (3.25), we can compute the different values of Γ_1 , Γ_2 and Γ_3 for different sets of parameters, such as baryon number B , mass m and potential parameter p , this is because the profile function we input into the integral of (3.23) and (3.24) comes from the solution of (2.30), where three parameters are needed. Within the same baryon number B , different sets of (m, p) lead to different profile functions and then of course the values of $(\Gamma_1, \Gamma_2, \Gamma_3)$ change. However, the eigenvectors of $(A^{-1} \cdot D)$ calculated with different sets of $(\Gamma_1, \Gamma_2, \Gamma_3)$ will not be affected by the changing values of Γ 's, but the eigenvalues will be. We will present the results which show how the eigenvalues vary with the mass m and the potential parameter p later.

Here we take $(\Gamma_1, \Gamma_2, \Gamma_3) = (4.28869, 0.872418, 0.370159)$, $(7.58651, 0.96429, 0.16419)$ and $(12.2868, 1.02577, 0.0895335)$ respectively to compute the eigenvectors and eigenvalues of $(A^{-1} \cdot D)$ for $(B, m, p) = (1, 0, 0)$, $(2, 0, 0)$ and $(4, 0, 0)$ ¹ by using two mathematical softwares Maple and Mathematica², and the results are as follows:

□ $B = 1$ ($\Gamma_1 = 4.28869, \Gamma_2 = 0.872418, \Gamma_3 = 0.370159$)³

$$\text{eigenvalues} = \begin{pmatrix} 0 & 0 & 0 & \Lambda_1 & \Lambda_1 & \Lambda_1 \end{pmatrix},$$

$$\text{eigenvectors} = \begin{pmatrix} -\varepsilon & 0 & 0 & \varepsilon & 0 & 0 \\ 0 & i\varepsilon & 0 & 0 & -i\varepsilon & 0 \\ \varepsilon & 0 & 0 & \varepsilon & 0 & 0 \\ 0 & i\varepsilon & 0 & 0 & i\varepsilon & 0 \\ 0 & 0 & 0 & 0 & 0 & \varepsilon \\ 0 & 0 & i\varepsilon & 0 & 0 & 0 \end{pmatrix},$$

with $\Lambda_1 = 0.573767$.

¹In fact, when $m = 0$, it does not matter what value we choose for p .

²Maple 10 and Mathematica 5.2.

³These Γ 's values are calculated from (3.25) by using numerical method.

Here we use the notation of putting the eigenvalues and eigenvectors into a row vector⁴ and matrix form respectively. The n -th entry of this “eigenvalues” row vector is the eigenvalue corresponding to the eigenvector represented as the n -th column in the “eigenvectors” matrix. For example, for the eigenvectors

$$\begin{pmatrix} 0 \\ i\varepsilon \\ 0 \\ i\varepsilon \\ 0 \\ 0 \end{pmatrix} \text{ and } \begin{pmatrix} \varepsilon \\ 0 \\ \varepsilon \\ 0 \\ 0 \\ 0 \end{pmatrix},$$

the eigenvalues are 0 and $\Lambda_1=0.5737$.

□ $B = 2$ ($\Gamma_1 = 7.58651$, $\Gamma_2 = 0.96429$, $\Gamma_3 = 0.16419$)

$$\text{eigenvalues} = \left(0 \ 0 \ 0 \ 0 \ 0 \ \Lambda_2 \ \Lambda_3 \ \Lambda_3 \ \Lambda_4 \ \Lambda_4 \right),$$

$$\text{eigenvectors} = \begin{pmatrix} 0 & -\varepsilon & 0 & 0 & 0 & 0 & 0 & \varepsilon & 0 & 0 \\ i\varepsilon & 0 & 0 & 0 & 0 & 0 & -i\varepsilon & 0 & 0 & 0 \\ 0 & 0 & 0 & -\varepsilon & 0 & 0 & 0 & 0 & 0 & \varepsilon \\ 0 & 0 & i\varepsilon & 0 & 0 & 0 & 0 & 0 & -i\varepsilon & 0 \\ 0 & 0 & 0 & \varepsilon & 0 & 0 & 0 & 0 & 0 & \varepsilon \\ 0 & 0 & i\varepsilon & 0 & 0 & 0 & 0 & 0 & i\varepsilon & 0 \\ 0 & \varepsilon & 0 & 0 & 0 & 0 & 0 & \varepsilon & 0 & 0 \\ i\varepsilon & 0 & 0 & 0 & 0 & 0 & i\varepsilon & 0 & 0 & 0 \\ 0 & 0 & 0 & 0 & 0 & \varepsilon & 0 & 0 & 0 & 0 \\ 0 & 0 & 0 & 0 & i\varepsilon & 0 & 0 & 0 & 0 & 0 \end{pmatrix},$$

with $\Lambda_2 = 0.227139$, $\Lambda_3 = 0.476128$, $\Lambda_4 = 0.981957$.

⁴For $B = 4$ case, we put all the eigenvalues in a column vector instead of a row vector.

□ $B = 4$ ($\Gamma_1 = 12.2868$, $\Gamma_2 = 1.02577$, $\Gamma_3 = 0.0895335$)

$$\text{eigenvalues} = \begin{pmatrix} 0 \\ 0 \\ 0 \\ 0 \\ 0 \\ 0 \\ 0.210307 \\ 0.210307 \\ 0.210307 \\ 0.371290 \\ 0.371290 \\ 0.371290 \\ 0.546893 \\ 0.546893 \\ 0.546893 \\ 0.669111 \\ 0.669111 \\ 1.289260 \end{pmatrix}, \quad \text{eigenvectors}^5 = \begin{pmatrix} 18 \times 18 \text{ matrix} \end{pmatrix}.$$

Now we try to understand the meaning of these eigenvalues and eigenvectors. Tracing back the origin of these eigenvectors, we can find that they are the vectors defined in (3.14), which are related to (3.8) and (3.9). Therefore we restore these eigenvectors to the perturbed rational maps as follows:

⁵Because the eighteen eigenvectors are hard to write as an 18×18 matrix on a single page, we give them separately in the following sections.

□ $B = 1$

$$\vec{v}_{R_1} = \begin{pmatrix} -\varepsilon \\ 0 \\ \varepsilon \\ 0 \\ 0 \\ 0 \end{pmatrix} \Rightarrow R_1 = \frac{\xi - \varepsilon}{1 + \varepsilon\xi}, \quad \vec{v}_{R_2} = \begin{pmatrix} 0 \\ i\varepsilon \\ 0 \\ i\varepsilon \\ 0 \\ 0 \end{pmatrix} \Rightarrow R_2 = \frac{\xi + i\varepsilon}{1 + i\varepsilon\xi},$$

$$\vec{v}_{R_3} = \begin{pmatrix} 0 \\ 0 \\ 0 \\ 0 \\ 0 \\ i\varepsilon \end{pmatrix} \Rightarrow R_3 = \frac{\xi}{1 + i\varepsilon}, \quad \vec{v}_{R_4} = \begin{pmatrix} \varepsilon \\ 0 \\ \varepsilon \\ 0 \\ 0 \\ 0 \end{pmatrix} \Rightarrow R_4 = \frac{\xi + \varepsilon}{1 + \varepsilon\xi},$$

$$\vec{v}_{R_5} = \begin{pmatrix} 0 \\ -i\varepsilon \\ 0 \\ i\varepsilon \\ 0 \\ 0 \end{pmatrix} \Rightarrow R_5 = \frac{\xi - i\varepsilon}{1 + i\varepsilon\xi}, \quad \vec{v}_{R_6} = \begin{pmatrix} 0 \\ 0 \\ 0 \\ 0 \\ \varepsilon \\ 0 \end{pmatrix} \Rightarrow R_6 = \frac{\xi}{1 + \varepsilon}.$$

□ $B = 2$

$$\vec{v}_{R_1} = \begin{pmatrix} 0 \\ i\varepsilon \\ 0 \\ 0 \\ 0 \\ 0 \\ 0 \\ i\varepsilon \\ 0 \\ 0 \end{pmatrix} \Rightarrow R_1 = \frac{\xi^2 + i\varepsilon\xi}{1 + i\varepsilon\xi}, \quad \vec{v}_{R_2} = \begin{pmatrix} -\varepsilon \\ 0 \\ 0 \\ 0 \\ 0 \\ 0 \\ 0 \\ \varepsilon \\ 0 \\ 0 \end{pmatrix} \Rightarrow R_2 = \frac{\xi^2 - \varepsilon\xi}{1 + \varepsilon\xi},$$

$$\vec{v}_{R_3} = \begin{pmatrix} 0 \\ 0 \\ 0 \\ i\varepsilon \\ 0 \\ i\varepsilon \\ 0 \\ 0 \\ 0 \\ 0 \end{pmatrix} \Rightarrow R_3 = \frac{\xi^2 + i\varepsilon}{1 + i\varepsilon\xi^2}, \quad \vec{v}_{R_4} = \begin{pmatrix} 0 \\ 0 \\ -\varepsilon \\ 0 \\ \varepsilon \\ 0 \\ 0 \\ 0 \\ 0 \\ 0 \end{pmatrix} \Rightarrow R_4 = \frac{\xi^2 - \varepsilon}{1 + \varepsilon\xi^2},$$

$$\vec{v}_{R_5} = \begin{pmatrix} 0 \\ 0 \\ 0 \\ 0 \\ 0 \\ 0 \\ 0 \\ 0 \\ 0 \\ i\varepsilon \end{pmatrix} \Rightarrow R_5 = \frac{\xi^2}{1+i\varepsilon}, \quad \vec{v}_{R_6} = \begin{pmatrix} 0 \\ 0 \\ 0 \\ 0 \\ 0 \\ 0 \\ 0 \\ 0 \\ \varepsilon \\ 0 \end{pmatrix} \Rightarrow R_6 = \frac{\xi^2}{1+\varepsilon},$$

$$\vec{v}_{R_7} = \begin{pmatrix} 0 \\ -i\varepsilon \\ 0 \\ 0 \\ 0 \\ 0 \\ 0 \\ 0 \\ i\varepsilon \\ 0 \\ 0 \end{pmatrix} \Rightarrow R_7 = \frac{\xi^2 - i\varepsilon\xi}{1+i\varepsilon\xi}, \quad \vec{v}_{R_8} = \begin{pmatrix} \varepsilon \\ 0 \\ 0 \\ 0 \\ 0 \\ 0 \\ 0 \\ \varepsilon \\ 0 \\ 0 \\ 0 \end{pmatrix} \Rightarrow R_8 = \frac{\xi^2 + \varepsilon\xi}{1+\varepsilon\xi},$$

$$\vec{v}_{R_9} = \begin{pmatrix} 0 \\ 0 \\ 0 \\ -i\varepsilon \\ 0 \\ i\varepsilon \\ 0 \\ 0 \\ 0 \\ 0 \end{pmatrix} \Rightarrow R_9 = \frac{\xi^2 - i\varepsilon}{1 + i\varepsilon\xi^2}, \quad \vec{v}_{R_{10}} = \begin{pmatrix} 0 \\ 0 \\ \varepsilon \\ 0 \\ \varepsilon \\ 0 \\ 0 \\ 0 \\ 0 \\ 0 \end{pmatrix} \Rightarrow R_{10} = \frac{\xi^2 + \varepsilon}{1 + \varepsilon\xi^2}.$$

□ $B = 4$

The eigenvectors for the $B = 4$ case will be presented soon in a separated section because of its complicated character.

It is mentioned in the previous paragraph of this section that the eigenvalues of the matrix $(A^{-1} \cdot D)$ vary with the mass m and potential parameter p and here we arrive at showing the relation between them in the following plots.

By solving (2.30) to generate the unperturbed profile functions $f_0(r)$ of different sets of parameters (m, p) and using them to compute the values $(\Gamma_1, \Gamma_2, \Gamma_3)$, we can then calculate the eigenvalues of the matrix $(A^{-1} \cdot D)$ for a certain set of parameter (m, p) . The parameter for the mass m is chosen out of the set $\{ 0, 0.2, 0.4, 0.6, 0.8, 1.0, 1.5, 2.0 \}$ and the potential parameter p is from $\{ 1, 2, 3, 4 \}$.

In the $B = 1$ case, there is only one degenerate eigenvalue, and we put all the data collected from different parameters (m, p) into one graph. We can see that as the mass parameter m increases, the eigenvalues for different potential parameters p increases as well. Furthermore, for any specific value of mass parameter m except for $m = 0$, the eigenvalue derived from the lower value of potential parameter p has the higher value and this phenomenon also happens in the cases of $B = 2$ and $B = 4$. We have to emphasize that the eigenvalue of the matrix $(A^{-1} \cdot D)$ represents

the vibrating frequency of the perturbed rational map around the unperturbed one, which is taken in the rational map ansatz for the Skyrmion.

In the $B = 2$ case, we also plot the data of three eigenvalues for different parameters (m, p) in single graph. However, there are five eigenvalues in the $B = 4$ case, and it would look crowded if we inserted the data into one graph. Hence, we choose to present them in four separate graphs, one for each potential parameter p .

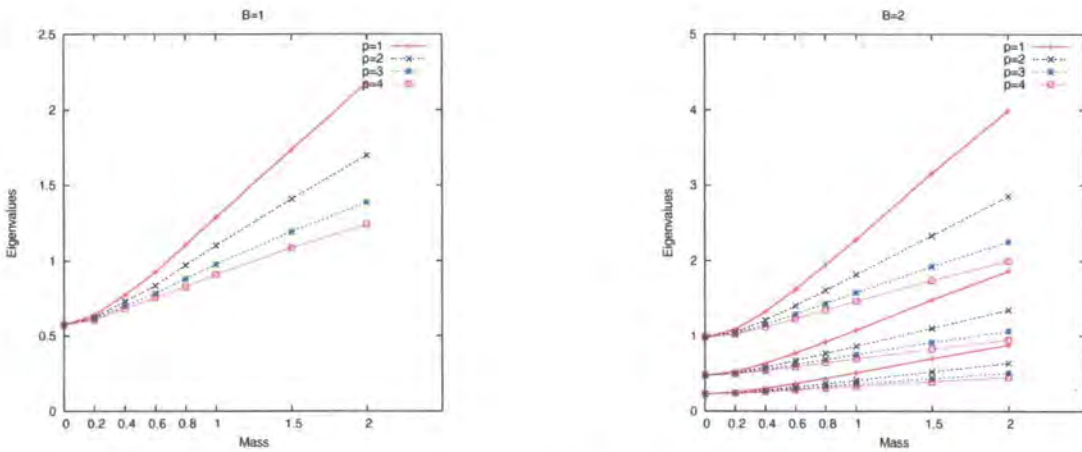


Figure 5.1: The eigenvalues versus mass for different potential parameters p . (Left) $B = 1$, (Right) $B = 2$.

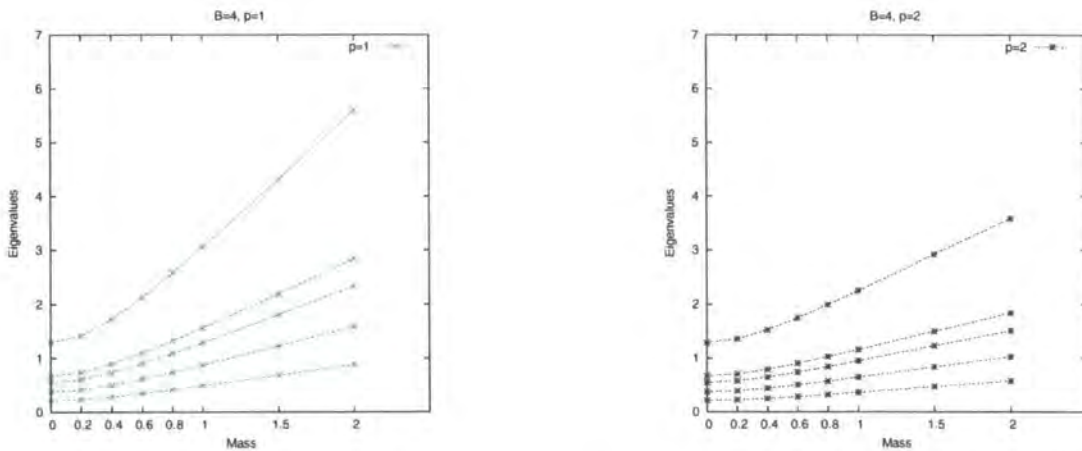


Figure 5.2: The eigenvalues versus mass for different potential parameters p for $B = 4$. (Left) $p = 1$, (Right) $p = 2$.

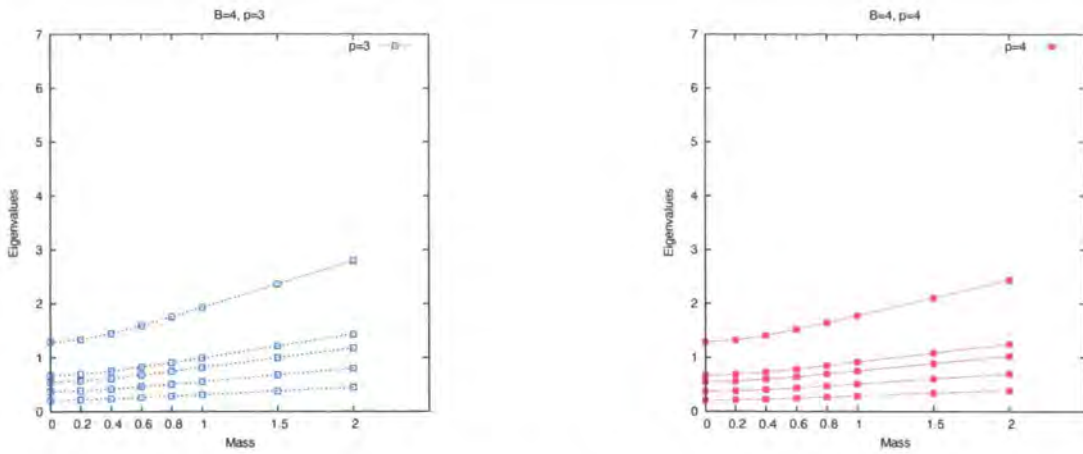


Figure 5.3: The eigenvalues versus mass for $B = 4$. (Left) $p = 3$, (Right) $p = 4$.

5.3 Broken Zero Mode

Simply speaking, a zero mode is a mode with an eigenvalue 0 resulting from the symmetry of the model; or the zero modes are the field configurations obtained by performing the symmetry transformations of the model on the stable, equilibrium field configuration without changing its energy. For the Skyrme model, there exists the rotational, isorotational, and translational symmetry for the Lagrangian, so that, in general, there are nine zero modes.

In this thesis, the Skyrmions are approximated by the rational map ansatz. The rational map can be obtained from the monopole in two different ways. The first one came from Donaldson [33], and the second from Jarvis [44]. It was shown by Jarvis that there exists a 1-1 correspondence between $SU(2)$ charge N monopole and degree N rational maps (here the Jarvis maps). Thus taking the rational map ansatz for the baryon B Skyrmion means that it was constructed indirectly from a monopole of charge B . Because of the exact correspondence between the monopole and the rational maps, the vibrations of the rational map therefore correspond to the monopole motion on the monopole moduli space. Furthermore, it implies that, to some extent, a monopole motion can be mapped to a path in the configuration space of the Skyrme fields, meaning the vibrations of the rational map will be associated to the vibrations of the Skyrmions, leading to the zero modes and the vibrational modes.

However, within the rational map ansatz, the origin of the coordinate is fixed.

Therefore, the translational modes would seem to be eliminated from the zero modes. As the argument above, we will show in this section that the translational zero modes do not completely disappear but are broken to become the non-genuine vibrational modes with a non-zero eigenvalue.

The rational map ansatz is based on treating the angular part of the domain space \mathbb{R}^3 as Riemann sphere \mathbb{S}^2 , and mapping it to the target space by the rational map. By taking the rational map ansatz, to fix the origin of the coordinate is necessary, and so that we can decompose the domain space into the radial part and the angular part. When a perturbation involving the translation in the domain space is carried out, the origin of the coordinate still can not be moved. It hence turns this translation into the angular part which at the end becomes the vibrational modes of the perturbed rational map. They are, however, not the genuine vibrational modes of the perturbed rational map but the broken translational zero modes, since it owes its origin to the translation, not to a real perturbation on the angular part, *i.e.* the rational map.

Based on this argument, we will show that some of our perturbed rational maps are the broken translational mode by discovering the coordinate transformation that turns the infinitesimal translations in the x , y and z direction into r , ξ and $\bar{\xi}$. To be precise, we are looking for the Jacobian matrix J for the coordinate transformation from (dx, dy, dz) to $(dr, d\xi, d\bar{\xi})$. Actually all we need is to find out how ξ is transformed under the translations. With the exact form of the transformations of ξ for dx , dy and dz discovered, we insert it to the unperturbed rational map, which is the BPS monopole solution adapted by the rational map ansatz, to get its associated perturbed rational map. Then we seek if any perturbed rational map obtained from the perturbation matches the rational map we just found and call it the broken translational zero mode.

However, we do not know how to derive the Jacobian matrix J directly. We then use an indirect way to develop J by combining J_1 and J_2 , which are Jacobian matrices for $(dr, d\phi, d\theta)$ to $(dr, d\xi, d\bar{\xi})$ and (dx, dy, dz) to $(dr, d\phi, d\theta)$ respectively,

with the definition of $\xi = \tan(\theta/2)e^{i\phi}$. Here is the relation between J , J_1 and J_2 :

$$\begin{pmatrix} dr \\ d\xi \\ d\bar{\xi} \end{pmatrix} = J \cdot \begin{pmatrix} dx \\ dy \\ dz \end{pmatrix} = J_1 \cdot \begin{pmatrix} dr \\ d\phi \\ d\theta \end{pmatrix} = J_1 \cdot J_2 \cdot \begin{pmatrix} dx \\ dy \\ dz \end{pmatrix},$$

with the definitions of J_1 and J_2 as

$$J_1 \equiv \begin{pmatrix} \frac{\partial r}{\partial r} & \frac{\partial r}{\partial \phi} & \frac{\partial r}{\partial \theta} \\ \frac{\partial \xi}{\partial r} & \frac{\partial \xi}{\partial \phi} & \frac{\partial \xi}{\partial \theta} \\ \frac{\partial \bar{\xi}}{\partial r} & \frac{\partial \bar{\xi}}{\partial \phi} & \frac{\partial \bar{\xi}}{\partial \theta} \end{pmatrix} = \begin{pmatrix} 1 & 0 & 0 \\ 0 & i\xi & \frac{\xi(1+|\xi|^2)}{2|\xi|} \\ 0 & -i\bar{\xi} & \frac{\bar{\xi}(1+|\xi|^2)}{2|\xi|} \end{pmatrix}$$

$$J_2 \equiv \begin{pmatrix} \frac{\partial r}{\partial x} & \frac{\partial r}{\partial y} & \frac{\partial r}{\partial z} \\ \frac{\partial \phi}{\partial x} & \frac{\partial \phi}{\partial y} & \frac{\partial \phi}{\partial z} \\ \frac{\partial \theta}{\partial x} & \frac{\partial \theta}{\partial y} & \frac{\partial \theta}{\partial z} \end{pmatrix} = \begin{pmatrix} \cos \phi \sin \theta & \sin \phi \sin \theta & \cos \theta \\ -\frac{\sin \phi}{r \sin \theta} & \frac{\cos \phi}{r \sin \theta} & 0 \\ \frac{\cos \phi \cos \theta}{r} & \frac{\sin \phi \cos \theta}{r} & -\frac{\sin \theta}{r} \end{pmatrix}.$$

Because of $\xi = \tan(\theta/2)e^{i\phi}$, using

$$\sin \theta = \frac{2|\xi|}{1+|\xi|^2}, \quad \cos \theta = \frac{1-|\xi|^2}{1+|\xi|^2}; \quad \sin \phi = \frac{-i(\xi - \bar{\xi})}{2|\xi|}, \quad \cos \phi = \frac{\xi + \bar{\xi}}{2|\xi|},$$

J hence takes the following form:

$$J = J_1 \cdot J_2 = \begin{pmatrix} \frac{\xi + \bar{\xi}}{1+|\xi|^2} & \frac{-i(\xi - \bar{\xi})}{1+|\xi|^2} & \frac{1-|\xi|^2}{1+|\xi|^2} \\ \frac{1-\xi^2}{2r} & \frac{i(1+\xi^2)}{2r} & -\frac{\xi}{r} \\ \frac{1-\bar{\xi}^2}{2r} & \frac{-i(1+\bar{\xi}^2)}{2r} & -\frac{\bar{\xi}}{r} \end{pmatrix}. \quad (5.3)$$

As we can see in the Jacobian matrix obtained above, there is an r dependence in some of the entries of the matrix J . However, as long as we set it to be r_0 for a fixed radius for the Riemann sphere, namely choosing a specific sphere, usually the unit sphere, it will not do any harm. Since it simply means that when the domain space decomposed into a set of concentric spheres with different radius r , the only difference for the effect of the transformation matrix J on the spheres of different radius, is the coefficients of the r dependence but not on the qualitative behaviour.

In the rest of this section, we want to show that some of the modes which seems to be the vibrational modes with non-zero eigenvalues are actually the broken zero modes, to be precise, the broken translational zero modes.

□ $B = 1$

From (5.3), we can see that under the transformation $z \rightarrow z + dz$ and $x \rightarrow x + dx$, the associated change in ξ will become

$$\begin{aligned} z \longrightarrow z + dz &\implies \xi \longrightarrow \xi + d\xi \equiv \xi(1 - \varepsilon), \quad \text{with } \varepsilon \equiv \frac{dz}{r}, \\ x \longrightarrow x + dx &\implies \xi \longrightarrow \xi + d\xi \equiv \xi + \varepsilon(1 - \xi^2), \quad \text{with } \varepsilon \equiv \frac{dx}{2r}. \end{aligned}$$

Here, by comparing with the result above, $R_6(\xi)$ and $R_4(\xi)$ can be shown as the broken z and x translational zero mode below:

$$R_6(\xi) = \frac{\xi}{1 + \varepsilon_6} \simeq \xi(1 - \varepsilon_6), \quad \text{with } \varepsilon_6 = \varepsilon = \frac{dz}{r},$$

$$R_4(\xi) = \frac{\xi + \varepsilon_4}{1 + \varepsilon_4\xi} \simeq (\xi + \varepsilon_4)(1 - \varepsilon_4\xi) \simeq \xi + \varepsilon_4(1 - \xi^2), \quad \text{with } \varepsilon_4 = \varepsilon = \frac{dx}{2r}.$$

Since the domain and target space of the perturbed rational map of $B = 1$ are the same, it is obvious that $R_6(\xi)$ and $R_4(\xi)$ have translations for $-\varepsilon_6\xi$ and $\varepsilon_4(1 - \xi^2)$ respectively from $R_0(\xi) = \xi$. Similarly, it can also be show that $R_5(\xi)$ is the y broken translational mode.

□ $B = 2$

For $B = 2$ case, since having had the Jacobian matrix J for the coordinate transformation, (5.3), we use the same way to show that $R_6(\xi)$ is the z broken translational mode as follows:

$$\begin{aligned} z &\longrightarrow z + dz \\ \implies \xi &\longrightarrow \xi + d\xi \equiv \xi(1 - \varepsilon), \quad \text{with } \varepsilon \equiv \frac{dz}{r}, \\ \implies \xi^2 &\longrightarrow \xi^2(1 - \varepsilon)^2 \simeq \xi^2(1 - 2\varepsilon), \end{aligned}$$

then

$$R_6(\xi) = \frac{\xi^2}{1 + \varepsilon_6} \simeq \xi^2(1 - \varepsilon_6), \quad \text{with } \varepsilon_6 = 2\varepsilon.$$

Since the rational map used for the rational map ansatz comes from the BPS monopole solution ξ^2 , we can see from the above that $R_6(\xi)$ indeed is the result from ξ^2 under the perturbation of $\xi \rightarrow \xi + d\xi$, which is the outcome of the translation in the z direction.

Likewise, $R_8(\xi)$ is the mode obtained under the x translation.

$$\begin{aligned} x &\longrightarrow x + dx, \\ \Rightarrow \quad \xi &\longrightarrow \xi + d\xi = \xi \left(1 + \frac{1 - \xi^2}{2r} dx\right) \equiv \xi + (1 - \xi^2)\varepsilon, \quad \varepsilon \equiv \frac{dx}{2r}, \\ \Rightarrow \quad \xi^2 &\longrightarrow (\xi + d\xi)^2 = (\xi + (1 - \xi^2)\varepsilon)^2 \simeq \xi^2 - 2\varepsilon\xi^3 + 2\varepsilon\xi, \end{aligned}$$

$$R_8 = \frac{\xi^2 + \varepsilon_8\xi}{1 + \varepsilon_8\xi} \simeq (\xi^2 + \varepsilon_8)(1 - \varepsilon_8\xi) = \xi^2 - 2\varepsilon\xi^3 + 2\varepsilon\xi, \quad \text{with } \varepsilon_8 = 2\varepsilon.$$

□ $B = 4$

As for the $B = 4$ case, the strategy is the same as we have been using for the $B = 1$ and $B = 2$ case. Under the translation in the z direction, *i.e.* $z \rightarrow z + dz$ and hence $\xi \rightarrow \xi(1 - \varepsilon)$, $R_0(\xi)$, the BPS monopole solution used for the rational map ansatz in the $B = 4$ case, then becomes

$$\begin{aligned} R_0(\xi) &= \frac{\xi^4 + 2\sqrt{3}i\xi^2 + 1}{\xi^4 - 2\sqrt{3}i\xi^2 + 1} = \frac{P_0}{Q_0} \\ &\longrightarrow \frac{\xi^4(1 - 4\varepsilon) + 2\sqrt{3}i\xi^2(1 - 2\varepsilon) + 1}{\xi^4(1 - 4\varepsilon) - 2\sqrt{3}i\xi^2(1 - 2\varepsilon) + 1} \simeq \frac{P_0 + 4\sqrt{3}i\varepsilon\xi^2 + 4\varepsilon}{Q_0 - 4\sqrt{3}i\varepsilon\xi^2 + 4\varepsilon} = R_7(\xi). \end{aligned}$$

With the identification of $\varepsilon_7 = 4\varepsilon$, $R_7(\xi)$ is the broken z translational mode.

Also, $\tilde{R}_9(\xi)$ can be proved to be the broken x translational mode as

$$\begin{aligned} R_0(\xi) &\longrightarrow \frac{[\xi^4 + 4\varepsilon\xi^3(1 - \xi^2)] + 2\sqrt{3}i[\xi^2 + 2\varepsilon\xi(1 - \xi^2)] + 1}{[\xi^4 + 4\varepsilon\xi^3(1 - \xi^2)] - 2\sqrt{3}i[\xi^2 + 2\varepsilon\xi(1 - \xi^2)] + 1} \\ &\simeq \frac{P_0 + 4\varepsilon\xi^3(1 + \sqrt{3}i) + 4\varepsilon\xi(1 + \sqrt{3}i)}{Q_0 + 4\varepsilon\xi^3(1 - \sqrt{3}i) + 4\varepsilon\xi(1 - \sqrt{3}i)} \\ &= \tilde{R}_9(\xi), \quad \text{with } \varepsilon_9 = -8\varepsilon. \end{aligned}$$

We can then conclude that in $B = 1$ case, R_4, R_5, R_6 are the broken x, y, z translational modes; in $B = 2$ case, R_6, R_7, R_8 are the broken z, y, x translational modes; in $B = 4$ case, $R_7, \tilde{R}_8, \tilde{R}_9$ are the broken z, y, x translational modes respectively.

5.4 Conjugacy Relation

Since we have already obtained the eigen-modes of the eigenvalue equation (5.1), it seems that we need to distinguish which modes represent inequivalent sets of solutions. The way of doing this is to classify these solutions in terms of the inequivalent irreducible representation of the symmetry group of the equation of motion or, in other words, of the Skymion because the equation of motion is derived from the perturbed Lagrangian L_2 around the Skymion.

Generally speaking, if a perturbation is performed at a local minimal equilibrium point in the configuration space of a topologically nontrivial field theory, then the fluctuations to linear approximation are very small and can be treated as vectors in the tangent space to the minimal point in the configuration space. These distortions, some of which would correspond to the vibrational modes, will lie in the tangent space, a vector space, to the Skymions. Furthermore, the vectors in the tangent space share the same symmetry of the Skymions because the space of solutions will have the same symmetry as the equation of motion. The solutions, the perturbed fields, are obtained from solving the equation of motion built around the Skymion, therefore the equation must have the same symmetry as the Skymion, and so must the vibrational modes. Thus the space of vibrational modes will constitute the representation space of the symmetry group of the Skymions. However, in our case, the distorted field configurations around the Skymions, the minimal energy field configurations, which is approximated by the rational map ansatz, can be obtained by varying the parameters in the rational map, which means that, by utilizing the rational map ansatz, the tangent space will reduce from infinite dimensional space to finite dimensional space.

In the following sections, we will show the details of the vibrational modes for

the rational map of the degrees, $\mathcal{N} = 1, 2$ and 4 , and use the property that the vibrational modes have the same symmetry group as the Skyrmion to connect those modes. Briefly, the modes with the same eigenvalue form an irreducible representation space of the symmetry group, meaning when the symmetry group acts on any vector, namely the perturbed field, in this space, the vector stays in the same space. That is the way we show the equivalence relation (or conjugate relation) among those modes with the same eigenvalue in case $B = 1$ and 2 . However, in the $B = 4$ case, the situation is more complicated, and hence it might make things simpler to find a set of basis by a suitable linear combinations of the degenerate eigen-modes to represent any vector in this space.

5.4.1 Möbius Transformation

Before investigating the properties of the perturbed rational maps obtained above, we would like to introduce the connection between the Möbius transformation and linear algebra [65]. We then can simplify the calculations and hence understand more about the rational map.

When adjoining a point at infinity to the complex plane \mathbb{C} , we obtain the complex projective line $\mathbb{C}\mathbb{P}^1$ [77] [79]. With the aid of the stereographic projection of the unit sphere \mathbb{S}^2 , the complex plane \mathbb{C} can be constructed. As a result, we can have a homeomorphism between the complex plane \mathbb{C} and the sphere \mathbb{S}^2 minus the point which is regarded as the infinity in the complex plane. Adding the point at the infinity hence leads us to that the $\mathbb{C}\mathbb{P}^1$ can be identified with the sphere \mathbb{S}^2 , which is called the Riemann sphere [84].

The set of the Möbius transformations [16] [65] [45] is the automorphism group of the Riemann sphere. A Möbius transformation take the general form as

$$\xi \mapsto T(\xi) = \frac{a\xi + b}{c\xi + d},$$

where a, b, c, d are complex numbers with the constraint $ad - bc \neq 0$. A Möbius transformation can be decomposed into a sequence of simpler transformations:

$$T(\xi) = T_4 \circ T_3 \circ T_2 \circ T_1(\xi) = \frac{a\xi + b}{c\xi + d},$$

where

$$\begin{aligned} T_1 : \xi &\mapsto \xi + \frac{d}{c}, && \text{translation;} \\ T_2 : \xi &\mapsto \frac{1}{\xi}, && \text{complex inversion;} \\ T_3 : \xi &\mapsto -\frac{ad-bc}{c^2}\xi, && \text{expansion and rotation;} \\ T_4 : \xi &\mapsto \xi + \frac{a}{c}, && \text{translation;} \end{aligned}$$

This decomposition makes it easy for us to understand the following properties of the Möbius transformation:

1. Möbius transformations preserve circles.
2. Möbius transformations are conformal.
3. Cross-ratio preservation, which means that cross-ratio [81] [72]

$$\frac{(\xi_1 - \xi_3)(\xi_2 - \xi_4)}{(\xi_1 - \xi_4)(\xi_2 - \xi_3)} = \frac{(\omega_1 - \omega_3)(\omega_2 - \omega_4)}{(\omega_1 - \omega_4)(\omega_2 - \omega_3)}$$

is unchanged under a Möbius transformation, *i.e.* $\omega = T(\xi)$.

It is useful to give the Möbius transformation $T(\xi)$ a representation as a 2×2 matrix:

$$T(\xi) = \frac{a\xi + b}{c\xi + d} \longleftrightarrow [T] = \begin{pmatrix} a & b \\ c & d \end{pmatrix}.$$

The advantage of this representation is that we can easily work out the composition of two Möbius transformations via the matrix multiplication of the corresponding matrices. If a map f from the general linear group $GL(2, \mathbb{C})$ to the Möbius group is defined, then f is a homomorphism [89]. Since f maps $\lambda[T]$, where λ is any scalar, to the same Möbius transformation, it is not an isomorphism but a homomorphism. But if we get the quotient group $GL(2, \mathbb{C})/Z(GL(2, \mathbb{C}))$, where $Z(GL(2, \mathbb{C}))$ is the kernel of the group $GL(2, \mathbb{C})$, then from group theory [75] [37] we can have the conclusion that the Möbius group is isomorphic to $PGL(2, \mathbb{C})$ [74], which is the quotient group $GL(2, \mathbb{C})/Z(GL(2, \mathbb{C}))$. Therefore the action of $PGL(2, \mathbb{C})$ on \mathbb{CP}^1

and that of the Möbius transformation on the Riemann sphere is the same when the sphere and the projective line are identified as follows:

$$[\xi_1 : \xi_2] \leftrightarrow \frac{\xi_1}{\xi_2},$$

where $[\xi_1 : \xi_2]$ are homogeneous coordinates on $\mathbb{C}\mathbb{P}^1$. If we restrict the matrix $[T]$ to those of unit determinant, then f is the map from special linear group $SL(2, \mathbb{C})$ to Möbius group, which is then isomorphic to $PSL(2, \mathbb{C})$.

In brief, if the pair $(\xi_1, \xi_2) \in \mathbb{C}^2$ represent a point in $\mathbb{C}\mathbb{P}^1$ by homogeneous coordinates, then the Möbius transformation can be represented as a 2×2 matrix. In the following, we explain more about the homogeneous coordinates [19].

In complex analysis, one can express a complex number ξ as the ratio of two complex numbers, z_1 and z_2 , instead of two real numbers, *i.e.* $\xi = x + iy$:

$$\xi = \frac{z_1}{z_2}.$$

These two complex numbers, z_1 and z_2 , are called homogeneous coordinates of ξ , and are expressed as (z_1, z_2) . The set of the ordered pairs (z_1, z_2) can then be denoted by the symbol \mathbb{C}^2 , just like for the case of sets of pairs of real numbers, (x, y) , as \mathbb{R}^2 . Therefore one can apply most of the concepts in \mathbb{R}^2 to \mathbb{C}^2 . First of all, one can write an ordered pair (z_1, z_2) as a column vector:

$$\xi = \frac{z_1}{z_2} \longleftrightarrow \boldsymbol{\xi} = \begin{pmatrix} z_1 \\ z_2 \end{pmatrix}.$$

A linear transformation in \mathbb{C}^2 , just as one in \mathbb{R}^2 , can be represented as a 2×2 complex matrix:

$$\begin{pmatrix} z_1 \\ z_2 \end{pmatrix} \mapsto \begin{pmatrix} w_1 \\ w_2 \end{pmatrix} = \begin{pmatrix} a & b \\ c & d \end{pmatrix} \begin{pmatrix} z_1 \\ z_2 \end{pmatrix} = \begin{pmatrix} a z_1 + b z_2 \\ c z_1 + d z_2 \end{pmatrix},$$

where the elements, a , b , c and d , in the matrix are complex constants. We can write the complex number ω , which is expressed previously by its homogeneous coordinates in \mathbb{C}^2 , now back to the form in \mathbb{C} as

$$\omega = \frac{w_1}{w_2} = \frac{a z_1 + b z_2}{c z_1 + d z_2}.$$

Similarly, we can apply the aforementioned method to the rational map, which has the general form

$$R(\xi) = \frac{P(\xi)}{Q(\xi)},$$

where $P(\xi)$ and $Q(\xi)$ are the polynomials of complex variables ξ . When applied, the rational map is expressed in terms of a column vector form as

$$R(\xi) = \frac{P(\xi)}{Q(\xi)} \longleftrightarrow \mathbf{R}(\xi) = \begin{pmatrix} P(\xi) \\ Q(\xi) \end{pmatrix}.$$

Likewise, we can have a linear transformation represented as a 2×2 matrix such that

$$\begin{pmatrix} P(\xi) \\ Q(\xi) \end{pmatrix} \mapsto \begin{pmatrix} M(\xi) \\ N(\xi) \end{pmatrix} = \begin{pmatrix} a & b \\ c & d \end{pmatrix} \begin{pmatrix} P(\xi) \\ Q(\xi) \end{pmatrix} = \begin{pmatrix} a P(\xi) + b Q(\xi) \\ c P(\xi) + d Q(\xi) \end{pmatrix},$$

where a, b, c and d in the matrix are complex constants. After the transformation, we restore the above expression to its rational map form as

$$W(\xi) = \frac{M(\xi)}{N(\xi)} = \frac{a P(\xi) + b Q(\xi)}{c P(\xi) + d Q(\xi)}.$$

What is more, one can write the complex number ω in the following form

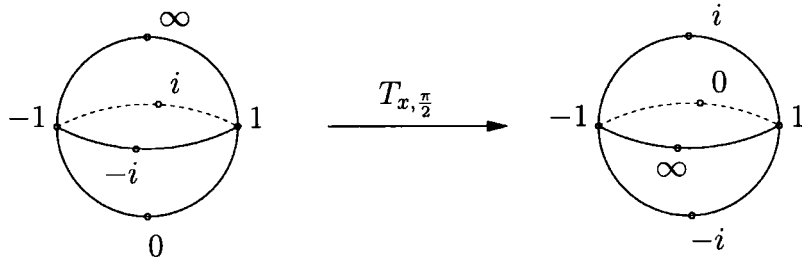
$$\omega = \frac{w_1}{w_2} = \frac{a z_1 + b z_2}{c z_1 + d z_2} = \frac{a (z_1/z_2) + b}{c (z_1/z_2) + d} = \frac{a\xi + b}{c\xi + d},$$

which is identified as the most general form of Mobius transformation. Next, we talk about some properties of Mobius transformation.

The expression of the rotation of the Riemann sphere about the x -axis, *i.e* 1 and -1 fixed, for $\pi/2$ is

$$T_{x, \pi/2}(\xi) = \frac{a\xi + b}{c\xi + d} \longleftrightarrow [T_{x, \pi/2}] = \begin{pmatrix} a & b \\ c & d \end{pmatrix},$$

where $ad - bc = 1$. $T_{x, \pi/2}(\xi)$ is a Mobius transformation on the complex plane. Its effect is to rotate the corresponding Riemann sphere such that

Figure 5.4: $\pi/2$ rotation of Riemann sphere about x -axis.

$$\left\{ \begin{array}{l} \xi \xrightarrow{T_{x, \frac{\pi}{2}}} T_{x, \frac{\pi}{2}}(\xi), \\ 1 \longrightarrow 1 \quad \Rightarrow \quad \frac{a+b}{c+d} = 1, \\ -1 \longrightarrow -1 \quad \Rightarrow \quad \frac{-a+b}{c+d} = -1, \\ i \longrightarrow \infty \quad \Rightarrow \quad ic + d = 0, \\ \infty \longrightarrow -i \quad \Rightarrow \quad \frac{a}{c} = -i, \\ -i \longrightarrow 0 \quad \Rightarrow \quad -ia + b = 0, \\ 0 \longrightarrow i \quad \Rightarrow \quad \frac{b}{d} = i. \end{array} \right.$$

According to the aforementioned conditions on $T_{x, \frac{\pi}{2}}(\xi)$, we hence fix the coefficients and have the explicit formula

$$T_{x, \frac{\pi}{2}}(\xi) = \frac{\xi + i}{i\xi + 1} \longleftrightarrow [T_{x, \frac{\pi}{2}}] = \frac{1}{\sqrt{2}} \begin{pmatrix} 1 & i \\ i & 1 \end{pmatrix}. \quad (5.4)$$

In the practical calculation, the normalization factor $\frac{1}{\sqrt{2}}$ is ignored because it would be cancelled out while applying to numerator and denominator at the same time. Therefore it is not necessary and would not do any help to include this normalization factor when we do the calculation in question. Applying similar conditions on finding

$T_{y, \frac{\pi}{2}}(\xi)$ and $T_{z, \frac{\pi}{2}}(\xi)$, we find

$$T_{y, \frac{\pi}{2}}(\xi) = \frac{\xi - 1}{\xi + 1} \longleftrightarrow [T_{y, \frac{\pi}{2}}] = \frac{1}{\sqrt{2}} \begin{pmatrix} 1 & -1 \\ 1 & 1 \end{pmatrix}, \quad (5.5)$$

$$T_{z, \frac{\pi}{2}}(\xi) = i\xi \longleftrightarrow [T_{z, \frac{\pi}{2}}] = \frac{1-i}{\sqrt{2}} \begin{pmatrix} i & 0 \\ 0 & 1 \end{pmatrix}. \quad (5.6)$$

Our next goal is to generalize the rotation to any angle θ , not just $\frac{\pi}{2}$, about the x , y and z -axis. We realize that it is achievable by starting from the expression of rotation about the z -axis for θ :

$$T_{z, \theta}(\xi) = e^{i\theta\xi} \longleftrightarrow [T_{z, \theta}] = e^{\frac{-i\theta}{2}} \begin{pmatrix} e^{i\theta} & 0 \\ 0 & 1 \end{pmatrix} = \begin{pmatrix} e^{\frac{i\theta}{2}} & 0 \\ 0 & e^{\frac{-i\theta}{2}} \end{pmatrix}. \quad (5.7)$$

By conjugation, we surely can get the formula for a rotation about the x and y -axis for any angle θ ; but all these can be obtained by the general expression⁶ as follows

$$T_{\mathbf{n}, \theta}(\xi) = \frac{(\cot(\frac{\theta}{2}) + in_3)\xi - (n_2 - in_1)}{(n_2 + in_1)\xi + \cot(\frac{\theta}{2}) - in_3}, \quad (5.8)$$

where $\mathbf{n} = (n_1, n_2, n_3)$ is a unit vector around which the angle θ is rotated.

For $\mathbf{n} = (1, 0, 0)$ and $(0, 1, 0)$, it represents respectively the rotations around x and y -axis about an angle θ and the associated matrix representations are

⁶It can be obtained from modifying the equation (A.2) in [42].

$$T_{x,\theta}(\xi) = \frac{\cos(\frac{\theta}{2})\xi + i\sin(\frac{\theta}{2})}{i\sin(\frac{\theta}{2})\xi + \cos(\frac{\theta}{2})} \longleftrightarrow [T_{x,\theta}] \propto \begin{pmatrix} \cos(\frac{\theta}{2}) & i\sin(\frac{\theta}{2}) \\ i\sin(\frac{\theta}{2}) & \cos(\frac{\theta}{2}) \end{pmatrix} \quad (5.9)$$

$$T_{y,\theta}(\xi) = \frac{\cos(\frac{\theta}{2})\xi - \sin(\frac{\theta}{2})}{\sin(\frac{\theta}{2})\xi + \cos(\frac{\theta}{2})} \longleftrightarrow [T_{y,\theta}] \propto \begin{pmatrix} \cos(\frac{\theta}{2}) & -\sin(\frac{\theta}{2}) \\ \sin(\frac{\theta}{2}) & \cos(\frac{\theta}{2}) \end{pmatrix} \quad (5.10)$$

Fixed Points of Perturbation

The fixed points of the mapping are those which stay invariant under the transformation, or, in other words, they are mapped or transformed back to themselves. However, there is another quite similar concept called fixed points of perturbation which are the points that are unmoved when a perturbation of the mapping is performed. This means for the mapping under a perturbation, $f \rightarrow f' = f + \delta f$, then the point p is called a fixed point of perturbation when $f(p) = f'(p)$. It is important to find the fixed point of perturbation because, while the perturbation is performed on the rational maps, it might induce a rotational zero mode, like, for example, a mode rotating about an axis with 2 fixed points. So the identification of the fixed points of perturbation will allow us to check, at least in the first step, whether or not a zero mode is a rotational mode and if they indeed are rotational zero modes, it is also helpful to show that these rotational zero modes, rotating about different axes, are actually equivalent. According to the aforesaid statement, we now want to find out the fixed points of the perturbed rational maps for $B = 1$ and $B = 2$:

$B = 1$ ($R_0 = \xi$, unperturbed rational map)

$$R_1(\xi) = \frac{\xi - \varepsilon}{1 + \varepsilon\xi} = \xi, \quad \forall \varepsilon \ll 1 \quad \Rightarrow \quad \xi = \pm i,$$

$B = 2$ ($R_0 = \xi^2$, unperturbed rational map)

$$R_1(\xi) = \frac{\xi^2 + i\varepsilon\xi}{1 + i\varepsilon\xi} = \xi^2, \quad \forall \varepsilon \ll 1 \quad \Rightarrow \quad \xi = 0^1, \infty^1, \pm 1.$$

We repeat the above method to obtain the fixed points of other perturbed rational maps and summarize in the following tables:

¹As we will show later, R_1 is a zero mode rotating about the x -axis for an infinitesimal angle ε . The expression of R_1 obtained from perturbing the original rational map ξ^2 is identified as the one taking the Taylor expansion of the full expression of the rotation only up to the leading order. Using this expression of the first-order Taylor expansion, we would have the fixed points, 0 and ∞ , which actually are the pseudo fixed points. What is meant by the pseudo fixed point is that, when the full expression, without taking the Taylor expansion, of the rotation is applied, this pseudo fixed point disappears. So we exclude it out of the table listed below.

Perturbed Rational Map	Fixed Points of Perturbation
Zero Mode	
$R_1(\xi) = \frac{\xi - \varepsilon}{1 + \varepsilon \xi}$	$\pm i$
$R_2(\xi) = \frac{\xi + i\varepsilon}{1 + i\varepsilon \xi}$	± 1
$R_3(\xi) = \frac{\xi}{1 + i\varepsilon}$	$0, \infty$
Broken Zero Mode	
$R_4(\xi) = \frac{\xi + \varepsilon}{1 + \varepsilon \xi}$	± 1
$R_5(\xi) = \frac{\xi - i\varepsilon}{1 + i\varepsilon \xi}$	$\pm i$
$R_6(\xi) = \frac{\xi}{1 + \varepsilon}$	$0, \infty$

Table 5.1: Fixed Points of Perturbed Rational Map in Baryon Number $B = 1$

Perturbed Rational Map	Fixed Points of Perturbation
Zero Mode	
$R_1(\xi) = \frac{\xi^2 + i\epsilon\xi}{1 + i\epsilon\xi}$	$\pm 1^*$
$R_2(\xi) = \frac{\xi^2 - \epsilon\xi}{1 + \epsilon\xi}$	$\pm i^*$
$R_3(\xi) = \frac{\xi^2 + i\epsilon}{1 + i\epsilon\xi^2}$	$\pm 1, \pm i$
$R_4(\xi) = \frac{\xi^2 - \epsilon}{1 + \epsilon\xi^2}$	$e^{\frac{i\pi}{4}}, e^{\frac{i3\pi}{4}}, e^{\frac{i5\pi}{4}}, e^{\frac{i7\pi}{4}}$
$R_5(\xi) = \frac{\xi^2}{1 + i\epsilon}$	$0, \infty$
$R_6(\xi) = \frac{\xi^2}{1 + \epsilon}$	$0, \infty$
$R_7(\xi) = \frac{\xi^2 - i\epsilon\xi}{1 + i\epsilon\xi}$	$\pm i^*$
$R_8(\xi) = \frac{\xi^2 + \epsilon\xi}{1 + \epsilon\xi}$	$\pm 1^*$
Vibrational Mode	
$R_9(\xi) = \frac{\xi^2 - i\epsilon}{1 + i\epsilon\xi^2}$	$e^{\frac{i\pi}{4}}, e^{\frac{i3\pi}{4}}, e^{\frac{i5\pi}{4}}, e^{\frac{i7\pi}{4}}$
$R_{10}(\xi) = \frac{\xi^2 + \epsilon}{1 + \epsilon\xi^2}$	$\pm 1, \pm i$

Table 5.2: Fixed Points of Perturbed Rational Map in Baryon Number $B = 2$.

The “ * ” in Table 5.2 means 0 and ∞ are the pseudo fixed points in the rational maps R_1 , R_2 , R_7 and R_8 respectively. More details of the origin of these pseudo fixed points will be given later.

The $R_3(\xi)$ in $B = 1$ and $R_5(\xi)$ in $B = 2$ are rotational zero mode, both rotating about the z -axis, that can be verified by (5.7) through doing Taylor expansion to the first order. According to the fixed points listed in the above tables, we think that those 6 rational maps in $B = 1$ might not be independent from each other and neither are the 10 rational maps in $B = 2$. Now, we introduce the concept of conjugation relation in order to show that some of them are conjugate, or equivalent, to each other.

5.4.2 Conjugacy relation, $B = 1$

$$\begin{array}{ccc}
 \xi & \xrightarrow{R_i} & R_i(\xi) \\
 \downarrow g & & \downarrow D_g \\
 \xi' = g(\xi) & \xrightarrow{R_j} & R_j(g(\xi)) = D_g \cdot R_i(\xi)
 \end{array}$$

The above commutative diagram tells us, given two maps, R_i and R_j , how to find their conjugation relation. Let us explain more in the following. There are two points of view to doing the transformations, active and passive. Here we take the active transformation point of view. The mapping is nothing but a rule of how to assign a point in the domain space to a point in the target space. When there is more than one mapping, one can try to find if there exists any relations among them, and then use the relations to classify them. One of the relations among the mappings which is useful for one to simplify classifications is the conjugation, or called equivalence, relation. One can then ask: by what criterion can one say whether or not any two mappings are conjugate (or equivalent) to each other? The basic idea of conjugation

relation is: Given two mappings, R_i and R_j , the points in the domain space ξ and ξ' of the mapping R_i and R_j are mapped to the points in target space $R_i(\xi)$ and $R_j(\xi')$ respectively. If a transformation g is performed on ξ to obtain $\xi' = g(\xi)$ and there exists a corresponding transformation D_g (of course also D_g^{-1}) in the target space to connect the values of $R_i(\xi)$ and $R_j(\xi')$, *i.e.* $R_j(\xi') = D_g \cdot R_i(\xi)$, then one can say that the mapping R_i and R_j are conjugate to each other. In other words, after the transformation D_g performed on points $R_i(\xi)$ in the target space, the points $D_g \cdot R_i(\xi)$ in the target space have the same “pattern” as those points $R_j(\xi')$ in target space mapped from the points ξ' in domain space that are obtained by a transformation g on points ξ in the domain space.

Here, we demonstrate the conjugacy relation between rational maps R_1 and R_3 using the way mentioned in the commutative diagram about the conjugation relation, to support our previous thought. The transformation on the domain space is first carried out:

$$\begin{aligned} \xi &\longrightarrow \xi' = [T_{x, \frac{\pi}{2}}] \cdot \xi = \begin{pmatrix} 1 & i \\ i & 1 \end{pmatrix} \cdot \begin{pmatrix} \xi \\ 1 \end{pmatrix} = \begin{pmatrix} \xi + i \\ i\xi + 1 \end{pmatrix} \\ \Rightarrow \quad \xi &\longrightarrow \xi' = g(\xi) = \frac{\xi + i}{i\xi + 1}. \end{aligned}$$

For the later convenience, we redefine the infinitesimal parameter ε as 2ε in $R_3(\xi)$:

$$R_3(\xi) = \frac{\xi}{1 + i\varepsilon} \xrightarrow{\varepsilon \rightarrow 2\varepsilon} \frac{\xi}{1 + 2i\varepsilon}.$$

The target space of the rational map R_1 with the original domain space,

$$R_1(\xi) = \frac{\xi - \varepsilon}{1 + \varepsilon\xi},$$

then, after taking the transformed domain space, becomes

$$\begin{aligned} R_1(g(\xi)) &= R_1(\xi') = \frac{\xi' - \varepsilon}{1 + \varepsilon\xi'} = \frac{\left(\frac{\xi+i}{i\xi+1}\right) - \varepsilon}{1 + \varepsilon\left(\frac{\xi+i}{i\xi+1}\right)} \\ &= \frac{(1 - i\varepsilon)\xi + (i - \varepsilon)}{(i + \varepsilon)\xi + (1 + i\varepsilon)} = \frac{\xi + \left(\frac{i-\varepsilon}{1-i\varepsilon}\right)}{\left(\frac{i+\varepsilon}{1-i\varepsilon}\right)\xi + \left(\frac{1+i\varepsilon}{1-i\varepsilon}\right)} \\ &= \frac{\xi + (i - 2\varepsilon)}{i\xi + (1 + 2i\varepsilon)} + O(\varepsilon^2). \end{aligned}$$

Meanwhile, on the other hand, we have transformed the target space of the rational map $R_3(\xi)$ to get

$$[T_{x, \frac{\pi}{2}}] \cdot \mathbf{R}_3(\xi) = \begin{pmatrix} 1 & i \\ i & 1 \end{pmatrix} \cdot \begin{pmatrix} \xi \\ 1 + 2i\varepsilon \end{pmatrix} = \begin{pmatrix} \xi + i - 2\varepsilon \\ i\xi + 1 + 2i\varepsilon \end{pmatrix}$$

$$\longleftrightarrow D_g \cdot R_3(\xi) = \frac{\xi + (i - 2\varepsilon)}{i\xi + (1 + 2i\varepsilon)} = R_1(g(\xi)) .$$

From the result obtained above, we can conclude, by the criterion in the commutative diagram of conjugation relation, that the rational maps R_1 and R_3 are conjugate to each other, using the notation below to denote the conjugation relation:

$$R_1(\xi) \sim R_3(\xi) \quad \Rightarrow \quad R_1 \sim R_3 .$$

Using exactly the same method, we understand that three zero modes in $B = 1$ are actually conjugate to one another. Besides these three zero modes, the other three vibrational modes in the $B = 1$ also forms a conjugacy class.

For $B = 1$, the rational map has six modes split into two sets of triplets; one is for the rotational zero modes, which in this case are the same as the iso-rotational zero modes because the domain space is exactly the same as the target space of the Skyrme field. The other triplet is the set of three broken translational zero modes, which are x , y and z translation respectively.

We summarize these facts for $B = 1$ in the following table:

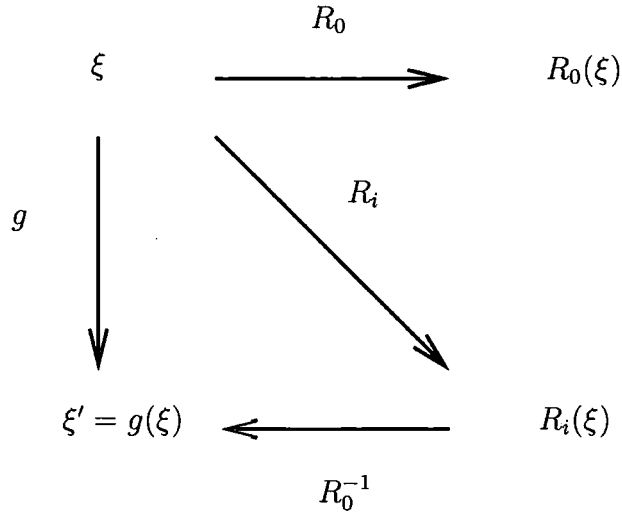
Perturbed Rational Map	Remarks
<p>Zero Mode</p> <p>Conjugacy Class $\left\{ \begin{array}{l} R_1(\xi) = \frac{\xi - \epsilon}{1 + \epsilon\xi} \\ R_2(\xi) = \frac{\xi + i\epsilon}{1 + i\epsilon\xi} \\ R_3(\xi) = \frac{\xi}{1 + i\epsilon} \end{array} \right.$</p>	<p>Rotation about y-axis for $\epsilon \ll 1$</p> <p>Rotation about x-axis for $\epsilon \ll 1$</p> <p>Rotation about z-axis for $\epsilon \ll 1$</p>
<p>Broken Zero Mode</p> <p>Conjugacy Class $\left\{ \begin{array}{l} R_4(\xi) = \frac{\xi + \epsilon}{1 + \epsilon\xi} \\ R_5(\xi) = \frac{\xi - i\epsilon}{1 + i\epsilon\xi} \\ R_6(\xi) = \frac{\xi}{1 + \epsilon} \end{array} \right.$</p>	<p>Broken x translational mode.*</p> <p>Broken y translational mode.*</p> <p>Broken z translational mode.*</p>

Table 5.3: Conjugacy Classes of Perturbed Rational Maps of Baryon Number $B = 1$

* See the Fig. 5.5, Fig. 5.6 and Fig. 5.7.

5.4.3 Conjugacy relation, $B = 2$

Of course, we can follow the same route to demonstrate the conjugacy relation among the rational maps in $B = 2$. But here we try a different way to identify the conjugate relation among the zero modes, using the concept indicated by the commutative diagram below:



This commutative diagram says that when the rational map R_0 is perturbed to become R_i , whose domain space is denoted as ξ , same as that of R_0 , we map the values $R_i(\xi)$ in the target space back, using the inverse mapping R_0^{-1} , to get the induced, transformed domain space $\xi' = g(\xi)$, where g is a transformation that can be applied on domain space ξ . Hence we can see what the deformation of the original domain space is induced by the perturbed rational map R_i . Through this route, we can show that $R_5(\xi)$, $R_1(\xi)$ and $R_2(\xi)$ are actually the rotational modes, rotating about the z -, x - and y -axis respectively, in $B = 2$, and therefore we claim that they are in the same conjugacy class, which of course can be verified by the criterion of conjugacy relation. We now demonstrate the conjugacy relation in the alternative way. According to (5.9), the expression of a rotation about x -axis for an infinitesimal angle ε is

$$[T_{x,\varepsilon}] = \begin{pmatrix} \cos(\frac{\varepsilon}{2}) & i \sin(\frac{\varepsilon}{2}) \\ i \sin(\frac{\varepsilon}{2}) & \cos(\frac{\varepsilon}{2}) \end{pmatrix}, \quad \varepsilon \ll 1.$$

The transformation g (or $[T_{x,\varepsilon}]$) is then performed on the domain space as follows

$$\begin{aligned} \xi &\longrightarrow \xi' = [T_{x,\varepsilon}] \cdot \xi \\ &= \begin{pmatrix} \cos(\frac{\varepsilon}{2}) & i \sin(\frac{\varepsilon}{2}) \\ i \sin(\frac{\varepsilon}{2}) & \cos(\frac{\varepsilon}{2}) \end{pmatrix} \cdot \begin{pmatrix} \xi \\ 1 \end{pmatrix} \\ &= \begin{pmatrix} \cos(\frac{\varepsilon}{2}) \xi + i \sin(\frac{\varepsilon}{2}) \\ i \sin(\frac{\varepsilon}{2}) \xi + \cos(\frac{\varepsilon}{2}) \end{pmatrix}, \\ \Rightarrow \xi &\longrightarrow \xi' = g(\xi) = \frac{\cos(\frac{\varepsilon}{2}) \xi + i \sin(\frac{\varepsilon}{2})}{i \sin(\frac{\varepsilon}{2}) \xi + \cos(\frac{\varepsilon}{2})}. \end{aligned}$$

Using the mapping R_0 to map the transformed domain space ξ' into target space $R_0(\xi') = \xi'^2$, we obtain

$$\begin{aligned} \xi'^2 &= \left[\frac{\cos(\frac{\varepsilon}{2}) \xi + i \sin(\frac{\varepsilon}{2})}{i \sin(\frac{\varepsilon}{2}) \xi + \cos(\frac{\varepsilon}{2})} \right]^2 \sim \frac{(\xi + \frac{i\varepsilon}{2})^2}{(\frac{i\varepsilon}{2}\xi + 1)^2} \\ &= \frac{\xi^2 + i\varepsilon\xi}{1 + i\varepsilon\xi} + O(\varepsilon^2) \\ &= R_1(\xi). \end{aligned} \tag{5.11}$$

As one can see that we have modified the route, which is supposed to map $R_1(\xi)$ back to the domain space. However, it is easier to map the transformed domain space ξ' , using R_0 , to the target space to see whether it matches the values of the perturbed rational map $R_1(\xi)$ in target space. As shown above, it matches to the leading order, and therefore we claim that R_1 in $B = 2$ is the rotational zero mode, which induces an infinitesimal rotation about the x -axis in the domain space. Using the same argument, we also claim that R_2 inducing an infinitesimal rotation about the y -axis in the domain space is another rotational zero mode in $B = 2$.

5.4.4 Finding the Iso-rotational Zero Mode, $B = 2$

From symmetry considerations, since we have already identified three rotational zero modes, it occurs to us that it is possible to show that the rest two zero modes are the iso-rotations. In the following, we will prove that $R_3(\xi)$ and $R_4(\xi)$, $B = 2$, are indeed the iso-rotations about the x and y -axis respectively.

In order to perform the rotation in target space (or, in short, iso-rotation), it is convenient for us to express the rational map R in terms of the Cartesian notation, which, via stereographic projection, presents the complex coordinates on a \mathbb{S}^2 sphere as the unit vector, \hat{n}_R . The iso-rotation is performed by the same way as that in the physical space, $\vec{V}' = O\vec{V}$, where \vec{V} is the original vector, \vec{V}' is the rotated vector and O is the rotation matrix. In this case, the \hat{n}_{R_0} and $\hat{n}_{\tilde{R}}$ represent the unit vectors of the unperturbed and iso-rotated rational maps, taking the following form:

$$\begin{aligned}\hat{n}_{R_0} &= \frac{1}{1 + |R_0|^2} (2\Re(R_0), 2\Im(R_0), 1 - |R_0|^2) = (n_1, n_2, n_3), \\ \hat{n}_{\tilde{R}} &= \frac{1}{1 + |\tilde{R}|^2} (2\Re(\tilde{R}), 2\Im(\tilde{R}), 1 - |\tilde{R}|^2) = (\tilde{n}_1, \tilde{n}_2, \tilde{n}_3),\end{aligned}$$

where n_1, n_2, \dots etc. are the Cartesian components of the unit vector.

Our strategy of finding the iso-rotation modes is to rotate the unit vector of the unperturbed rational map to get the iso-rotated unit vector. Then use this formula

$$\tilde{R} = \frac{\tilde{n}_1 + i\tilde{n}_2}{1 + \tilde{n}_3} = \Re(\tilde{R}) + i\Im(\tilde{R}), \quad (5.12)$$

to have the rational map of the iso-rotated zero modes. In the end, we compare this iso-rotated rational map with our previously obtained rational map, R_3 and R_4 , to see if we can identify them.

To find out the iso-rotated rational map about the x -axis, we first need to compute the components of unit vector of the iso-rotated rational map.

$$\begin{pmatrix} \tilde{n}_1 \\ \tilde{n}_2 \\ \tilde{n}_3 \end{pmatrix} = \begin{pmatrix} 1 & 0 & 0 \\ 0 & \cos \theta & \sin \theta \\ 0 & -\sin \theta & \cos \theta \end{pmatrix} \begin{pmatrix} n_1 \\ n_2 \\ n_3 \end{pmatrix} = \begin{pmatrix} n_1 \\ n_2 \cos \theta + n_3 \sin \theta \\ -n_2 \sin \theta + n_3 \cos \theta \end{pmatrix}.$$



Choosing the parametrization, $\xi = re^{i\alpha}$, we can have

$$\begin{aligned}\tilde{n}_1 = n_1 &\Rightarrow \frac{2\Re(\tilde{R}_{iso,x})}{1 + |\tilde{R}_{iso,x}|^2} = \frac{2\Re(R_0)}{1 + |R_0|^2} = \frac{2r^2 \cos 2\alpha}{1 + r^4}, \\ \tilde{n}_2 = n_2 \cos \theta + n_3 \sin \theta &\Rightarrow \frac{2\Im(\tilde{R}_{iso,x})}{1 + |\tilde{R}_{iso,x}|^2} = \frac{2r^2 \sin 2\alpha \cos \theta + (1 - r^4) \sin \theta}{1 + r^4}, \\ \tilde{n}_3 = -n_2 \sin \theta + n_3 \cos \theta &\Rightarrow \frac{1 - |\tilde{R}_{iso,x}|^2}{1 + |\tilde{R}_{iso,x}|^2} = \frac{-2r^2 \sin 2\alpha \sin \theta + (1 - r^4) \cos \theta}{1 + r^4}.\end{aligned}$$

From the first two equalities, we realize

$$\begin{aligned}|\tilde{R}_{iso,x}|^2 &= |R_0|^2 = r^4, \\ \Re(\tilde{R}_{iso,x}) &= \Re(R_0) = r^2 \cos 2\alpha, \\ \Im(\tilde{R}_{iso,x}) &= r^2 \sin 2\alpha \cos \theta + \frac{1}{2}(1 - r^4) \sin \theta.\end{aligned}$$

With those components obtained, the rotated rational map can be constructed to the linear order of approximation, as

$$\begin{aligned}\tilde{R}_{iso,x} &= \Re(\tilde{R}_{iso,x}) + i\Im(\tilde{R}_{iso,x}) \\ &= r^2 \cos 2\alpha + ir^2 \sin 2\alpha \cos \theta + \frac{i}{2}(1 - r^4) \sin \theta \\ &\simeq r^2 e^{2i\alpha} + \frac{i\theta}{2}(1 - r^4) \\ &= \xi^2 + \frac{i\theta}{2}(1 - |\xi|^2).\end{aligned}$$

In the meanwhile, we rationalize R_3 to the first order of ε to have

$$\begin{aligned}R_3 &= \frac{\xi^2 + i\varepsilon}{1 + i\varepsilon\xi^2} = \frac{(\xi^2 + i\varepsilon)(1 - i\varepsilon\bar{\xi}^2)}{(1 + i\varepsilon\xi^2)(1 - i\varepsilon\bar{\xi}^2)} \\ &\simeq \xi^2 + i\varepsilon(1 - |\xi|^2) = \tilde{R}_{iso,x}, \quad \text{with } \varepsilon = \frac{\theta}{2}.\end{aligned}$$

Therefore, we can identify R_3 as the iso-rotated zero mode about the x -axis up to the linear order.

Following the same method mentioned above but using $\tilde{R} = \frac{\tilde{n}_1 + i\tilde{n}_2}{1 + \tilde{n}_3}$ instead of $\Re(\tilde{R}) + i\Im(\tilde{R})$, it can be easily shown that \tilde{R} is the iso-rotation about the y -axis, with $\varepsilon = \frac{-\theta}{2}$. Performing the iso-rotation for the unit vector about the y -axis leads to

$$\begin{pmatrix} \tilde{n}_1 \\ \tilde{n}_2 \\ \tilde{n}_3 \end{pmatrix} = \begin{pmatrix} \cos \theta & 0 & \sin \theta \\ 0 & 1 & 0 \\ -\sin \theta & 0 & \cos \theta \end{pmatrix} \begin{pmatrix} n_1 \\ n_2 \\ n_3 \end{pmatrix} = \begin{pmatrix} n_1 \cos \theta + n_3 \sin \theta \\ n_2 \\ -n_1 \sin \theta + n_3 \cos \theta \end{pmatrix}.$$

We then construct the rational map as

$$\begin{aligned} \tilde{R}_{iso,y} &= \frac{\tilde{n}_1 + i\tilde{n}_2}{1 + \tilde{n}_3} = \frac{\frac{2r^2 \cos 2\alpha \cos \theta + (1 - r^4) \sin \theta}{1 + r^4} + i \frac{2r^2 \sin 2\alpha}{1 + r^4}}{1 + \frac{-2r^2 \cos 2\alpha \sin \theta + (1 - r^4) \cos \theta}{1 + r^4}} \\ &\simeq \frac{r^2 \cos 2\alpha + ir^2 \sin 2\alpha + (1 - r^4)\theta}{1 - \theta r^2 \cos 2\alpha} = \frac{\xi^2 + \frac{\theta}{2}(1 - |\xi|^4)}{1 - \theta r^2 \cos 2\alpha}. \end{aligned}$$

Rewrite R_4 to make a comparison with $R_{iso,y}$, then

$$\begin{aligned} R_4 &= \frac{\xi^2 - \varepsilon}{1 + \varepsilon \xi^2} = \frac{(\xi^2 - \varepsilon)(1 + \varepsilon \bar{\xi}^2)}{(1 + \varepsilon \xi^2)(1 + \varepsilon \bar{\xi}^2)} \simeq \frac{\xi^2 - \varepsilon(1 - |\xi|^4)}{1 + 2\varepsilon r^2 \cos 2\alpha} \\ &= \tilde{R}_{iso,y}, \quad \text{with } \varepsilon = \frac{-\theta}{2}. \end{aligned}$$

As expected, R_4 is the iso-rotated zero mode.

5.4.5 Conjugacy Relation Between $R_7(\xi)$ and $R_8(\xi)$, $B = 2$

We show the conjugacy relation between broken translational modes $R_7(\xi)$ and $R_8(\xi)$ in $B = 2$ as follows. Before proving the existence of the conjugacy relation between $R_7(\xi)$ and $R_8(\xi)$, which share the same eigenvalue, we would like to show there is a geometrical connection among $R_6(\xi)$, $R_7(\xi)$ and $R_8(\xi)$. Even though there is a geometrical connection among them, only $R_7(\xi)$ and $R_8(\xi)$ are conjugate to each other.

Consider a Mobius transformation, $[A_{z,\varepsilon}]$, the form of which is very similar to the rotation about the z -axis for infinitesimal angles:

$$[A_{z,\varepsilon}] = \begin{pmatrix} e^\varepsilon & 0 \\ 0 & 1 \end{pmatrix}, \quad \forall \varepsilon \ll 1,$$

where the lower index z means that the effect it causes is along the z -axis of its Riemann sphere corresponding to the complex plane ξ . Its geometric meaning will be clearer later. We then can obtain its action on the x and y -axis respectively:

$$\begin{aligned}
[A_{x,\epsilon}] &\propto [T_{y,\frac{\epsilon}{2}}] \cdot [A_{z,\epsilon}] \cdot [T_{y,\frac{\epsilon}{2}}]^{-1} \\
&\propto \begin{pmatrix} 1 & -1 \\ 1 & 1 \end{pmatrix} \cdot \begin{pmatrix} e^\epsilon & 0 \\ 0 & 1 \end{pmatrix} \cdot \begin{pmatrix} 1 & 1 \\ -1 & 1 \end{pmatrix} \\
&\propto \begin{pmatrix} e^\epsilon + 1 & e^\epsilon - 1 \\ e^\epsilon - 1 & e^\epsilon + 1 \end{pmatrix} \\
&\propto \begin{pmatrix} e^{\frac{\epsilon}{2}} + e^{-\frac{\epsilon}{2}} & e^{\frac{\epsilon}{2}} - e^{-\frac{\epsilon}{2}} \\ e^{\frac{\epsilon}{2}} - e^{-\frac{\epsilon}{2}} & e^{\frac{\epsilon}{2}} + e^{-\frac{\epsilon}{2}} \end{pmatrix}, \\
\Rightarrow [A_{x,\epsilon}] &= \begin{pmatrix} \cosh \frac{\epsilon}{2} & \sinh \frac{\epsilon}{2} \\ \sinh \frac{\epsilon}{2} & \cosh \frac{\epsilon}{2} \end{pmatrix}.
\end{aligned}$$

Similarly,

$$[A_{y,\epsilon}] = \begin{pmatrix} \cosh \frac{\epsilon}{2} & i \sinh \frac{\epsilon}{2} \\ -i \sinh \frac{\epsilon}{2} & \cosh \frac{\epsilon}{2} \end{pmatrix}.$$

So now to show the conjugacy relation between $R_6(\xi)$ and $R_8(\xi)$, we first find

$$\xi \longrightarrow \xi' = [A_{z,\frac{\epsilon}{2}}] \cdot \xi = \begin{pmatrix} e^{-\frac{\epsilon}{2}} \xi \\ 1 \end{pmatrix}$$

$$\Rightarrow \xi \longrightarrow \xi' = e^{-\frac{\epsilon}{2}} \xi,$$

therefore

$$\xi'^2 = e^{-\varepsilon} \xi^2 = R_6(\xi).$$

Using $[A_{x,\varepsilon}]$, we transform the domain space to

$$\begin{aligned} \xi &\longrightarrow \xi' = [A_{x,\varepsilon}] \cdot \xi \\ &= \begin{pmatrix} \cosh \frac{\varepsilon}{2} & \sinh \frac{\varepsilon}{2} \\ \sinh \frac{\varepsilon}{2} & \cosh \frac{\varepsilon}{2} \end{pmatrix} \cdot \begin{pmatrix} \xi \\ 1 \end{pmatrix}, \quad \varepsilon \ll 1. \end{aligned}$$

Hence we get

$$\xi' = \frac{\xi \cosh \frac{\varepsilon}{2} + \sinh \frac{\varepsilon}{2}}{\xi \sinh \frac{\varepsilon}{2} + \cosh \frac{\varepsilon}{2}}.$$

We follow the same procedure mentioned in the last paragraph and take Taylor expansion in the final step

$$\begin{aligned} \xi'^2 &= \frac{(\xi \cosh \frac{\varepsilon}{2} + \sinh \frac{\varepsilon}{2})^2}{(\xi \sinh \frac{\varepsilon}{2} + \cosh \frac{\varepsilon}{2})^2} \\ &= \frac{\xi^2 \cosh^2 \frac{\varepsilon}{2} + \sinh^2 \frac{\varepsilon}{2} + 2\xi \cosh \frac{\varepsilon}{2} \sinh \frac{\varepsilon}{2}}{\xi^2 \sinh^2 \frac{\varepsilon}{2} + \cosh^2 \frac{\varepsilon}{2} + 2\xi \cosh \frac{\varepsilon}{2} \sinh \frac{\varepsilon}{2}} \\ &= \frac{\xi^2 + 2\xi \cdot 1 \cdot \frac{\varepsilon}{2}}{1 + 2\xi \cdot \frac{\varepsilon}{2} \cdot 1} + O(\varepsilon^2) \\ &\sim \frac{\xi^2 + \varepsilon\xi}{1 + \varepsilon\xi} = R_8(\xi). \end{aligned} \tag{5.13}$$

Similarly, $R_7(\xi)$ can be obtained in the same way. So we can conclude that $R_6(\xi)$, $R_7(\xi)$ and $R_8(\xi)$ are connected to one another geometrically. However this geometrical connection does not guarantee the conjugacy relation among them since the conjugacy relation has to respect the symmetry of the unperturbed rational map, which in this $B = 2$ case is the continuous rotation symmetry about the z -axis. The conjugacy relation between $R_7(\xi)$ and $R_8(\xi)$ can be obtained as follows:

$$\begin{aligned} \xi &\longrightarrow \xi' = [T_{z, \frac{\pi}{2}}] \cdot \xi = \begin{pmatrix} i\xi \\ 1 \end{pmatrix} \\ \Rightarrow \xi &\longrightarrow \xi' = g(\xi) = i\xi, \end{aligned}$$

therefore

$$R_8(g(\xi)) = \frac{\xi'^2 + \varepsilon\xi'}{1 + \varepsilon\xi'} = \frac{-\xi^2 + i\varepsilon\xi}{1 + i\varepsilon\xi}.$$

Assume there exists a matrix D_g ,

$$D_g = \begin{pmatrix} a & b \\ c & d \end{pmatrix},$$

such that $R_8(g(\xi)) = D_g \cdot R_7(\xi)$, meaning

$$\begin{pmatrix} -\xi^2 + i\varepsilon_8\xi \\ 1 + i\varepsilon_8\xi \end{pmatrix} = \begin{pmatrix} a & b \\ c & d \end{pmatrix} \cdot \begin{pmatrix} \xi^2 - i\varepsilon_7\xi \\ 1 + i\varepsilon_7\xi \end{pmatrix},$$

where ε_7 and ε_8 are infinitesimal parameters for $R_7(\xi)$ and $R_8(\xi)$ respectively.

After a simple calculation, we then can easily identify that

$$D_g = \begin{pmatrix} -1 & 0 \\ 0 & 1 \end{pmatrix},$$

provided $\varepsilon_7 = \varepsilon_8$.

Since such a D_g matrix exists, it can be concluded that $R_7(\xi)$ and $R_8(\xi)$ are conjugate to each other, *i.e.*

$$R_7(\xi) \sim R_8(\xi).$$

As mentioned previously, the conjugacy relation has to respect the symmetry of the unperturbed rational map. If we try to prove that there exists a conjugacy relation between $R_6(\xi)$ and $R_7(\xi)$ or $R_6(\xi)$ and $R_8(\xi)$, we then need a rotation symmetry which rotate about the x or y -axis. But unfortunately these are not the symmetry that the $B = 2$ Skyrminion has. So $R_6(\xi)$ is neither conjugate to $R_7(\xi)$ nor to $R_8(\xi)$.

The vibrational modes in $B = 2$ can be sorted by the conjugation relation into three different classes. We list all the facts in the following table:

Perturbed Rational Map	Remarks
<p style="text-align: center;">Zero Mode</p> <p>Conjugacy Class $\left\{ \begin{array}{l} R_5(\xi) = \frac{\xi^2}{1+i\varepsilon} \\ R_1(\xi) = \frac{\xi^2+i\varepsilon\xi}{1+i\varepsilon\xi} \\ R_2(\xi) = \frac{\xi^2-\varepsilon\xi}{1+\varepsilon\xi} \end{array} \right.$</p> <p>Conjugacy Class $\left\{ \begin{array}{l} R_3(\xi) = \frac{\xi^2+i\varepsilon}{1+i\varepsilon\xi^2} \\ R_4(\xi) = \frac{\xi^2-\varepsilon}{1+\varepsilon\xi^2} \end{array} \right.$</p>	<p>Rotation about z-axis for $\varepsilon \ll 1$. See Figure 5.15 and 5.16.</p> <p>Rotation about x-axis for $\varepsilon \ll 1$. See Figure 5.11 and 5.12.</p> <p>Rotation about y-axis for $\varepsilon \ll 1$.</p> <p>Iso-rotation about x-axis for $\varepsilon \ll 1$. See Figure 5.13 and 5.14</p> <p>Iso-rotation about y-axis for $\varepsilon \ll 1$.</p>
<p style="text-align: center;">Broken Zero Mode</p> <p>Conjugacy Class $\left\{ \begin{array}{l} R_6(\xi) = \frac{\xi^2}{1+\varepsilon} \\ R_7(\xi) = \frac{\xi^2-i\varepsilon\xi}{1+i\varepsilon\xi} \\ R_8(\xi) = \frac{\xi^2+\varepsilon\xi}{1+\varepsilon\xi} \end{array} \right.$</p>	<p>Broken z translational node. See Figure 5.17 and 5.18.</p> <p>Broken y translational mode.</p> <p>Broken x translational mode. See Figure 5.21 and 5.22.</p>
<p style="text-align: center;">Vibrational Mode</p> <p>Conjugacy Class $\left\{ \begin{array}{l} R_9(\xi) = \frac{\xi^2-i\varepsilon}{1+i\varepsilon\xi^2} \\ R_{10}(\xi) = \frac{\xi^2+\varepsilon}{1+\varepsilon\xi^2} \end{array} \right.$</p>	<p>Squeeze</p> <p>Squeeze</p> <p>See Figure 5.25 and 5.26.</p>

Table 5.4: Conjugacy Classes of Perturbed Rational Maps in Baryon Number $B = 2$

We here give more details of the origin of the pseudo fixed points of perturbation. As one has seen in (5.11) and (5.13), we realize that the expressions of $R_1(\xi) = \frac{\xi^2 + i\varepsilon\xi}{1 + i\varepsilon\xi}$ and $R_8(\xi) = \frac{\xi^2 + \varepsilon\xi}{1 + \varepsilon\xi}$ are merely the results of Taylor expansion of the following expression, called the full expression, to the first order:

$$R_1(\xi) = \left[\frac{\xi \cos(\frac{\varepsilon}{2}) + i \sin(\frac{\varepsilon}{2})}{i\xi \sin(\frac{\varepsilon}{2}) + \cos(\frac{\varepsilon}{2})} \right]^2 ,$$

$$R_8(\xi) = \left[\frac{\xi \cosh(\frac{\varepsilon}{2}) + \sinh(\frac{\varepsilon}{2})}{\xi \sinh(\frac{\varepsilon}{2}) + \cosh(\frac{\varepsilon}{2})} \right]^2 .$$

In searching for the fixed points of the perturbation, we have

$$R_1(\xi) = \left[\frac{\xi \cos(\frac{\varepsilon}{2}) + i \sin(\frac{\varepsilon}{2})}{i\xi \sin(\frac{\varepsilon}{2}) + \cos(\frac{\varepsilon}{2})} \right]^2 = \xi^2 \Rightarrow \xi = \pm 1 ,$$

$$R_8(\xi) = \left[\frac{\xi \cosh(\frac{\varepsilon}{2}) + \sinh(\frac{\varepsilon}{2})}{\xi \sinh(\frac{\varepsilon}{2}) + \cosh(\frac{\varepsilon}{2})} \right]^2 = \xi^2 \Rightarrow \xi = \pm 1 .$$

The fixed point which only appears in the first order of Taylor expansion of the full expression of the rational map is what we called the pseudo fixed point.

5.5 Plots of Rational Maps and Energy Density

In this section, we will present the deformations of the rational maps under the perturbations from the original rational map for $B = 1, 2,$ and $4,$ and their associated energy density.

5.5.1 $B = 1$

□ Plots of rational maps

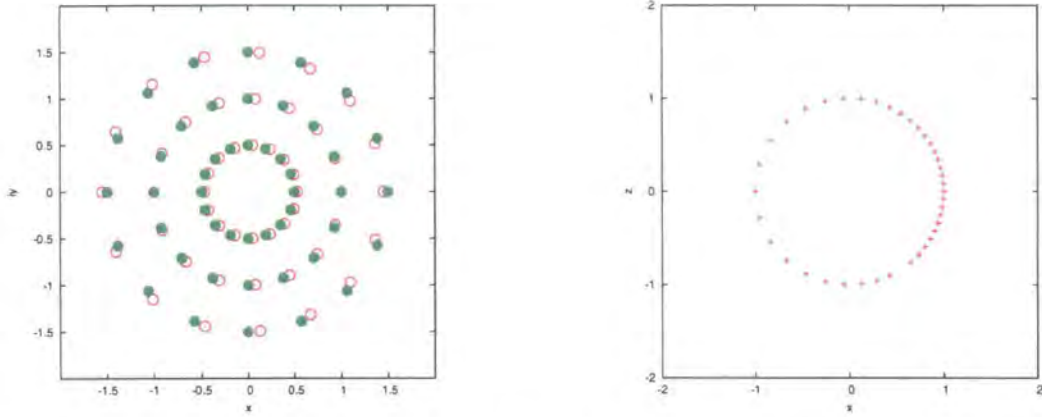


Figure 5.5: (Left) Green dots: The sample points of the domain(or physical) space. Red circles: The corresponding sample points of the deformed domain space of R_4 of $B = 1$. (Right) A slice of the stereographic projection of the complex plane.

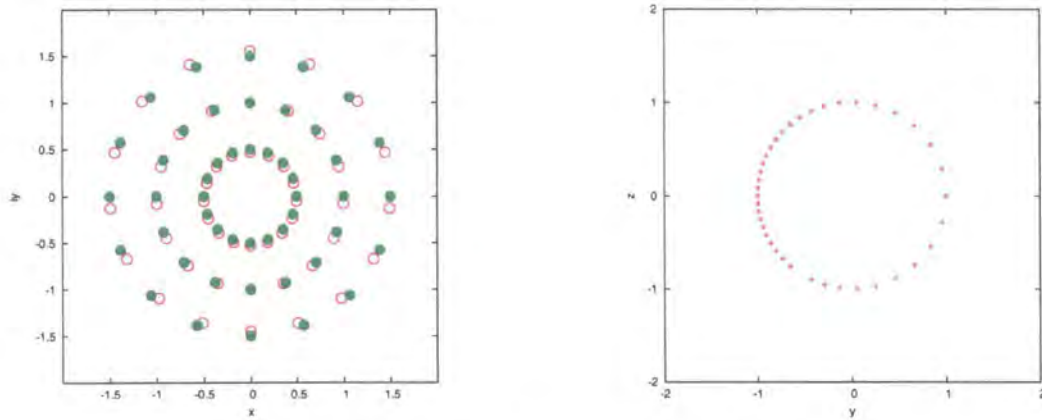


Figure 5.6: Perturbed rational map R_5 of $B = 1$.

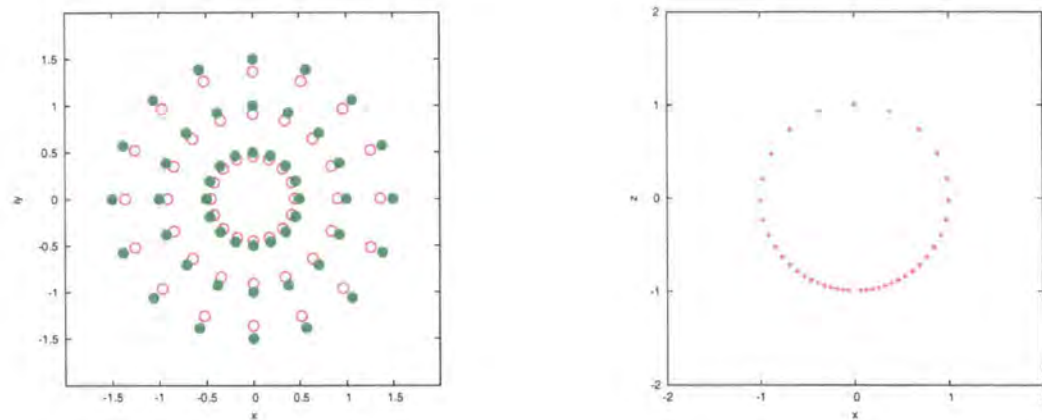
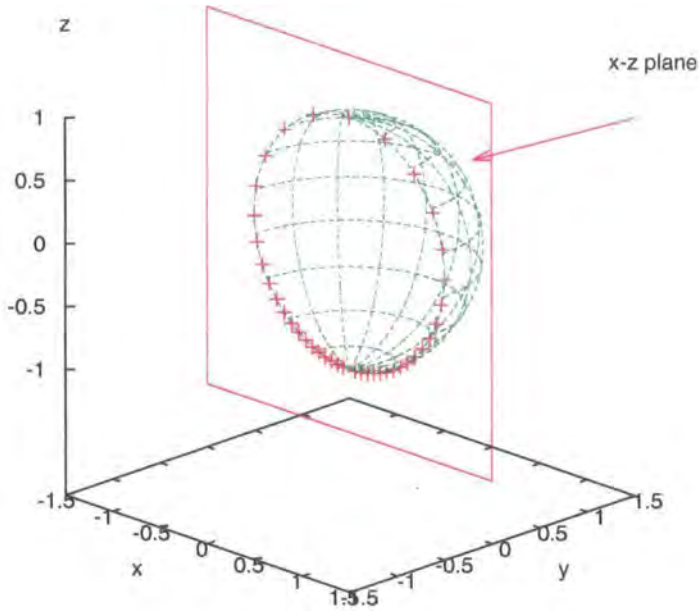


Figure 5.7: Perturbed rational map R_6 of $B = 1$.

Figure 5.8: $R_6, B=1$

Here we give an explanation to the figures in Fig. 5.5, 5.6 and 5.7. As mentioned previously, a rational map is a mapping from \mathbb{S}^2 to \mathbb{S}^2 . Via the stereographic projection, we can map \mathbb{S}^2 to the complex plane \mathbb{C} , which is the one we use in the left plots of the Fig. 5.5, 5.6 and 5.7. Since we would like to understand the deformations of the original domain space induced by the perturbed rational maps R_i , by taking some sample points in the domain space, we then can have a basic idea of how the domain space changes, or deforms, under the perturbed rational maps. Those green dots and red circles in the left part of Fig. 5.5, 5.6 and 5.7 represent respectively the sample points of the original domain space and of the deformed domain space of the rational maps. While obtaining the deformed domain space in the realization of the complex plane \mathbb{C} , we can find their corresponding deformations in \mathbb{S}^2 by taking the stereographic projection for different perturbed rational maps R_i . We demonstrate a part of the stereographic projection of R_6 of $B = 1$ in Fig. 5.8 by slicing \mathbb{S}^2 with x - z plane and that appears as the right part of Fig. 5.7. The other two plots in the right part of Fig. 5.5 and 5.6 can be also obtained by doing the similar actions

on \mathbb{S}^2 for R_4 and R_5 of $B = 1$ with the x - z and y - z plane. Furthermore, as one can see in the right part of Fig. 5.5, 5.6 and 5.7, those deformed sample points are not distributed uniformly as they were in the original domain space, instead they stretch around the x , y and z -axis respectively. Because the stretching behavior is only on the angular part, we call it “angular stretching”. It has to be noted that these modes are the broken translational modes, rather than the genuine vibrational modes.

In addition to the plots of the perturbed rational map presented previously, we also show the plots of the energy density, which are obtained by the method mentioned in section 2.3, in the next page. Since these three broken translational modes in $B = 1$ are conjugate to each other, we only display the plots of the energy density of the rational map R_6 , which is the mode of angular stretching about the z -axis. The perturbation parameter ε used for producing the plots of the positive mode, namely the mode with a positive perturbation parameter ε , in the left part of Figure 5.9 and Figure 5.10 is 2; the one used in the negative mode, shown in the right part of Figure 5.9 and Figure 5.10, is -0.67 . The reason why we choose two different parameters for ε is to demonstrate the deformation clearly. As one can see, the energy density is axially symmetric about the z -axis but not about the x or y -axis, which matches the results shown in the Figure 5.7.

There is one thing needed to be pointed out that when generating the plots of the energy density, we choose the parameter of the pion mass to be zero. Since the effect caused by the pion mass is merely on the profile function but not on the rational map, which means the the angular part of the Skyrmion will not be influenced, we thus still can have the reasonable plots of the energy density with such a value of the pion mass.

□ Plots of energy density

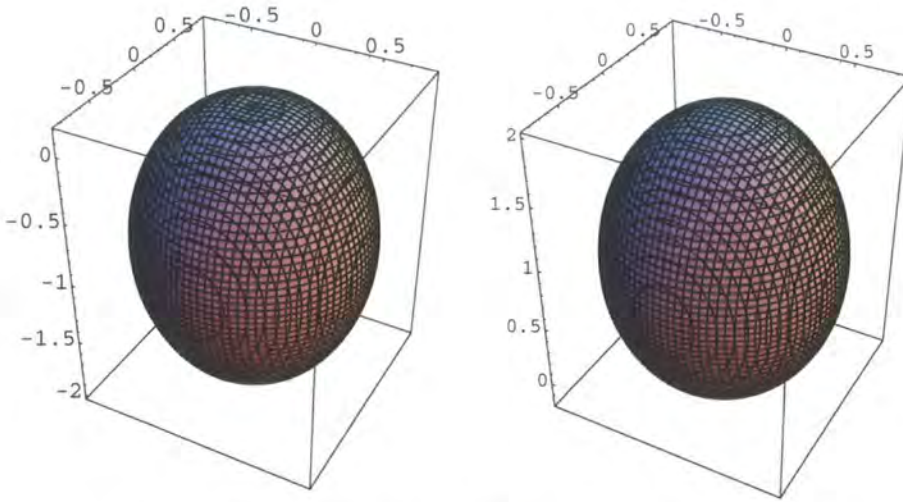


Figure 5.9: $B = 1$: (Left) $R_6(\xi)$, $\varepsilon = 2$; (Right) $R_6(\xi)$, $\varepsilon = -0.670$.

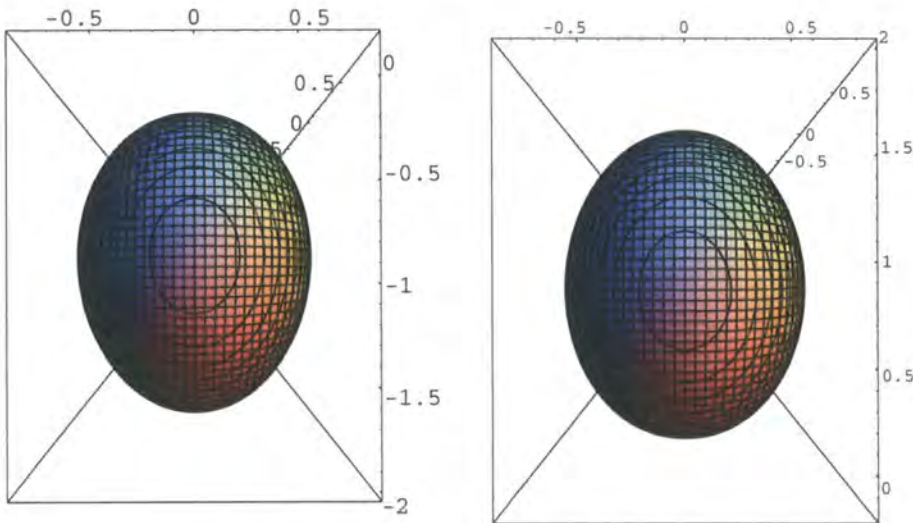


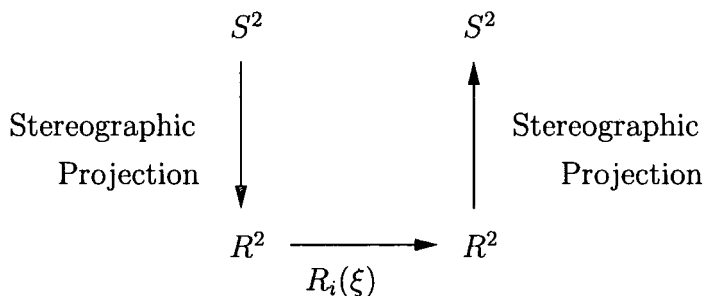
Figure 5.10: $B = 1$, $R_6(\xi)$, side view: (Left) $\varepsilon = 2$; (Right) $\varepsilon = -0.67$.

Rational Map	Description of Energy Density
Zero Mode	
$R_0(\xi)$	A sphere.
$\left\{ \begin{array}{l} R_1(\xi) \\ R_2(\xi) \\ R_3(\xi) \end{array} \right.$	<p>Rotational zero mode about y-axis.</p> <p>Rotational zero mode about x-axis.</p> <p>Rotational zero mode about z-axis.</p>
Broken Zero Mode	
$\left\{ \begin{array}{l} R_4(\xi) \\ R_5(\xi) \\ R_6(\xi) \end{array} \right.$	<p>Angular stretching about x-axis.</p> <p>Angular stretching about y-axis.</p> <p>Angular stretching about z-axis. See in Figure 5.9 and Figure 5.10.</p>

Table 5.5: Description of the energy density of the perturbed rational maps, $B = 1$.

5.5.2 $B = 2$

Although it is simple to present the results on the complex plane, topologically equivalent to \mathbb{R}^2 , instead of on \mathbb{S}^2 itself, it is not very easy to visualize the real deformations of S^2 from those projected onto \mathbb{R}^2 . But it still would be nice to find a special way to have the results in three dimensional space shown in two dimensional plane. Thus, we have determined a method of being able to demonstrate the deformations of \mathbb{S}^2 clearly in two dimensional space; however, we need to take use of the stereographic projection once more, *i.e.*



Then we project the outcomes on S^2 onto the x - y , y - z and x - z plane respectively to realize our idea of showing S^2 clearly on R^2 .

We now give more information about how to read these projected figures which are presented later. The green dots in the figures represent the sample points in domain space S^2 and we want to study how these sample points deform under the perturbed rational maps. First, we map the sample points to the target space S^2 through the perturbed rational map, $R_i(\xi)$. However, we need to put these two sets of points in the same space (either domain or target space) to understand how one set of points change from the other set under the influence of the perturbed rational map, and the pattern of the change. Therefore, we choose to take the set of points mapped to the target space back to the domain space via $R_0^{-1}(\xi)$, and call these points the deformation of S^2 . Once we have the two sets of points in the same space S^2 , we project them onto the subspace R^2 of R^3 , into which S^2 is embedded, so that one can easily see the change between the original and deformed sample points. The planes to which we choose to project from S^2 are x - y , y - z , and x - z plane of R^3 .

The figures in the next pages are the representatives of the conjugacy classes of the perturbed rational maps of baryon number $B = 2$.

□ Plots of zero modes

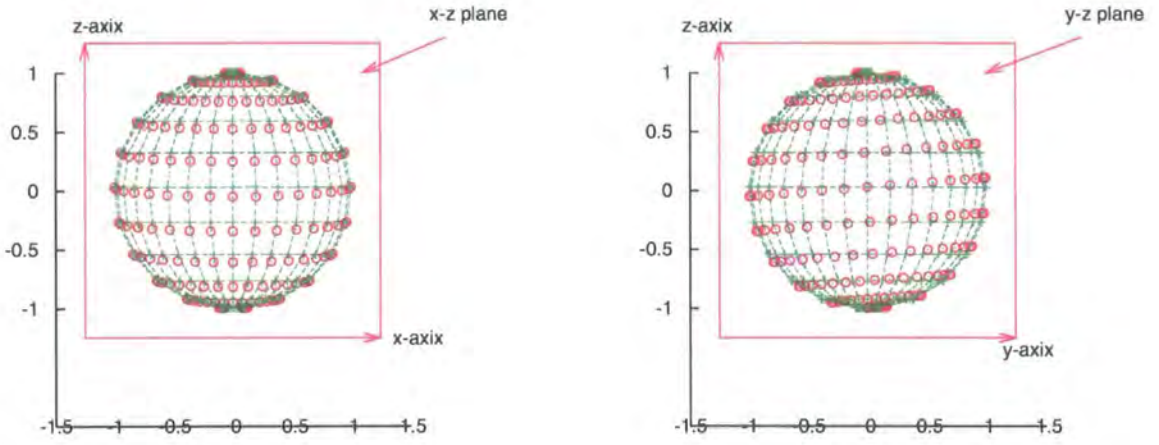


Figure 5.11: $R_1, B=2$

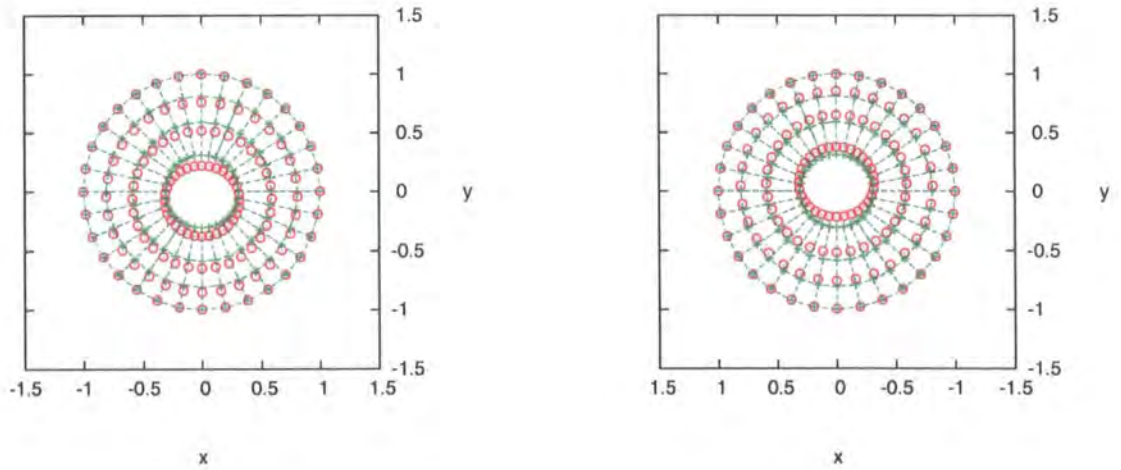


Figure 5.12: Northern(left) and southern(right) hemisphere of Riemann sphere of $R_1, B=2$

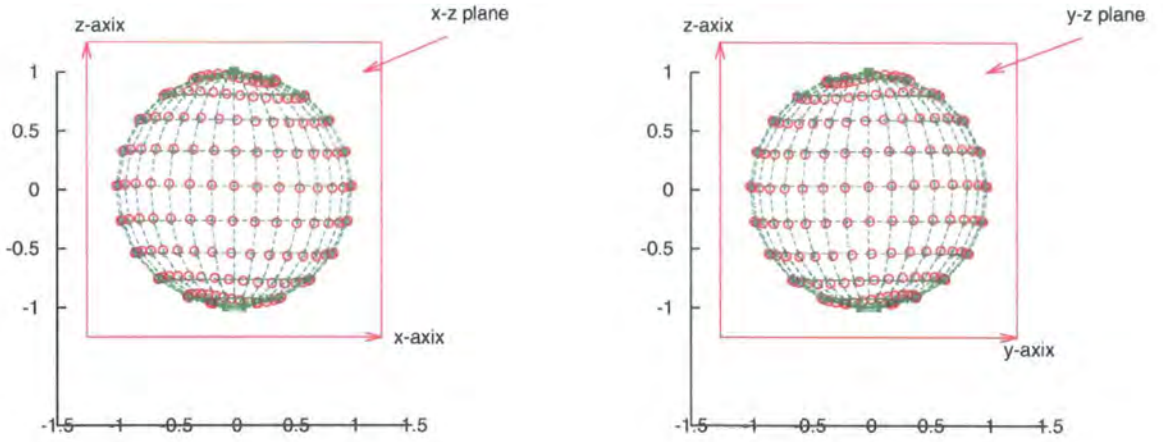


Figure 5.13: $R_3, B=2$

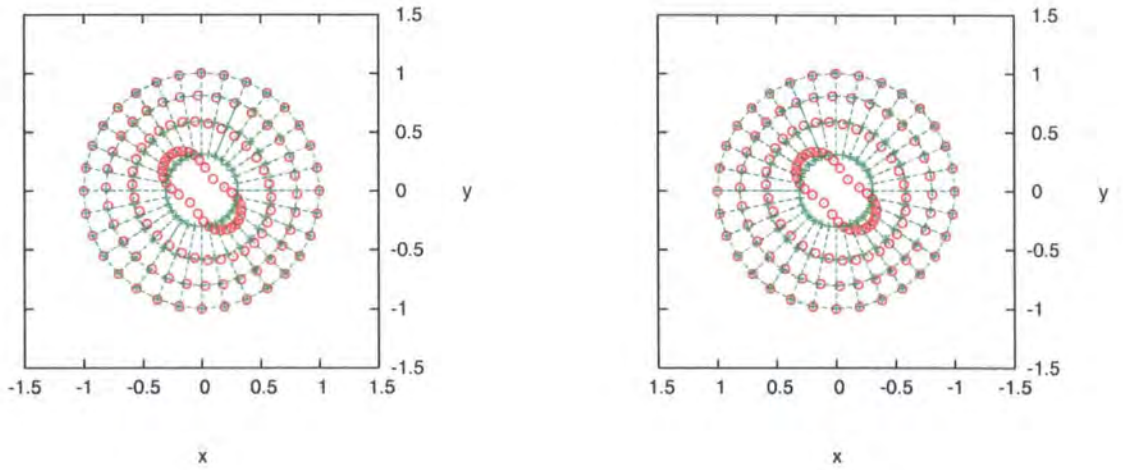


Figure 5.14: Northern(left) and southern(right) hemisphere of Riemann sphere of $R_3, B=2$

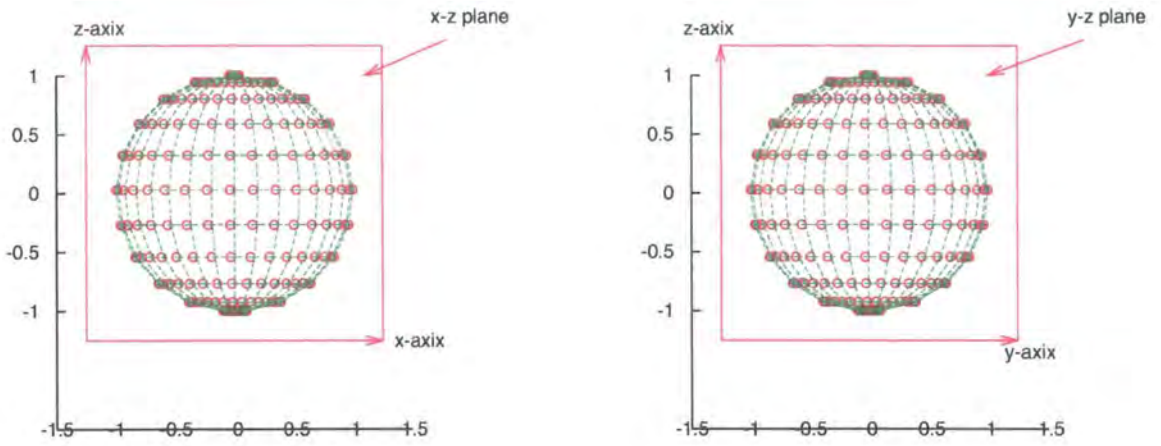


Figure 5.15: $R_5, B=2$

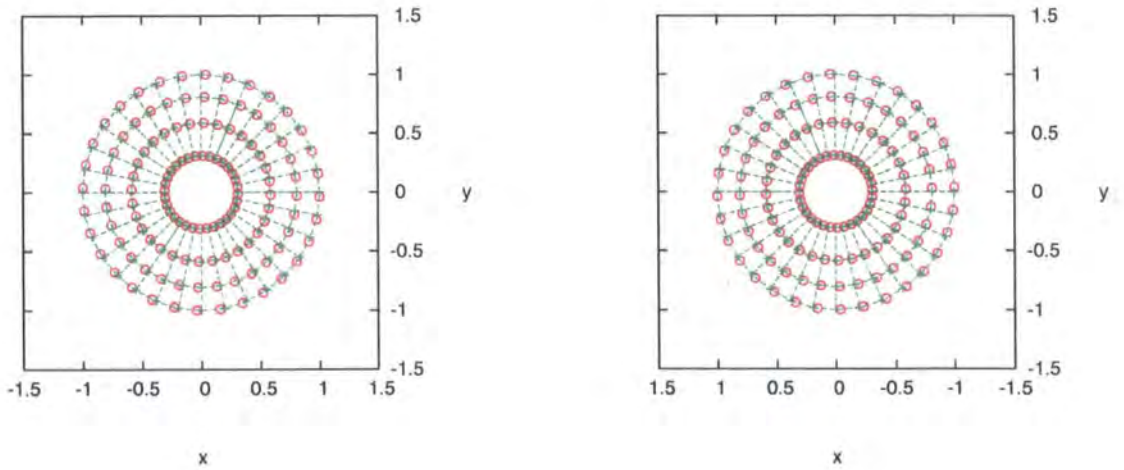


Figure 5.16: Northern(left) and southern(right) hemisphere of Riemann sphere of $R_5, B=2$

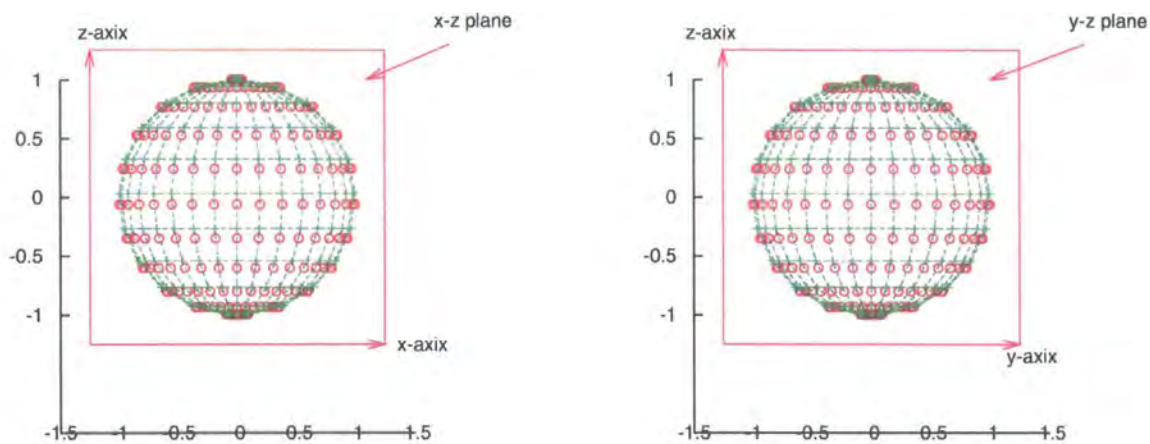


Figure 5.17: $R_6, B=2$

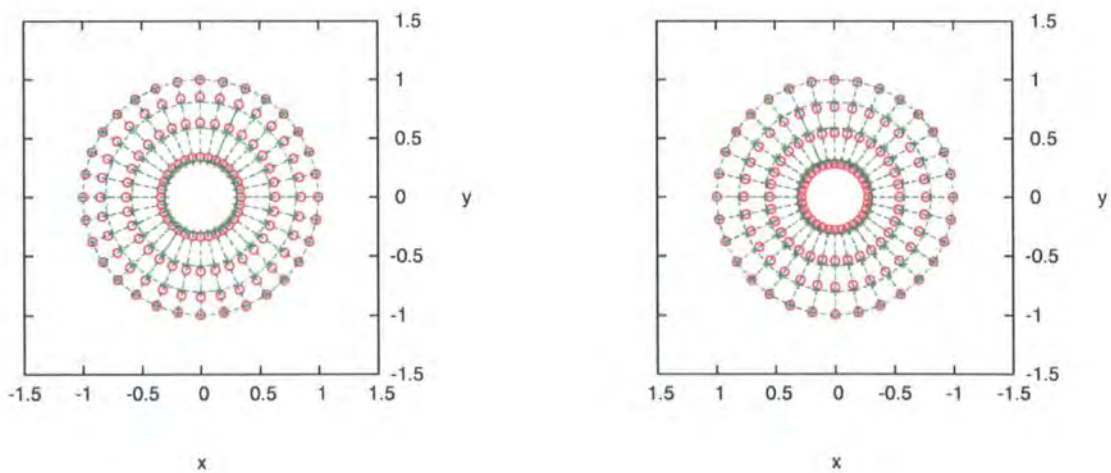


Figure 5.18: Northern(left) and southern(right) hemisphere of Riemann sphere of $R_6, B=2$

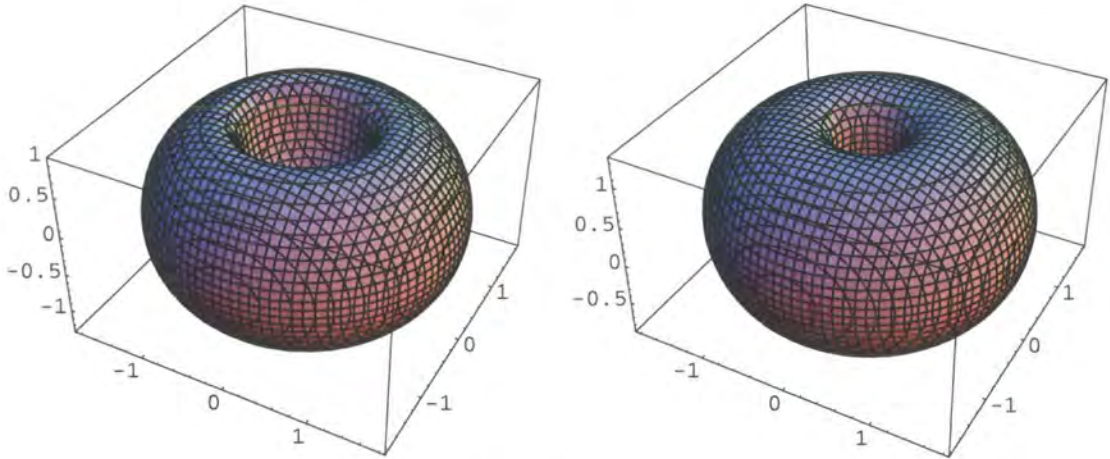


Figure 5.19: $B = 2$, $R_6(\xi)$: (Left) $\varepsilon > 0$; (Right) $\varepsilon < 0$.

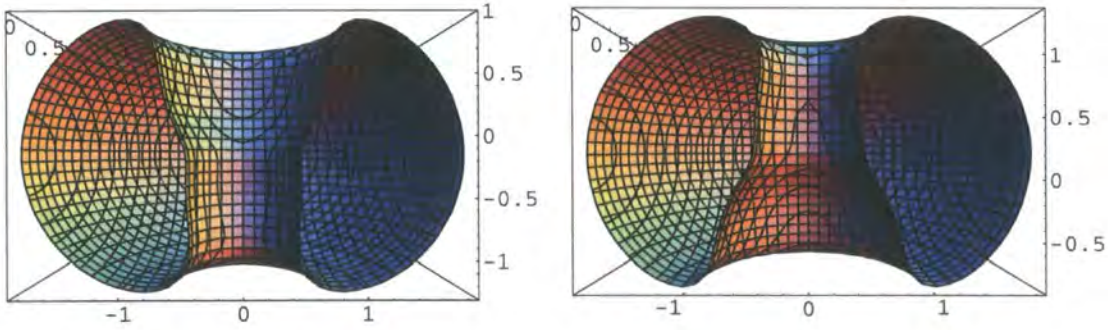


Figure 5.20: $B = 2$, $R_6(\xi)$, half side view: (Left) $\varepsilon > 0$; (Right) $\varepsilon < 0$.

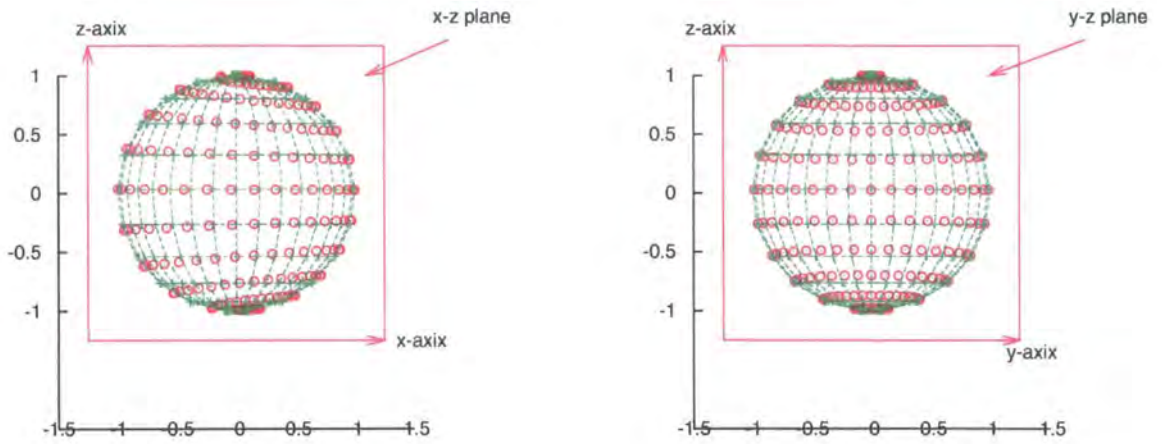


Figure 5.21: $R_8, B=2$

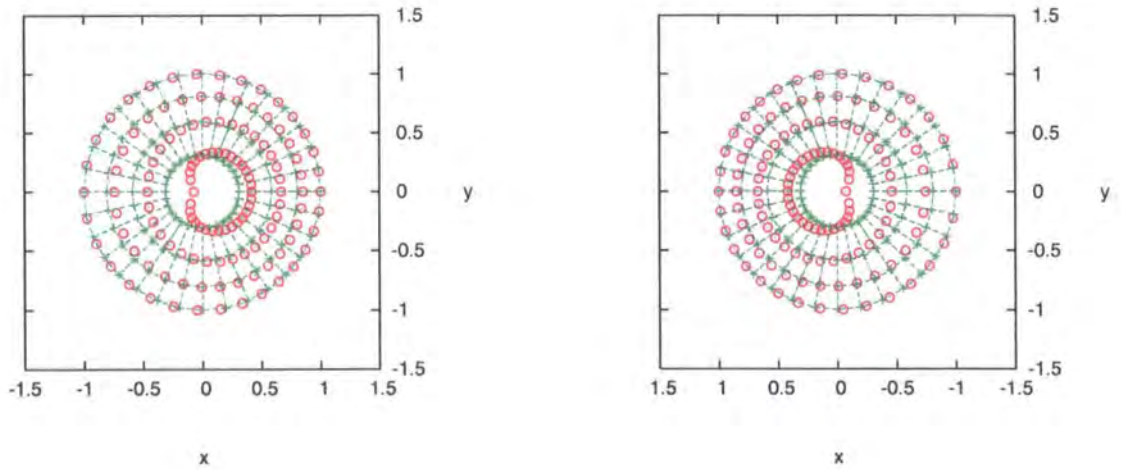


Figure 5.22: Northern(left) and southern(right) hemisphere of Riemann sphere of $R_8, B=2$

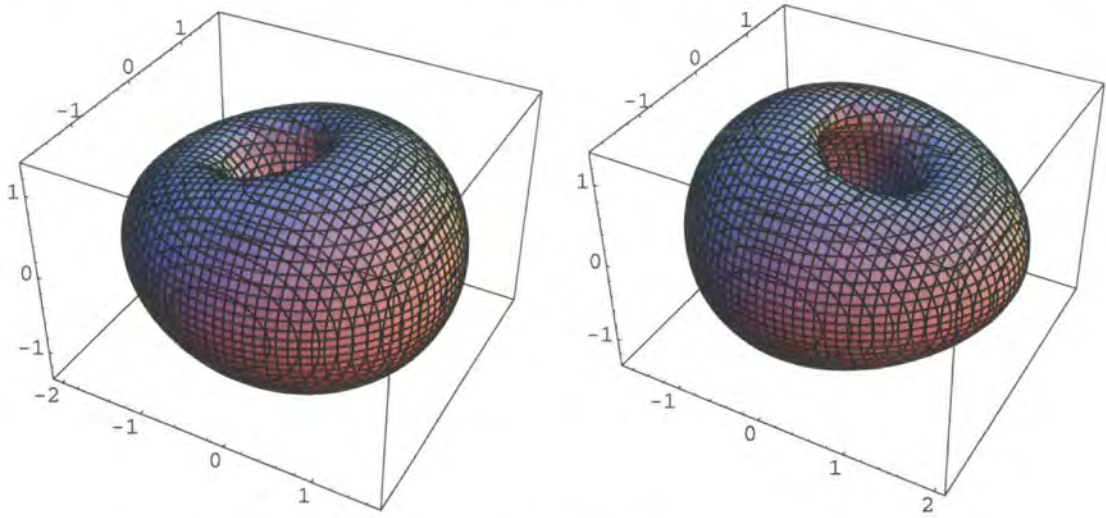


Figure 5.23: $B = 2$, $R_8(\xi)$: (Left) $\varepsilon > 0$; (Right) $\varepsilon < 0$.

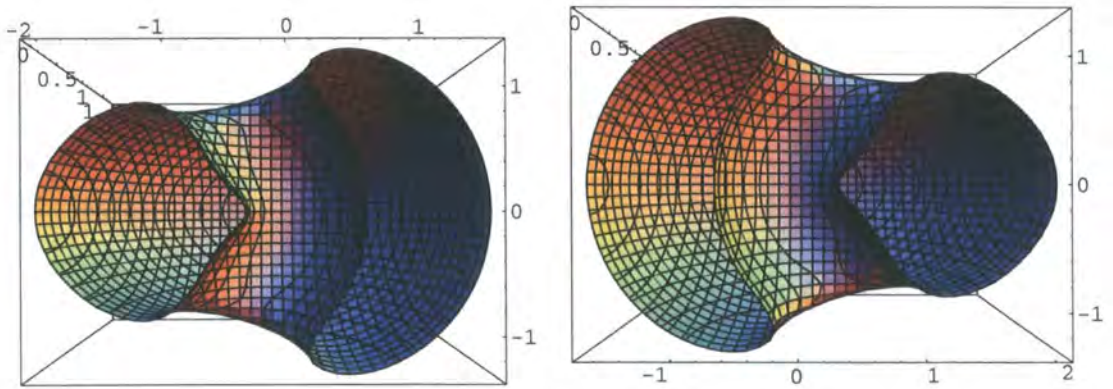


Figure 5.24: $B = 2$, $R_8(\xi)$, half side view: (Left) $\varepsilon > 0$; (Right) $\varepsilon < 0$.

□ Plots of vibrational modes

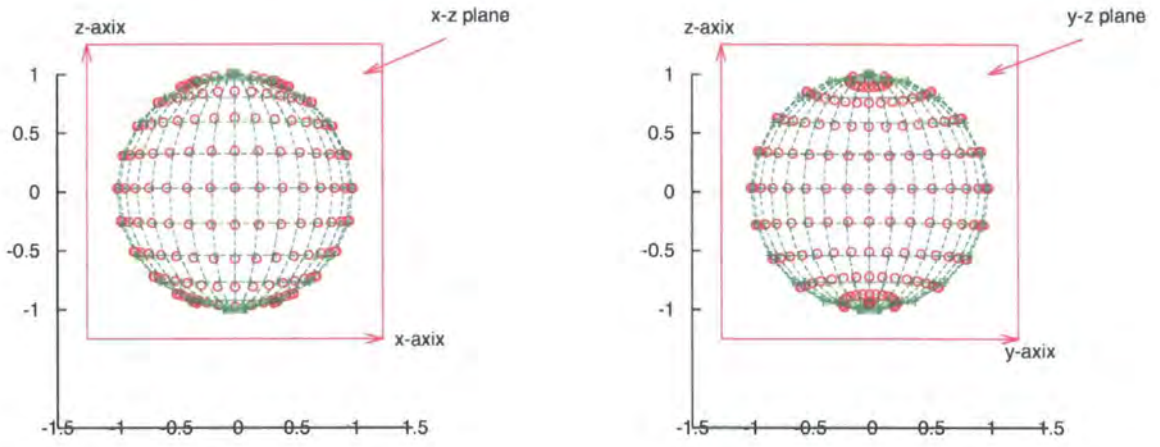


Figure 5.25: $R_{10}, B=2$

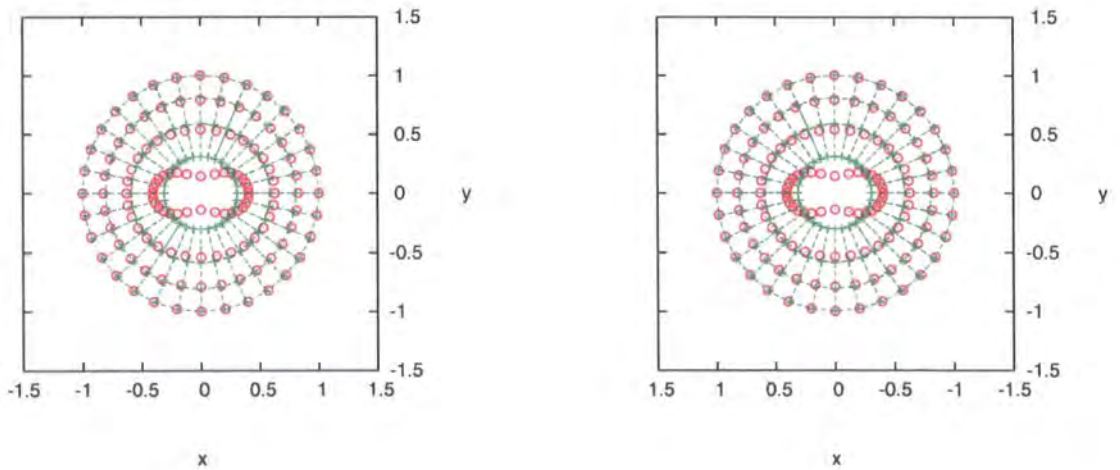


Figure 5.26: Northern(left) and southern(right) hemisphere of Riemann sphere of $R_{10}, B=2$

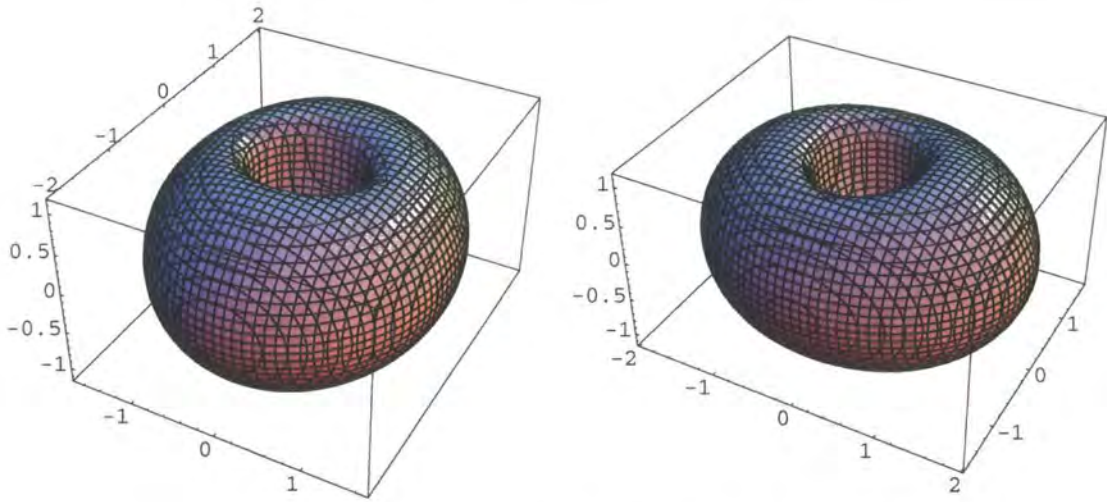


Figure 5.27: $B = 2$, $R_{10}(\xi)$: (Left) $\varepsilon > 0$; (Right) $\varepsilon < 0$.

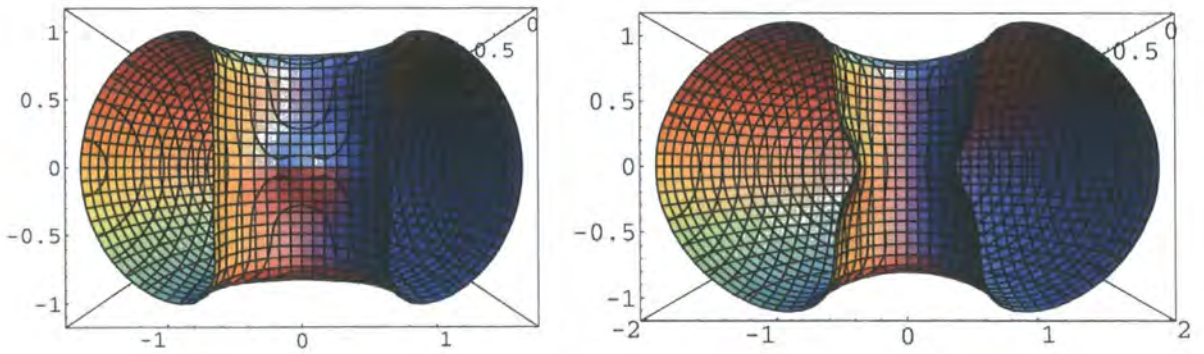


Figure 5.28: $B = 2$, $R_{10}(\xi)$, half side view: (Left) $\varepsilon > 0$; (Right) $\varepsilon < 0$.

Rational Map	Description of Energy density
Zero Mode	
$R_0(\xi)$	A torus.
$\left\{ \begin{array}{l} R_1(\xi) \\ R_2(\xi) \\ R_5(\xi) \end{array} \right.$	Rotational zero mode about x -axis.
	Rotational zero mode about y -axis.
	Rotational zero mode about z -axis.
$\left\{ \begin{array}{l} R_3(\xi) \\ R_4(\xi) \end{array} \right.$	Iso-rotational zero mode about x -axis.
	Iso-rotational zero mode about y -axis.
Broken Zero Mode	
$R_6(\xi)$	Broken z translational zero mode. One of the upper and lower part of the hole expands and the other shrinks. See in Figure 5.19.
$\left\{ \begin{array}{l} R_7(\xi) \\ R_8(\xi) \end{array} \right.$	Broken y translational zero mode.
	Broken x translational zero mode. One end of the torus inflates and the opposite end deflates. See in Figure 5.23.
Vibrational Mode	
$\left\{ \begin{array}{l} R_9(\xi) \\ R_{10}(\xi) \end{array} \right.$	Two opposite ends of the torus stretches and two other ends, whose connecting line is perpendicular to that of the previous pair of opposite ends, contracts. See in Figure 5.27.
	Same as $R_9(\xi)$.

Table 5.6: Description of the energy density of the perturbed rational maps, $B = 2$.

We here briefly review all the modes obtained by perturbing the rational map in the $B = 2$ case. There are ten rational modes, five of them are zero modes, another three are broken zero mode and the other two are the genuine vibrational modes. The five zero modes are recognized as a triplet for the rotational zero modes, a doublet for the iso-rotational zero modes. Three broken zero modes are divided into a singlet for the broken z translational zero mode, and a doublet for the other broken translational zero modes. The two genuine vibrational modes comprise a doublet.

Since the translational zero modes are broken, the effect of the broken z translation causes the deformation on the rational map that the upper part of the hole expands when the lower part of that shrinks, and vice versa, as seen in Figure 5.17 and 5.18. As for the broken x and y translational modes, the representative seen in Figure 5.23, the deformation is the inflation at one end of the torus and the deflation at the opposite end. The doublet for the vibrational modes corresponds to two squeezing modes. The description of one of the squeezing mode, R_{10} , is that two opposite ends of the torus stretches and two other ends, whose connecting line is perpendicular to that of the previous pair of opposite ends, contracts, as shown in Figure 5.27.

Chapter 6

Eigen Mode of Rational Map (II)

In this chapter, we will follow the procedure taken in the previous chapter to study the eigen mode of the rational map for the $B = 4$ case.

6.1 $R_{18}(\xi)$, $B = 4$

The eigenvector of the highest eigenvalue and hence its corresponding perturbed rational map in the $B = 4$ case is as follows

$$\left(0 \ 0 \ 0 \ 0 \ 0 \ 0 \ 0 \ 0 \ 0 \ -0.26726 \varepsilon \ 0 \ 0 \ 0 \ 0 \ 0.92582 \ i \varepsilon \ 0 \ 0 \ -0.26726 \varepsilon \ 0 \right)^t$$

$$\Rightarrow R_{18}(\xi) = \frac{P_0}{Q_0 - 0.26726 \varepsilon \xi^4 + 0.92582 \ i \varepsilon \xi^2 - 0.26726 \varepsilon} \xrightarrow{\text{rescale}} \frac{P_0}{Q_0(1 - \varepsilon)}, \quad (6.1)$$

where $P_0 = \xi^4 + 2\sqrt{3} \ i \xi^2 + 1$ and $Q_0 = \xi^4 - 2\sqrt{3} \ i \xi^2 + 1$.

This vibrational mode $R_{18}(\xi)$ is a tetrahedral mode since a one parameter family of rational map of degree four with the tetrahedral symmetry takes the form [42]

$$R(z) = c \frac{\xi^4 + 2\sqrt{3} \ i \xi^2 + 1}{\xi^4 - 2\sqrt{3} \ i \xi^2 + 1},$$

where c is a real number parameter. Comparing the above rational map with the one in (6.1) tells us that $R_{18}(z)$ is indeed a tetrahedral mode with $c = (1 + \varepsilon)$.

Taking the same procedure used previously to analyze or to visualize a vibrational mode of $B = 4$, rational map $R_{18}(\xi)$, we present the plots

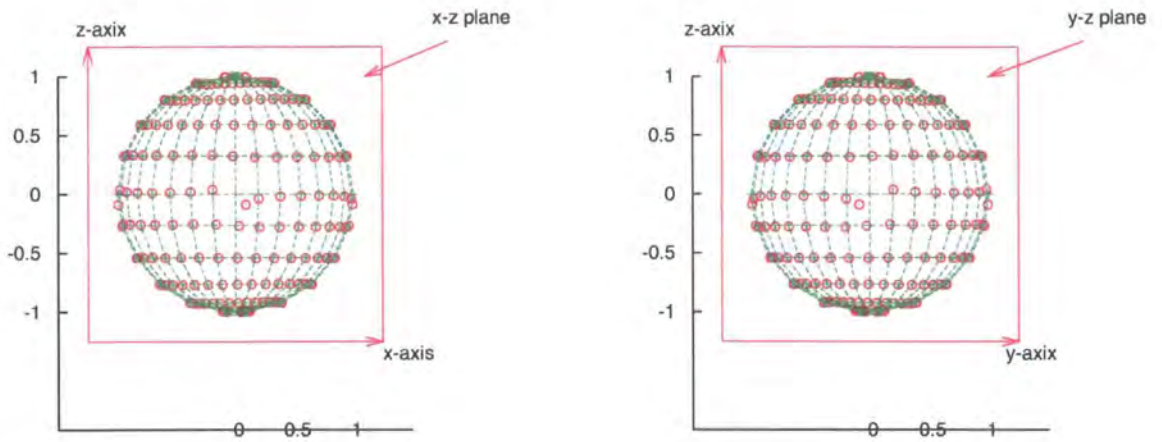


Figure 6.1: R_{18} , $B=4$

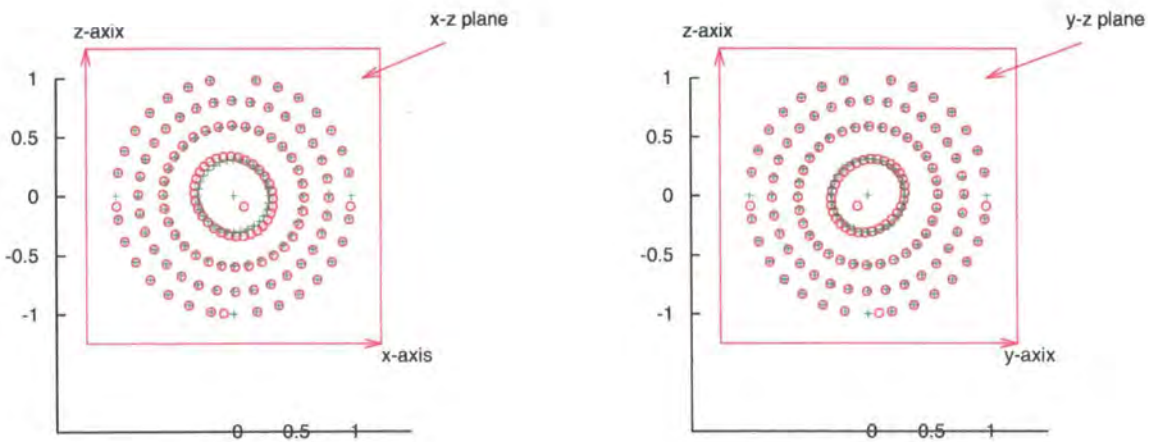


Figure 6.2: R_{18} , $B=4$

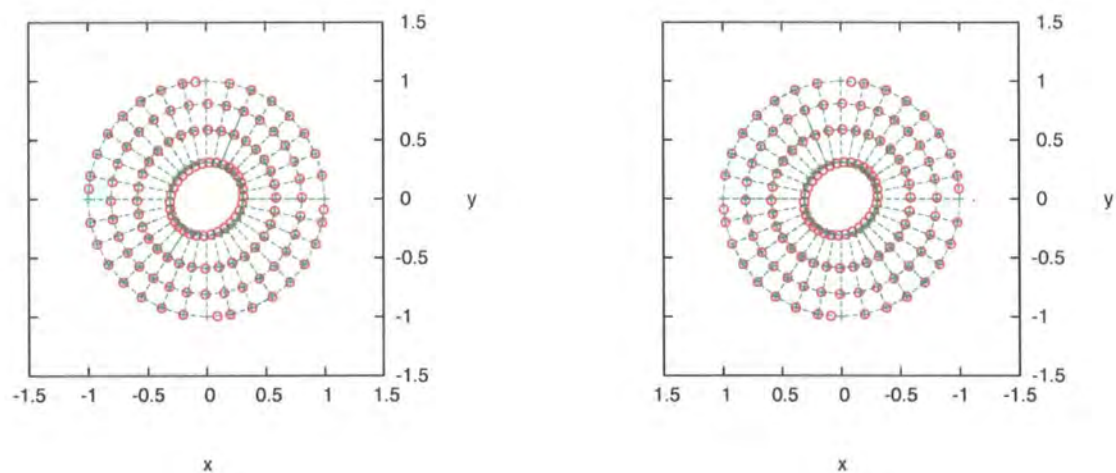


Figure 6.3: Northern(left) and southern(right) hemisphere of Riemann sphere of R_{18} , $B=4$.

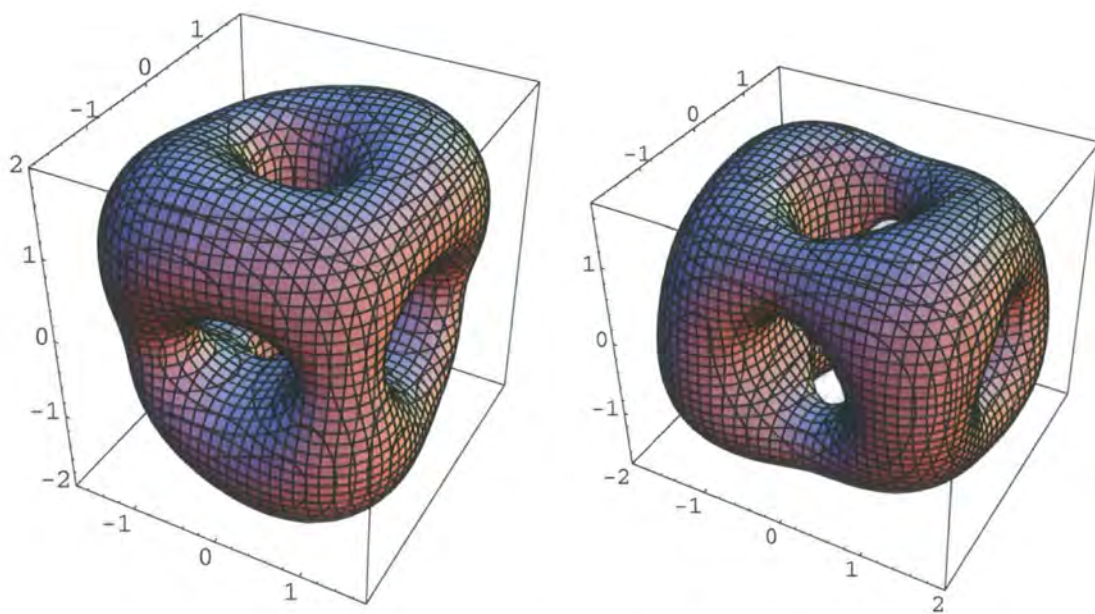


Figure 6.4: $B = 4$, $R_{18}(\xi)$: (Left) $\varepsilon > 0$; (Right) $\varepsilon < 0$.

As we have mentioned earlier, the green points in the figures above are the sampling points of the domain space \mathbb{S}^2 of the rational map, and the red points are the perturbed points obtained from inserting the sample points into the perturbed rational map and then taking those associated points in target space back to the domain space via the inverse map of the unperturbed rational map, R_0^{-1} . We hence refer these perturbed points as the deformation of the unperturbed rational map or just simply as the perturbed rational map.

The deformation, projected on the x - y plane, of the rational map $R_{18}(\xi)$ in the northern hemisphere and in the southern hemisphere are out of phase, meaning that the deformations of $R_{18}(\xi)$ in the northern and southern hemisphere are perpendicular to each other. If one looks at the deformation without the aid of the projection, the diameter of the circle on the northern hemisphere is stretched and its two ends move downwards to the equator, and the other diameter perpendicular to the previous one is contracted and its two ends move upwards to the north pole. The circle of the same size on the southern hemisphere deforms similarly to the equator and south pole.

Furthermore, as one can see in the both sides of the Figure 6.1, there is a discontinuity in the middle of the equator of the Riemann sphere. It seems quite unnatural and, hence, it is necessary for us to understand the essence of this discontinuity, which is identified as at the point, $\xi = 1$, in the complex plane that is projected onto the Riemann sphere by the stereographic projection. We therefore divide the neighborhood of the point, $\xi = 1$, into sixteen small parts, where the same color will be assigned to two regions that are reflective with respect to $\xi = 1$ and their corresponding parts in the target space, as done in Figure 6.6 later figures, and map each of the parts into the target space of the rational maps to see how it covers the target space. The reason for doing so is to check whether this discontinuity is due to the incomplete covering of the target space from the domain space. We try to apply four different numerical values of parameter ε , which are 0, 0.01, 0.05 and 0.1 respectively, to the rational map to realize how it varies as ε changes. The results are presented in the following.

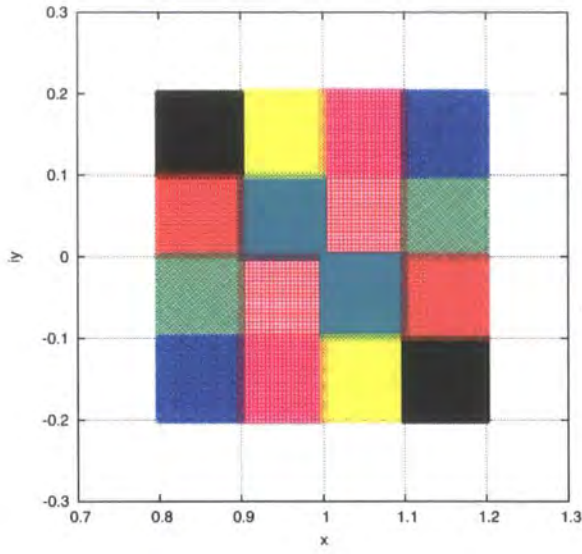


Figure 6.5: The neighborhood of $\xi = 1$

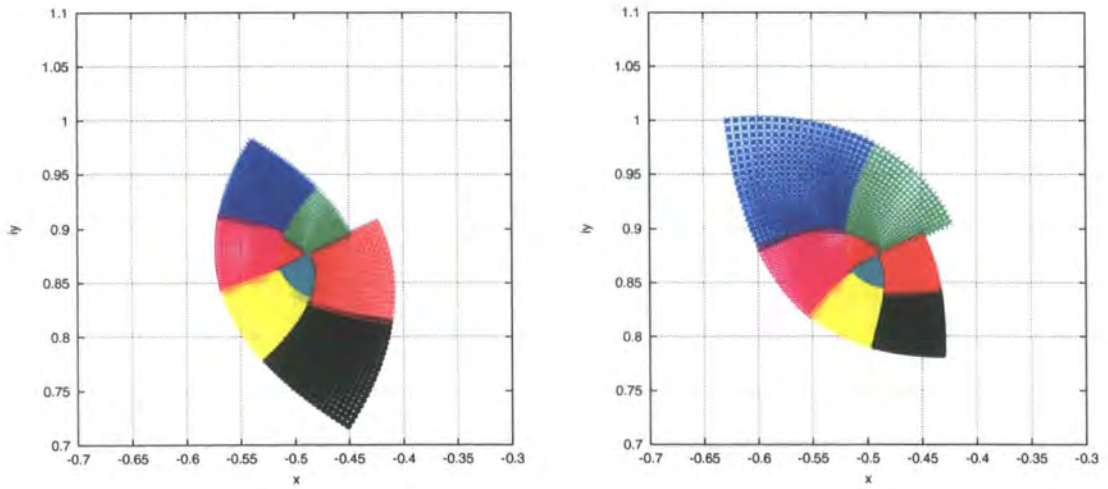


Figure 6.6: Parameter $\varepsilon = 0$, (left)upper half plane and (right)lower half plane of the target space of the rational map $R_{18}(\xi)$, $B=4$

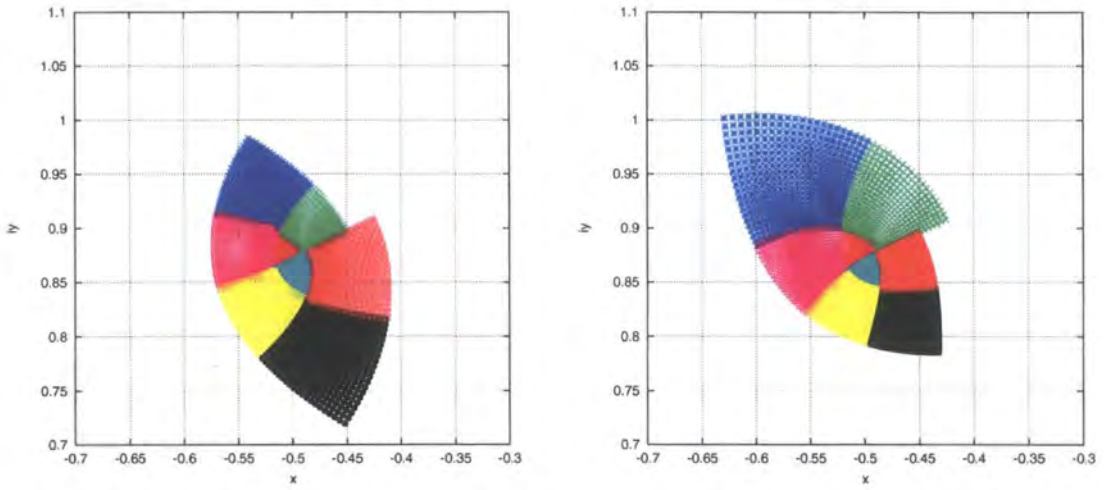


Figure 6.7: Parameter $\epsilon = 0.01$, (left)upper half plane and (right)lower half plane of the target space of the rational map $R_{18}(\xi)$, $B=4$

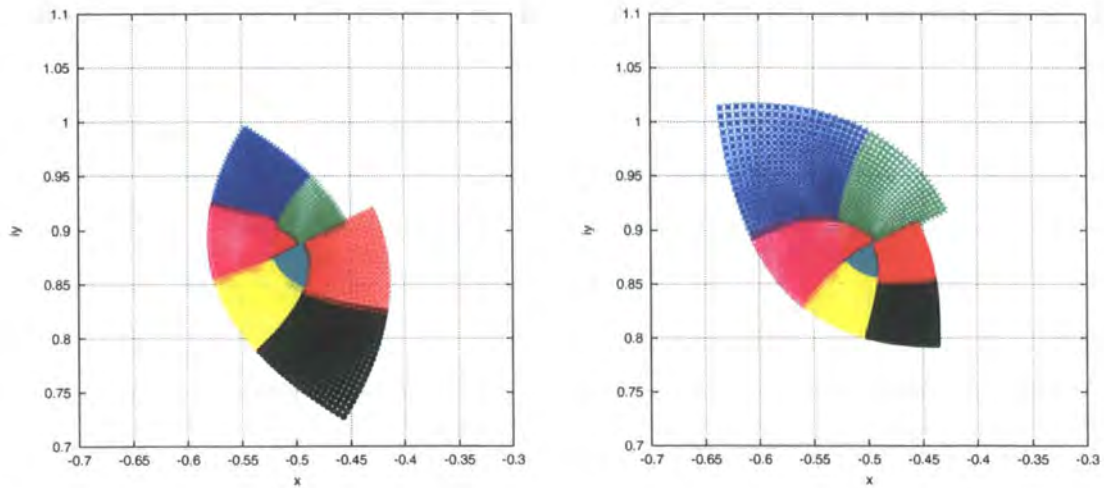


Figure 6.8: Parameter $\epsilon = 0.05$, (left)upper half plane and (right)lower half plane of the target space of the rational map $R_{18}(\xi)$, $B=4$

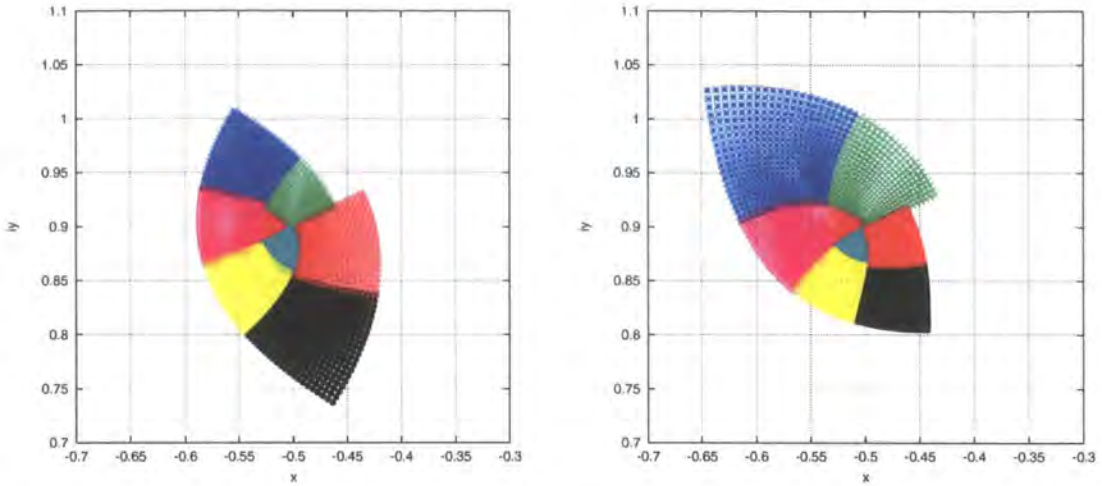


Figure 6.9: Parameter $\varepsilon = 0.1$, (left) upper half plane and (right) lower half plane of the target space of the rational map $R_{18}(\xi)$, $B=4$

The outcome shown from the figures above is very clear that in the neighborhood of $\xi = 1$ the target space is covered completely and in fact it is a double covering which means that a point in the target space has two pre-images; in other words, two different points in the domain space can map into the same point in the target space. However, it is well-known that the target space of the rational map with winding number four is covered four times instead of twice mentioned here. The truth is that indeed there are four pre-images for each point in the target space, and a further explanation will be given in the next paragraph. Another noticeable fact coming from these figures is that different values of parameters ε only induce the translation of the pattern mapped from the domain space without deformation. Since the target space is obviously continuous, the question of what causes this discontinuity still remains. In fact, the problem appears from the action, mentioned in the commutative diagram in section 5.3.2, of taking the point in target space back to domain space using inverse mapping of the unperturbed rational map when we try to understand or visualize how a perturbed rational map induces the movement of the points in the physical space. Hence the next step is to map the aforementioned areas in target space back to the domain space to check how they change from the original area, composed of sixteen small squares, under the perturbed rational map. Here are the consequences.

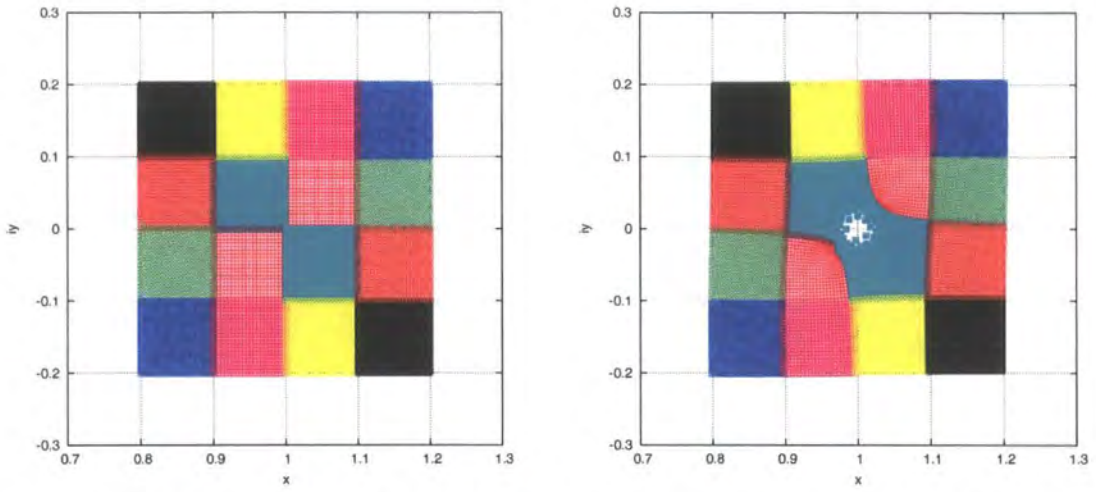


Figure 6.10: Neighborhood of $\xi = 1$ under the perturbed rational map R_{18} , $B=4$, with parameter $\varepsilon = 0$ (left) and parameter $\varepsilon = 0.01$ (right)

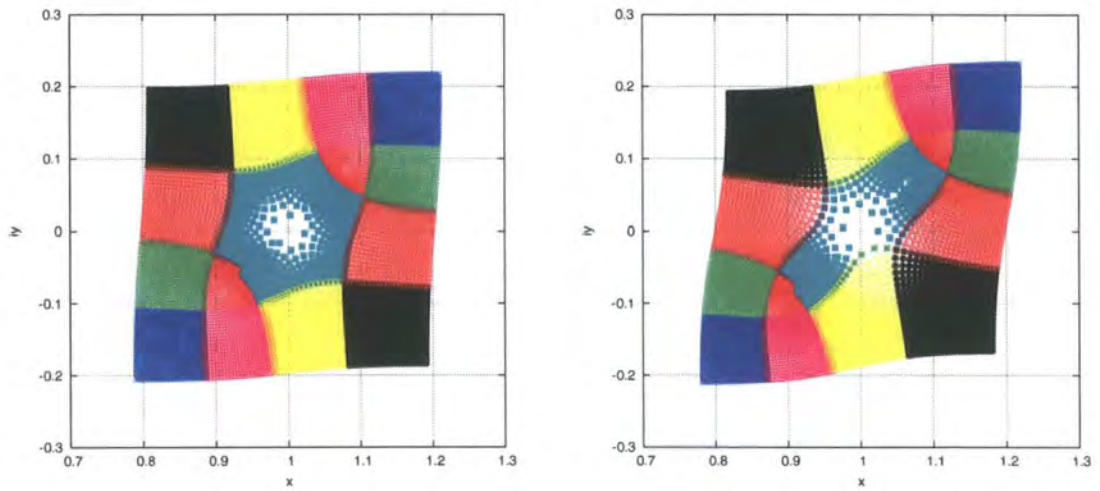


Figure 6.11: Neighborhood of $\xi = 1$ under the perturbed rational map R_{18} , $B=4$, with parameter $\varepsilon = 0.05$ (left) and parameter $\varepsilon = 0.1$ (right)

As expected and seen in the figures, while mapping the points in the target space back to domain space, the discontinuity shows up. The deeper explanation to this phenomenon can be traced back to the property of double covering. However, as mentioned in the previous paragraph, the target space is four-covered not just only double-covered. Here we come to sort out this inconsistency. When a point, say p , in the domain space is mapped via the perturbed rational map to a point t , to be precise $t = R_{18}(p)$, in the target space, there are also three other points, q , r and s , can be mapped to the same point t . As mapping the point t , coming from p , back to domain space using inverse rational map R_0^{-1} , we have four choices, *i.e.* p'_1 , p'_2 , p'_3 and p'_4 . Because of the perturbation, the principle of choosing among p'_1 , p'_2 , p'_3 and p'_4 is to pick the nearest one to p , say p'_1 , for example. The same principle is applied while mapping t , result from q , r and s respectively, back to domain space. According to the investigation shown in Fig. 6.6 - 6.9, we understand that two pre-images of t , say p and q , are close to each other in the neighborhood of $\xi = 1$ while the other two, r and s , are near the neighborhood of $\xi = -1$, which is at the other end of the Riemann sphere. That is the reason we call it double covering around $z = 1$. Because of the essential property of this rational map R_{18} , p'_1 and q'_1 are away from each other that causes the splitting in the central areas of Fig. 6.10 and 6.11 for parameters $\varepsilon = 0.01, 0.05$ and 0.1 . That explains the discontinuity in Fig. 6.1 and actually it is an artificial, not a genuine property of $R_{18}(\xi)$.

6.2 $R_{16}(\xi)$ & $R_{17}(\xi)$, $B = 4$

Two degenerate eigenvectors, $\vec{v}_{R_{17}}$ and $\vec{v}_{R_{16}}$, and their corresponding rational maps, $R_{17}(\xi)$ and $R_{16}(\xi)$, are listed as follows:

$$\vec{v}_{R_{17}} = \left(0 \ 0 \ -2\sqrt{3}\varepsilon \ 0 \ 0 \ 0 \ 0 \ 0 \ 0 \ 0 \ i\varepsilon \ 0 \ 0 \ 0 \ 0 \ 0 \ 0 \ 0 \ i\varepsilon \right)^t,$$

$$\vec{v}_{R_{16}} = \left(0 \ 0 \ 0 \ i\varepsilon \ 0 \ 0 \ 0 \ 0 \ 0 \ 0 \ 0 \ 0 \ 0 \ 0 \ -i\varepsilon \ 0 \ 0 \ 0 \ 0 \right)^t.$$

$$\Rightarrow \begin{cases} R_{17}(\xi) = \frac{P_0(\xi) - 2\sqrt{3}\varepsilon\xi^2}{Q_0(\xi) + i\varepsilon\xi^4 + i\varepsilon}, \\ R_{16}(\xi) = \frac{P_0(\xi) + i\varepsilon\xi^2}{Q_0(\xi) - i\varepsilon\xi^2}. \end{cases}$$

Since the eigenvectors $\vec{v}_{R_{17}}$ and $\vec{v}_{R_{16}}$ are with the same eigenvalues, these two form a two dimensional subspace of the eigenspace. So any vector in this subspace can be expressed in terms of the linear combinations of $\vec{v}_{R_{17}}$ and $\vec{v}_{R_{16}}$ as

$$\vec{v}_{16-17} = a \vec{v}_{R_{17}} + b \vec{v}_{R_{16}},$$

with a and b are two real coefficients. Hence its corresponding rational map is

$$\begin{aligned} R_{16-17}(\xi) &= \frac{P_0(\xi) - 2\sqrt{3}\varepsilon_a \xi^2 + i\varepsilon_b \xi^2}{Q_0(\xi) + i\varepsilon_a \xi^4 - i\varepsilon_b \xi^2 + i\varepsilon_a}, \\ &= \frac{P_{16-17}(\xi)}{Q_{16-17}(\xi)}, \end{aligned} \tag{6.2}$$

where $\varepsilon_a = a \cdot \varepsilon \ll 1$ and $\varepsilon_b = b \cdot \varepsilon \ll 1$.

By having the general expression for any rational map in the subspace, it is easier and more efficient for us to understand the relationship between these two rational maps. Because of their having the same eigenvalue, the first thing we want

to know is whether $R_{17}(\xi)$ and $R_{16}(\xi)$ are conjugate to each other or not. The way to investigate their conjugation relations is to take the method modified from the commutative diagram about the symmetry, which is shown below, to check if the equality stands

$$D_g^{-1} \cdot R_{16-17}(g(\xi)) \stackrel{?}{=} R_{16-17}(\xi), \quad (6.3)$$

where g 's are the $\pi/2$ rotations about the x , y and z -axis respectively. With $[D_{T_z, \frac{\pi}{2}}]$, $[D_{T_y, \frac{\pi}{2}}]$ and $[D_{T_x, \frac{\pi}{2}}]$ given previously, we then can have their inverse matrices

$$\left\{ \begin{array}{l} [D_{T_z, \frac{\pi}{2}}^{-1}] = \begin{pmatrix} 0 & 1 \\ 1 & 0 \end{pmatrix}, \\ [D_{T_y, \frac{\pi}{2}}^{-1}] = \frac{1}{4} \begin{pmatrix} 0 & 1 + \sqrt{3}i \\ 1 - \sqrt{3}i & 0 \end{pmatrix}, \\ [D_{T_x, \frac{\pi}{2}}^{-1}] = \frac{1}{4} \begin{pmatrix} 0 & -1 + \sqrt{3}i \\ -1 - \sqrt{3}i & 0 \end{pmatrix}. \end{array} \right.$$

Therefore, the application of the $\pi/2$ rotation of the domain space to (6.3) leads to

$$D_{T_z, \frac{\pi}{2}}^{-1} \cdot R_{16-17}(T_{z, \frac{\pi}{2}}(\xi)) = \frac{P_0(\xi) + 2\sqrt{3}\varepsilon_a \xi^2 + i\varepsilon_b \xi^2}{Q_0(\xi) - i\varepsilon_a \xi^4 - i\varepsilon_b \xi^2 - i\varepsilon_a}.$$

Comparing the above result with (6.2), we have

$$\left\{ \begin{array}{l} R_{17}(\xi, \varepsilon) \xrightarrow{T_z, \frac{\pi}{2}} R_{17}(\xi, -\varepsilon), \\ R_{16}(\xi, \varepsilon) \xrightarrow{T_z, \frac{\pi}{2}} R_{16}(\xi, \varepsilon). \end{array} \right.$$

This outcome tells us that, under $\pi/2$ rotation about the z -axis, $R_{17}(\xi)$ and $R_{16}(\xi)$ are self-conjugated, with that the parameter ε in $R_{17}(\xi)$ changes sign and $R_{16}(\xi)$ remains invariant.

The situation is however a bit complicated when the $\pi/2$ rotation about the y -axis is performed. The result is

$$D_{T_{y, \frac{\pi}{2}}}^{-1} \cdot R_{16-17}(T_{y, \frac{\pi}{2}}(\xi))$$

$$= \frac{P_0(\xi) - (\sqrt{3}\varepsilon_a + \frac{\sqrt{3}}{2}\varepsilon_b)\xi^2 + i(3\varepsilon_a - \frac{1}{2}\varepsilon_b)\xi^2}{Q_0(\xi) + i(\frac{1}{2}\varepsilon_a + \frac{1}{4}\varepsilon_b)\xi^4 + i(-3\varepsilon_a + \frac{1}{2}\varepsilon_b)\xi^2 + i(\frac{1}{2}\varepsilon_a + \frac{1}{4}\varepsilon_b)}$$

The comparison of this consequence with (6.3) comes in

$$R_{16-17}(\xi, \varepsilon_a, \varepsilon_b) \xrightarrow{T_{y, \frac{\pi}{2}}} R_{16-17}\left(\xi, \frac{\varepsilon_a}{2} + \frac{\varepsilon_b}{4}, 3\varepsilon_a - \frac{\varepsilon_b}{2}\right),$$

which is equivalent to

$$\left\{ \begin{array}{l} \varepsilon_a \xrightarrow{T_{y, \frac{\pi}{2}}} \frac{\varepsilon_a}{2} + \frac{\varepsilon_b}{4}, \\ \varepsilon_b \xrightarrow{T_{y, \frac{\pi}{2}}} 3\varepsilon_a - \frac{\varepsilon_b}{2}. \end{array} \right.$$

These relations obtained above give us a hint to show the conjugation relation, that is if we can find a pair of suitable coefficients ε_a and ε_b , or equivalently a and b in $\vec{v}_{R_{16-17}}$, such that

$$R_{16-17}(\xi, \varepsilon_a, \varepsilon_b) = D_{T_{y, \frac{\pi}{2}}}^{-1} \cdot R_{16-17}(T_{y, \frac{\pi}{2}}(\xi), \varepsilon_a, \varepsilon_b)$$

$$= R_{16-17}\left(\xi, \frac{\varepsilon_a}{2} + \frac{\varepsilon_b}{4}, 3\varepsilon_a - \frac{\varepsilon_b}{2}\right),$$

hence

$$\left\{ \begin{array}{l} \varepsilon_a = \frac{\varepsilon_a}{2} + \frac{\varepsilon_b}{4} \\ \varepsilon_b = 3\varepsilon_a - \frac{\varepsilon_b}{2} \end{array} \right. \Rightarrow \varepsilon_b = 2\varepsilon_a.$$

With this pair of coefficients, the conjugation relation is therefore shown

$$R_{16-17}(\xi, \varepsilon_a, 2\varepsilon_a) \xrightarrow{T_{y, \frac{\pi}{2}}} R_{16-17}(\xi, \varepsilon_a, 2\varepsilon_a).$$

We can also find the other pair of $(\varepsilon_a, \varepsilon_b)$ through

$$\begin{cases} \varepsilon_a = -\frac{\varepsilon_a}{2} - \frac{\varepsilon_b}{4} \\ \varepsilon_b = -3\varepsilon_a + \frac{\varepsilon_b}{2} \end{cases} \Rightarrow \varepsilon_b = -6\varepsilon_a,$$

then

$$R_{16-17}(\xi, \varepsilon_a, -6\varepsilon_a) \xrightarrow{T_{y, \frac{\pi}{2}}} R_{16-17}(\xi, -\varepsilon_a, 6\varepsilon_a).$$

Similarly, for the $\pi/2$ rotation about the x -axis, it results in

$$\begin{aligned} & D_{T_{x, \frac{\pi}{2}}}^{-1} \cdot R_{16-17}(T_{x, \frac{\pi}{2}}(\xi)) \\ &= \frac{P_0(\xi) - (\sqrt{3}\varepsilon_a + \frac{\sqrt{3}}{2}\varepsilon_b)\xi^2 + i(3\varepsilon_a - \frac{1}{2}\varepsilon_b)\xi^2}{Q_0(\xi) + i(\frac{1}{2}\varepsilon_a + \frac{1}{4}\varepsilon_b)\xi^4 + i(-3\varepsilon_a + \frac{1}{2}\varepsilon_b)\xi^2 + i(\frac{1}{2}\varepsilon_a + \frac{1}{4}\varepsilon_b)}, \end{aligned}$$

and leads to

$$R_{16-17}(\xi, \varepsilon_a, \varepsilon_b) \xrightarrow{T_{x, \frac{\pi}{2}}} R_{16-17}\left(\xi, \frac{\varepsilon_a}{2} - \frac{\varepsilon_b}{4}, -3\varepsilon_a - \frac{\varepsilon_b}{2}\right),$$

or equivalently

$$\begin{cases} \varepsilon_a \xrightarrow{T_{x, \frac{\pi}{2}}} \frac{\varepsilon_a}{2} - \frac{\varepsilon_b}{4}, \\ \varepsilon_b \xrightarrow{T_{x, \frac{\pi}{2}}} -3\varepsilon_a - \frac{\varepsilon_b}{2}. \end{cases}$$

Following the same procedure to show the conjugation relation, we have

$$\begin{aligned} R_{16-17}(\xi, \varepsilon_a, \varepsilon_b) &= D_{T_{x, \frac{\pi}{2}}}^{-1} \cdot R_{16-17}(T_{x, \frac{\pi}{2}}(\xi), \varepsilon_a, \varepsilon_b) \\ &= R_{16-17}\left(\xi, \frac{\varepsilon_a}{2} - \frac{\varepsilon_b}{4}, -3\varepsilon_a - \frac{\varepsilon_b}{2}\right). \end{aligned}$$

Choosing $(\varepsilon_a, \varepsilon_b)$ as

$$\begin{cases} \varepsilon_a = \frac{\varepsilon_a}{2} - \frac{\varepsilon_b}{4}, \\ \varepsilon_b = -3\varepsilon_a - \frac{\varepsilon_b}{2}. \end{cases} \Rightarrow \varepsilon_b = -2\varepsilon_a,$$

the conjugate relation comes to light

$$R_{16-17}(\xi, \varepsilon_a, -2\varepsilon_a) \xrightarrow{T_{x, \frac{\pi}{2}}} R_{16-17}(\xi, \varepsilon_a, -2\varepsilon_a).$$

Another pair of $(\varepsilon_a, \varepsilon_b)$ can be chosen as

$$\Rightarrow \begin{cases} \varepsilon_a = -\frac{\varepsilon_a}{2} + \frac{\varepsilon_b}{4} \\ \varepsilon_b = 3\varepsilon_a + \frac{\varepsilon_b}{2} \end{cases} \Rightarrow \varepsilon_b = 6\varepsilon_a,$$

to discover the conjugate relation

$$R_{16-17}(\xi, \varepsilon_a, 6\varepsilon_a) \xrightarrow{T_{x, \frac{\pi}{2}}} R_{16-17}(\xi, -\varepsilon_a, -6\varepsilon_a).$$

Here we present the plots of the perturbed rational map $R_{16}(\xi)$:

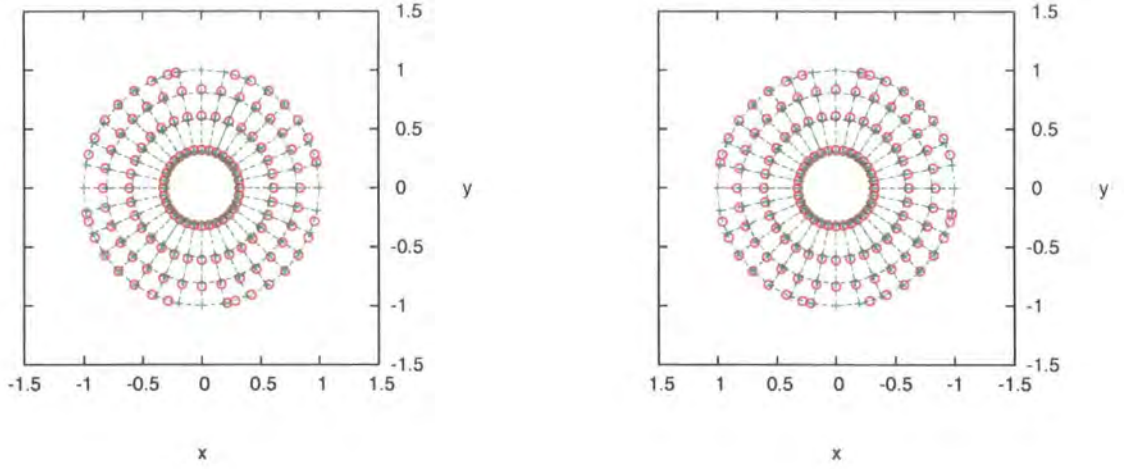


Figure 6.12: Northern(left) and southern(right) hemisphere of Riemann sphere of $R_{16}(\xi)$, $B=4$.

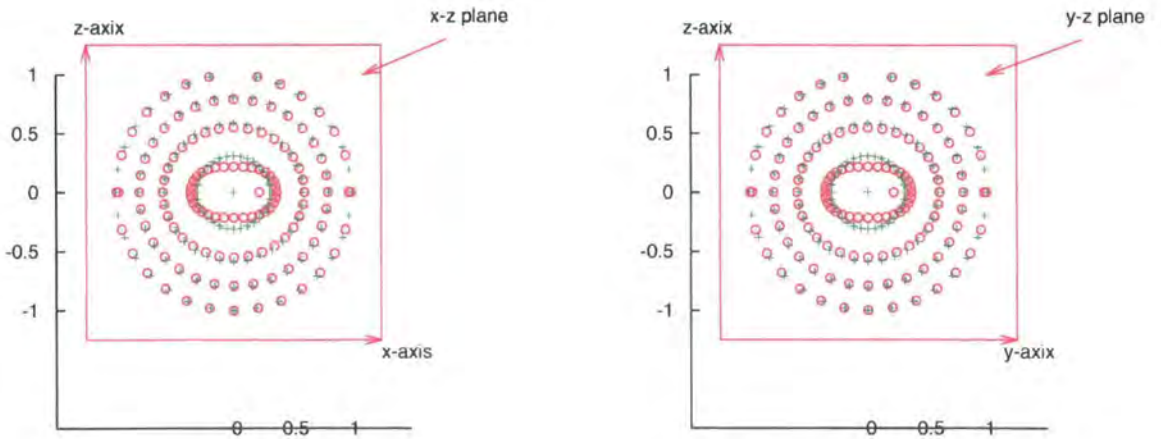


Figure 6.13: $R_{16}(\xi)$, $B=4$

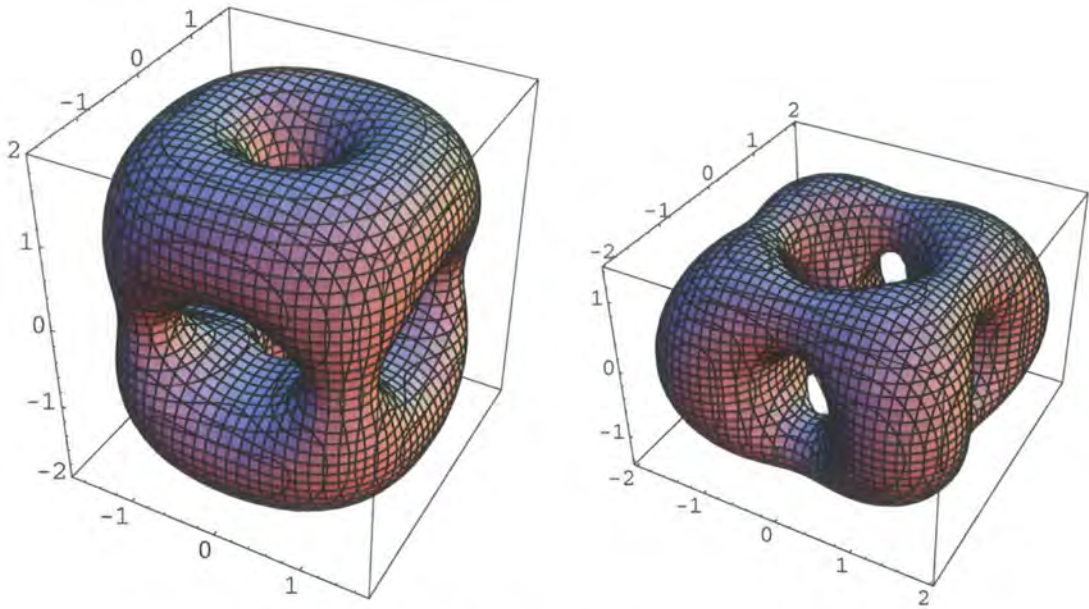


Figure 6.14: $B = 4$, $R_{16}(\xi)$: (Left) $\varepsilon > 0$; (Right) $\varepsilon < 0$.

The description of the perturbed rational map $R_{16}(\xi)$ is that the northern hemisphere is stretching uniformly downwards to the equator, and the southern hemisphere is doing the same but upwards to the equator. The energy density shows that the deformation of a cube that pulls it into two toruses in two perpendicular directions.

6.3 $R_{15}(\xi)$, $R_{14}(\xi)$ & $R_{13}(\xi)$, $B = 4$

The three degenerate eigenvector with eigenvalue 0.546893 and their corresponding rational maps are given

$$\vec{v}_{R_{15}} = \begin{pmatrix} 0.47145 \varepsilon \\ 0.49156 i \varepsilon \\ 0 \\ 0 \\ -0.0915 \varepsilon \\ 0.16654 i \varepsilon \\ 0 \\ 0 \\ 0 \\ 0 \\ 0 \\ 0.0915 \varepsilon \\ 0.16654 i \varepsilon \\ 0 \\ 0 \\ -0.47145 \varepsilon \\ 0.49156 i \varepsilon \\ 0 \\ 0 \end{pmatrix}, \quad \vec{v}_{R_{14}} = \begin{pmatrix} 0.16295 \varepsilon \\ -0.09524 i \varepsilon \\ 0 \\ 0 \\ -0.49085 \varepsilon \\ -0.4727 i \varepsilon \\ 0 \\ 0 \\ 0 \\ 0 \\ 0 \\ 0.49085 \varepsilon \\ -0.4727 i \varepsilon \\ 0 \\ 0 \\ -0.16295 \varepsilon \\ -0.09524 i \varepsilon \\ 0 \\ 0 \end{pmatrix}, \quad \vec{v}_{R_{13}} = \begin{pmatrix} 0 \\ 0 \\ 0 \\ -\sqrt{3} i \varepsilon \\ 0 \\ 0 \\ -\varepsilon \\ 0 \\ -\varepsilon \\ 0 \\ 0 \\ 0 \\ 0 \\ 0 \\ \sqrt{3} i \varepsilon \\ 0 \\ 0 \\ 0 \\ 0 \end{pmatrix}.$$

$$\Rightarrow \begin{cases} R_{15}(\xi) = \frac{P_0(\xi) + (0.47145 \varepsilon + 0.49156 i \varepsilon)\xi^3 + (-0.0915 \varepsilon + 0.16654 i \varepsilon)\xi}{Q_0(\xi) + (0.0915 \varepsilon + 0.16654 i \varepsilon)\xi^3 + (-0.47145 \varepsilon + 0.49156 i \varepsilon)\xi}, \\ R_{14}(\xi) = \frac{P_0(\xi) + (0.16295 \varepsilon - 0.09524 i \varepsilon)\xi^3 + (-0.49085 \varepsilon - 0.4727 i \varepsilon)\xi}{Q_0(\xi) + (0.49085 \varepsilon - 0.4727 i \varepsilon)\xi^3 + (-0.16295 \varepsilon - 0.09524 i \varepsilon)\xi}, \\ R_{13}(\xi) = \frac{P_0(\xi) - \sqrt{3} i \varepsilon \xi^2 - \varepsilon}{Q_0(\xi) - \varepsilon \xi^4 + \sqrt{3} i \varepsilon \xi^2}. \end{cases}$$

Since we realize the procedure of finding the conjugate relation between these three rational maps ($R_{15}(\xi)$, $R_{14}(\xi)$, $R_{13}(\xi)$) is the same as that for the other two

sets of $(R_{12}(\xi), R_{11}(\xi), R_{10}(\xi))$ and $(R_9(\xi), R_8(\xi), R_7(\xi))$, we provide some details of the derivation here once and for all.

By doing a linear combination of $\vec{v}_{R_{14}}$ and $\vec{v}_{R_{15}}$, we can obtain a new set of $\tilde{R}_{14}(\xi)$ and $\tilde{R}_{15}(\xi)$ in a simpler expression which is easier to show their conjugacy relations:

$$\tilde{R}_{15}(\xi) = \frac{P_0(\xi) + \left(\frac{1}{2} + \frac{\sqrt{3}i}{2}\right)\varepsilon\xi^3 + \left(\frac{1}{2} + \frac{\sqrt{3}i}{2}\right)\varepsilon\xi}{Q_0(\xi) - \left(\frac{1}{2} - \frac{\sqrt{3}i}{2}\right)\varepsilon\xi^3 - \left(\frac{1}{2} - \frac{\sqrt{3}i}{2}\right)\varepsilon\xi},$$

$$\tilde{R}_{14}(\xi) = \frac{P_0(\xi) + \left(\frac{\sqrt{3}}{2} + \frac{i}{2}\right)\varepsilon\xi^3 - \left(\frac{\sqrt{3}}{2} + \frac{i}{2}\right)\varepsilon\xi}{Q_0(\xi) + \left(\frac{\sqrt{3}}{2} - \frac{i}{2}\right)\varepsilon\xi^3 - \left(\frac{\sqrt{3}}{2} - \frac{i}{2}\right)\varepsilon\xi}.$$

In obtaining $\tilde{R}_{15}(\xi)$, we set $(\varepsilon_{15}, \varepsilon_{14}) = (1.5099\varepsilon, -1.30006\varepsilon)$ in $(\vec{v}_{R_{15}} + \vec{v}_{R_{14}})$ to reduce the number of the parameters from two to one; similarly, two parameters $(\varepsilon_{15}, \varepsilon_{14}) = (1.31164\varepsilon, 1.51982\varepsilon)$ are set to determine $\tilde{R}_{14}(\xi)$, where ε_{14} and ε_{15} are the parameters from the rational maps $R_{14}(\xi)$ and $R_{15}(\xi)$ respectively.

The conjugate relation is then shown as follows

$$\begin{aligned} & D_{T_{x, \frac{\pi}{2}}}^{-1} \cdot R_{13}(T_{x, \frac{\pi}{2}}(\xi), \varepsilon) \\ &= \frac{P_0(\xi) - \left(\frac{\sqrt{3}}{2} + \frac{i}{2}\right)\varepsilon\xi^3 + \left(\frac{\sqrt{3}}{2} + \frac{i}{2}\right)\varepsilon\xi}{Q_0(\xi) - \left(\frac{\sqrt{3}}{2} - \frac{i}{2}\right)\varepsilon\xi^3 + \left(\frac{\sqrt{3}}{2} - \frac{i}{2}\right)\varepsilon\xi} \\ &= \tilde{R}_{14}(\xi, -\varepsilon), \end{aligned}$$

so we have

$$R_{13}(\xi) \sim \tilde{R}_{14}(\xi).$$

Using the same method, we can show

$$\begin{aligned} & D_{T_{y, \frac{\pi}{2}}}^{-1} \cdot R_{13}(T_{y, \frac{\pi}{2}}(\xi), \varepsilon) \\ &= \frac{P_0(\xi) + \left(\frac{1}{2} + \frac{\sqrt{3}i}{2}\right)\varepsilon\xi^3 + \left(\frac{1}{2} + \frac{\sqrt{3}i}{2}\right)\varepsilon\xi}{Q_0(\xi) - \left(\frac{1}{2} - \frac{\sqrt{3}i}{2}\right)\varepsilon\xi^3 - \left(\frac{1}{2} - \frac{\sqrt{3}i}{2}\right)\varepsilon\xi}, \\ &= \tilde{R}_{15}(\xi, \varepsilon), \end{aligned}$$

which means

$$R_{13}(\xi) \sim \tilde{R}_{15}(\xi) .$$

From the transitive relation, we have

$$R_{13}(\xi) \sim \tilde{R}_{14}(\xi) \sim \tilde{R}_{15}(\xi) .$$

Similarly,

$$\begin{aligned} & D_{T_{z, \frac{\pi}{2}}}^{-1} \cdot R_{13}(T_{z, \frac{\pi}{2}}(\xi), \varepsilon) \\ &= \frac{P_0(\xi) + \sqrt{3}i\varepsilon\xi^3 + \varepsilon}{Q_0(\xi) + \varepsilon\xi^4 - \sqrt{3}i\varepsilon\xi^2} \\ &= R_{13}(\xi, -\varepsilon) . \end{aligned}$$

It leads us to the relation

$$R_{13}(\xi, \varepsilon) \xrightarrow{T_{z, \frac{\pi}{2}}} R_{13}(\xi, -\varepsilon) .$$

Repeatedly doing the aforementioned method will yield us other relations among these three rational maps and the results are summarized as follows:

$$\left\{ \begin{array}{l} R_{13}(\xi, \varepsilon) \xrightarrow{T_{x, \frac{\pi}{2}}} \tilde{R}_{14}(\xi, -\varepsilon) , \\ R_{13}(\xi, \varepsilon) \xrightarrow{T_{y, \frac{\pi}{2}}} \tilde{R}_{15}(\xi, \varepsilon) , \\ R_{13}(\xi, \varepsilon) \xrightarrow{T_{z, \frac{\pi}{2}}} R_{13}(\xi, -\varepsilon) , \\ \\ \tilde{R}_{14}(\xi, \varepsilon) \xrightarrow{T_{x, \frac{\pi}{2}}} R_{13}(\xi, \varepsilon) , \\ \tilde{R}_{14}(\xi, \varepsilon) \xrightarrow{T_{y, \frac{\pi}{2}}} \tilde{R}_{14}(\xi, -\varepsilon) , \\ \tilde{R}_{14}(\xi, \varepsilon) \xrightarrow{T_{z, \frac{\pi}{2}}} \tilde{R}_{15}(\xi, -\varepsilon) , \end{array} \right.$$

and

$$\left\{ \begin{array}{l} \tilde{R}_{15}(\xi, \varepsilon) \xrightarrow{T_x, \frac{\pi}{2}} \tilde{R}_{15}(\xi, -\varepsilon), \\ \tilde{R}_{15}(\xi, \varepsilon) \xrightarrow{T_y, \frac{\pi}{2}} R_{13}(\xi, -\varepsilon), \\ \tilde{R}_{15}(\xi, \varepsilon) \xrightarrow{T_z, \frac{\pi}{2}} \tilde{R}_{14}(\xi, \varepsilon). \end{array} \right.$$

Let us show the graph of the perturbed rational map $R_{13}(\xi)$ here:

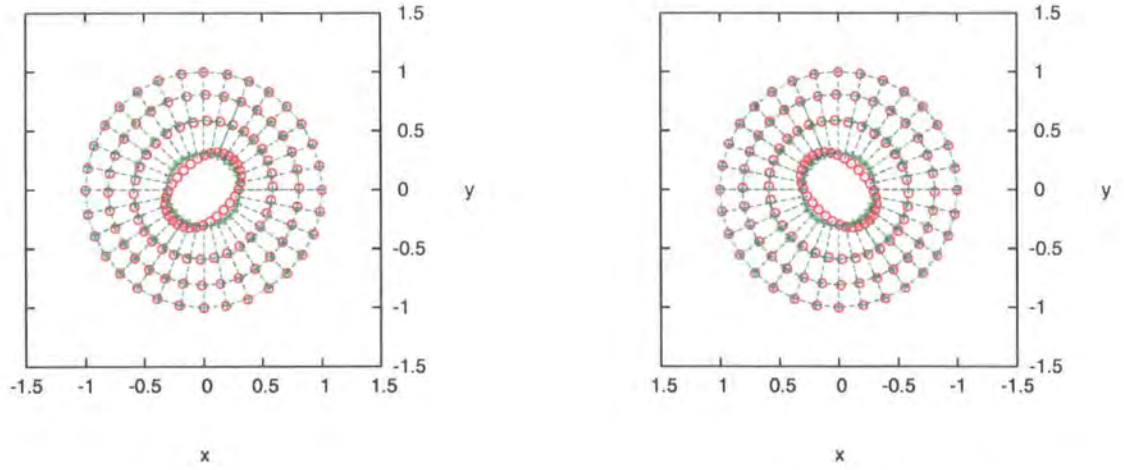


Figure 6.15: Northern(left) and southern(right) hemisphere of Riemann sphere of $R_{13}(\xi)$, $B=4$.

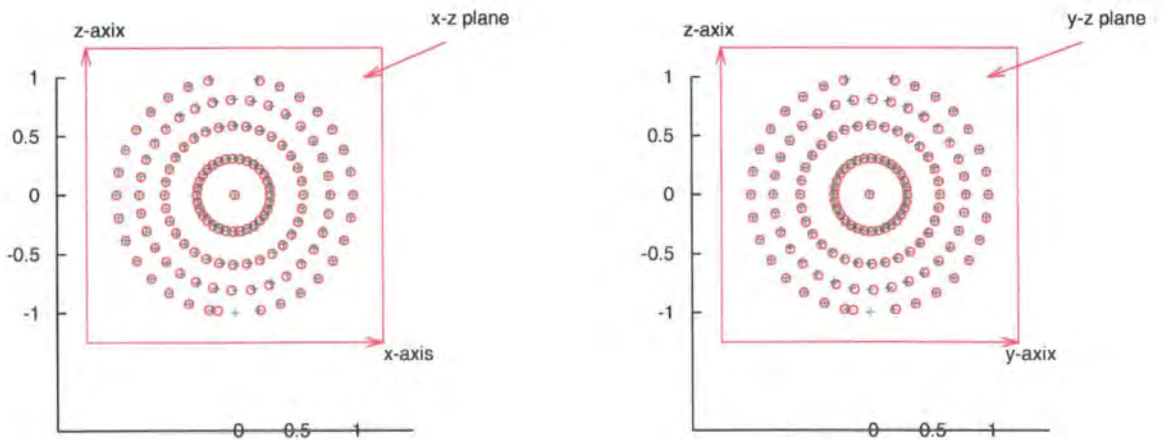


Figure 6.16: $R_{13}(\xi)$, $B=4$

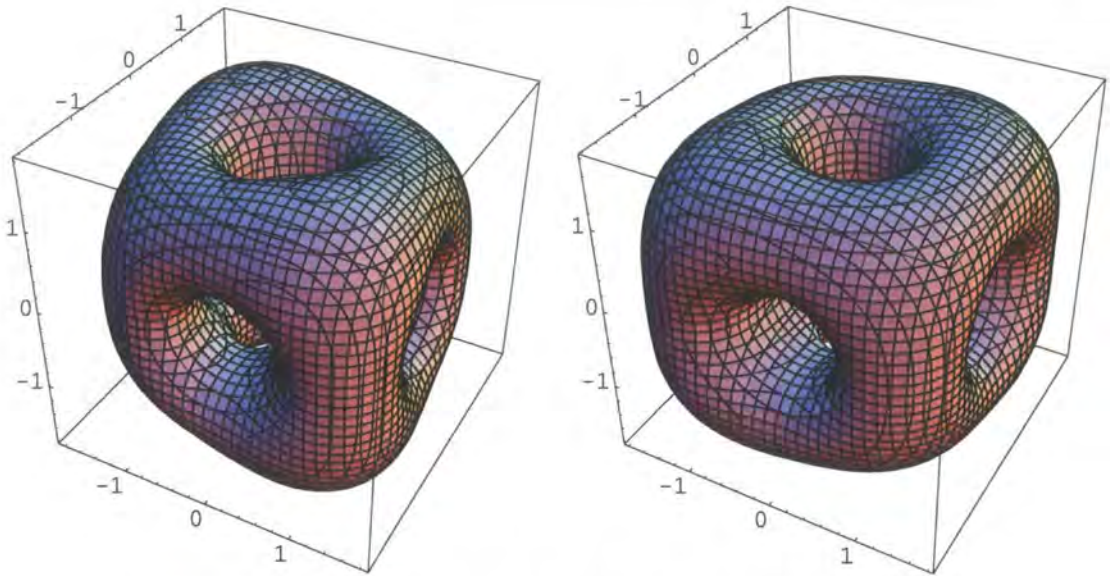


Figure 6.17: $B = 4$, $R_{13}(\xi)$: (Left) $\varepsilon > 0$; (Right) $\varepsilon < 0$.

For the perturbed rational map $R_{13}(\xi)$, a circle on the northern hemisphere, when projected on the x - y plane, deforms into an ellipse whose long axis makes an angle of about $\pi/4$ with the x -axis. The deformation of the same size of the circle on the southern hemisphere is in phase with that on the northern hemisphere. If we look at the deformation of this circle on the northern hemisphere of \mathbb{S}^2 without the projection, two ends of its diameter will be lengthened and move downwards to the equator, and two ends of another diameter, perpendicular to the former one, will be shortened and move upwards to the north pole. The situation is similar to that on the southern hemisphere. However, the circles of the same size on the other hemispheres do not seem to deform at all. The energy density displays the deformation that makes a cube become a rhombus.

6.4 $R_{12}(\xi)$, $R_{11}(\xi)$ & $R_{10}(\xi)$, $B = 4$

The eigenvectors with eigenvalue 0.37129 are presented here

$$\vec{V}_{R_{12}} = \begin{pmatrix} -0.48029 \varepsilon \\ 0.48545 i \varepsilon \\ 0 \\ 0 \\ -0.11976 \varepsilon \\ -0.13901 i \varepsilon \\ 0 \\ 0 \\ 0 \\ 0 \\ -0.11976 \varepsilon \\ 0.13901 i \varepsilon \\ 0 \\ 0 \\ -0.48029 \varepsilon \\ -0.48545 i \varepsilon \\ 0 \\ 0 \end{pmatrix}, \quad \vec{V}_{R_{11}} = \begin{pmatrix} 0.1403 \varepsilon \\ 0.11845 i \varepsilon \\ 0 \\ 0 \\ 0.48577 \varepsilon \\ -0.47991 i \varepsilon \\ 0 \\ 0 \\ 0 \\ 0 \\ 0.48577 \varepsilon \\ 0.47991 i \varepsilon \\ 0 \\ 0 \\ 0.1403 \varepsilon \\ -0.11845 i \varepsilon \\ 0 \\ 0 \end{pmatrix}, \quad \vec{V}_{R_{10}} = \begin{pmatrix} 0 \\ 0 \\ \sqrt{3} \varepsilon \\ 0 \\ 0 \\ 0 \\ 0 \\ -i \varepsilon \\ 0 \\ -i \varepsilon \\ 0 \\ 0 \\ -\sqrt{3} \varepsilon \\ 0 \\ 0 \\ 0 \\ 0 \\ 0 \end{pmatrix}.$$

Following the same procedure we demonstrated in the previous section, with $(\varepsilon_{12}, \varepsilon_{11}) = (1.38186 \varepsilon, -1.44215 \varepsilon)$, $\tilde{R}_{12}(\xi)$ is obtained, and with $(\varepsilon_{12}, \varepsilon_{11}) = (1.44584 \varepsilon, 1.38576 \varepsilon)$, we can have $\tilde{R}_{11}(\xi)$:

$$\left\{ \begin{array}{l} \tilde{R}_{12}(\xi) = \frac{P_0(\xi) - (\frac{\sqrt{3}}{2} - \frac{i}{2})\varepsilon\xi^3 - (\frac{\sqrt{3}}{2} - \frac{i}{2})\varepsilon\xi}{Q_0(\xi) - (\frac{\sqrt{3}}{2} + \frac{i}{2})\varepsilon\xi^3 - (\frac{\sqrt{3}}{2} + \frac{i}{2})\varepsilon\xi}, \\ \tilde{R}_{11}(\xi) = \frac{P_0(\xi) - (\frac{1}{2} - \frac{\sqrt{3}i}{2})\varepsilon\xi^3 + (\frac{1}{2} - \frac{\sqrt{3}i}{2})\varepsilon\xi}{Q_0(\xi) + (\frac{1}{2} + \frac{\sqrt{3}i}{2})\varepsilon\xi^3 - (\frac{1}{2} + \frac{\sqrt{3}i}{2})\varepsilon\xi}, \\ R_{10}(\xi) = \frac{P_0(\xi) + \sqrt{3}\varepsilon\xi^2 - i\varepsilon}{Q_0(\xi) - i\varepsilon\xi^4 - \sqrt{3}\varepsilon\xi^2}. \end{array} \right.$$

Therefore, the conjugate relations among $\tilde{R}_{12}(\xi)$, $\tilde{R}_{11}(\xi)$ and $R_{10}(\xi)$ are shown here:

$$D_{T_x, \frac{\pi}{2}}^{-1} \cdot R_{10}(T_x, \frac{\pi}{2}(\xi), \varepsilon) = R_{11}(\xi, -\varepsilon) \Rightarrow R_{10}(\xi) \sim \tilde{R}_{11}(\xi),$$

$$D_{T_y, \frac{\pi}{2}}^{-1} \cdot R_{10}(T_y, \frac{\pi}{2}(\xi), \varepsilon) = R_{12}(\xi, \varepsilon) \Rightarrow R_{10}(\xi) \sim \tilde{R}_{12}(\xi).$$

Obviously, we find

$$R_{10}(\xi) \sim \tilde{R}_{11}(\xi) \sim \tilde{R}_{12}(\xi).$$

Two more useful relations are

$$D_{T_z, \frac{\pi}{2}}^{-1} \cdot \tilde{R}_{11}(T_z, \frac{\pi}{2}(\xi), \varepsilon) = \tilde{R}_{12}(\xi, \varepsilon).$$

$$D_{T_z, \frac{\pi}{2}}^{-1} \cdot R_{10}(T_z, \frac{\pi}{2}(\xi), \varepsilon) = R_{10}(\xi, -\varepsilon).$$

Putting all the results above together, we come to the following conclusions:

$$\left\{ \begin{array}{l} R_{10}(\xi, \varepsilon) \xrightarrow{T_x, \frac{\pi}{2}} \tilde{R}_{11}(\xi, -\varepsilon), \\ R_{10}(\xi, \varepsilon) \xrightarrow{T_y, \frac{\pi}{2}} \tilde{R}_{12}(\xi, \varepsilon), \\ R_{10}(\xi, \varepsilon) \xrightarrow{T_z, \frac{\pi}{2}} R_{10}(\xi, -\varepsilon), \end{array} \right.$$

$$\left\{ \begin{array}{l} \tilde{R}_{11}(\xi, \varepsilon) \xrightarrow{T_x, \frac{\pi}{2}} R_{10}(\xi, \varepsilon) , \\ \tilde{R}_{11}(\xi, \varepsilon) \xrightarrow{T_y, \frac{\pi}{2}} \tilde{R}_{11}(\xi, -\varepsilon) , \\ \tilde{R}_{11}(\xi, \varepsilon) \xrightarrow{T_z, \frac{\pi}{2}} \tilde{R}_{12}(\xi, -\varepsilon) , \end{array} \right.$$

and

$$\left\{ \begin{array}{l} \tilde{R}_{12}(\xi, \varepsilon) \xrightarrow{T_x, \frac{\pi}{2}} \tilde{R}_{12}(\xi, -\varepsilon) , \\ \tilde{R}_{12}(\xi, \varepsilon) \xrightarrow{T_y, \frac{\pi}{2}} R_{10}(\xi, -\varepsilon) , \\ \tilde{R}_{12}(\xi, \varepsilon) \xrightarrow{T_z, \frac{\pi}{2}} \tilde{R}_{11}(\xi, \varepsilon) . \end{array} \right.$$

The graph of the perturbed rational map $R_{10}(\xi)$ is shown as follows:

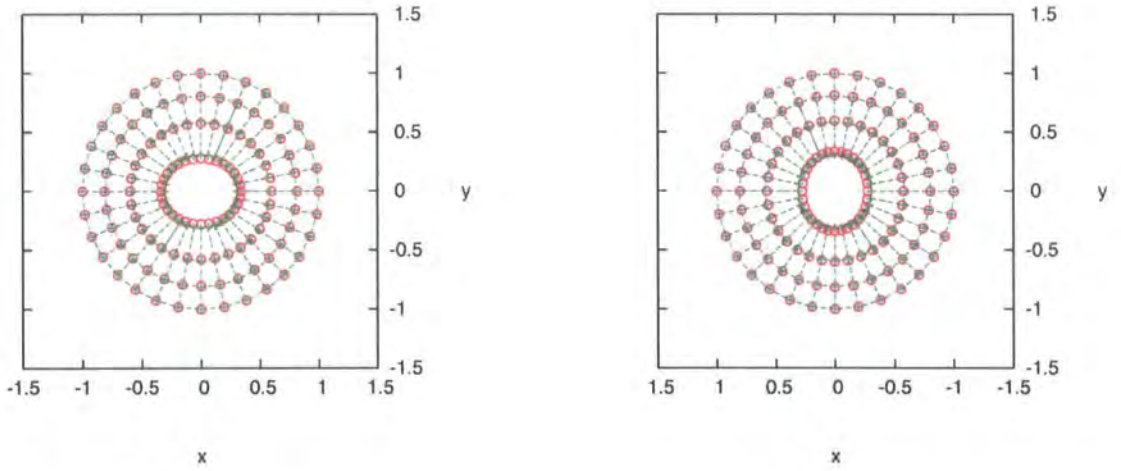


Figure 6.18: Northern(left) and southern(right) hemisphere of Riemann sphere of $R_{10}(\xi)$, $B=4$.

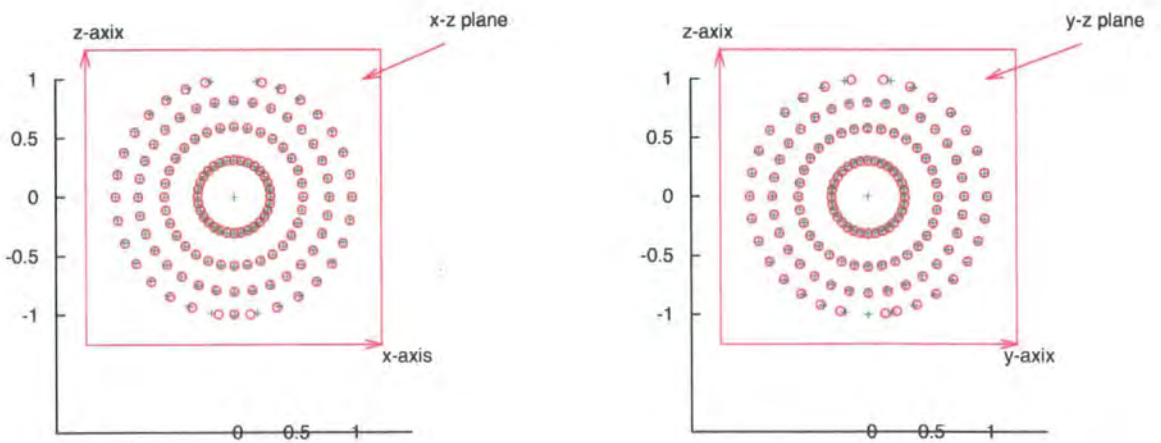


Figure 6.19: $R_{10}(\xi)$, $B=4$

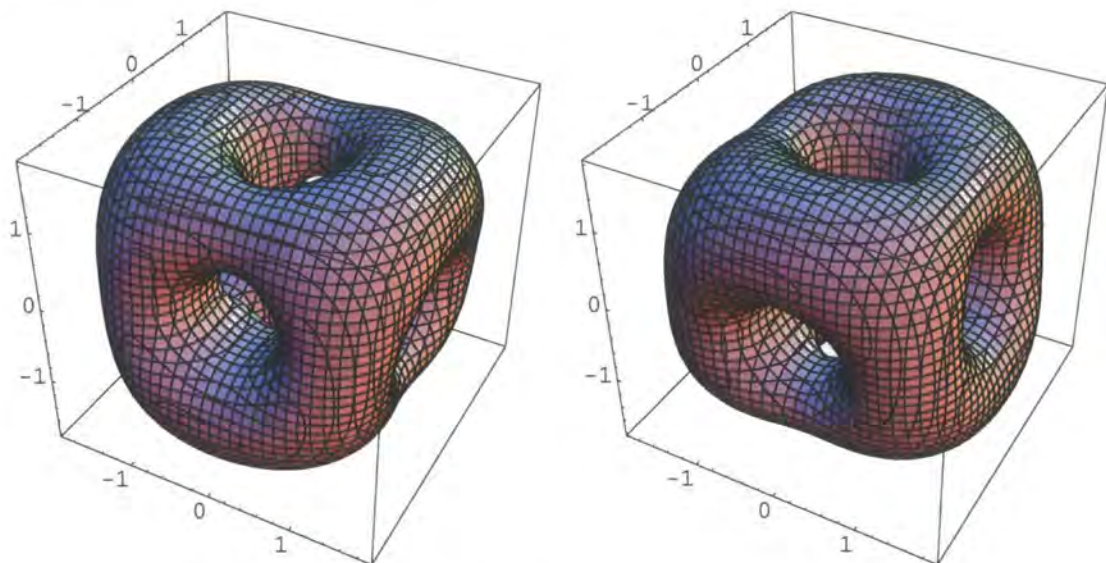


Figure 6.20: $B = 4$, $R_{10}(\xi)$: (Left) $\varepsilon > 0$; (Right) $\varepsilon < 0$.

The projected deformation of the circle of the hemisphere on the x - y plane is stretched along x -direction, and that from the southern hemisphere is contracted in the y -direction. On \mathbb{S}^2 , two ends of the diameter of the circle lengthened and move downwards to the equator and two ends of the shortened diameter perpendicular to the former one move upwards to the north pole. The deformation of the southern hemisphere is out of phase to those on the northern hemisphere. The energy density demonstrates the deformation of inflating two opposite edges on one face and deflating the other two opposite edges on that face.

6.5 $R_9(\xi)$, $R_8(\xi)$ & $R_7(\xi)$, $B = 4$

The three eigenvectors with the same eigenvalue, 0.210307, are listed as follows:

$$\vec{V}_{R_9} = \begin{pmatrix} -0.48317 \varepsilon \\ -0.48276 i \varepsilon \\ 0 \\ 0 \\ 0.13017 \varepsilon \\ -0.12864 i \varepsilon \\ 0 \\ 0 \\ 0 \\ 0 \\ 0 \\ 0.13017 \varepsilon \\ 0.12864 i \varepsilon \\ 0 \\ 0 \\ -0.48317 \varepsilon \\ 0.48276 i \varepsilon \\ 0 \\ 0 \end{pmatrix}, \quad \vec{V}_{R_8} = \begin{pmatrix} -0.1321 \varepsilon \\ 0.12676 i \varepsilon \\ 0 \\ 0 \\ 0.48367 \varepsilon \\ 0.48225 i \varepsilon \\ 0 \\ 0 \\ 0 \\ 0 \\ 0 \\ 0.48367 \varepsilon \\ -0.48225 i \varepsilon \\ 0 \\ 0 \\ -0.1321 \varepsilon \\ -0.12676 i \varepsilon \\ 0 \\ 0 \end{pmatrix}, \quad \vec{V}_{R_7} = \begin{pmatrix} 0 \\ 0 \\ 0 \\ \sqrt{3} i \varepsilon \\ 0 \\ 0 \\ \varepsilon \\ 0 \\ 0 \\ 0 \\ 0 \\ 0 \\ 0 \\ 0 \\ 0 \\ 0 \\ -\sqrt{3} i \varepsilon \\ 0 \\ \varepsilon \\ 0 \end{pmatrix}.$$

By a linear combination of $(\vec{v}_{R_9} + \vec{v}_{R_8})$ with $(\varepsilon_9, \varepsilon_8) = (0.1422 \varepsilon, -1.41624 \varepsilon)$, $\tilde{R}_9(\xi)$ is determined, and with $(\varepsilon_9, \varepsilon_8) = (1.4064 \varepsilon, 1.41176 \varepsilon)$, we have $\tilde{R}_8(\xi)$:

$$\left\{ \begin{aligned} \tilde{R}_9(\xi) &= \frac{P_0(\xi) - (\frac{1}{2} + \frac{\sqrt{3}i}{2}) \varepsilon \xi^3 - (\frac{1}{2} + \frac{\sqrt{3}i}{2}) \varepsilon \xi}{Q_0(\xi) - (\frac{1}{2} - \frac{\sqrt{3}i}{2}) \varepsilon \xi^3 - (\frac{1}{2} - \frac{\sqrt{3}i}{2}) \varepsilon \xi}, \\ \tilde{R}_8(\xi) &= \frac{P_0(\xi) - (\frac{\sqrt{3}}{2} + \frac{i}{2}) \varepsilon \xi^3 + (\frac{\sqrt{3}}{2} + \frac{i}{2}) \varepsilon \xi}{Q_0(\xi) + (\frac{\sqrt{3}}{2} - \frac{i}{2}) \varepsilon \xi^3 - (\frac{\sqrt{3}}{2} - \frac{i}{2}) \varepsilon \xi}, \\ R_7(\xi) &= \frac{P_0(\xi) + \sqrt{3} i \varepsilon \xi^2 + \varepsilon}{Q_0(\xi) - \sqrt{3} i \varepsilon \xi^2 + \varepsilon}. \end{aligned} \right.$$

The conjugate relations among $\tilde{R}_9(\xi)$, $\tilde{R}_8(\xi)$ and $R_7(\xi)$ are then revealed as:

$$D_{T_x, \frac{\pi}{2}}^{-1} \cdot R_7(T_x, \frac{\pi}{2}(\xi), \varepsilon) = R_8(\xi, \varepsilon) \quad \Rightarrow \quad R_7(\xi) \sim \tilde{R}_8(\xi) ,$$

$$D_{T_y, \frac{\pi}{2}}^{-1} \cdot R_7(T_y, \frac{\pi}{2}(\xi), \varepsilon) = R_9(\xi, -\varepsilon) \quad \Rightarrow \quad R_7(\xi) \sim \tilde{R}_9(\xi) .$$

Manifestly, we arrive at finding

$$R_7(\xi) \sim \tilde{R}_8(\xi) \sim \tilde{R}_9(\xi) .$$

Besides the relations above, here are two other useful relations

$$D_{T_z, \frac{\pi}{2}}^{-1} \cdot \tilde{R}_8(T_z, \frac{\pi}{2}(\xi), \varepsilon) = \tilde{R}_9(\xi, \varepsilon) .$$

$$D_{T_z, \frac{\pi}{2}}^{-1} \cdot R_7(T_z, \frac{\pi}{2}(\xi), \varepsilon) = R_7(\xi, \varepsilon) .$$

With some more work, we come to the following conclusions:

$$\left\{ \begin{array}{l} R_7(\xi, \varepsilon) \xrightarrow{T_x, \frac{\pi}{2}} \tilde{R}_8(\xi, \varepsilon) , \\ R_7(\xi, \varepsilon) \xrightarrow{T_y, \frac{\pi}{2}} \tilde{R}_9(\xi, -\varepsilon) , \\ R_7(\xi, \varepsilon) \xrightarrow{T_z, \frac{\pi}{2}} R_7(\xi, \varepsilon) , \end{array} \right.$$

$$\left\{ \begin{array}{l} \tilde{R}_8(\xi, \varepsilon) \xrightarrow{T_x, \frac{\pi}{2}} R_7(\xi, -\varepsilon) , \\ \tilde{R}_8(\xi, \varepsilon) \xrightarrow{T_y, \frac{\pi}{2}} \tilde{R}_8(\xi, \varepsilon) , \\ \tilde{R}_8(\xi, \varepsilon) \xrightarrow{T_z, \frac{\pi}{2}} \tilde{R}_9(\xi, \varepsilon) , \end{array} \right.$$

and

$$\left\{ \begin{array}{l} \tilde{R}_9(\xi, \varepsilon) \xrightarrow{T_x, \frac{\pi}{2}} \tilde{R}_9(\xi, \varepsilon) , \\ \tilde{R}_9(\xi, \varepsilon) \xrightarrow{T_y, \frac{\pi}{2}} R_7(\xi, \varepsilon) , \\ \tilde{R}_9(\xi, \varepsilon) \xrightarrow{T_z, \frac{\pi}{2}} \tilde{R}_8(\xi, -\varepsilon) . \end{array} \right.$$

The plots of the perturbed rational map $R_7(\xi)$ are given here:

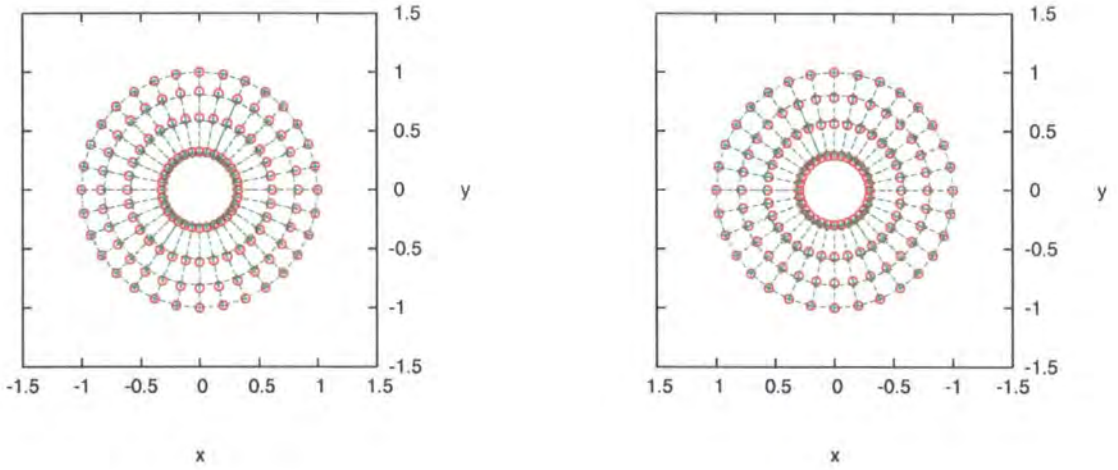


Figure 6.21: Northern(left) and southern(right) hemisphere of Riemann sphere of $R_7(\xi)$, $B=4$

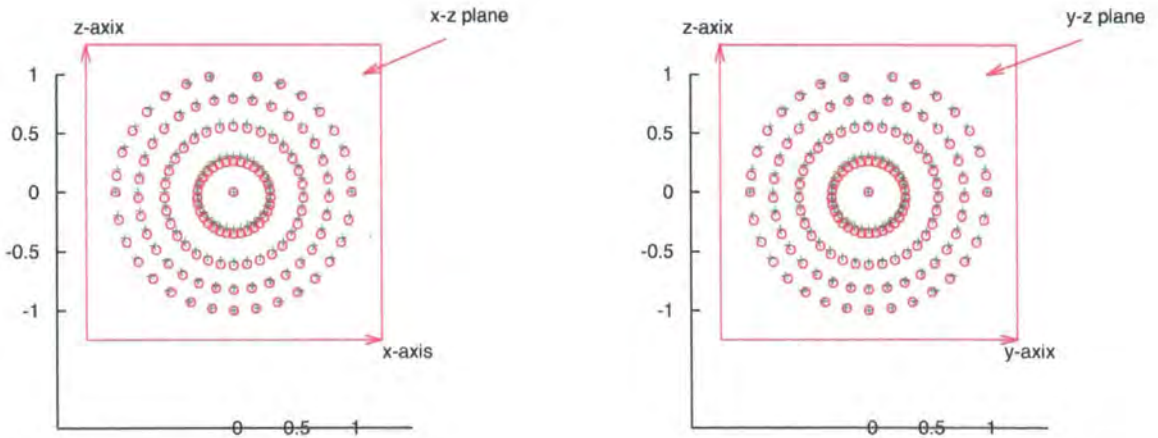


Figure 6.22: $R_7(\xi)$, $B=4$

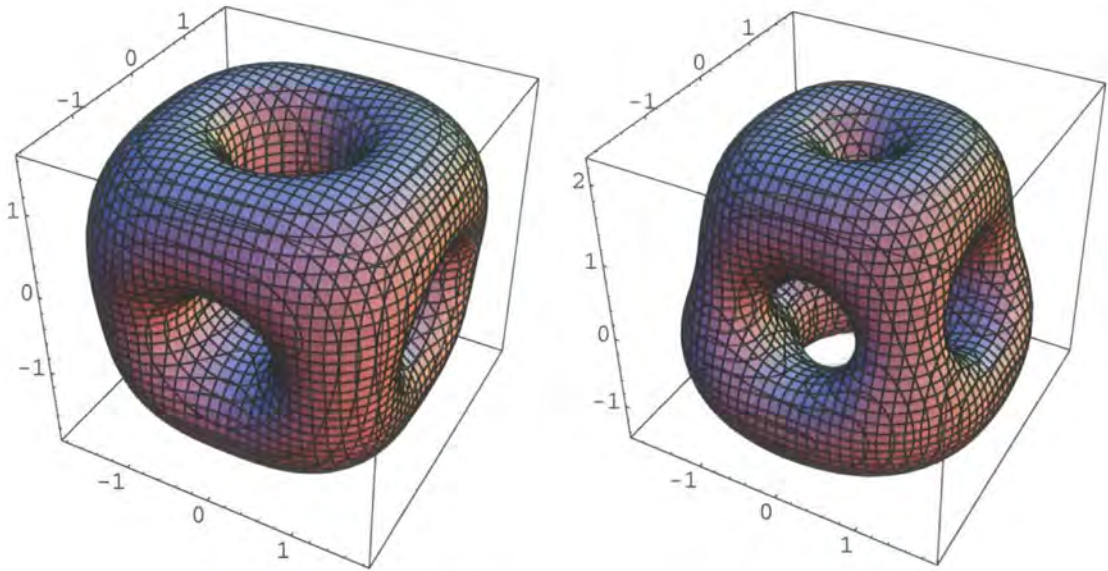


Figure 6.23: $B = 4$, $R_7(\xi)$: (Left) $\varepsilon > 0$; (Right) $\varepsilon < 0$.

Both the norther and southern hemisphere stretches uniformly downwards to the south pole. The energy density shows that the deformation of a cube such that one of the upper and lower part of the cube inflates and the other deflates.

$$\vec{v}_{R_4} = \begin{pmatrix} -0.13610 \varepsilon \\ -0.12272 i\varepsilon \\ 0 \\ 0 \\ -0.48471 \varepsilon \\ 0.48113 i\varepsilon \\ 0 \\ 0 \\ 0 \\ 0 \\ 0 \\ 0.48471 \varepsilon \\ 0.48113 i\varepsilon \\ 0 \\ 0 \\ 0.13610 \varepsilon \\ -0.12272 i\varepsilon \\ 0 \\ 0 \end{pmatrix}, \quad \vec{v}_{R_5} = \begin{pmatrix} -0.48038 \varepsilon \\ 0.48537 i\varepsilon \\ 0 \\ 0 \\ -0.12001 \varepsilon \\ -0.13870 i\varepsilon \\ 0 \\ 0 \\ 0 \\ 0 \\ 0 \\ 0.12001 \varepsilon \\ -0.13870 i\varepsilon \\ 0 \\ 0 \\ 0 \\ 0.48038 \varepsilon \\ 0.48537 i\varepsilon \\ 0 \\ 0 \end{pmatrix}, \quad \vec{v}_{R_6} = \begin{pmatrix} 0 \\ 0 \\ 0 \\ -0.92582 i\varepsilon \\ 0 \\ 0 \\ 0 \\ 0 \\ -0.26726 \varepsilon \\ 0 \\ 0 \\ 0 \\ 0 \\ 0 \\ 0 \\ 0 \\ 0 \\ 0 \\ -0.26726 \varepsilon \\ 0 \end{pmatrix}.$$

(6.4)

By (3.14) and (5.2), we can have the rational maps of the zero modes, which are respectively

$$R_1(\xi) = \frac{P_0(\xi) - 0.68624 \varepsilon \xi^2 - 0.17053 i \varepsilon}{Q_0(\xi) + 0.68624 \varepsilon \xi^2 - 0.17053 i \varepsilon}, \quad (6.5)$$

$$R_2(\xi) = \frac{P_0(\xi) - 0.14171 \varepsilon \xi^2 + 0.69276 i \varepsilon}{Q_0(\xi) + 0.14171 \varepsilon \xi^2 + 0.69276 i \varepsilon}, \quad (6.6)$$

$$R_3(\xi) = \frac{P_0(\xi) + 0.57206 \varepsilon \xi^2 - 0.1799 i \varepsilon}{Q_0(\xi) + 0.36391 i \varepsilon \xi^4 + 0.68855 \varepsilon \xi^2 + 0.18401 i \varepsilon}, \quad (6.7)$$

$$R_4(\xi) = \frac{P_0(\xi) + (-0.1361 \varepsilon - 0.12272 i \varepsilon) \xi^3 + (-0.48471 \varepsilon + 0.48113 i \varepsilon) \xi}{Q_0(\xi) + (0.48471 \varepsilon + 0.48113 i \varepsilon) \xi^3 + (0.1361 \varepsilon - 0.12272 i \varepsilon) \xi}, \quad (6.8)$$

$$R_5(\xi) = \frac{P_0(\xi) + (-0.48038 \varepsilon + 0.48537 i \varepsilon) \xi^3 + (-0.12001 \varepsilon - 0.1387 i \varepsilon) \xi}{Q_0(\xi) + (0.12001 \varepsilon - 0.1387 i \varepsilon) \xi^3 + (0.48038 \varepsilon + 0.48537 i \varepsilon) \xi}, \quad (6.9)$$

$$R_6(\xi) = \frac{P_0(\xi) - 0.92582 i \varepsilon \xi^2}{Q_0(\xi) - 0.26726 \varepsilon \xi^4 - 0.26726 \varepsilon}. \quad (6.10)$$

It is well known that the rotation modes are the zero modes of the Skyrme model. Therefore our first task of analyzing these zero modes is to identify those, among the six rational maps listed above, corresponding to the rotation modes, or as the linear combinations of the rotation modes.

Instead of plotting all the plots of the rational maps from R_1 to R_6 and then finding out which of them are the rotational modes, we take a different route, *i.e.* we utilize the mathematical expressions of the rotation modes in the first place and then see if there are any rational maps of zero modes matching these expressions. If not, then we try to take the linear combinations of the obtained zero modes to fit the mathematical expressions of the rotation modes.

To get the mathematical expressions of the rotation modes, we have the domain space, \mathbb{S}^2 , infinitesimally rotated around the x , y and z -axis to derive the forms of the rotated domain space and then plug them into unperturbed rational map, $R_0(\xi)$. Because of infinitesimal rotation, to the first order of expansion of expressions of rotation matrix in Riemann sphere, three rotation matrix, $[Q_{x,\theta}]$, $[Q_{y,\theta}]$ and $[Q_{z,\theta}]$,

have the following forms:

$$[T_{z,\theta}] = \begin{pmatrix} e^{\frac{i\theta}{2}} & 0 \\ 0 & e^{-\frac{i\theta}{2}} \end{pmatrix} \xrightarrow{\theta \rightarrow 0} \begin{pmatrix} 1 + \frac{i\theta}{2} & 0 \\ 0 & 1 + \frac{i\theta}{2} \end{pmatrix},$$

$$[T_{y,\theta}] = \begin{pmatrix} \cos(\frac{\theta}{2}) & -\sin(\frac{\theta}{2}) \\ \sin(\frac{\theta}{2}) & \cos(\frac{\theta}{2}) \end{pmatrix} \xrightarrow{\theta \rightarrow 0} \begin{pmatrix} 1 & -\frac{\theta}{2} \\ \frac{\theta}{2} & 1 \end{pmatrix},$$

$$[T_{x,\theta}] = \begin{pmatrix} \cos(\frac{\theta}{2}) & i \sin(\frac{\theta}{2}) \\ i \sin(\frac{\theta}{2}) & \cos(\frac{\theta}{2}) \end{pmatrix} \xrightarrow{\theta \rightarrow 0} \begin{pmatrix} 1 & \frac{i\theta}{2} \\ \frac{i\theta}{2} & 1 \end{pmatrix}.$$

Therefore, under rotation around the x , y and z -axis, the domain space becomes

$$\xi \xrightarrow{\theta \rightarrow 0} \xi' = T_{z,\theta}(\xi) = \frac{\xi(1 + \frac{i\theta}{2})}{1 - \frac{i\theta}{2}} \sim \xi(1 + i\theta),$$

$$\xi \xrightarrow{\theta \rightarrow 0} \xi' = T_{y,\theta}(\xi) = \frac{\xi - \frac{\theta}{2}}{\frac{\theta}{2}\xi + 1} = \frac{2\xi - \theta}{\theta\xi + 2},$$

$$\xi \xrightarrow{\theta \rightarrow 0} \xi' = T_{x,\theta}(\xi) = \frac{\xi + \frac{i\theta}{2}}{\frac{i\theta}{2}\xi + 1} = \frac{2\xi + i\theta}{i\theta\xi + 2}.$$

Putting them into the unperturbed rational map $R_0(\xi) = \frac{\xi^4 + 2\sqrt{3}i\xi^2 + 1}{\xi^4 - 2\sqrt{3}i\xi^2 + 1}$, we then can have the expressions of the rational maps for the rotation modes, which are rotating around the z , y and x -axis respectively:

$$R_0(T_{z,\theta_z}(\xi)) = \frac{P_0(\xi) + 4\sqrt{3}\theta_z\xi^2 - 4i\theta_z}{Q_0(\xi) - 4\sqrt{3}\theta_z\xi^2 - 4i\theta_z}, \quad (6.11)$$

$$R_0(T_{y,\theta_y}(\xi)) = \frac{P_0(\xi) + (2\sqrt{3}i\theta_y - 2\theta_y)\xi^3 + (-2\sqrt{3}i\theta_y + 2\theta_y)\xi}{Q_0(\xi) + (-2\sqrt{3}i\theta_y - 2\theta_y)\xi^3 + (2\sqrt{3}i\theta_y + 2\theta_y)\xi}, \quad (6.12)$$

$$R_0(T_{x,\theta_x}(\xi)) = \frac{P_0(\xi) + (2i\theta_x - 2\sqrt{3}\theta_x)\xi^3 + (2i\theta_x - 2\sqrt{3}\theta_x)\xi}{Q_0(\xi) + (2i\theta_x + 2\sqrt{3}\theta_x)\xi^3 + (2i\theta_x + 2\sqrt{3}\theta_x)\xi}, \quad (6.13)$$

where the subscript x , y , and z of θ is just used to remind us of its rotation axis.

The corresponding vector forms to the rational maps for the rotation modes are

$$\vec{v}_{R_z,\theta_z} = \begin{pmatrix} 0 \\ 0 \\ 4\sqrt{3}\theta_z \\ 0 \\ 0 \\ 0 \\ 0 \\ 0 \\ -4i\theta_z \\ 0 \\ 0 \\ 0 \\ 0 \\ 0 \\ 0 \\ -4\sqrt{3}\theta_z \\ 0 \\ 0 \\ 0 \\ 0 \\ 0 \\ -4i\theta_z \end{pmatrix}, \quad \vec{v}_{R_y,\theta_y} = \begin{pmatrix} -2\theta_y \\ 2\sqrt{3}i\theta_y \\ 0 \\ 0 \\ 2\theta_y \\ -2\sqrt{3}i\theta_y \\ 0 \\ 0 \\ 0 \\ 0 \\ 0 \\ -2\theta_y \\ -2\sqrt{3}i\theta_y \\ 0 \\ 0 \\ 0 \\ 0 \\ 2\theta_y \\ 2\sqrt{3}i\theta_y \\ 0 \\ 0 \end{pmatrix}, \quad \vec{v}_{R_x,\theta_x} = \begin{pmatrix} -2\sqrt{3}\theta_x \\ 2i\theta_x \\ 0 \\ 0 \\ -2\sqrt{3}\theta_x \\ 2i\theta_x \\ 0 \\ 0 \\ 0 \\ 0 \\ 0 \\ 2\sqrt{3}\theta_x \\ 2i\theta_x \\ 0 \\ 0 \\ 0 \\ 0 \\ 2\sqrt{3}\theta_x \\ 2i\theta_x \\ 0 \\ 0 \end{pmatrix}. \quad (6.14)$$

Obviously, the comparisons of $R_0(Q_{z,\theta_z}(\xi))$, $R_1(Q_{z,\theta_z}(\xi))$ and $R_2(Q_{z,\theta_z}(\xi))$ with any rational maps from (6.5) to (6.10) show that there is no instance where the zero modes we obtained are rotation modes alone. However, as mentioned previously, the rotation modes must be the zero modes of the Skyrme model. Hence, some of the zero modes we have are probably linear combinations of the rotation modes. By further inspection, it seems that two zero modes $R_1(\xi)$ and $R_2(\xi)$ have similar structures to rotational mode $R_0(Q_{z,\theta_z}(\xi))$ but not with the correct values. We then consider a simple linear combinations of $R_1(\xi)$ and $R_2(\xi)$ to check whether or not it can be our required rotation modes $R_0(Q_{z,\theta_z}(\xi))$. Through the following identification

$$\begin{aligned}
 & a \vec{v}_{R_1} + b \vec{v}_{R_2} = \vec{v}_{R_{z,\theta_z}} , \\
 \Rightarrow & \frac{P_0(\xi) - (0.68624 \varepsilon_a + 0.14171 \varepsilon_b) \xi^2 + i (0.69276 \varepsilon_b - 0.17053 \varepsilon_a)}{Q_0(\xi) + (0.68624 \varepsilon_a + 0.14171 \varepsilon_b) \xi^2 + i (0.69276 \varepsilon_b - 0.17053 \varepsilon_a)} = R_0(T_{z,\theta_z}(\xi)) , \\
 & \hspace{20em} (6.15)
 \end{aligned}$$

$$\Rightarrow \begin{cases} 0.68624 \varepsilon_a + 0.14171 \varepsilon_b = -4\sqrt{3} \theta_z \\ 0.69276 \varepsilon_b - 0.17053 \varepsilon_a = -4\theta_z \end{cases} ,$$

we find that while the parameters take the values below

$$\begin{cases} \varepsilon_a = a \cdot \varepsilon = -8.47285 \theta_z \\ \varepsilon_b = b \cdot \varepsilon = -7.85968 \theta_z \end{cases} ; \quad \theta_z \rightarrow 0 ,$$

the linear combination of $R_1(\xi)$ and $R_2(\xi)$ can result in the rotational mode $R_0(T_{z,\theta_z}(\xi))$, which is an infinitesimal rotation around the z -axis.

This fact immediately tells us that we can represent $R_1(\xi)$ and $R_2(\xi)$ in terms of the rotation mode $R_0(T_{z,\theta_z}(\xi))$ and another mode, which does not contain the $R_0(T_{z,\theta_z}(\xi))$ component in it and that would make things easier and clearer. So we choose $\tilde{R}_2(\xi) \equiv R_0(T_{z,\theta_z}(\xi))$ to take the place of $R_2(\xi)$. To find the new one to replace $R_1(\xi)$, it is crucial to remove the rotational mode from $R_1(\xi)$. By setting

$(0.68624 \varepsilon_a + 0.14171 \varepsilon_b)$ in (6.15) to be zero, we can take the $R_0(T_{z,\theta_z}(\xi))$ component out of $R_1(\xi)$ as much as possible and that is because the part involving ξ^2 , which is related to the rotation mode $R_0(T_{z,\theta_z}(\xi))$, in $(a \vec{V}_{R_1} + b \vec{V}_{R_2})$ has been taken away. In this case, we have $\varepsilon_b = -4.84257 \varepsilon_a$, and therefore the new mode is

$$\tilde{R}_1(\xi) \equiv \frac{P_0(\xi) - 0.35253 i \varepsilon}{Q_0(\xi) - 0.35253 i \varepsilon} \stackrel{\text{redefine}}{=} \frac{P_0(\xi) + i \varepsilon}{Q_0(\xi) + i \varepsilon}.$$

Similarly, we also realize that $R_4(\xi)$ and $R_5(\xi)$ have the same structures, which means that they have the terms of the same powers of ξ , as $R_0(T_{x,\theta_x}(\xi))$ and $R_0(T_{y,\theta_y}(\xi))$ and therefore, by suitable linear combinations of two rotation modes, we have

$$R_4(\xi) = R_0(T_{x,\theta_x}(\xi)) + R_0(T_{y,\theta_y}(\xi))$$

with

$$\begin{cases} \theta_x = 0.08961 \varepsilon \\ \theta_y = -0.08716 \varepsilon \end{cases} ; \quad \varepsilon \rightarrow 0,$$

and

$$R_5(\xi) = R_0(T_{x,\theta_x}(\xi)) + R_0(T_{y,\theta_y}(\xi))$$

with

$$\begin{cases} \theta_x = 0.08667 \varepsilon \\ \theta_y = 0.09008 \varepsilon \end{cases} ; \quad \varepsilon \rightarrow 0.$$

Since it is possible to generate $R_4(\xi)$ and $R_5(\xi)$ from linearly combining $R_0(Q_{x,\theta_x}(\xi))$ and $R_0(T_{y,\theta_y}(\xi))$, it is proper to replace them with these two zero modes and to define:

$$\begin{cases} \tilde{R}_4(\xi) \equiv R_0(T_{y,\theta}(\xi)) \\ \tilde{R}_5(\xi) \equiv R_0(T_{x,\theta}(\xi)) \end{cases}$$

So far, we have already understood that some of the zero modes acquired from the mechanism out of which the eigenvectors are obtained, can be reproduced by three rotational modes, *i.e.* $R_0(Q_{x,\theta}(\xi))$, $R_0(Q_{y,\theta}(\xi))$ and $R_0(Q_{z,\theta}(\xi))$, and $\tilde{R}_1(\xi)$. Our next task in analyzing the zero modes is to find out what the rest of the zero modes, $R_3(\xi)$ and $R_6(\xi)$, really are.

The act of getting rid of some modes already known seems to be quite reasonable as the first step toward understanding them more. For that reason, we take the next move

$$\vec{v}_{\tilde{R}_3} \equiv \vec{v}_{R_3} - \vec{v}_{R_{z,\theta}} - \vec{v}_{\tilde{R}_1},$$

$$\Rightarrow \tilde{R}_3(\xi) = \frac{P_0(\xi) + (4\sqrt{3}\theta_z + 0.57206\varepsilon)\xi^2 - i(\varepsilon_1 + 0.1799\varepsilon)}{Q_0(\xi) + 0.36391i\varepsilon\xi^4 + (0.68855\varepsilon - 4\sqrt{3}\theta_z)\xi^2 + i(0.18401\varepsilon - \varepsilon_1)}.$$

We then set $\varepsilon_1 + 0.1799\varepsilon = 0$ and $0.68855\varepsilon - 4\sqrt{3}\theta_z = 0$ to make the removal so that the precise relation between the parameters are

$$\begin{cases} \varepsilon_1 = -0.1799\varepsilon \\ \theta_z = 0.09938\varepsilon \end{cases},$$

where the parameters θ_z , ε_1 and ε come from $R_0(T_{z,\theta}(\xi))$, $\tilde{R}_1(\xi)$ and $R_3(\xi)$ respectively.

As a result, $R_3(\xi)$ can be replaced with $\tilde{R}_3(\xi)$, which involves the other zero modes as little as possible:

$$\tilde{R}_3(\xi) = \frac{P_0(\xi) + 1.26061\varepsilon\xi^2}{Q_0(\xi) + 0.36391i\varepsilon\xi^4 + 0.36391i\varepsilon}$$

$$\equiv \frac{P_0(\xi) + \varepsilon\xi^2}{Q_0(\xi) + 0.28868i\varepsilon\xi^4 + 0.28868i\varepsilon}$$

$$\xrightarrow{\text{redefine}} \frac{P_0(\xi) + 2\sqrt{3}\varepsilon\xi^2}{Q_0(\xi) + i\varepsilon\xi^4 + i\varepsilon}.$$

Taking a further look at $\tilde{R}_3(\xi)$ will lead us to find out that its structure is almost exactly the same as $R_6(\xi)$'s except that the coefficient for each term other than

those in the unperturbed map, P_0 and Q_0 , is different from each other by a factor of i . Comparison of $\tilde{R}_3(\xi)$ and $R_6(\xi)$ with the one's obtained originally shows that there are hardly any component that can be taken away from these two zero modes. Therefore we list in the following the new zero modes instead of the previous old ones.

$$\tilde{R}_1(\xi) = \frac{P_0(\xi) + i\varepsilon_1}{Q_0(\xi) + i\varepsilon_1} = \frac{P_0(\xi) + \tilde{P}_1(\xi)}{Q_0(\xi) + \tilde{Q}_1(\xi)}, \quad (6.16)$$

$$\tilde{R}_2(\xi) = \frac{P_0(\xi) + 4\sqrt{3}\theta_z\xi^2 - 4i\theta_z}{Q_0(\xi) - 4\sqrt{3}\theta_z\xi^2 - 4i\theta_z} = \frac{P_0(\xi) + \tilde{P}_2(\xi)}{Q_0(\xi) + \tilde{Q}_2(\xi)}, \quad (6.17)$$

$$\tilde{R}_3(\xi) = \frac{P_0(\xi) + 2\sqrt{3}\varepsilon_3\xi^2}{Q_0(\xi) + i\varepsilon_3\xi^4 + i\varepsilon_3} = \frac{P_0(\xi) + \tilde{P}_3(\xi)}{Q_0(\xi) + \tilde{Q}_3(\xi)}, \quad (6.18)$$

$$\tilde{R}_4(\xi) = \frac{P_0(\xi) + (2\sqrt{3}i\theta_y - 2\theta_y)\xi^3 + (-2\sqrt{3}i\theta_y + 2\theta_y)\xi}{Q_0(\xi) + (-2\sqrt{3}i\theta_y - 2\theta_y)\xi^3 + (2\sqrt{3}i\theta_y + 2\theta_y)\xi} = \frac{P_0(\xi) + \tilde{P}_4(\xi)}{Q_0(\xi) + \tilde{Q}_4(\xi)}, \quad (6.19)$$

$$\tilde{R}_5(\xi) = \frac{P_0(\xi) + (2i\theta_x - 2\sqrt{3}\theta_x)\xi^3 + (2i\theta_x - 2\sqrt{3}\theta_x)\xi}{Q_0(\xi) + (2i\theta_x + 2\sqrt{3}\theta_x)\xi^3 + (2i\theta_x + 2\sqrt{3}\theta_x)\xi} = \frac{P_0(\xi) + \tilde{P}_5(\xi)}{Q_0(\xi) + \tilde{Q}_5(\xi)}, \quad (6.20)$$

$$\tilde{R}_6(\xi) = \frac{P_0(\xi) + 2\sqrt{3}i\varepsilon_6\xi^2}{Q_0(\xi) + \varepsilon_6\xi^4 + \varepsilon_6} = \frac{P_0(\xi) + \tilde{P}_6(\xi)}{Q_0(\xi) + \tilde{Q}_6(\xi)}, \quad (6.21)$$

where the parameters ε_1 , ε_3 , ε_6 , θ_x , θ_y , and $\theta_z \ll 1$.

We now are interested in knowing how these zero modes relate to one another under the transformations of some finite rotations, to be specific, $\pi/2$ rotation around the x , y and z -axis. In order to perform such transformations, we take a general expression for the zero modes, treating it as a general vector, $\vec{V}_{R_{zm}}$, containing all aforementioned zero modes.

$$\vec{v}_{R_{zm}} \equiv \vec{v}_{\tilde{R}_1} + \vec{v}_{\tilde{R}_2} + \vec{v}_{\tilde{R}_3} + \vec{v}_{\tilde{R}_4} + \vec{v}_{\tilde{R}_5} + \vec{v}_{\tilde{R}_6} ,$$

$$\Rightarrow R_{zm}(\xi) \equiv \frac{P_0(\xi) + \tilde{P}_1(\xi) + \tilde{P}_2(\xi) + \tilde{P}_3(\xi) + \tilde{P}_4(\xi) + \tilde{P}_5(\xi) + \tilde{P}_6(\xi)}{Q_0 + \tilde{Q}_1(\xi) + \tilde{Q}_2(\xi) + \tilde{Q}_3(\xi) + \tilde{Q}_4(\xi) + \tilde{Q}_5(\xi) + \tilde{Q}_6(\xi)} .$$

Recall that the Skyrmion has a symmetry when the relation $R(g(\xi)) = D_g \cdot R(\xi)$ is realized, where g is a group element of the transformations on domain space and D_g is the corresponding group element of the transformations on target space. Since we try to apply the transformations of some finite rotations, g , on domain space and we then need to find out the corresponding transformations, D_g , on target space. The way to obtain these D_g transformations is through performing the transformations of the $\pi/2$ rotations on the domain space. Here are the consequences:

$$\begin{cases} R_0(T_{z, \frac{\pi}{2}}(\xi)) = D_{T_{z, \frac{\pi}{2}}} \cdot R_0(\xi) , \\ R_0(T_{y, \frac{\pi}{2}}(\xi)) = D_{T_{y, \frac{\pi}{2}}} \cdot R_0(\xi) , \\ R_0(T_{x, \frac{\pi}{2}}(\xi)) = D_{T_{x, \frac{\pi}{2}}} \cdot R_0(\xi) , \end{cases}$$

$$\Rightarrow \begin{cases} [T_{Q_z, \frac{\pi}{2}}] = \begin{pmatrix} 0 & 1 \\ 1 & 0 \end{pmatrix} , \\ [D_{T_{y, \frac{\pi}{2}}}] = \begin{pmatrix} 0 & -1 - \sqrt{3}i \\ -1 + \sqrt{3}i & 0 \end{pmatrix} , \\ [D_{T_{x, \frac{\pi}{2}}}] = \begin{pmatrix} 0 & 1 - \sqrt{3}i \\ 1 + \sqrt{3}i & 0 \end{pmatrix} , \end{cases} \quad (5.32)$$

where the explicit expressions of $[T_{x, \frac{\pi}{2}}]$, $[T_{y, \frac{\pi}{2}}]$ and $[T_{z, \frac{\pi}{2}}]$ are shown in the previous section.

Performing the $\pi/2$ rotations around the x , y and z -axis leads to the following results:

$$R_{zm}(T_{z, \frac{\pi}{2}}(\xi)) = D_{T_{z, \frac{\pi}{2}}} \cdot R_{zm}(\xi)$$

$$\Rightarrow \left\{ \begin{array}{l} \varepsilon_1 \xrightarrow{T_{z, \frac{\pi}{2}}} \tilde{\varepsilon}_1 = \varepsilon_1 + 4\varepsilon_3 \\ \varepsilon_3 \longrightarrow \tilde{\varepsilon}_3 = -\varepsilon_3 \\ \varepsilon_6 \longrightarrow \tilde{\varepsilon}_6 = -\varepsilon_6 \\ \theta_x \longrightarrow \tilde{\theta}_x = \theta_y \\ \theta_y \longrightarrow \tilde{\theta}_y = -\theta_x \\ \theta_z \longrightarrow \tilde{\theta}_z = \theta_z + \varepsilon_3 \end{array} \right.$$

$$R_{zm}(T_{y, \frac{\pi}{2}}(\xi)) = D_{T_{y, \frac{\pi}{2}}} \cdot R_{zm}(\xi)$$

$$\Rightarrow \left\{ \begin{array}{l} \varepsilon_1 \xrightarrow{T_{y, \frac{\pi}{2}}} \tilde{\varepsilon}_1 = -\frac{1}{2}\varepsilon_1 + \varepsilon_3 + \sqrt{3}\varepsilon_6 \\ \varepsilon_3 \longrightarrow \tilde{\varepsilon}_3 = -\varepsilon_3 \\ \varepsilon_6 \longrightarrow \tilde{\varepsilon}_6 = \frac{\sqrt{3}}{4}\varepsilon_1 + \frac{\sqrt{3}}{2}\varepsilon_3 + \frac{1}{2}\varepsilon_6 \\ \theta_x \longrightarrow \tilde{\theta}_x = -\theta_z + \frac{1}{4}\varepsilon_1 \\ \theta_y \longrightarrow \tilde{\theta}_y = \theta_y \\ \theta_z \longrightarrow \tilde{\theta}_z = \theta_x - \frac{1}{8}\varepsilon_1 + \frac{1}{4}\varepsilon_3 + \frac{\sqrt{3}}{4}\varepsilon_6 \end{array} \right.$$

$$R_{zm}(Q_{x, \frac{\pi}{2}}(\xi)) = D_{T_{x, \frac{\pi}{2}}} \cdot R_{zm}(\xi)$$

$$\Rightarrow \left\{ \begin{array}{l} \varepsilon_1 \xrightarrow{T_{x, \frac{\pi}{2}}} \tilde{\varepsilon}_1 = -\frac{1}{2} \varepsilon_1 + \varepsilon_3 - \sqrt{3} \varepsilon_6 \\ \varepsilon_3 \longrightarrow \tilde{\varepsilon}_3 = -\varepsilon_3 \\ \varepsilon_6 \longrightarrow \tilde{\varepsilon}_6 = -\frac{\sqrt{3}}{4} \varepsilon_1 - \frac{\sqrt{3}}{2} \varepsilon_3 + \frac{1}{2} \varepsilon_6 \\ \theta_x \longrightarrow \tilde{\theta}_x = \theta_x \\ \theta_y \longrightarrow \tilde{\theta}_y = \theta_z - \frac{1}{4} \varepsilon_1 \\ \theta_z \longrightarrow \tilde{\theta}_z = -\theta_y - \frac{1}{8} \varepsilon_1 + \frac{1}{4} \varepsilon_3 - \frac{\sqrt{3}}{4} \varepsilon_6 \end{array} \right.$$

6.6.1 Identification of Iso-rotational Modes, $B = 4$

Since we have already identified that three of the zero modes are the rotational zero modes, it is reasonable to check if the other three zero modes are the iso-rotational zero modes because of the symmetry consideration. In the following, we will generalize the method of identifying iso-rotational zero modes which is used in section 5.3.3.

The Cartesian notation for the unit vector of the rational map is

$$\hat{n}_{R_0} = \frac{1}{1 + |R_0|^2} (2\Re(R_0), 2\Im(R_0), 1 - |R_0|^2) = (n_1, n_2, n_3).$$

Then the iso-rotated unit vector about the x , y , and z -axis can be shown respectively below as

$$\hat{\tilde{n}} = O_i \hat{n}_{R_0}, \quad i = x, y, z,$$

where O_x , O_y , and O_z are the iso-rotation matrices, taking the following form

$$O_x = \begin{pmatrix} 1 & 0 & 0 \\ 0 & \cos \theta & \sin \theta \\ 0 & -\sin \theta & \cos \theta \end{pmatrix}, \quad O_y = \begin{pmatrix} \cos \theta & 0 & \sin \theta \\ 0 & 1 & 0 \\ -\sin \theta & 0 & \cos \theta \end{pmatrix},$$

$$O_z = \begin{pmatrix} \cos \theta & \sin \theta & 0 \\ -\sin \theta & \cos \theta & 0 \\ 0 & 0 & 1 \end{pmatrix}.$$

The associated iso-rotated rational maps constructed using the formula (5.12) up to the linear order are

$$R_{iso,x} = \frac{R_0 + i\frac{\theta}{2}(1 - |R_0|^2)}{1 - \theta \cdot \Im(R_0)},$$

$$R_{iso,y} = \frac{R_0 + \frac{\theta}{2}(1 - |R_0|^2)}{1 - \theta \cdot \Re(R_0)},$$

$$R_{iso,z} = R_0 \cdot (1 + i\theta).$$

In the case of $B = 2$, it is easy to show that the rational maps R_3 and R_4 are those of the iso-rotational zero modes. In the case of $B = 4$, the situation is more complicated and the iso-rotated rational maps will be demonstrated as the linear combinations of some other zero modes. Therefore the strategy used here should be different from that in the previous $B = 2$ case. We first find out the iso-rotated zero mode about the z -axis and then use the conjugation to obtain the rest iso-rotational modes. Afterwards, we will show how these iso-rotational zero modes can be the linear combinations of some other zero modes.

The rational map of iso-rotated zero mode about the z -axis obtained above is

$$R_{iso,z} = R_0 \cdot (1 + i\theta) \simeq \frac{P_0}{Q_0 \cdot (1 - i\theta)} = \frac{\xi^4 + 2\sqrt{3}i\xi^2 + 1}{(1 - i\theta)(\xi^4 - 2\sqrt{3}i\xi^2 + 1)}.$$

We then want to express it as the linear combinations of the zero modes, \tilde{R}_1 , \tilde{R}_2 , and \tilde{R}_3 :

$$\vec{v}_{R_{iso,z}} = \vec{v}_{\tilde{R}_1} + \vec{v}_{\tilde{R}_2} + \vec{v}_{\tilde{R}_3} .$$

Rewriting the above vector form to the expression of the rational map, we have

$$\begin{aligned} & \frac{\xi^4 + 2\sqrt{3}i\xi^2 + 1}{(1 - i\theta)(\xi^4 - 2\sqrt{3}i\xi^2 + 1)} \\ = & \frac{\xi^4 + (2\sqrt{3}i + 4\sqrt{3}\theta_z + \varepsilon_3)\xi^2 + (i\varepsilon_1 - 4i\theta_z + 1)}{(1 + \frac{i\varepsilon_3}{2\sqrt{3}})\xi^4 - (2\sqrt{3}i + 4\sqrt{3}\theta_z)\xi^2 + (i\varepsilon_1 - 4i\theta_z + \frac{i\varepsilon_3}{2\sqrt{3}} + 1)} . \end{aligned}$$

Hence, after solving the equation above, we find the relation between the iso-rotational angle θ and the parameters which the other rational maps of zero mode take:

$$\begin{cases} \varepsilon_1 = 2\theta , \\ \varepsilon_3 = -2\sqrt{3}\theta , \\ \theta_z = \frac{\theta}{2} . \end{cases}$$

As mentioned previously, the iso-rotational modes about the x and y -axis are not easy to obtain from the general formula, we therefore choose to use conjugation to find the other two rational maps of the iso-rotational zero modes. Here we first take this strategy to obtain the iso-rotational mode about the x -axis.

We first use the matrix (5.4) to rotate the axis of the target space, *i.e.* the rotation of the x -axis into z -axis.

$$R'_0 = [T_{y, \frac{\pi}{2}}]^{-1} \cdot R_0 ,$$

$$\begin{pmatrix} P'_0 \\ Q'_0 \end{pmatrix} = \begin{pmatrix} 1 & 1 \\ -1 & 1 \end{pmatrix} \begin{pmatrix} P_0 \\ Q_0 \end{pmatrix} = \begin{pmatrix} \xi^4 + 1 \\ -2\sqrt{3}i\xi^2 \end{pmatrix} .$$

Then the iso-rotation about the z -axis is performed on R'_0 to have the iso-rotational rational map.

$$R'_0 \longrightarrow R'_0 \cdot (1 + i\theta).$$

In the end, we perform the rotation by using the matrix (5.4) to take this iso-rotational map about the z -axis back to that about the x -axis to obtain the rational map of the iso-rotational mode about the x -axis, *i.e.* $R_{iso,x}$.

$$R_{iso,x} = [T_{y, \frac{\pi}{2}}] \cdot (R'_0 \cdot (1 + i\theta)),$$

$$\begin{pmatrix} P_{iso,x} \\ Q_{iso,x} \end{pmatrix} = \begin{pmatrix} 1 & -1 \\ 1 & 1 \end{pmatrix} \begin{pmatrix} P'_0 \\ Q'_0(1 - i\theta) \end{pmatrix} = \begin{pmatrix} P_0 + 2\sqrt{3}\theta\xi^2 \\ Q_0 - 2\sqrt{3}\theta\xi^2 \end{pmatrix}.$$

Using the conjugation, the iso-rotational mode is then

$$R_{iso,x} = \frac{P_0 + 2\sqrt{3}\theta\xi^2}{Q_0 - 2\sqrt{3}\theta\xi^2}.$$

Since the iso-rotational mode about the x -axis is obtained, we are interested in finding how it can be linearly combined from the other zero modes. After some observations, we can find that

$$\vec{v}_{R_{iso,x}} = \vec{v}_{\tilde{R}_1} + \vec{v}_{\tilde{R}_2}.$$

In terms of the rational map, it is expressed as

$$\frac{P_0 + 2\sqrt{3}\theta\xi^2}{Q_0 - 2\sqrt{3}\theta\xi^2} = \frac{P_0 + 4\sqrt{3}\theta_z\xi^2 - 4i\theta_z + i\varepsilon_1}{Q_0 - 4\sqrt{3}\theta_z\xi^2 - 4i\theta_z + i\varepsilon_1}.$$

Identification of the coefficients of each terms in the above equation leads us to have the connection between the parameters:

$$\begin{cases} \theta_z = \frac{\theta}{2}, \\ \varepsilon_1 = 2\theta. \end{cases}$$

Similarly, the iso-rotational mode about the y -axis can be obtained by using the procedure taken above, with the matrix $[T_{x, \frac{\pi}{2}}]$ in (5.3) instead $[T_{y, \frac{\pi}{2}}]$ in (5.4). Hence, $R_{iso,y}$, the rational map of the iso-rotational rational mode about the y -axis, is

$$\begin{aligned}
R_{iso,y} &= \frac{(1 + \frac{\theta}{2} - \frac{i\theta}{2})\xi^4 + 2\sqrt{3}i(1 - \frac{\theta}{2} - \frac{i\theta}{2})\xi^2 + (1 + \frac{\theta}{2} - \frac{i\theta}{2})}{(1 - \frac{\theta}{2} - \frac{i\theta}{2})\xi^4 - 2\sqrt{3}i(1 + \frac{\theta}{2} - \frac{i\theta}{2})\xi^2 + (1 - \frac{\theta}{2} - \frac{i\theta}{2})} \\
&\simeq \frac{\xi^4 + 2\sqrt{3}i\xi^2(1 - \theta) + 1}{(1 - \theta)\xi^4 - 2\sqrt{3}i\xi^2 + (1 - \theta)} \\
&= \frac{P_0 - 2\sqrt{3}i\theta}{Q_0 - \theta\xi^4 - \theta} \\
&= \tilde{R}_6, \quad \text{with } \varepsilon_6 = -\theta.
\end{aligned}$$

Since all these iso-rotational modes can be expressed as the linear combinations of some other zero modes, it is natural to take the iso-rotational modes as the basis of the subspace of the vector space of the zero modes. We therefore rearrange the zero modes as

$$R_{rot,x}(\xi) = \frac{P_0(\xi) + (2i\theta_x - 2\sqrt{3}\theta_x)\xi^3 + (2i\theta_x - 2\sqrt{3}\theta_x)\xi}{Q_0(\xi) + (2i\theta_x + 2\sqrt{3}\theta_x)\xi^3 + (2i\theta_x + 2\sqrt{3}\theta_x)\xi},$$

$$R_{rot,y}(\xi) = \frac{P_0(\xi) + (2\sqrt{3}i\theta_y - 2\theta_y)\xi^3 + (-2\sqrt{3}i\theta_y + 2\theta_y)\xi}{Q_0(\xi) + (-2\sqrt{3}i\theta_y - 2\theta_y)\xi^3 + (2\sqrt{3}i\theta_y + 2\theta_y)\xi},$$

$$R_{rot,z}(\xi) = \frac{P_0(\xi) + 4\sqrt{3}\theta_z\xi^2 - 4i\theta_z}{Q_0(\xi) - 4\sqrt{3}\theta_z\xi^2 - 4i\theta_z},$$

$$R_{iso,x}(\xi) = \frac{P_0 + 2\sqrt{3}\theta_1\xi^2}{Q_0 - 2\sqrt{3}\theta_1\xi^2},$$

$$R_{iso,y}(\xi) = \frac{P_0 - 2\sqrt{3}i\theta_2\xi^2}{Q_0 - \theta_2\xi^4 - \theta_2},$$

$$R_{iso,z}(\xi) = \frac{P_0 \cdot (1 + i\theta_3)}{Q_0}.$$

6.6.2 Plots of the Zero Modes, $B = 4$

The plots of the new zero modes are presented in the following:

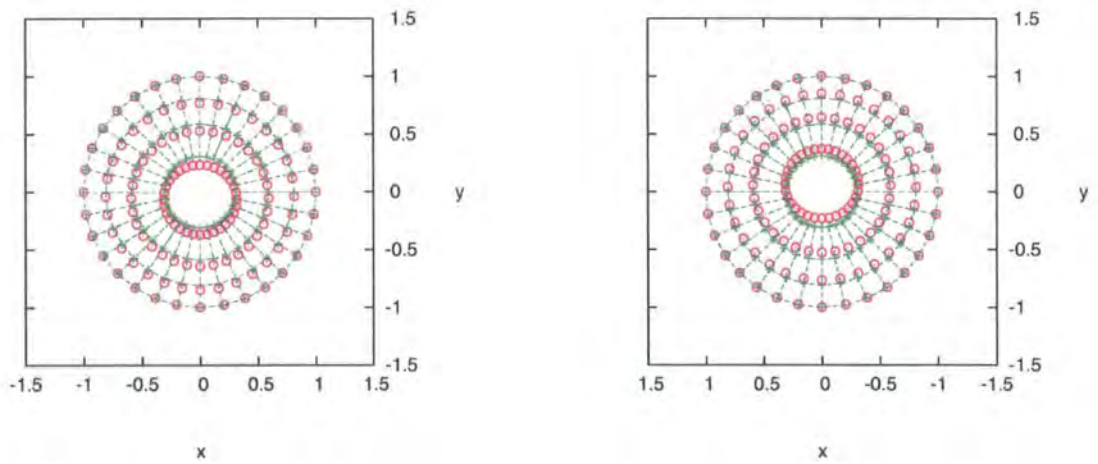


Figure 6.24: Northern(left) and southern(right) hemisphere of Riemann sphere of $R_{rot,x}(\xi)$, $B=4$.

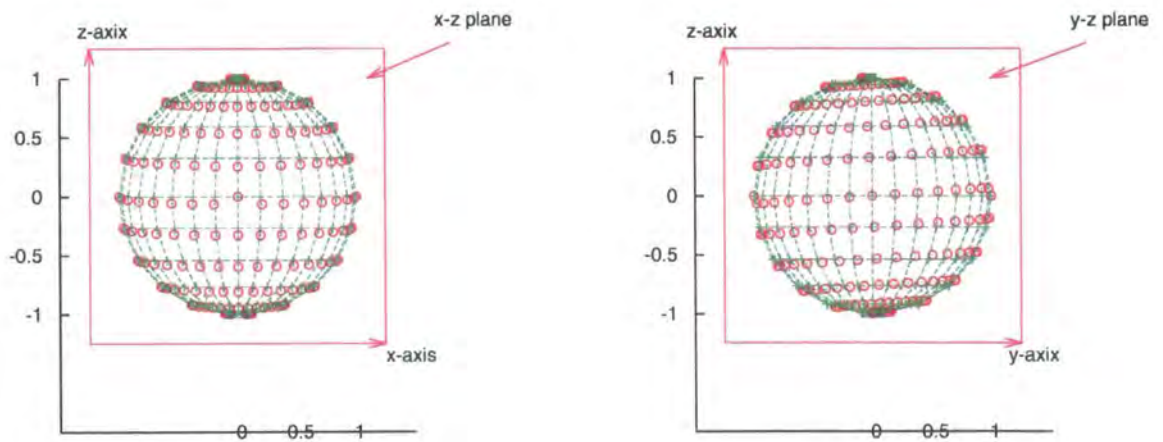


Figure 6.25: $R_{rot,x}(\xi)$, $B=4$

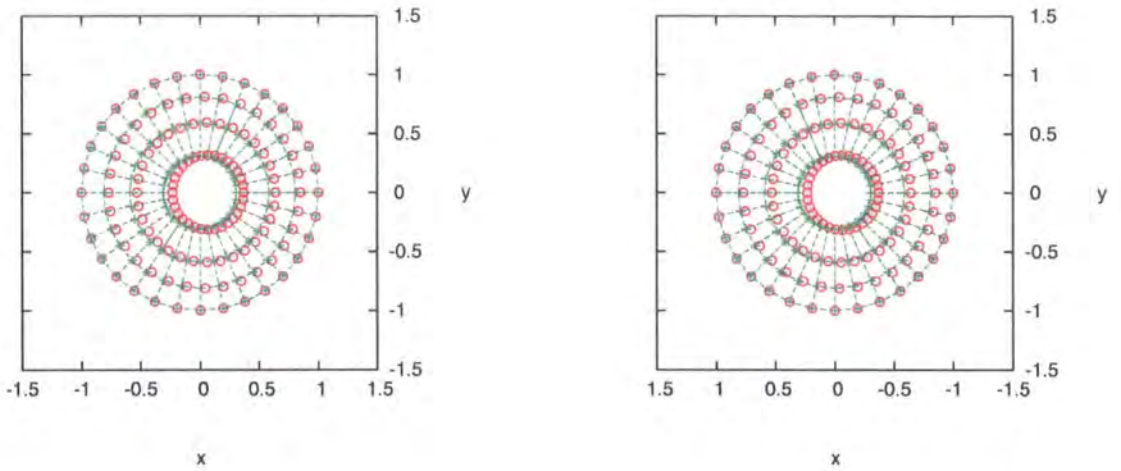


Figure 6.26: Northern(left) and southern(right) hemisphere of Riemann sphere of $R_{rot,y}(\xi)$, $B=4$.

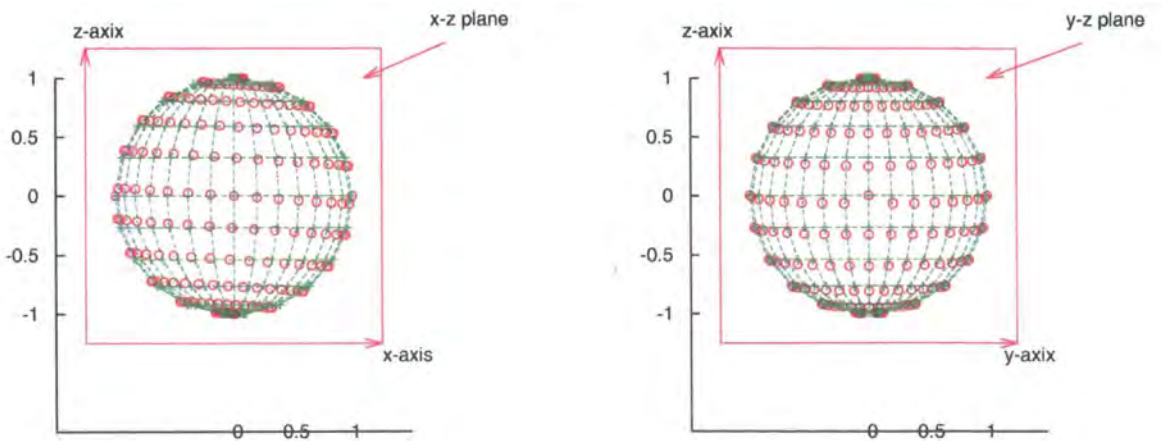


Figure 6.27: $R_{rot,y}(\xi)$, $B=4$

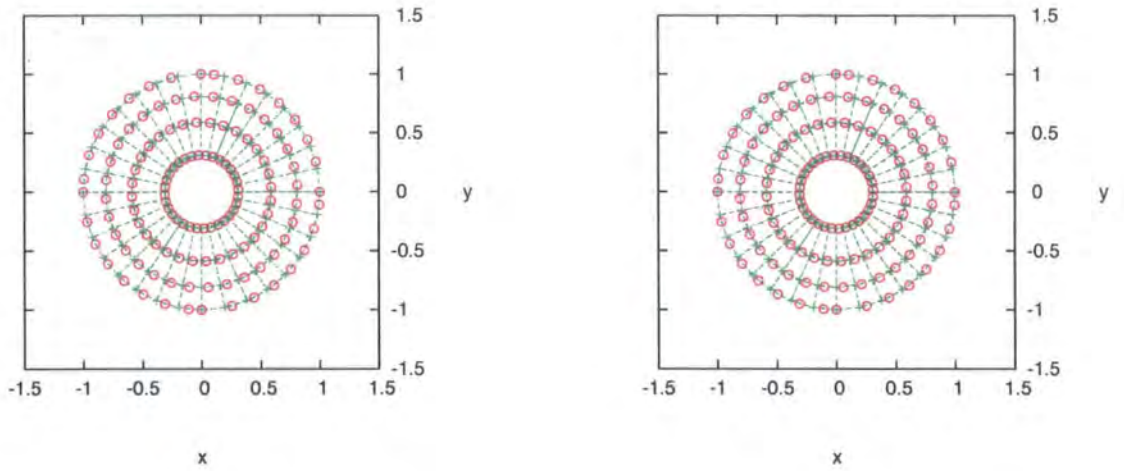


Figure 6.28: Northern(left) and southern(right) hemisphere of Riemann sphere of $R_{rot,z}(\xi)$, $B=4$.

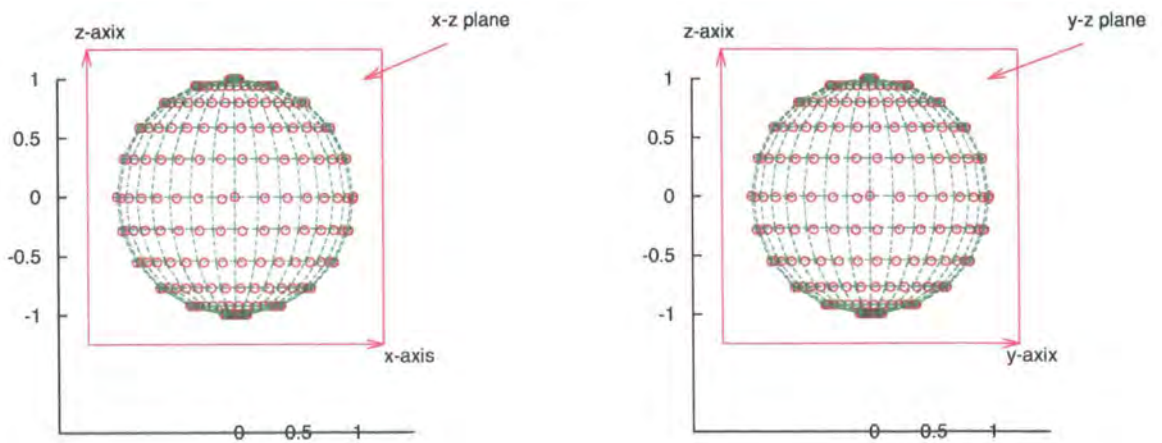


Figure 6.29: $R_{rot,z}(\xi)$, $B=4$

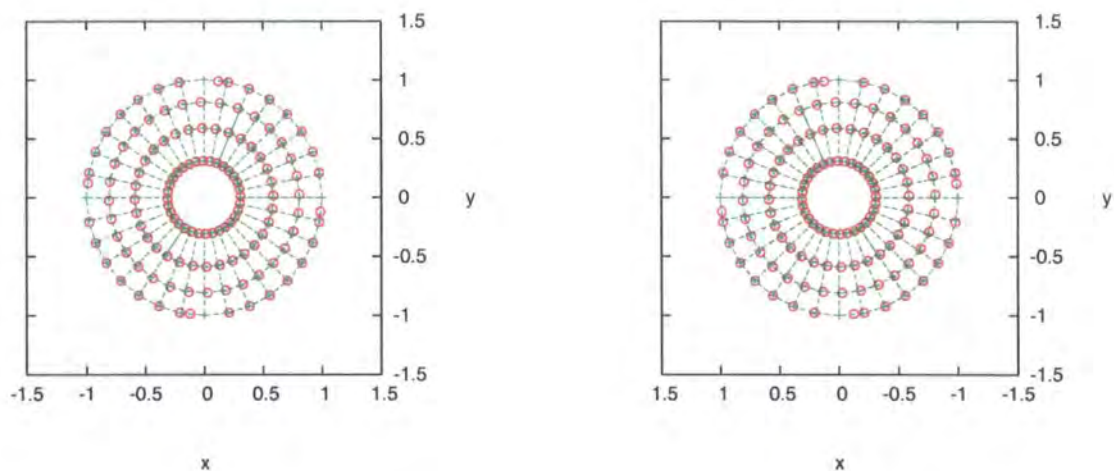


Figure 6.30: Northern(left) and southern(right) hemisphere of Riemann sphere of $R_{iso,x}(\xi)$, $B=4$.

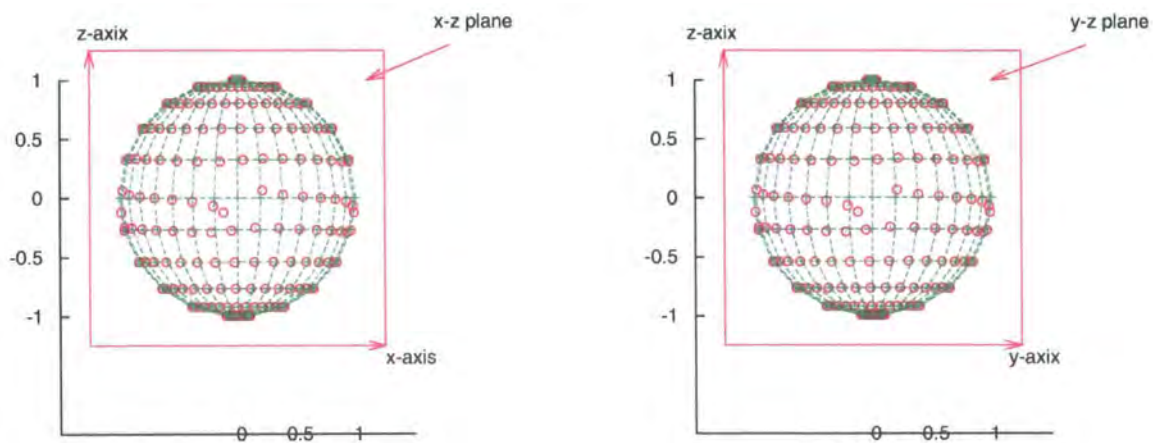


Figure 6.31: $R_{iso,x}(\xi)$, $B=4$

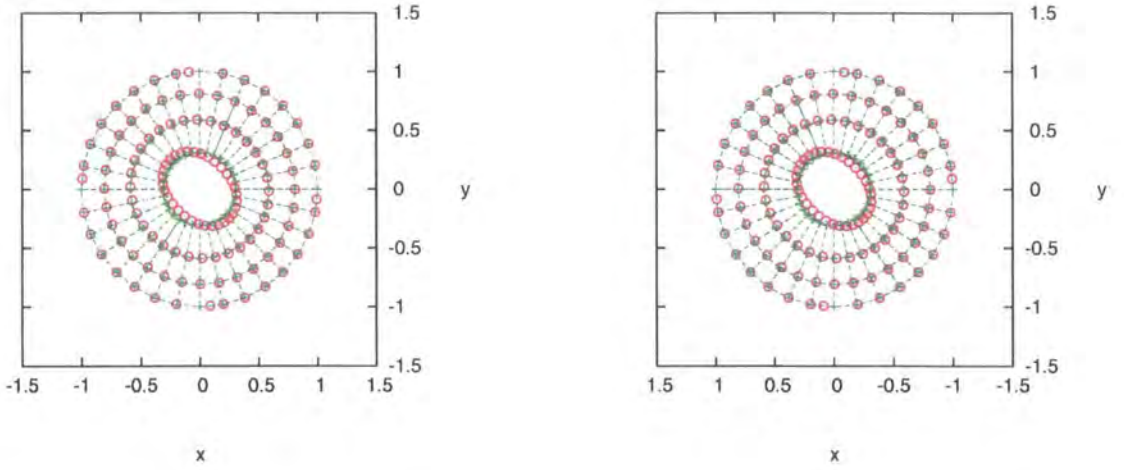


Figure 6.32: Northern(left) and southern(right) hemisphere of Riemann sphere of $R_{iso,y}(\xi)$, $B=4$.

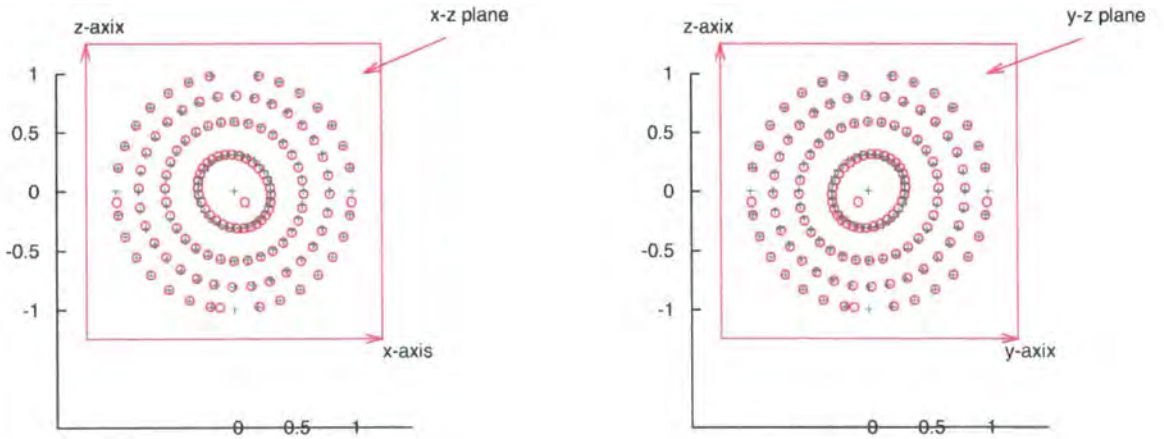


Figure 6.33: $R_{iso,y}(\xi)$, $B=4$

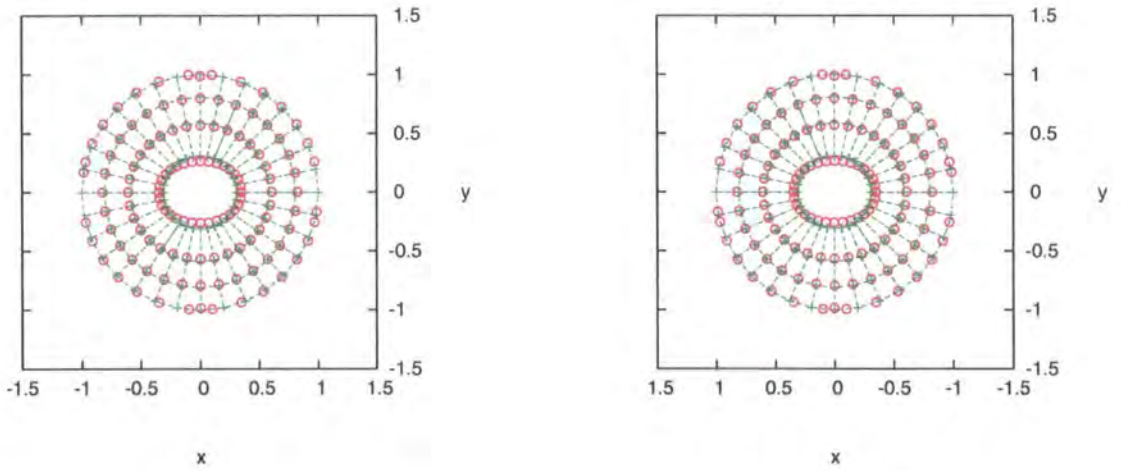


Figure 6.34: Northern(left) and southern(right) hemisphere of Riemann sphere of $R_{iso,z}(\xi)$, $B=4$.

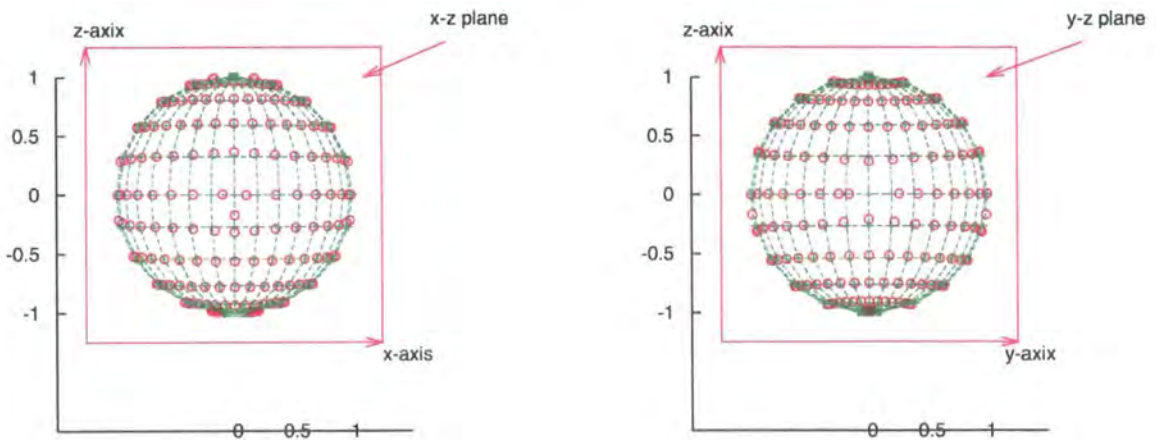


Figure 6.35: $R_{iso,z}(\xi)$, $B=4$

Rational Map	Description	
Zero Mode		
$\left\{ \begin{array}{l} R_{rot,x}(\xi) \\ R_{rot,y}(\xi) \\ R_{rot,z}(\xi) \end{array} \right.$	<p>Rotational mode around the x-axis. See Figure 6.24 and 6.25.</p> <p>Rotational mode around the y-axis. See Figure 6.26 and 6.27.</p> <p>Rotational mode around the z-axis. See Figure 6.28 and 6.29.</p>	
	$\left\{ \begin{array}{l} R_{iso,x}(\xi) \\ R_{iso,y}(\xi) \\ R_{iso,z}(\xi) \end{array} \right.$	<p>Iso-rotational mode around the x-axis. See Figure 6.30 and 6.31.</p> <p>Iso-rotational mode around the y-axis. See Figure 6.32 and 6.33.</p> <p>Iso-rotational mode around the z-axis. See Figure 6.34 and 6.35.</p>
		Broken Zero Mode
$\left\{ \begin{array}{l} R_7(\xi) \\ \tilde{R}_8(\xi) \\ \tilde{R}_9(\xi) \end{array} \right.$		<p>Broken z translational mode. See in Figure 6.23. One of the upper and lower part of the cube inflates and the other deflates.</p> <p>Broken y translational mode. Same as $R_7(\xi)$.</p> <p>Broken x translational mode. Same as $R_7(\xi)$.</p>

Table 6.1: Descriptions of the zero modes and the broken zero modes of the perturbed rational maps, $B = 4$.

Rational Map	Description of Energy density
Vibrational Mode	
$R_{10}(\xi)$	Deform by inflating two opposite edges on one face and deflating the other two opposite edges on that face. See in Figure 6.20.
$\tilde{R}_{11}(\xi)$	Same as $R_{10}(\xi)$
$\tilde{R}_{12}(\xi)$	Same as $R_{10}(\xi)$.
$R_{13}(\xi)$	The deformation makes a cube become a rhombus. See in Figure 6.17.
$\tilde{R}_{14}(\xi)$	Same as $R_{13}(\xi)$
$\tilde{R}_{15}(\xi)$	Same as $R_{13}(\xi)$.
$R_{16}(\xi)$	Deform a cube by pulling it into two toruses in two perpendicular directions. See in Figure 6.14.
$R_{17}(\xi)$	Same as $R_{16}(\xi)$.
$R_{18}(\xi)$	Deform by pulling and inflating one edge on one face and inflating the opposite edge on the same face. The deformation is performed in two perpendicular directions. See in Figure 6.4.

Table 6.2: Description of the energy density for the vibrational modes of the perturbed rational maps, $B = 4$.

We summarize all the vibrational modes obtained in the $B = 4$ case and briefly describe the corresponding energy density here.

In the $B = 4$ case, the rational map has eighteen modes. Six of them are zero modes, three are the broken zero modes and the other nine modes are vibrational modes. The zero modes can be identified as two set of triplets, which are that of the rotation zero modes and of the iso-rotation zero modes. The broken translational zero modes comprises a triplet. The nine vibrational modes can be grouped into one singlet, one doublet and three triplets.

The descriptions of the energy density for the broken zero modes and the vibrational modes are as follows. For the broken translational zero modes, the representative seen in Figure 6.23, the deformation of a cube such that one of the upper and lower part of the cube inflates and the other deflates. As for the vibrational modes: The singlet is the mode of the deformation of a cube, which is pulling and inflating one edge on one face and inflating the opposite edge on the same face, which can be seen in Figure 6.4. The doublet consists of the two modes, each of which is the deformation of a cube, pulling it into two toruses in two perpendicular directions, as can be seen Figure 6.14. As in Figure 6.17, one of the triplets is composed of three modes, corresponding to the deformation that makes a cube become a rhombus. Another triplet consists of the three modes, each of which is a deformation of inflating two opposite edges on one face and deflating the other two opposite edges on that face, and one can see this in Figure 6.20.

Chapter 7

Conclusion

7.1 Comparisons

After all the work has been done, we now want to compare our results obtained by using the rational map ansatz with the numerical results done by Barnes et al. [10] [11]. We list the frequencies and the degeneracies of the vibrational modes in the following tables to do the comparison. The first table is for the $B = 2$ case, and the second is for $B = 4$.

It is necessary to give a brief description of Barnes et al.'s work. In their first paper [10], they compute the deuteron spectra for two different sizes of box, $L = 6$ and $L = 8$. We choose the data listed in the graph of $L = 8$ because they claimed that the box size $L = 8$ is a reasonable approximation to the infinite separation limit. Since they did not provide the details of the frequencies in the context, we read those roughly from the graph to do the comparison. To do the comparison correctly, we need to make sure that the normalization factors are the same. In their notation, they define $\beta = m_\pi/F_\pi e = 0.263$, following Adkins and Nappi [1], and then we can identify our definition for the pion mass m equal to $2\beta=0.526$. Since our breathing mode is quite sensitive to the mass parameter, we therefore have its frequency by using the set of parameters $(m, p) = (0.526, 1)$, where m is for pion mass and p is for the potential parameter. The other modes listed in the first table are from the perturbation of the rational map.

In the $B = 4$ case, our breathing mode is obtained by $(m, p)=(0.526,1)$ as well.

The other modes are from the deformation of the rational map.

To make the comparisons easy to read, we list the data obtained in Table 7.2 and Table 7.3 for $B = 2$ and $B = 4$ case respectively. The data listed in Table 7.2 are the numerical results about the frequencies of the vibrational modes, from Barnes et al. [10] and our results from using rational map ansatz. In Table 7.3, besides our results, there is also the numerical data done by Barnes et al. [11] and the results from Houghton et al. [42] by using group theory, about the dimensions of the multiplets in which the vibrational modes lie.

7.1.1 Analysis for $B = 2$ case

For $B = 2$ case, Barnes et al. [10] have seen 13 modes in total, including five finite energy bound modes from their analysis for the power spectrum of the perturbation and eight zero modes from the group theory analysis. But actually there are two rotational zero modes (around x, y axes) broken. Our result from the rational map ansatz contains eleven modes in which there are five zero modes, three broken zero modes and three genuine vibrational modes.

We first focus on the results from Barnes et al. and give some descriptions to these modes. From the computation of the bound state spectrum, they have obtained six distinct normal modes. They then identified the vibrational modes from the radiative modes, and determined the degeneracy and the symmetry of these modes. As a result, they stated that among these six peaks only three are genuine bound modes, which corresponds to five finite energy bound modes, another peak is two broken rotational zero modes around x and y axes, and the other two are the radiation modes.

As for the zero modes, they can be obtained by using group theory analysis as follows. The rational map for $B = 2$ Skyrminion is given by the 2-monopole solution $R(\xi) = \xi^2$ with the $D_{\infty h}$ symmetry. The general perturbed rational map can take the form

$$R(\xi) = \frac{\xi^2 + a\xi + b}{c\xi^2 + d\xi + 1 + e},$$

where a, b, c, d, e are small complex parameters. Under the $D_{\infty h}$, the symmetry

transformations act linearly on these parameters via a 5×5 matrix (or 10×10 matrix in real representation). Using the character table

	E	C_∞	σ_v	I	S_∞	C_2
$A_{1g} \equiv \Sigma_g^+$	1	1	1	1	1	1
$A_{2g} \equiv \Sigma_g^-$	1	1	-1	1	1	-1
$E_{1g} \equiv \Pi_g$	2	$2\cos(\theta)$	0	2	$-2\cos(\theta)$	0
$E_{2g} \equiv \Delta_g$	2	$2\cos(2\theta)$	0	2	$2\cos(2\theta)$	0
$E_{3g} \equiv \Phi_g$	2	$2\cos(3\theta)$	0	2	$-2\cos(3\theta)$	0
$A_{1u} \equiv \Sigma_u^+$	1	1	1	-1	-1	-1
$A_{2u} \equiv \Sigma_u^-$	1	1	-1	-1	-1	1
$E_{1u} \equiv \Pi_u$	2	$2\cos(\theta)$	0	-2	$2\cos(\theta)$	0
$E_{2u} \equiv \Delta_u$	2	$2\cos(2\theta)$	0	-2	$-2\cos(2\theta)$	0
$E_{3u} \equiv \Phi_u$	2	$2\cos(3\theta)$	0	-2	$2\cos(3\theta)$	0

Table 7.1: Character table for $D_{\infty h}$.

this ten-dimensional representation can be decomposed into irreducible representations $E_{2g} + E_{2u} + E_{1g} + A_{2g} + E_{1u} + A_{1u}$ ¹. However, we can use the following method to find the representations associated with the zero modes. Consider the perturbation of the the rational map

$$R_0(\xi) \mapsto R(\xi) = \frac{(1 + i\varepsilon_1)R_0(\xi) + (\varepsilon_2 + i\varepsilon_3)}{-(\varepsilon_2 - i\varepsilon_3)R_0(\xi) + (1 - i\varepsilon_3)},$$

where $\varepsilon_1, \varepsilon_2, \varepsilon_3$ are small real numbers, and $R_0(\xi) = \xi^2$. It is clear that we only need to find the characters of the symmetry transformations I and σ_v to determine a singlet representation; I, σ_v and C_∞ for a doublet.

¹In [10], the irreducible representations obtained are $E_{2g} + E_{2u} + E_{1g} + A_{2g} + E_{1u} + A_{2u}$. We believe that A_{2u} is a typo and should be A_{1u} instead.

Now we compute the effect of I leaving $R_0(\xi)$ unchanged

$$I: \xi \mapsto \frac{-1}{\bar{\xi}} \quad ; \quad R_0\left(\frac{-1}{\bar{\xi}}\right) = \frac{1}{\bar{R}_0(\xi)} \quad \Rightarrow \quad R_0(\xi) = \frac{1}{\bar{R}_0\left(\frac{-1}{\bar{\xi}}\right)},$$

$$\sigma_v: \xi \mapsto \bar{\xi} \quad ; \quad R_0(\bar{\xi}) = \bar{R}_0(\xi) \quad \Rightarrow \quad R_0(\xi) = \bar{R}_0(\bar{\xi}),$$

$$C_\infty: \xi \mapsto e^{i\theta}\xi \quad ; \quad R_0(e^{i\theta}\xi) = e^{2i\theta}R_0(\xi) \quad \Rightarrow \quad R_0(\xi) = e^{-2i\theta}R_0(e^{i\theta}\xi),$$

on the perturbed rational map $R(\xi)$ as

$$I: R(\xi) \mapsto \frac{1}{\bar{R}\left(\frac{-1}{\bar{\xi}}\right)} = \frac{(1 + i\varepsilon_1)R_0(\xi) - (\varepsilon_2 + i\varepsilon_3)}{(\varepsilon_2 - i\varepsilon_3)R_0(\xi) + (1 - i\varepsilon_3)},$$

$$\sigma_v: R(\xi) \mapsto \bar{R}(\bar{\xi}) = \frac{(1 - i\varepsilon_1)R_0(\xi) + (\varepsilon_2 - i\varepsilon_3)}{-(\varepsilon_2 + i\varepsilon_3)R_0(\xi) + (1 + i\varepsilon_3)},$$

$$C_\infty: R(\xi) \mapsto e^{-2i\theta}R(e^{i\theta}\xi) = \frac{(1 - i\varepsilon_1)R_0(\xi) + (\varepsilon_2 + i\varepsilon_3)e^{-2i\theta}}{-(\varepsilon_2 - i\varepsilon_3)e^{2i\theta}R_0(\xi) + (1 - i\varepsilon_3)}.$$

We can find that under I , σ_v and C_∞ , three small real parameters become

$$I: \begin{pmatrix} \varepsilon_1 \\ \varepsilon_2 \\ \varepsilon_3 \end{pmatrix} \longrightarrow \begin{pmatrix} \varepsilon_1 \\ -\varepsilon_2 \\ -\varepsilon_3 \end{pmatrix} = \begin{pmatrix} 1 & 0 & 0 \\ 0 & -1 & 0 \\ 0 & 0 & -1 \end{pmatrix} \begin{pmatrix} \varepsilon_1 \\ \varepsilon_2 \\ \varepsilon_3 \end{pmatrix},$$

$$\sigma_v: \begin{pmatrix} \varepsilon_1 \\ \varepsilon_2 \\ \varepsilon_3 \end{pmatrix} \longrightarrow \begin{pmatrix} -\varepsilon_1 \\ \varepsilon_2 \\ -\varepsilon_3 \end{pmatrix} = \begin{pmatrix} -1 & 0 & 0 \\ 0 & 1 & 0 \\ 0 & 0 & -1 \end{pmatrix} \begin{pmatrix} \varepsilon_1 \\ \varepsilon_2 \\ \varepsilon_3 \end{pmatrix},$$

$$C_\infty: \begin{pmatrix} \varepsilon_1 \\ \varepsilon_2 \\ \varepsilon_3 \end{pmatrix} \longrightarrow \begin{pmatrix} \varepsilon_1 \\ \varepsilon_2 \cos(2\theta) + \varepsilon_3 \sin(2\theta) \\ \varepsilon_3 \cos(2\theta) - \varepsilon_2 \sin(2\theta) \end{pmatrix} = \begin{pmatrix} 1 & 0 & 0 \\ 0 & \cos(2\theta) & \sin(2\theta) \\ 0 & -\sin(2\theta) & \cos(2\theta) \end{pmatrix} \begin{pmatrix} \varepsilon_1 \\ \varepsilon_2 \\ \varepsilon_3 \end{pmatrix}.$$

Thus the characters of I , σ_v and C_∞ are $\chi(I) = -1$, $\chi(\sigma_v) = -1$, and $\chi(C_\infty) = 1 + 2\cos(2\theta)$. From Table 7.1, we understand that the iso-rotational modes transform as $E_{2u} + A_{2g}$. Similarly, the rotaional modes transform as $E_{1g} + A_{2g}$ since $\chi(I) = 3$, $\chi(\sigma_v) = -1$, and $\chi(C_\infty) = 1 + 2\cos(\theta)$; translational mode as $E_{1u} + A_{1u}$. However,

because of the symmetry consideration, the domain space and target space of the rational map share the same z -axis. Therefore the iso-rotational modes comprise E_{2u} and the rotational modes $E_{1g} + A_{2g}$. Removing all the zero modes from the ten-dimensional representations, we then can have E_{2g} , which is regarded as a genuine vibrational mode.

Since the representations form by the zero modes have been determined by the aforementioned method, we next move to seek the representations of the perturbed rational maps obtained by us. Consider $R_7(\xi)$ and $R_8(\xi)$ of the frequency 0.846727, which are shown conjugate to each other in the previous chapter. We form them as

$$R_{7-8}(\xi) = \frac{\xi^2 - i\varepsilon_7\xi + \varepsilon_8\xi}{1 + i\varepsilon_7\xi + \varepsilon_8\xi},$$

and, under the transformation I , σ_v and C_∞ , they perform as

$$I: R(\xi) \mapsto \frac{1}{\bar{R}(\frac{-1}{\xi})} = \frac{\xi^2 + i\varepsilon_7\xi - \varepsilon_8\xi}{1 - i\varepsilon_7\xi - \varepsilon_8\xi},$$

$$\sigma_v: R(\xi) \mapsto \bar{R}(\bar{\xi}) = \frac{\xi^2 + i\varepsilon_7\xi + \varepsilon_8\xi}{1 - i\varepsilon_7\xi + \varepsilon_8\xi},$$

$$C_\infty: R(\xi) \mapsto e^{-2i\theta} R(e^{i\theta}\xi) = \frac{\xi^2 + (\varepsilon_8 - i\varepsilon_7)e^{-i\theta}\xi}{1 + (\varepsilon_8 + i\varepsilon_7)e^{i\theta}\xi}.$$

We hence follow the same procedure taken previously to get the characters $\chi(I) = -2$, $\chi(\sigma_v) = 0$, and $\chi(C_\infty) = 2\cos(\theta)$ that is E_{1u} . So for $R_{9-10}(\xi)$ and $R_6(\xi)$, the representations they comprise are E_{2g} and A_{1u} . As for the brething mode, it was obtained numerically, and hence we can not determine its representation of symmetry using this method, but we assume that it has the same symmetry of that from Barnes et al.

We list in Table 7.2 the normal modes from the analysis for the power spectrum of the perturbation in Barnes et al. [10], and all the perturbed rational maps obtained by us, to make the comparison easy to read. The data from Barnes et al. are listed in increasing order of frequency, and the data from us are arranged in order to match the symmetry representations formed by the modes from the result of numerical study..

In Barnes et al., all the zero modes except two rotational modes around x , y axes, are not contained in the normal modes spectrum. In our result, we have the three rotational zero modes and two isorotational zero modes but the translational modes are broken since the rational map ansatz requires to set the origin of the coordinate fixed. The first two modes from the numerical result are the x , y rotational modes, which are slightly broken because of the finite size effects. We both have the same ‘2 Skyrmions scattering mode’ with the symmetry E_{2g} , which is the only genuine vibrational mode from the group theory analysis, but our results are with a large difference in frequency. It was claimed that they have two radiative modes of frequencies 0.49 and 0.52. We found that our broken z translational mode has the same symmetry, A_{1g} , as one of their radiative modes and the plots of both of our energy density are quite similar. However, we still do not have the conclusive evidence to claim that these two modes are the same. So we do not put them in the same line. As for the breathing mode, a mode must exist in every multi-Skyrmions and is a rescaling of the size of the Skyrmion, our result is obtained numerically from solving the perturbed profile function. With the parameters for the mass m and the potential p taken the values $(m, p) = (0.526, 1)$, the vibrational frequency acquired is higher than the value of the mass parameter and that means our breathing mode is not a genuine vibrational mode but a pseudo-vibrational mode, and the relevant discussion is in section 4.2. It therefore implies that the result from Barnes et al. might be the same, which means if the time frame they took is long enough, their breathing mode would have disappeared as the result obtained by Bizon et al. [18]. The frequencies of our results are very close, which are 0.75 and 0.761375 respectively; however, since the symmetry representation for our breathing mode can not be determined directly, we take it as A_{1g} but with parenthesis, same as that from Barnes et al. One important property for the breathing mode is that the modes obtained from the variations of the parameters of the rational map are below the breathing mode. The final mode of the frequency 0.84 in the numerical study is called ‘a dipole breathing mode’ by Barnes et al., whose description for the energy density is the same as our broken x , y translational modes with the frequency 0.846727.

To summarise, we can identify seven modes out of eleven with the numerical

result of Barnes et al.'s. Without taking the frequency into consideration, the qualitative properties, as in the representations of the symmetry and the degeneracy, of these seven modes obtained from the rational map ansatz match those result from Barnes et al. But we can not identify the modes corresponding to the isorotations in their data and also it is not conclusive to treat one of their radiative mode as our broken z translational mode. Furthermore their z rotational mode seems to be missing and it could be that the mode is slightly broken so that the frequency is too small to recognize in the power spectrum. The frequencies from the the breathing mode, broken rotational modes and broken translational modes have a very good agreement. However, the frequencies of both our genuine vibrational modes seem to have a large difference, for that it might be that the rational map ansatz is too stiff.

7.1.2 Analysis for $B = 4$ case

For $B = 4$ case, there is total of twenty-five modes in the power spectrum of the perturbation from [11], in which they claimed it contains three broken rotational zero mode, six radiative modes, sixteen vibrational modes respectively. The result obtained by us by using the rational map ansatz contains eighteen modes, including six zero modes, three broken translational zero modes and nine genuine vibrational modes.

Following the same group theory analysis mentioned in the previous section, we have determined the symmetry representations of our perturbed rational maps. Since, from the character table below, it is sufficient to determine the symmetry representations by calculating the characters of C_4 and C_4^2 and I for the rational maps of $B = 4$.

O_h	E	C_2	C_3	C_4	C_4^2	I	σ_v	S_6	$C_4\sigma_h$	σ_h
A_{1g}	1	1	1	1	1	1	1	1	1	1
A_{2g}	1	-1	1	-1	1	1	-1	1	-1	1
E_g	2	0	-1	0	2	2	0	-1	0	2
F_{1g}	3	-1	0	1	-1	3	1	0	-1	-1
F_{2g}	3	1	0	-1	-1	3	-1	0	1	-1
A_{1u}	1	1	1	1	1	-1	-1	-1	-1	-1
A_{2u}	1	-1	1	-1	1	-1	1	-1	1	-1
E_u	2	0	-1	0	2	-2	0	1	0	-2
F_{1u}	3	-1	0	1	-1	-3	-1	0	1	1
F_{2u}	3	1	0	-1	-1	-3	1	0	-1	1

The result is presented as follows:

1. rotational mode, $\chi(C_4) = 1$, $\chi(C_4^2) = -1$, $\chi(C_2) = -1$, $\chi(C_3) = 0$: symmetry representation F_{1g} .
2. isorotational mode, $\chi(C_4) = -1$, $\chi(C_4^2) = 3$, $\chi(C_2) = -1$, $\chi(C_3) = 0$, $\chi(I) = -3$: symmetry representation $E_{1u} + A_{2u}$.
3. $R_7, \tilde{R}_8, \tilde{R}_9$ (broken translational mode), $\chi(C_4) = 1$, $\chi(C_4^2) = -1$, $\chi(I) = -3$: symmetry representation F_{1u} .
4. $R_{10}, \tilde{R}_{11}, \tilde{R}_{12}$, $\chi(C_4) = -1$, $\chi(C_4^2) = -1$, $\chi(I) = -3$: symmetry representation F_{2u} .
5. $R_{13}, \tilde{R}_{14}, \tilde{R}_{15}$, $\chi(C_4) = -1$, $\chi(C_4^2) = -1$, $\chi(I) = 3$: symmetry representation F_{2g} .
6. R_{16}, R_{17} , $\chi(C_4) = 0$, $\chi(C_4^2) = 2$, $\chi(I) = 2$: symmetry representation E_g .
7. R_{18} , $\chi(C_4) = -1$, $\chi(C_4^2) = 1$, $\chi(I) = -1$: symmetry representation A_{2u} .

This result is consistent with that in Houghton et al. [42].

In increasing order of frequency, we list the data from Barnes et al. in Table 7.3. We then sort our data in order to match the symmetry and degeneracy of that in Barnes et al. instead of by the vibrational frequency. We also check both of our energy density plots of the vibrational modes for the auxiliary support and it

is found that the plots are exactly the same, even though the frequencies are very different in some modes. We both have in common the deuteron scattering mode, tetrahedral mode, rhombus mode, 4-Skyrmions mode, and breathing mode, which has the frequencies of 0.605 and 0.640537 from Barnes et al. and us. With the mass parameter m and the potential parameter p taken the values $(m, p) = (0.526, 1)$, the breathing mode for $B = 4$ case is quite similar to that in $B = 2$ case, *i.e.* it is also a pseudo-vibrational mode. Furthermore Barnes et al. have a slightly broken rotational zero mode. However, similar to the $B = 2$ case, we still can not conclusively regard one of their radiative modes as one of our isorotations, even though the symmetry representation is the same, A_{2u} . We hence put them in two different lines to avoid the confusion. The mode of frequency 0.655 from Barnes et al. is regarded as a genuine vibrational mode that has the same description for the energy density as ours, which, however, is identified as a broken translational modes by us. From the result of Barnes et al., the only vibrational mode that we do not have from the rational map ansatz, is the one of frequency 0.738.

To summarise, although the frequencies for both our results are quite different in some of the modes, the symmetry representations, the degeneracy and the energy density plots are matched very well. Except one isorotational mode E_u , we basically can identify our perturbed rational maps in the numerical data. Among these modes, the frequencies of the breathing mode from both our data are close. Again, in the numerical data, the isorotational modes are missing in the power spectrum. The numerical mode of frequency 0.655 is treated as a genuine mode but, according to our analysis, it is actually a broken translational zero mode. Barnes et al. have a mode of frequency 0.738 that we do not have in our result.

Numerical [10]				Ansatz			
Frequency	Degeneracy	Description	Symmetry	Frequency	Degeneracy	Description	Symmetry
0.03	2	broken rotational modes (around x and y axes)	E_{1g}	0	2	x, y isorotation (R_3, R_4)	E_{2u}
0.31	2	2 Skyrmions scattering mode	E_{2g}	0	3	x, y rotational modes (R_1, R_2) and z (iso)rotational mode (R_5)	$E_{1g} + A_{2g}$
0.49	1	radiative mode	A_{1u}	1.225536	2	2 Skyrmions scattering mode (R_9, R_{10})	E_{2g}
0.52	2	radiative mode	E_{2g}	0.583500	1	broken z translation (R_6)	A_{1u}
0.75	1	breathing mode	A_{1g}	(0.76)	1	breathing mode*	(A_{1g})
0.84	2	a dipole 'breathing' motion†	E_{1u}	0.846727	2	broken x, y translation (R_7, R_8)	E_{1u}

Table 7.2: Comparison of vibrational frequency between the numerical results and the rational map ansatz, $B = 2$.

* It is a pseudo-vibrational mode, and we hence enclose the frequency with the parenthesis.

† Its description of the energy density matches that of the broken x, y translational zero mode obtained from the rational map ansatz; however, this representation, E_{1u} , coincides with the doublet of x, y translational zero mode of the 2-monopole toroidal BPS solution.

Numerical [11]				Ansatz				Group Theory	Analysis [42]
Frequency	Degeneracy	Description	Symmetry	Frequency	Degeneracy	Description	Symmetry	Notation [40]	Degeneracy
				0	2	isorotation ($R_{iso,x}, R_{iso,y}$)	E_u	E^O	2
0.070	3	broken rotation	F_{1g}	0	3	rotation ($R_{rot,x}, R_{rot,y}, R_{rot,z}$)	F_{1g}	F_1^O	3
0.367	2	deuteron scattering mode	E_g	1.006370	2	deuteron scattering mode (R_{16}, R_{17})	E_g	E^O	2
0.405	1	tetrahedral mode	A_{2u}	1.402608	1	tetrahedral mode (R_{18})	A_{2u}	A_2^O	1
0.419	3	rhombus mode	F_{2g}	0.911260	3	rhombus mode ($R_{13}, \bar{R}_{14}, \bar{R}_{15}$)	F_{2g}	F_2^O	3
0.513	3	4 Skyrmions mode	F_{2u}	0.750841	3	4 Skyrmions mode ($R_{10}, \bar{R}_{11}, \bar{R}_{12}$)	F_{2u}	F_2^O	3
0.545	2	radiative mode	E_g						
				0	1	isorotation ($R_{iso,z}$)	A_{2u}	A_2^O	1
0.587	1	radiative mode	A_{2u}						
0.605	1	breathing mode	A_{1g}	(0.64)	1	breathing mode*	(A_{1g})		
0.655	3	broken translation	F_{1u}	0.562538	3	broken translation ($R_7, \bar{R}_8, \bar{R}_9$)	F_{1u}	F_1^O	3
0.738	3	diagonal mode	F_{2g}						
0.908	3	lowest nonzero radiative mode							

Table 7.3: Comparison of vibrational frequency between the numerical result and the rational map ansatz, $B = 4$.

* It is a pseudo-vibrational mode, and we hence enclose the frequency with the parenthesis.

7.2 Conclusion

We have studied the vibrational modes of the massive Skyrme solutions for $B = 1, 2$ and 4 within the rational map ansatz. Traditionally, the mass term used by researchers to study the massive Skyrme model is $m^2 \text{Tr}(U - 1)$; however, the mass term for this model is not unique and Kopeliovich et al. [49] have shown that there is a family of mass terms that can be used. Furthermore, Battye et al. [15] also demonstrates both the qualitative and quantitative changes in the configurations of the Skyrme solutions with the introduction of a nonzero pion mass with values larger than the standard one. Kopeliovich et al. sought to see whether there is a mass term different from the traditional one, with a value close to the standard value of the pion mass that allows us to have the Skyrme solutions similar to that obtained by Battye et al., whose shape is not shell-like but closes to real nuclei. Following Kopeliovich et al. the mass term that we took, is $\frac{m^2}{p^2} \text{Tr}(U^p - 1)$, with $p = 1, 2, 3$ and 4 .

We then performed perturbations around static Skyrme solutions approximated by the rational map ansatz to find out the vibrational modes of these solutions. These perturbations are realized by the most general fluctuation of the rational map that minimizes the energy for a given baryon number B of the Skyrme field, and by the fluctuation of the radial profile function.

When inserting this perturbed Skyrme field into the Lagrangian of the Skyrme model, it turns out that the radial perturbation, coming from the profile function, and angular vibrations, coming from the rational map, are decoupled. We then have two independent sets of equations of motion derived from this Lagrangian, namely the equation for the vibration of the profile function and that of the perturbed rational map. Solutions of these two sets of the eigenvalue equations provide the vibrational modes. The solutions that can be obtained by solving the equation of motion for the perturbed profile function for a given baryon number B are called breathing modes. As for the eigenvalue equation for the perturbed rational map, the solutions are not independent from each other. There exists an equivalence relation (or conjugate relation) among these solutions, namely zero modes and vibrational modes. They can be grouped into different multiplets based on symmetry considerations.

For $B = 1$, a trivial case, the rational map has six modes split into two sets of triplets; one is for the rotational zero modes, which in this case are the same as the iso-rotational zero modes because the domain space is exactly the same as the target space of the Skyrme field. The other three modes are the broken translational zero modes, which is the result of the rational map ansatz. The only one genuine vibrational mode comes from the breathing mode, which is the perturbed radial profile function.

For $B = 2$ case, there are ten rational modes and one perturbed radial mode, namely breathing mode. Five of the rational modes are zero modes, three broken translational zero modes and the other two are the genuine vibrational modes. The five zero modes are recognized as a triplet for the rotational zero modes, and a doublet for the isorotational zero modes. The three broken translational zero modes split into one doublet and singlet, E_{1u} and A_{1u} ; the singlet corresponds to a mode of broken z translational mode and the doublet to x and y translation. The only vibrational modes from the rational modes comprise a doublet. The breathing mode is another genuine vibrational mode, which is from the perturbed radial profile function.

In the case $B = 4$, the rational map has eighteen modes and the perturbed profile function has one vibrational mode, the breathing mode. Six of the rational modes are zero modes, three broken translational zero modes and the other nine are the vibrational modes. From symmetry consideration, the zero modes can be identified as two sets of triplets, which are that of the rotational zero modes and of the iso-rotational zero modes. The three broken translational zero modes form a triplet, whose energy density is the deformation of a cube such that one of the upper and lower part of the cube inflates and the other deflates. As for the nine vibrational modes, they can be grouped into one singlet, one doublet, and two triplets. The singlet is the mode of the deformation of a cube, which is pulling and inflating one edge on one face and inflating the opposite edge on the same face; the doublet consists of the two modes, each of which is the deformation of a cube, pulling it into two toruses in two perpendicular directions. One of the triplets is composed of three modes, corresponding to the deformation that makes a cube

become a rhombus. Another triplet consists of the three modes, each of which is a deformation of inflating two opposite edges on one face and deflating the other two opposite edges on that face.

Our result for symmetry representations of the vibrational modes of $B = 4$ is in a very good agreement with the analysis using the group theory done by Houghton et al. [42], except the triplet of the translational modes are broken by the rational map ansatz. We also compared our results with the numerical results obtained by Barnes et al. [10] [11]. In the $B = 2$ case, if we only focus on the symmetry representations and the degeneracy of the modes, *i.e.* the qualitative feature, and do not take the vibrational frequency into account, then there is only one broken z translational zero mode, and x, y isorotational zero modes can not be identified. In the $B = 4$ case, without taking into consideration the values of the vibrational frequencies and these ordering, we can match all our genuine vibrational modes, which are nine, three zero modes, three broken translational zero modes and one breathing mode with the numerical data from Barnes et al. In other words, we can find all our modes in the numerical data except three isorotational modes, which is good. There are merely some radiative modes in their result that we do not have. So qualitatively speaking, to some degree, our results are not so different from theirs. In the quantitative aspect, the reason why the frequencies are different from each other might come from the intrinsic property of the rational map.

The critical pion mass is another result that we can obtain from our data. When trying to solve the eigenvalue equation for the perturbed profile function, we need two parameters, one for the pion mass m and the other is for the potential parameter p . In the Table 4.1 to 4.3, we list the vibrational frequencies of the modes allowed by the equation of motion for $B = 1, 2$ and 4. The value of the critical mass then can be obtained for the different parameters p and listed in the Table 4.4. The values of the critical mass obtained by us are decreasing with the increasing potential parameter p for a give B . Likewise, the values of the critical mass are decreasing with the increasing B for a fixed p . Among these values of the critical mass for different sets of (B, p) , the values from $B = 1$ are the most important ones since they are obtained from the hedgehog ansatz, *i.e.* exact solutions of the Skyrme equation. It

thus means that the critical values of m set an upper bound for the value of the pion mass that we can take for the Skyrme model. In particular the upper bound is $m = 1.6$ when $p = 1$.

Generally speaking, from our results, the rational map ansatz is not a very good approximation to the Skyrmions. In the quantitative aspect, the frequencies of the vibrational modes that we obtained, are not in a good agreement with numerical study except for the breathing modes in $B = 2$ and $B = 4$ cases, and one vibrational mode in $B = 2$ case. Furthermore, within the rational map ansatz, the translational zero modes are not well described but are broken to the low energy modes. It shows that the rational map ansatz has much space to be improved quantitatively. However, in the qualitative aspect, most of the vibrational modes can be found in the numerical result with the same energy density descriptions, and therefore we might conclude that it is not bad in the qualitative aspect.

Bibliography

- [1] G. S. Adkins and C. R. Nappi, *The Skyrme Model with Pion Masses*, Nucl. Phys. **B233**: 109 (1984).
- [2] G. S. Adkins, C. R. Nappi and E. Witten, *Static Properties of Nucleons in the Skyrme Model*, Nucl. Phys. **B228**: 552 (1983).
- [3] H. Asano, H. Kanada, and H. So, *Quantization of the Non-linear Sigma Model and the Skyrme Model*, Phys. Rev. **D44**: 277-288 (1991).
- [4] I. J. R. Aitchison, *Effective Lagrangians and Soliton Physics I. Derivative Expansion and Decoupling*, Acta Physica Polonica **B18**: 191-205 (1987).
- [5] M. A. Armstrong, *Groups and Symmetry*, Springer-Verlag, New York, 1988.
- [6] M. F. Atiyah and N. S. Manton, *Skyrmions from instantons*, Phys. Lett. **B 222**: 438 (1989).
- [7] M. F. Atiyah and N. S. Manton, *Geometry and Kinematics of Two Skyrmions*, Comm. Math. Phys. **153**: 391-422 (1993).
- [8] M. F. Atiyah and P. M. Sutcliffe, *Skyrmions, instantons, mass and curvature*, Physics Letters **B 605**: 106-114 (2005).
- [9] B. S. Balakrishna, V. Sanyuk, J. Schechter, and A. Subbaraman, *Cutoff quantization and the Skyrmion*, Phys. Rev. **D45**: 344-351 (1992).
- [10] C. Barnes, K. Baskerville and N. Turok, *Normal Modes Spectrum of the Deuteron in the Skyrme Model*, Phys. Rev. B **441**: 180 (1997).

-
- [11] C. Barnes, K. Baskerville and N. Turok, *Normal Modes of the $B = 4$ Skyrme Soliton*, Phys. Rev. Lett. **79**: 367 (1997).
- [12] R. A. Battye and P. M. Sutcliffe, *Solitonic fullerene structures in light atomic nuclei*, Phys. Rev. Lett. **86**: 3989-3992 (2001).
- [13] R. A. Battye and P. M. Sutcliffe, *Skyrmions, Fullerenes and Rational Maps*, Reviews in Mathematical Physics **14**: 29-85 (2002).
- [14] R. A. Battye, S. Krusch, and P. M. Sutcliffe *Spinning Skyrmions and the Skyrme Parameters*, Phys.Lett. **B626**: 120-126 (2005).
- [15] R. A. Battye and P. M. Sutcliffe, *Skyrmions and the Pion Mass*, Nucl. Phys. **B705**: 384 (2005)
- [16] D. A. Brannan, M. F. Esplen, J. J. Gray, *Geometry*, Cambridge University Press, 1999.
- [17] D. M. Bishop, *Group Theory and Chemistry*, Dover Publications, 1993.
- [18] P. Bizon, T. Chmaj, and A. Rostworowski, *Asymptotic Stability of the Skyrmion*, Phys. Rev. D **75**: 121702(R) (2007)
- [19] A. Beutelspacher and U. Rosenbaum, *Projective Geometry: From Foundations to Applications*, Cambridge University Press, 1998.
- [20] E. Braaten and J. P. Ralston, *Limitations of A Semiclassical Treatment of the Skyrme Soliton*, Phys. Rev. bf B31: 598 (1985).
- [21] E. Braaten and L. Carson, *Deuteron as a toroidal Skyrmion*, Phys. Rev. **D38**: 3525-3539 (1988).
- [22] J. D. Breit and C. R. Nappi, *Phase Shifts of the Skyrmion Breathing Mode*, Phys. Rev. Lett. **53**: 889 (1984).
- [23] G. Burns, *Introduction to Group Theory with Applications*, Academic Press, 1977.

- [24] L. Carson, *B = 3 Nuclei as Quantized Multi-Skyrmions*, Phys. Rev. Lett. **66**: 1406-1409 (1991).
- [25] D. P. Cebula, A. Klein, and N. R. Walet, *Quantization of the Skyrmion*, Phys. Rev. **D47**: 2113-2131 (1993).
- [26] A. Chodor, E. Hadjimichael and C. Tze , editor, *Skyrmions and QCD; In: Solitons in Nuclear and Elementary Particle Physics*, World Scientific, p.306-312, 1984.
- [27] S. Coleman, *Aspects of symmetry*, Cambridge University Press, 1985.
- [28] J. F. Cornwell, *Group Theory in Physics*, Academic Press, 1984.
- [29] H. S. M. Coxeter, *Regular Polytopes*, Dover Publications, 1973.
- [30] B. S. DeWitt, *Point Transformations in Quantum Mechanics*, Phys. Rev. **85**: 653-661 (1952).
- [31] B. S. DeWitt, *Dynamical Theory in Curved Spaces. I. A Review of the Classical and Quantum Action Principles*, Rev. Mod. Phys. **29**: 377-397 (1957).
- [32] B. S. DeWitt, *Dynamical Theory of Groups and Fields*, (Les Houches Lectures 1963), Gordon and Breach, New York, 1965.
- [33] S. K. Donaldson, *Nahm's equations and the classification of monopoles*, Commun. Math. Phys. **96**: 387 (1984).
- [34] N. Dorey, J. Hughes and M. P. Mattis, *Skyrmion Quantization and the Decay of the Delta*, Phys. Rev. **D50**: 5816 (1994).
- [35] D. Finkelstein and J. Rubinstein, *Connection Between Spin, Statistics, and Kinks*, J. Math. Phys **9**: 1762 (1968).
- [36] K. Fujii, A. Kobushkin, K. Sato, and N. Toyota, *Skyrme-Model Lagrangian in Quantum Mechanics: SU(2) Case*, Phys. Rev. **D35**: 1896-1907 (1987).
- [37] D. J. H. Garling, *A Course in Galois Theory*, Cambridge University Press, 1986.

- [38] I. Grossman and W. Magnus, *Groups and Their Graphs*, The Mathematical Association of America, 1964.
- [39] J. Goldstone, *Field Theories with "Superconductor" Solutions*, *Nuovo Cimento* **19**: 154 (1961).
- [40] M. Hamermesh, *Group Theory and Its Application to Physical Problems*, Addison-Wesley, Reading, 1962.
- [41] Allen Hatcher, *Algebraic Topology*, Cambridge University Press, 2002.
- [42] C. J. Houghton, N. S. Manton and P. M. Sutcliffe, *Rational Maps, Monopoles and Skyrmions*, *Nucl. Phys.* **B510**: 507 (1998).
- [43] P. Irwin, *Zero Mode Quantization of Multi-Skyrmions*, *Phys. Rev.* **D61**: 114024 (2000).
- [44] S. Jarvis, *A Rational Map for Euclidean Monopoles via Radial Scattering*, *J. Reine Angew. Math.* **524**: 1741 (2000).
- [45] G. A. Jones, D. Singerman, *Complex Functions: An Algebraic and Geometric Viewpoint*, Cambridge University Press, 1987.
- [46] N. Kaiser, and Ulf-G Meiner, *On the axial charge in Skyrme models with vector mesons*, *Phys. Lett.* **B311**(1-4): 1-3 (1993).
- [47] K. D. Kokkotas and B. G. Schmidt, *Quasi-Normal Modes of Stars and Black Holes*, *Living Reviews in Relativity*, Vol. 2, No. 1999-2, (1999).
- [48] V. B. Kopeliovich, *Quantization of the Rotations of Axially Symmetric Systems in the Skyrme Model*, *Sov. J. Nucl. Phys.* **47**: 949-953 (1988).
- [49] V. B. Kopeliovich, B. Piette and W. J. Zakrzewski, *Mass terms in the Skyrme Model*, *Phys. Rev.* **D73**: 014006 (2006).
- [50] S. Krusch, *Homotopy of Rational Maps and the Quantization of Skyrmions*, *Ann. Phys.* **304**: 103-127 (2003).

- [51] S. Krusch, *Finkelstein-Rubinstein Constraints for the Skyrme Model with Pion Masses*, Proc. Roy. Soc. **A462**: 20012016 (2006).
- [52] P. D. Lax, R. S. Phillips, *Scattering theory*, Academic Press, New York, 1967.
- [53] T. D. Lee and C. N. Yang, *Question of Parity Conservation in Weak Interactions*, Phys. Rev. **104**: 254-258 (1956).
- [54] R. A. Leese and N. S. Manton, *Stable instanton-generated Skyrme fields with baryon numbers three and four*, Nucl. Phys. **A572**: 575-599 (1994).
- [55] R. A. Leese, N. S. Manton, and B. J. Schroers, *Attractive Channel Skyrmions and the Deuteron*, Nucl. Phys. **B442**: 228 (1995).
- [56] N.S. Manton and P.J. Ruback, *Skyrmions in Flat Space and Curved Space*, Phys. Lett. **B181**: 137-140 (1986).
- [57] L. Marleau, *The Skyrme Model and Higher Order Terms*, Phys. Lett. **B235**(1-2): 141-146 (1990).
- [58] L. Marleau, *All-orders Skyrmions*, Phys. Rev. **D45**: 1776-1781 (1992).
- [59] M. P. Mattis, *Skyrmions and Vector Mesons*, Phys. Rev. Lett. **56**: 1103-1106 (1986).
- [60] R. Mirman, *Point Groups, Space Groups, Crystals, Molecules*, World Scientific, 1999.
- [61] M. Mukerjee and M.P. Mattis, *Skyrmions and Vector Mesons II: Strange New Formulae*, KEK 88-11-188.
- [62] R. S. Mulliken, J. Chem. Phys., **23**: 1997 (1955).
- [63] R. S. Mulliken, J. Chem. Phys., **24**: 1118 (1956).
- [64] Y. Nambu and G. Jona-Lasinio, *Dynamical Model of Elementary Particles Based on an Analogy with Superconductivity. I*, Phys. Rev. **122**: 345-358 (1961).

- [65] T. Needham, *Visual Complex Analysis*, Oxford University Press, 2003.
- [66] V. G. Makhankov, Y. P. Rybakov and V. I. Sanyuk, *The Skyrme Model*, Springer-Verlag, 1993.
- [67] S. Sternberg, *Group Theory and Physics*, Cambridge University Press, 1994.
- [68] G. t' Hooft, *A Planar Diagram Theory for Strong Interactions*, Nucl. Phys. **B72**: 461-473 (1974).
- [69] N. S. Manton and P. M. Sutcliffe, *Topological Solitons*, Cambridge University Press, 2004.
- [70] A. Pais, *Isotopic Spin and Mass Quantization*, Physica **19**: 869-887 (1953).
- [71] A. Pais, *On the Program of Systematization of Particles and Interactions*, Proc. Nat. Acad. Sci.(USA) **40**: 484-492 (1954).
- [72] B. P. Palka, *An Introduction to Complex Function Theory.*, Springer-Verlag, New York, 1991.
- [73] R. Rajaraman, H. M. Sommermann, J. Wambach and H. W. Wyld, *Stability of the Rotating Skyrmion*, Phys. Rev. **D33**: 287 (1986).
- [74] E. G. Rees, *Notes on Geometry*, Springer-Verlag, New York, 1983.
- [75] D. J. S. Robinson, *A Course in the Theory of Groups*, Springer-Verlag, New York, 1982.
- [76] V. N. Romanov, I. V. Frolov and A. S. Schwarz, *Spherically Symmetric Solitons*, Teor. Mat. Fizika **37**: 305-319(in Russian), [English Translation Teor. & Mat. Physics **37**: 1038-1046, (1978)].
- [77] W. Rossmann, *Lie Groups: An Introduction Through Linear Groups*, Oxford University Press, 2002.
- [78] B. J. Schroers, *Dynamics of Moving and Spinning Skyrmions*, Z. Phys. **C61**: 479 (1994).

- [79] P. Samuel, *Projective Geometry*, Springer-Verlag, New York, 1988.
- [80] S. Sawada and K. Yang, *Stability of Quantized Chiral Soliton with the Skyrme Term*, Phys. Rev. **D44**: 1578-1584 (1991).
- [81] Hans Schwerdtfeger, *Geometry of Complex Numbers*, Dover Publications, 1979.
- [82] J. Schechter and H. Weigel, *Breathing Mode in the $SU(3)$ Skyrme Model*, Phys. Rev. **D44**: 2916-2927 (1991).
- [83] J.-P. Serre, *Linear Representations of Finite Groups*, Springer-Verlag, New York, 1994.
- [84] R. A. Silverman, *Introductory Complex Analysis*, Dover Publications, 1984.
- [85] M. A. Singer and P. M. Sutcliffe, *Symmetric Instantons and Skyrme Fields*, Nonlinearity **12**: 987-1003 (1999).
- [86] T. H. R. Skyrme, *A Nonlinear Field Theory*, Proc. Roy. Soc. London **A260**: 127 (1961).
- [87] T. H. R. Skyrme, *The Origins of Skyrmions*, Int. J. Mod. Phys. **A3**: 2745-2751 (1988).
- [88] P. M. Sutcliffe, *Instantons and the Buckyball*, Proc. R. Soc. London, **A460**: 2903-2912 (2004).
- [89] W.-K. Tung, *Group Theory in Physics*, World Scientific, 1985.
- [90] J. J. M. Verbaarschot, *Axial Symmetry of bound Baryon Number Two Solution of the Skyrme Model*, Phys. Lett. **B195**: 235-239 (1987).
- [91] T. S. Walhout, *Quantizing the Four Baryon Skyrmion*, Nucl. Phys. **A547**: 423 (1992).
- [92] H. Walliser, *The $SU(n)$ Skyrme model*, Nucl. Phys. **A548**: 649 (1992).
- [93] E. Witten, *Baryons in the $1/N$ Expansion*, Nucl. Phys. **B160**: 57-115 (1979).

Appendix A

Symmetry Groups

In Appendix A, we basically follow the book “Group Theory and Its Application to Physical Problems” [40] to briefly introduce the symmetry groups. If one is interested in more details of the symmetry groups, we refer to other books [5] [60] [23] [38] [67] [28] [17].

A.1 Introduction to Symmetry Groups

An object is said to have a certain symmetry when it is brought back to itself or is left invariant after a set of transformations which do not change the distance between any pairs of points of the object. This set of transformations, called symmetry transformations, forms the symmetry group of the object. The isometric transformations, or distance-preserving transformation, come from the combinations of three basic types:

1. Finite rotation.
2. Reflection.
3. Translation.

In physics, there is a class of groups which are important, named “symmetry groups”. The symmetry groups of finite bodies are called point groups since there must be at least one point of the body fixed for all transformations of the symmetry group of the finite body. However, translation is not a symmetry for a body of

finite extension. Therefore only the finite rotations and reflection in a plane are the possible fundamental types of transformations used to build up the point groups. We will introduce them in the following sections of this appendix.

A.2 Fundamental Symmetry Transformations

A.2.1 Finite rotation.

Suppose that the body is invariant after being rotated through an angle $\theta = 2\pi/n$ (n is an integer) about an axis. We then call this axis an n -fold axis. For a crystal, the n is restricted to the values 1, 2, 3, 4 or 6 only, whose associated rotation angle is $\theta = 2\pi, 2\pi/2, 2\pi/3, 2\pi/4$ and $2\pi/6$. By the symbol C_n we denote the symmetry transformation of finite rotation through $2\pi/n$. Multiple applications of the operation will be denoted by C_n^k , which is the rotation through $2k\pi/n$. If n can be divided by k , then

$$C_n^k = C_{\frac{n}{k}}. \quad (\text{A.2.1})$$

It is obvious that the application of rotation through $2\pi/n$ about the same axis n times will take this object back to its initial configuration, and hence give the identity transformation. By (A.2.1), we have $C_n^n = E$, where E is the symbol for the identity transformation.

An axis with 2-fold symmetry has just two symmetry operations (rotations through π and 2π); one with 4-fold symmetry has four symmetry transformations (rotations through $\pi/2, \pi, 3\pi/2$ and 2π). It means an axis with 4-fold symmetry will also have 2-fold symmetry. It is said that a 4-fold axis has higher symmetry than a 2-fold axis and the axis with the highest symmetry is then defined as the principal axis.

A.2.2 Reflection.

The second type of fundamental transformation, *i.e.* reflection in a plane, is different from the rotation, which can move an object from its initial to its final configuration;

however, the reflection does not correspond to any physical displacement. Simply speaking, the reflection transforms the object to one which is the original seen in a mirror.

The symbol used to denote a reflection in the plane is σ . Two successive reflections in the same mirror give the initial configuration, then we have

$$\sigma^2 = E . \quad (\text{A.2.2})$$

However, there are several ways to specify the reflection plane, which can be denoted as $\sigma_h, \sigma_v, \sigma_d, \sigma_{xy} = \sigma_h, \sigma_{xz} = \sigma_v$, etc.. The symbol σ_h and σ_v stand for the reflection plane is horizontal (h) and vertical (v) that is perpendicular and passing through to the principal axis respectively and σ_d denotes diagonal mirror between two rotational axes.

The combination of two fundamental transformations, a rotation about an axis C_n and reflection σ_h in the plane perpendicular to the axis of C_n , gives a symmetry operation which will be called a rotation-reflection or improper rotation, denoted by S_n :

$$S_n = C_n \sigma_h = \sigma_h C_n . \quad (\text{A.2.3})$$

If an object is said to have an n -fold rotation-reflection axis, then when being applied by a rotation of $2\pi/n$ about the axis and together with reflection in a plane perpendicular to the rotation axis, it is brought back to itself. It also should be noted that the C_n and σ_h commute with each other. From (A.2.2), (A.2.3) and together with $C_n^n = E$, we have

$$(S_n)^n = (C_n \sigma_h)^n = C_n^n (\sigma_h)^n = \begin{cases} E & , \text{ for even } n. \\ \sigma_h & , \text{ for odd } n. \end{cases} \quad (\text{A.2.4})$$

Furthermore, S_2 is an important case for rotation-reflection symmetry since it will result in the inversion, which reflects the object relative to the origin. Inversion is denoted by another symbol, I , and defined as

$$I = S_2 = C_2 \sigma_h . \quad (\text{A.2.5})$$

Three transformations, I , σ_h and C_2 , commute since by $C_2^2 = \sigma_h^2 = E$, we have

$$C_2 = I\sigma_h \quad , \quad \sigma_h = IC_2 . \quad (\text{A.2.6})$$

It means that when any two of the elements, I , σ_h and C_2 , are in the symmetry group, so is the third one.

In the following table, we summarize the notations for the symmetry transformation:

Notation	Description
E	Identity.
C_n	Proper rotation by $2\pi/n$ about an axis.
σ	Reflection in a plane.
σ_h	Reflection in a horizontal plane perpendicular to the principal axis.
σ_v	Reflection in a vertical plane passing through the principal axis.
σ_d	Reflection in a diagonal plane.
S_n	Rotation-reflection (Improper rotation).
I	Inversion.

Table A.1: Notations for the elements of point groups

A.3 Groups of Pure Rotations

In this section, we consider the groups with the elements only from the pure rotations. This kind of groups can be categorized by the number and the order of the axis. When there is only one rotation axis, we have a uniaxial group. When there is one n -fold axis and a set of 2-fold axes perpendicular to it, this is dihedral group. A group with more than one n -fold axis is called polyhedral group.

A.3.1 Uniaxial Group: C_n

Groups with only one rotation axis of n -fold: C_n . An object with this symmetry will coincide with itself after a rotation by $2\pi/n$ (n is an integer) is performed.

A.3.2 Dihedral Group: D_n

Groups with an n -fold principal axis and a set of 2-fold axes perpendicular to it, are called dihedral groups and are denoted by D_n .

One way to expand the uniaxial groups C_n to other groups of pure rotations, is to adjoin some 2-fold axes to the principal axis of n -fold. As the first step, we consider only to adjoin a single 2-fold axis to C_n . One should then note that the angle for adjoining this 2-fold axes matters, since if it does not take the correct angle, then a second n -fold axis will be obtained by rotating about the 2-fold axis through π . Therefore one should adjoin the 2-fold axis at a right angle, *i.e.* $\pi/2$, to the n -fold principal axis.

The simplest case for D_n is to adjoin a set of 2-fold axes to C_2 , leading to D_2 . This set of 2-fold axes contains two axes, C_a and C_b , which are orthogonal to each other and both are perpendicular to the 2-fold principal axis. D_2 has four elements in four classes:

$$E ; C_2 ; C_a ; C_b . \quad (\text{A.3.7})$$

For $n = 3$, one has a single 2-fold axis, C_a , at a right angle to the 3-fold principal axis, and by rotating the 2-fold axis about the principal axis through $2\pi/3$ and $4\pi/3$ respectively, one then has the other two equivalent 2-fold axes, C_b and C_c . The six elements of D_3 are in three conjugacy classes:

$$E ; C_3 , C_3^2 ; C_a ; C_b ; C_c . \quad (\text{A.3.8})$$

For higher values of n for D_n , it can be obtained similarly as D_2 or D_3 .

A.3.3 Regular Polyhedron (Platonic Solids)

The other way to expand the uniaxial groups C_n to other groups of pure rotations, is to adjoin more than one n -fold ($n > 2$) axis. They are the symmetry groups for the regular polyhedron, or platonic solids. Before discussing these symmetry groups with elements having more than one n -fold axis with $n > 2$, we briefly describe these regular polyhedrons.

There are actually only five regular polyhedra, which are listed in the table below:

Name	p^*	q^{**}	V (Vertices)	E (Edges)	F (Faces)
Tetrahedron	3	3	4	6	4
Cube	4	3	8	12	6
Octahedron	3	4	6	12	8
Dodecahedron	5	3	20	30	12
Icosahedron	3	5	12	30	20

Table A.2: Combinatorial properties of the polyhedron.

* p - the number of sides of each face (or the number of vertices of each face).

** q - the number of faces meeting at each vertex (or the number of edges meeting at each vertex).

The relations among p , q , V , E and F are

$$pF = 2E = qV . \quad (\text{A.3.9})$$

Meanwhile, the Euler characteristic is

$$V - E + F = 2 . \quad (\text{A.3.10})$$

From (A.3.9) and (A.3.10), V , E and F can be expressed in terms of p and q only:

$$V = \frac{4p}{2p + 2q - pq} , \quad E = \frac{2pq}{2p + 2q - pq} , \quad F = \frac{4q}{2p + 2q - pq} . \quad (\text{A.3.11})$$

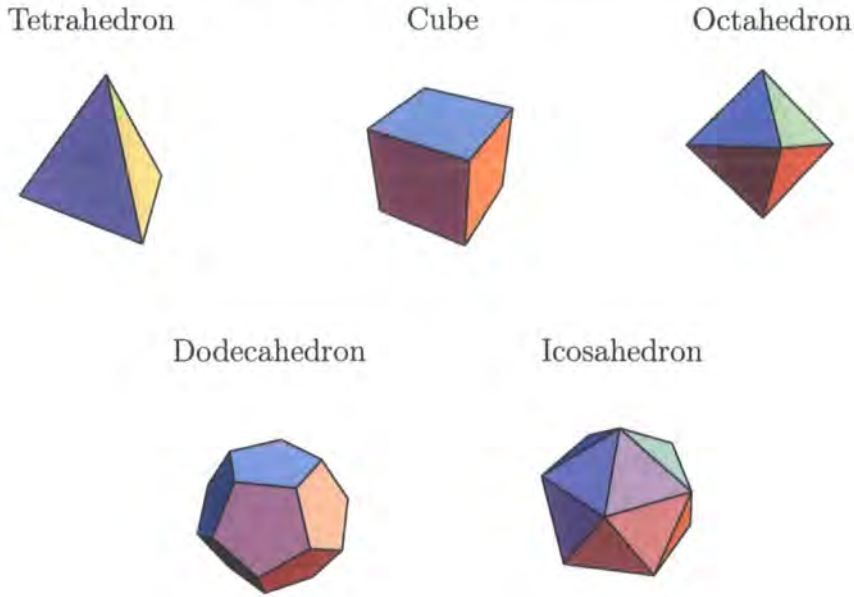


Figure A.1: Five regular polyhedra (or platonic solids).

Tetrahedral Symmetry, T

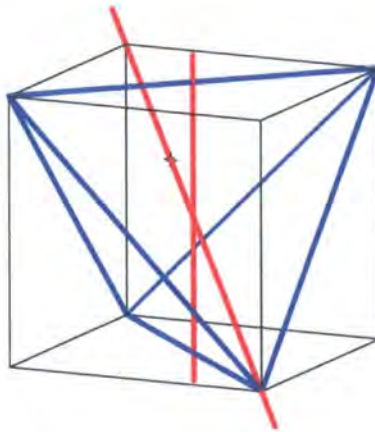


Figure A.2: Tetrahedron and the rotation axes.

A regular tetrahedra can be fit into a cubic, like Figure A.4, which has two different rotational axes, 3-fold and 2-fold respectively. The 3-fold axis is the line which is passing through one vertex of the tetrahedra and is normal to one face of the tetrahedron, and hence there are four 3-fold axis. In Figure A.4, this 3-fold axis is presented as the line connection two diagonal points of the cube. The 2-fold axis is the line joining two midpoints of the “opposite” edges of the tetrahedron, and there

are three 2-fold axis. Rotations about one 2-fold axis will take any of 3-fold axis into the other, so that all four 3-fold axis are equivalent. Similar situation applied to the 2-fold axis will lead us to find that three 2-fold axis are equivalent to one another. However, C_3 rotations are not the same as C_3^2 , since by conjugate relation $C_2C_3C_2^{-1} \neq C_3^2$. Therefore, the tetrahedral group has 12 symmetry transformations (or 12 elements), which can be categorized into 4 classes:

$$E ; C_2 ; C_3 ; C_3^2 . \quad (\text{A.3.12})$$

Octahedral Symmetry, O

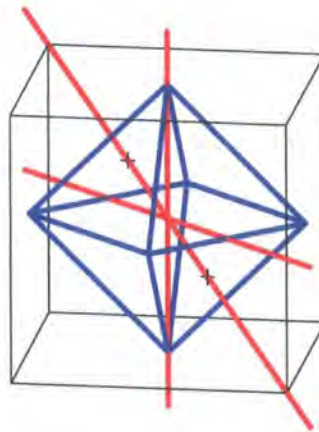


Figure A.3: Octahedron and the rotation axes.

The regular octahedron shown in Figure A.3 has three different rotational axes, which are a set of three 4-fold, a set of four 3-fold axis and a set of six 2-fold axes. The 4-fold axis is the line connecting centers of opposite face of the cube; the 3-fold axis joins two diagonal points of the cube; joining the midpoints of the opposite edges of the cube is the 2-fold axis. Application of the 3-fold and 4-fold rotation to any one of the 2-fold axes will get the other five equivalent 2-fold axes, which means these six elements are in the same class. It is also easy to show that all 3-fold axes are equivalent to one another. All 4-fold axes are equivalent to one another but these elements are in the two conjugacy classes. So the octahedral group has 24

elements, in 5 conjugacy classes:

$$E; C_2; C_3, C_3^2; C_4, C_4^3; C_4^2. \quad (\text{A.3.13})$$

A cube has the same set of symmetries as that of an octahedron, since it is the dual to each other.

A.4 Groups with Pure Rotations and Rotation Reflections

After the discussion of all the possible symmetry groups with elements only about the rotations, it is necessary to add the elements of the second type, the reflection-rotations S . Let S be an element of the group. There are two possible actions for S : the product of S with the rotation is still a rotation-reflection; the product of two rotation-reflection leads to a rotation. However, when adjoining the rotation-reflections S , we do not allow the new rotations, since all the rotations should already be the elements in the group of the pure rotations. So there are only two kinds of choices for S : $S^2 = E$; $S^2 \neq E$. The possibility for $S^2 = E$ is $S = \sigma$, reflection in a plane, and $S = I$, the inversion.; for $S^2 \neq E$ is $S^2 = C_n$ [40]. This leaves us with three possible ways for S to adjoin the groups of pure rotations: $S = \sigma$, $S = I$ and $S^2 = C_n$.

A.4.1 Adjunction of Reflection to C_n

1. $S^2 = C_n$.

(1) $n = 1$: $S^2 = C_1 = E$, so we have $S = \sigma$ and $S = I$, which will be discussed later.

(2) $n = 2$: $S^2 = C_2$, then $S = S_4$.

(3) $n = 3$: $S^2 = C_3$, so $S = S_6$.

(4) $n \geq 4$: It then would lead to a rotation-reflection axis of order greater than 6, which was excluded.

2. $S = \sigma$. If no new rotations are allowed, then there are only two possible ways to include the reflection plane: perpendicular to, or passing through the principal axis.

(1) $C_{nh} = \sigma_h \times C_n$: When the σ is adjoined to the C_n , the new group is called C_{nh} . The new groups in this case are

$$C_s, C_{2h}, C_{3h}, C_{4h}, C_{6h}, \quad (\text{A.4.14})$$

where $C_s \equiv C_{1h}$, which only contains two elements, *i.e.* E and σ_h .

(2) $C_{nv} = \sigma_v \times C_n$: Since $n = 1$ gives C_s , which is obtained in the former case, the adjunction of σ_v to C_n leads to the new groups

$$C_{2v}, C_{3v}, C_{4v}, C_{6v}, \quad (\text{A.4.15})$$

3. $S = I$. The only new group that can be obtained in this case is for $n = 1$, and it gives C_i , or S_2 , which contains two elements E and I .

A.4.2 Adjunction of Reflection to D_n

Similar actions taken previously can be done to the dihedral group D_n . In adjoining dihedral group, we only consider reflection symmetry, since when trying to adjoin inversion, we obtain $D_n \times C_i$, *i.e.* D_{nh} for n even, and D_{nd} for n odd; when adjoining rotation-reflection, it gives no new groups.

1. Adjunction of σ_h . If σ_h is taken into consideration, we will obtain the reflection in the vertical plane through any 2-fold axis by the product of σ_h with the rotation about this axis. It means that adjunction of σ_h gives n vertical reflection planes with n operations σ_v . The new groups obtained from this procedure are D_{nh} , which can be written as

$$D_{nh} = D_n \times C_s, \quad (\text{A.4.16})$$

the direct product of D_n and C_s . There are $2n$ elements of the pure rotations from D_n , n reflections elements in the n vertical plane and n rotation reflections elements in D_n group. Therefore the new groups are

$$D_{2h}, D_{3h}, D_{4h}, D_{6h}. \quad (\text{A.4.17})$$

- Adjunction of σ_d . There is another possibility to adjoin a reflection plane to D_n , namely a vertical plane that bisects the angle between two 2-fold axes. This set of new groups is called D_{nd} . But there are only two choices for n , $n=2$ and 3, and for $n > 3$ the order of the rotation-reflection axis would be greater than 6, which was excluded earlier. Hence these two new groups are D_{2d} and D_{3d} .

A.4.3 Adjunction of Reflection to T , O

Finally we want to add rotation-reflections to the tetrahedral group T and octahedral group O .

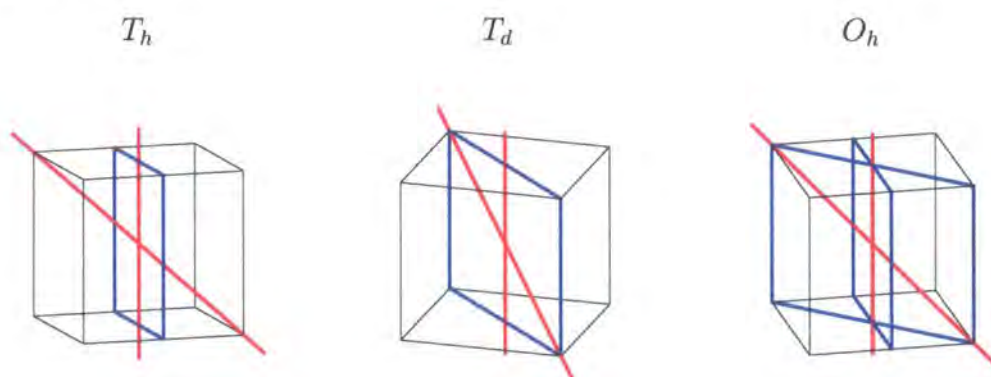


Figure A.4: T_h , T_d and O_h

In adjoining the reflection plane to T , we only have two choice for the plane: either pass through two opposite edges of the cube or is the parallel plane in the middle of the two opposite faces.

- Adjunction of σ_h to T : T_h . The subscript h here means that the plane is horizontal to 2-fold axes shown in Figure A.4. Since the angles between the 3-fold axes are bisected by the planes, these reflection planes turn those 3-fold axes into 6-fold rotation-reflection axes. We may write $T_h = T \times C_i$, and therefore there are 24 elements in T_h , distributed in 8 conjugacy classes.
- Adjunction of σ_v to T : T_d . That the planes added in T bisects the angles between two horizontal 2-fold axes, gives this new group denoted by T_d . It means that the 2-fold rotation axes are converted into 4-fold rotation-reflection

axes S_4 . Hence there are 24 elements of T_d in 5 conjugacy classes:

$$E; C_3, C_3^2; S_4, S_4^3; C_2 = S_4^2; \sigma_d. \quad (\text{A.4.18})$$

It has to be noted that the group T_d is the full symmetry group of the tetrahedron.

1. Adjunction of σ_h to O : O_h . Although the position for adding reflection planes is confined in the same way as that for T , the adjunction of one type of plane will generate the other. The 3-fold C_3 -axes convert to S_6 -axes for the same reason for that in T_h . We can express the group O_h as the direct product of O and C_i , or as $O_h = O \times C_i$. O_h is the group of the symmetry transformation for a cube, and it contains 48 elements in 10 classes:

$$\begin{aligned} E; C_2; C_3, C_3^2; C_4, C_4^3; C_4^2; \\ I; \sigma_v; S_6, \sigma_6^5; C_4\sigma_h, C_4^3\sigma_h; \sigma_h. \end{aligned} \quad (\text{A.4.19})$$

A.5 Character Tables for Some Important Point Groups

In this section we give the character tables of the irreducible representations of some important point groups as the basis for studying the symmetry of the Skyrmions.

The symbols introduced in the character tables are Mulliken Symbols [62] [63], which are used to denote the irreducible representations of groups. The notations and explanations of the symbols are given in the following table.

Symbol	Description
A	One dimensional representations symmetric with respect to rotation about the principal C_n axis.
B	One dimensional representations which is antisymmetric with respect to rotation about the principal C_n axis.
E	Two dimensional representations.
T (or F)	Three dimensional representations.
X_g	g attached to symbols for representations symmetric under inversion.
X_u	u attached to symbols for representations antisymmetric under inversion.
X_1	Subscript 1 attached to symbols A or B only; symmetric with respect to a vertical mirror plane perpendicular to the principal axis.
X_2	Subscript 2 attached to symbols A or B only; antisymmetric with respect to a vertical mirror plane perpendicular to the principal axis.
'	Prime attached to symbols for the representations symmetric with respect to a mirror plane horizontal to the principal rotational axis.
"	Double primes attached to symbols for the representations antisymmetric with respect to a mirror plane horizontal to the principal rotational axis.

In the group C_s , x and y are symmetric under reflection, whose reflection plane is the $X - Y$ plane, and therefore denote by the symbol A' ; z is antisymmetric under reflection and denote by A'' . In the group C_i , that x , y and z are all antisymmetric under inversion results in using the denotation A_u . In the group C_4 and S_4 , there are two two dimensional representations E that are complex conjugate.

The character tables are listed as follows

			C_1	E
			A	1

			C_i	E	I
			C_2	E	C_2
			C_s	E	σ

A_g	$A; z$	$A'; x, y$	1	1
$A_u; x, y, z$	$B; x, y$	$A''; z$	1	-1

C_{2h}			E	C_2	σ_h	I
		C_{2v}	E	C_2	σ_v	$\sigma_{v'}$
		D_2	E	C_z	C_y	C_x
A_g	$A_1; z$	A_1	1	1	1	1
B_g	$B_2; y$	$B_3; x$	1	-1	-1	1
$A_u; z$	A_2	$B_1; z$	1	1	-1	-1
$B_u; x, y$	$B_1; x$	$B_1; y$	1	-1	1	-1

C_4		E	C_4	C_4^2	C_4^3
		E	S_4	S_4^2	S_4^3
$A; z$	A	1	1	1	1
B	$B; z$	1	-1	1	-1
$E; x + iy$	$E; x + iy$	1	i	-1	$-i$
$E; x - iy$	$E; x - iy$	1	$-i$	-1	i

C_3	E	C_3	C_3^2
$A; z$	1	1	1
$E; x + iy$	1	ϵ	ϵ^2
$E; x - iy$	1	ϵ^2	ϵ

$$\epsilon = e^{-2\pi i/3}.$$

C_{3v}		E	C_3	σ_v
		E	C_3	C_x
$A_1; z$	A_1	1	1	1
A_2	$A_2; z$	1	1	-1
$E; x, y$	$E; x, y$	2	-1	0

C_{3h}	E	C_3	C_3^2	σ_h	$\sigma_h C_3$	σC_6^2
A'	1	1	1	1	1	1
A''	1	-1	1	-1	1	-1
E'	1	ϵ	ϵ^2	1	ϵ	ϵ^2
E''	1	ϵ^2	ϵ	1	ϵ^2	ϵ
E'	1	ϵ	ϵ^2	-1	$-\epsilon$	$-\epsilon^2$
E''	1	ϵ	ϵ^2	-1	$-\epsilon^2$	$-\epsilon$

$$\epsilon = e^{-2\pi i/3}.$$

C_6	E	C_6	C_6^2	C_6^3	C_6^4	C_6^5
$A; z$	1	1	1	1	1	1
$B; z$	1	-1	1	-1	1	-1
E_1	1	ω^2	$-\omega$	1	ω^2	$-\omega$
E_2	1	$-\omega$	ω^2	1	$-\omega$	ω^2
$E_3; x + iy$	1	ω	ω^2	-1	$-\omega$	$-\omega^2$
$E_4; x - iy$	1	$-\omega^2$	$-\omega$	-1	ω^2	ω

$$\omega = e^{2\pi i/6}.$$

C_{4v}	D_4		E	C_4^2	C_4	σ_v	σ_v'
			E	C_4^2	C_4	C_2	C_2'
			E	C_2	S_4	C_2'	σ_d
$A_1; z$	A_1	A_1	1	1	1	1	1
A_2	$A_2; z$	A_2	1	1	1	-1	-1
B_1	B_1	B_1	1	1	-1	1	-1
B_2	B_2	$B_2; z$	1	1	-1	-1	1
$E; x, y$	$E; x, y$	$E; x, y$	2	-2	0	0	0

x axis coincident with C_2' axis.

C_6			E	C_6^3	C_6^2	C_6	C_2	$C_{2'}$
C_{6v}			E	C_6^3	C_6^2	C_6	σ_v	$\sigma_{v'}$
D_{3h}			E	σ_h	S_6^2	S_6	C_2	σ_v
A_1	$A_1; z$	A'_1	1	1	1	1	1	1
$A_2; z$	A_2	A'_2	1	1	1	1	-1	-1
B_1	B_2	A''_1	1	-1	1	-1	1	-1
B_2	B_1	$A''_2; z$	1	-1	1	-1	-1	1
E_2	E_1	$E'; x, y$	2	2	-1	-1	0	0
$E_1; x, y$	$E_2; x, y$	E''	2	-2	-1	1	0	0

T	E	C_2	C_3	C_3^2
A	1	1	1	1
E	1	1	ϵ	ϵ^2
E	1	1	ϵ^2	ϵ
$F; x, y, z$	3	-1	0	0

$$\epsilon = e^{-2\pi i/3}$$

O		E	C_3	C_4^2	C_2	C_4
T_d		E	C_3	S_4^2	σ_d	S_4
A_1	A_1	1	1	1	1	1
A_2	A_2	1	1	1	-1	-1
E	E	2	-1	2	0	0
F_2	$F_2; x, y, z$	3	0	-1	1	-1
$F_1; x, y, z$	F_1	3	0	-1	-1	1

O_h	E	C_2	C_3	C_4	C_4^2	I	σ_v	S_6	$C_4\sigma_h$	σ_h
A_{1g}	1	1	1	1	1	1	1	1	1	1
A_{2g}	1	-1	1	-1	1	1	-1	1	-1	1
E_g	2	0	-1	0	2	2	0	-1	0	2
F_{1g}	3	-1	0	1	-1	3	1	0	-1	-1
F_{2g}	3	1	0	-1	-1	3	-1	0	1	-1
A_{1u}	1	1	1	1	1	-1	-1	-1	-1	-1
A_{2u}	1	-1	1	-1	1	-1	1	-1	1	-1
E_u	2	0	-1	0	2	-2	0	1	0	-2
F_{1u}	3	-1	0	1	-1	-3	-1	0	1	1
F_{2u}	3	1	0	-1	-1	-3	1	0	-1	1

